UNIVERSITÀ DEGLI STUDI DI TRIESTE

XXXV CICLO DEL DOTTORATO DI RICERCA IN CHIMICA

SYNTHESIS OF ATP-COMPETITIVE CK1δ INHIBITORS: EXPLORING HETEROAROMATIC SYSTEMS AS PROMISING TOOLS FOR NEURODEGENERATIVE DISEASES

Settore scientifico-disciplinare: **CHIM-08**

DOTTORANDO / A

ILENIA GRIECO

COORDINATORE

PROF. ENZO ALESSIO

SUPERVISORE DI TESI

PROF. STEPHANIE FEDERICO
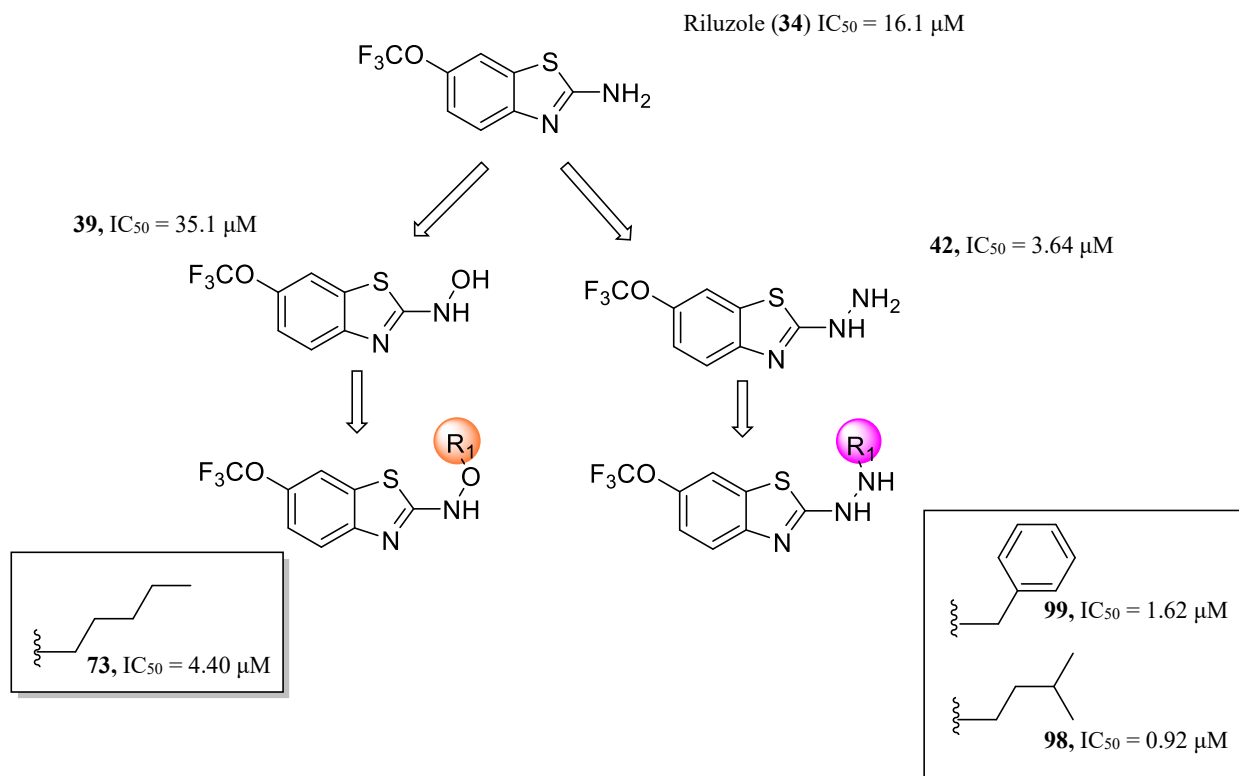
ANNO ACCADEMICO 2021/2022

Abstract

Protein kinases (PKs) are a family of 518 enzymes that catalyze the phosphorylation of substrates containing serine, threonine or tyrosine residues (Ser/Thr/Tyr). One of the members of this superfamily is Casein Kinase 1 (CK1), a subset that is composed by six isoforms: the isoform δ (CK1δ), in particular, is the protein on which the PhD thesis is focused. This target is involved in several physiological processes modulating different signaling pathways and deregulations can lead to the development of pathological conditions including cancer, circadian rhythm disorders and neurodegenerative diseases. CK1δ results implied in Alzheimer's, Parkinson's diseases (AD; PD) and Amyotrophic Lateral Sclerosis (ALS) which are all characterized by hyperphosphorylation of proteins and accumulation of aggregates contributing to trigger neuroinflammatory and neurodegenerative processes. Given the role of CK1δ in these disorders, the kinase appears an appealing target to be studied. In this PhD thesis, series of ATP-competitive CK1δ inhibitors have been developed to obtain promising candidates that can be used as tools in neurodegenerative diseases. Several heteroaromatic systems have been functionalized to outline and deepen a structure-activity relationship profile (SAR). Metabolism-based, new scaffold-based and molecular simplification-based strategies has been applied to gain the fixed goal.

Synthesis and characterization of benzo[*d*]thiazole derivatives: a metabolism-based strategy

Riluzole (**34**), an approved drug for ALS, is characterized by an intricated and unclear mechanism of action. It has proved to reduce the excitotoxic effects of glutamate in brain mitigating the disease's progression. The research group in which I conducted the PhD and the collaborators of Padua, have *in silico* postulated and experimentally demonstrated an activity of this candidate on CK1δ with an IC$_{50}$ of 16.1 μM. Riluzole (**34**) underwent a strong hepatic and extrahepatic metabolism; one of the main metabolites produced is the hydroxylamine that is subjected to quick glucuronoconjugation. Therefore, the first purpose is represented by the achievement of this metabolite to establish an additional link between CK1δ and riluzole (**34**). N-hydroxylamine metabolite (**39**) displays an IC$_{50}$ in the high micromolar range of 35.1 μM that agrees with the reported one for riluzole. This represents an important achievement since provides the validation of the hypothesis for which the CK1δ-mediated action can be one of the mechanisms of action explicated by riluzole. Moreover, a series of functionalized derivatives has been developed to modify phase II metabolism of the approved candidate. Several types of alkyl and arylalkyl chains have been introduced and most of the synthesized compounds have proved to be inactive with the exception of pentyl derivative that has registered an activity of 4.40 μM (**73**). In addition, another starting point is represented by the hydrazine derivative (**42**) that, according to the computational studies, seems to conserve the capability of binding the target. Surprisingly, it has revealed an IC$_{50}$ of 3.64 μM denoting a marked improvement of the activity. To outline the structure-activity relationship profile of this series, the hydrazine moiety has been functionalized with linear and branched chains as well as aryl and arylalkyl groups. All the developed compounds have proved to be active excepting ethylhexyl derivative and, in particular, isopentyl and benzyl candidates have proved to be the best of the series achieving IC$_{50}$s of 0.92 (**98**) and 1.62 (**99**), respectively. Final derivatives have been characterized from biochemical and biological point of view. The BBB-permeability using BBB-PAMPA (Parallel Artificial Membrane Permeability Assay) has been predicted and all the synthesized compounds have proved to be permeable. Moreover, the ATP-competitive behavior as well as the stability effect of the binding towards the target with TSA (Thermal Shift Assay) have been carried out for the best compound of the series. To explore a preliminary selectivity profile of candidates, the screening on GSK3β, another kinase involved in neurodegeneration has been performed for riluzole, its hydroxylamine metabolite and the two best derivatives; N-hydroxylamine metabolite has reported an IC$_{50}$ of 23.1 μM, in the same range for the registered one for CK1δ. Finally, *in vitro* assays on neuroblastoma cell lines (SH-SY5Y) has been performed; preliminary

Abstract

MTT (3-(4,5-dimethylthiazol-2-yl)-2,5-diphenyltetrazolium bromide) test to establish if derivatives are toxic has highlighted a strong toxicity for N-hydroxylamine metabolite (**39**). Neuroprotection assays, conducted for compounds that have displayed to be harmless for cells, have been denoted an important effect of riluzole but non-positive contributions for best derivatives of the series. Thus, a preliminary Western Blot analysis has been carried out for riluzole but the drug has not determined a decrease in the phosphorylation of TDP-43. In conclusion, preliminary results have been achieved by assaying riluzole in *Drosophila* models overexpressing TDP-43: an improvement in the lifespan of flies has been observed. Nevertheless, further results are required to validate all the collected data.

Riluzole (**34**) IC$_{50}$ = 16.1 μM

39, IC$_{50}$ = 35.1 μM

42, IC$_{50}$ = 3.64 μM

73, IC$_{50}$ = 4.40 μM

99, IC$_{50}$ = 1.62 μM

98, IC$_{50}$ = 0.92 μM

Development of tri- and tetra-substituted pyrazines: new scaffold-based strategy

A routinely screening of in-house molecules designed for a completely different purpose has highlighted the activity on CK1δ in the high micromolar range of three tetra-substituted 2-amino pyrazines bearing 2-fluoro-6-methylpyridine at the 6-position and 4-fluorophenyl ring at the 5-location. The three compounds differ for the alkyl chain introduced at the 3-position of the scaffold. Starting from these compounds, several moieties have been inserted in 3 of the 4 positions of the nucleus trying different combinations in order to enhance the activity towards CK1δ. Some synthetic precursors of 3-alkyl derivatives have been assayed on the target revealing the crucial substitution at the 5-location to obtain activity. This SAR hypothesis has been confirmed by developing 3-amino derivatives functionalized with a 4-fluorophenyl at the 6-location: without moieties at the 5-position, these compounds have reported no activity towards CK1δ. The situation changes introducing 4-fluorophenyl moiety at the 5-position while inserting an ester at the 3-position: ethyl ester derivative showed an IC$_{50}$ of 12.3 μM (**125**). Interestingly, the exploration of the position 5 of the ring has led to promising results: introducing a double fluorophenyl ring at -5 and -6 location, an IC$_{50}$ of 1.86 μM (**137**) has been achieved and the activity improves when 4-fluorophenyl moiety has been substituted with pyridine achieving an IC$_{50}$ of 69.0 nM (**138**), the best compound of the series. Then, functionalizing bis fluorophenyl derivative with amino groups at the 3-position such as piperazine, the activity of 0.86 μM (**136**) has been reached. Changing nature of substituent, inserting a butyl chain at the 3-location, the activity improves (**120**, IC$_{50}$ = 0.20 μM). Given the promising results of the series, biochemical and biological investigations have been conducted. Firstly, the

Abstract

BBB-permeabilities have been evaluated: 3-piperazine derivative as well as the most potent compound of the series have displayed borderline values while the double fluorophenyl candidate has shown a CNS+ feature according to the performed BBB-PAMPA. The ATP-competitive behavior as well as the capability to stabilize the target have been evaluated for the most potent candidate. Moreover, the most promising derivatives have been screened on GSK3β: it is interesting to explore the selectivity of this new scaffold-based series towards other kinases. The derivatives have proved to be inactive on GSK3β. Most potent compounds of the series have been assayed on neuroblastoma cell lines: they have proved to be harmless for cells in MTT assay at the concentrations of 5 and 10 μM; in neuroprotection assay, in particular, the most active derivative has shown a neuroprotective effect at the concentration of 1 μM. The Western Blot preliminary experiment has been conducted to observe a decrease in TDP-43 phosphorylation; in this case two contradictory results have been obtained suggesting that further investigations are required to confirm the results.
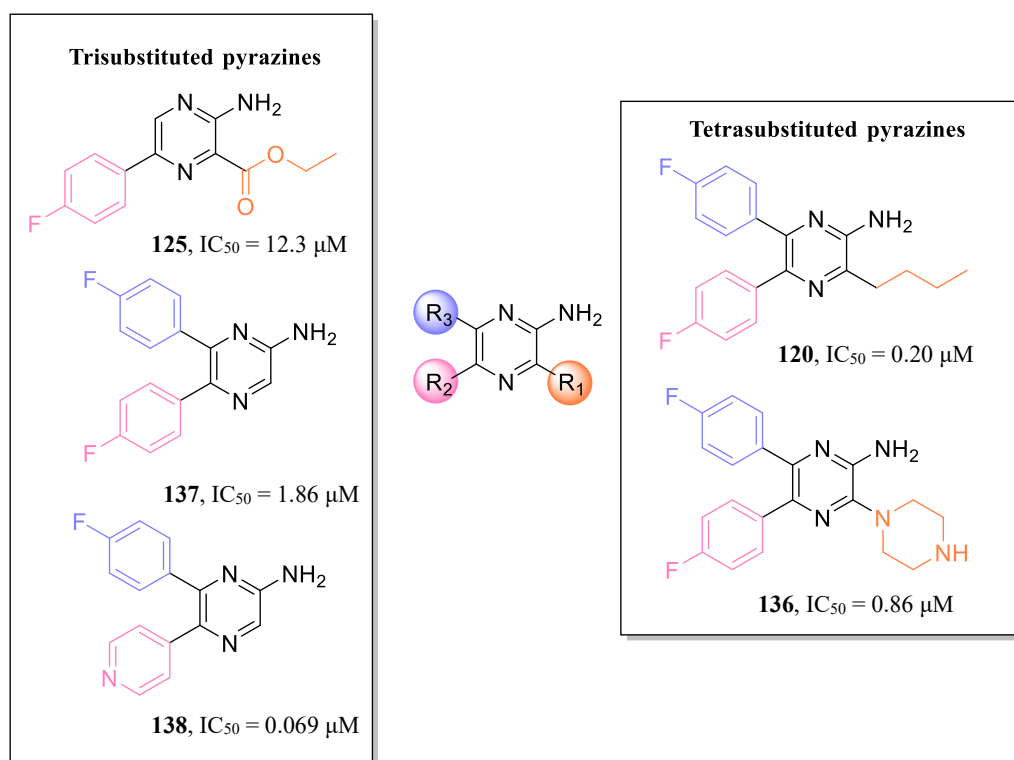
1,3,5-Triazines as CK1δ inhibitors: a simplification strategy

The bicyclic derivative 5-(7-amino-5-(benzylamino)-[1,2,4]triazolo[1,5-*a*][1,3,5]triazin-2-yl)benzen-1,3-diol (**35**) that has reported an IC$_{50}$ of 0.18 μM on CK1δ. Moreover, it has proved to be not cytotoxic against peripheral blood lymphocytes as well as neuroblastoma cells. The synthetic strategy to obtain [1,2,4]triazolo[1,5-*a*]triazine (TT) derivatives involves eight steps and, in particular, the intramolecular cyclization leads to low yields. In order to simplify the synthetic approach, a molecular simplification has been applied functionalizing the 1,3,5-triazine nucleus opening the possibility to develop a quick and deep SAR profile. Several substituents have been considered: amino moieties have been inserted at 6-position of the scaffold maintaining poly methoxy and hydroxyphenyl groups as R$_2$ linked by a linker of different size and nature including hydrazide, alkyl chain, amino moiety as well as ureido group. A few compounds of the series have proved to be active in the high micromolar range, the best one displayed an IC$_{50}$ of 19.6 μM (**174**). Its activity suggests that it behaves more as fragment than full inhibitor; therefore, a molecular hybrid has been developed by fusing N-benzyl-4,6-dichloro-1,3,5-triazin-2-amine and 4-fluoro-1*H*-indazol-3-amine, heteroaromatic molecule discovered in a Fragment-Based Drug Discovery work published by the research group that reported an activity of 24.9 μM. The molecular hybrid has determined an improvement in the IC$_{50}$

Abstract

(**142**, 3.86 μM) confirming this strategy as challenging. This molecule has been confirmed as an ATP-competitive CK1δ inhibitor. Moreover, the screening on GSK3β, that allows to obtain some information about the activity towards another kinase involved in neurodegeneration, has led to an inactive derivative. Nevertheless, despite the promising CNS-predicted permeability of the candidate, the *in vitro* investigation on neuroblastoma cell lines has highlighted a strong toxicity of the derivative in MTT assay. Thus, applying this strategy the optimization of the compound by functionalizing the indazole fragment can be available to might allow the development of a new series of inhibitors.

35, IC$_{50}$ = 0.18 μM   **174**, IC$_{50}$ = 19.6 μM
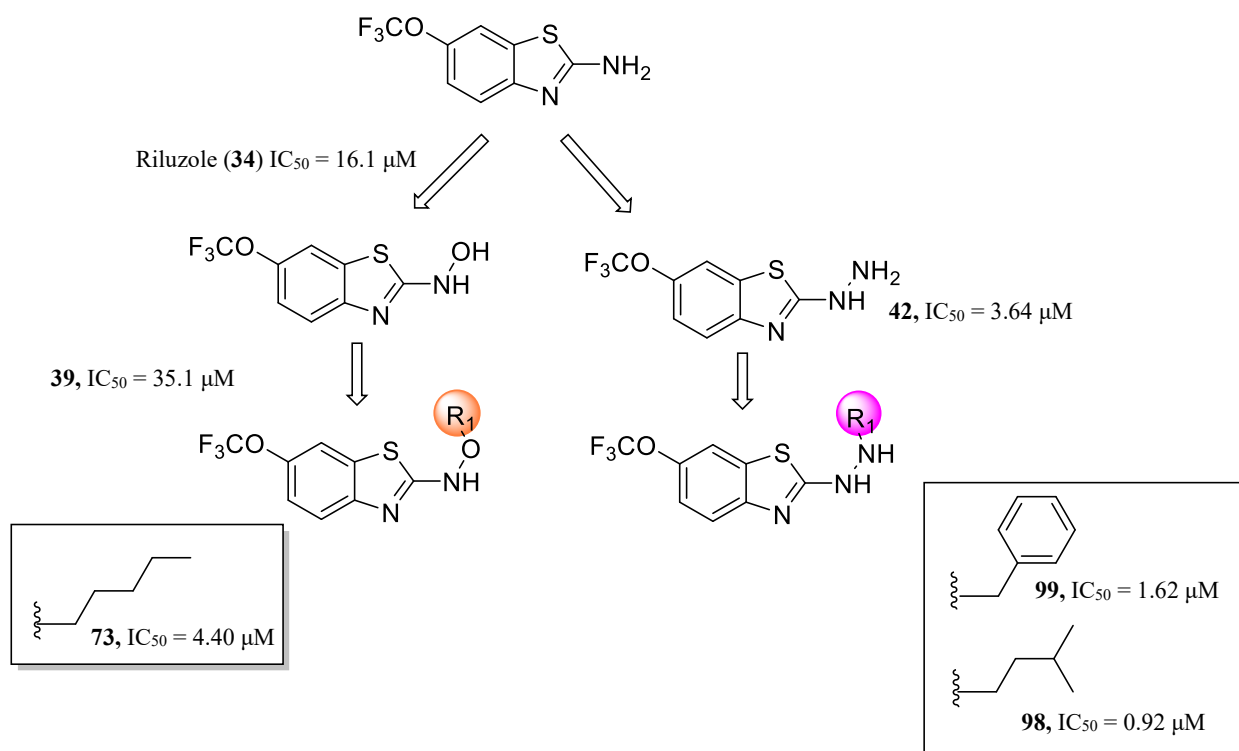
142, IC$_{50}$ = 3.86 μM
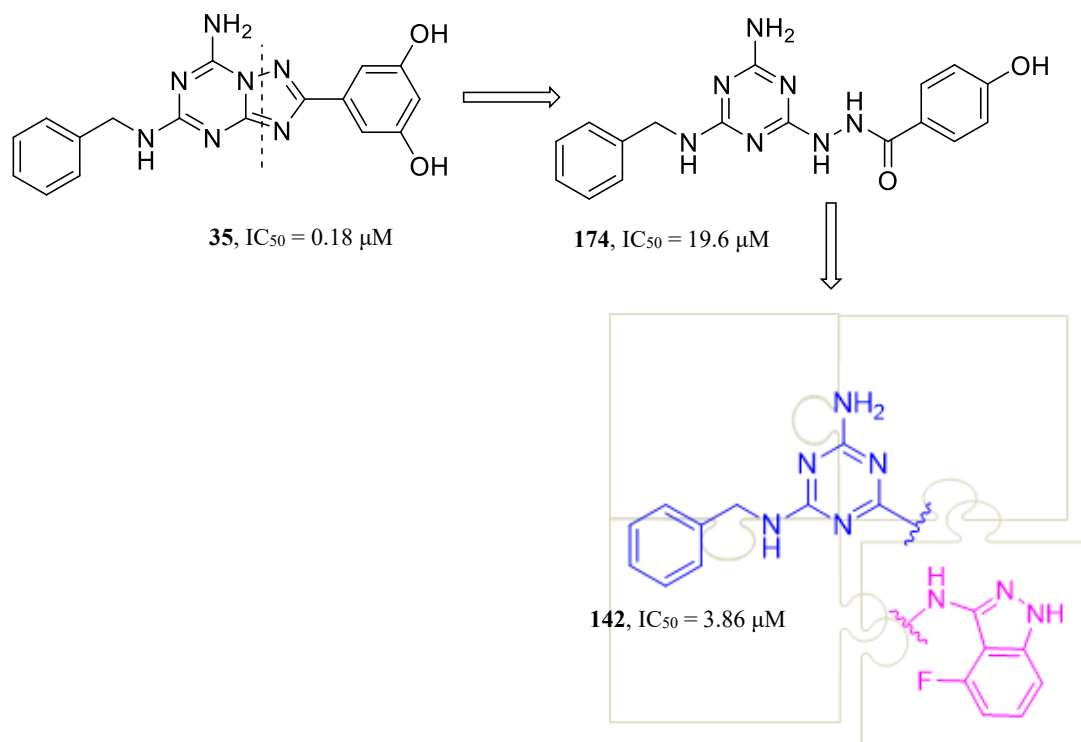
Riassunto

Le protein kinasi sono un'importante famiglia di 518 enzimi che catalizzano la fosforilazione di substrati che contengono residui di serina, treonina o tirosina. Uno dei membri di questa superfamiglia è la Casein Kinase 1, un insieme di enzimi composto da sei isoforme: l'isoforma δ (CK1δ), in particolare, è la proteina su cui si focalizza questa tesi. Questo bersaglio è coinvolto in diversi processi fisiologici che modulano diversi percorsi di segnalazione e le deregolazioni possono portare allo sviluppo di condizioni patologiche tra cui cancro, disturbi del ritmo circadiano e malattie neurodegenerative. I risultati di CK1δ sono impliciti nell'Alzheimer, nel morbo di Parkinson (AD; PD) e nella sclerosi laterale amiotrofica (SLA), che sono tutti caratterizzati da iperfosforilazione delle proteine e accumulo di aggregati che contribuiscono a innescare processi neuroinfiammatori e neurodegenerativi. Dato il ruolo di CK1δ in questi disturbi, la chinasi appare un interessante bersaglio da studiare. In questa tesi di dottorato, sono state sviluppate serie di inibitori CK1δ ATP-competitivi per ottenere candidati promettenti che possono essere utilizzati come strumenti nelle malattie neurodegenerative. Diversi sistemi eteroaromatici sono stati funzionalizzati per delineare e approfondire un profilo di relazione struttura-attività (SAR). Per raggiungere l'obiettivo prefissato sono state applicate nuove strategie basate sul metabolismo, basate su scaffold e basate sulla semplificazione molecolare.

Sintesi e caratterizzazione di derivati benzo[*d*]thiazolici: una strategia "*metabolism-based*"

Il riluzolo (**34**), un farmaco approvato per la SLA, è caratterizzato da un meccanismo d'azione intricato e poco chiaro. Ha dimostrato di ridurre gli effetti citotossici del glutammato nel cervello mitigando la progressione della malattia. Il gruppo di ricerca in cui ho condotto il dottorato e i collaboratori di Padova, hanno postulato *in silico* e dimostrato sperimentalmente un'attività di questo candidato su CK1δ con una IC_{50} di 16.1 μM. Il riluzolo (**34**) ha subito un forte metabolismo epatico ed extraepatico; uno dei principali metaboliti prodotti è l'idrossilammina che viene sottoposta a rapida glucuronoconiugazione. Pertanto, il primo scopo è rappresentato dal raggiungimento di questo metabolita per stabilire un legame aggiuntivo tra CK1δ e il riluzolo (**34**). Il metabolita N-idrossilamminico (**39**) ha mostrato un IC_{50} nell'intervallo micromolare di 35.1 μM che concorda con quello riportato per il riluzolo. Questo rappresenta un risultato importante poiché fornisce la convalida dell'ipotesi per cui l'azione mediata da CK1δ può essere uno dei meccanismi di azione esplicati dal riluzolo. Inoltre, è stata sviluppata una serie di derivati funzionalizzati per modificare il metabolismo di fase II del candidato approvato. Sono stati introdotti diversi tipi di catene alchiliche e arilalchiliche e la maggior parte dei composti sintetizzati si è rivelata inattiva ad eccezione del derivato pentilico che ha registrato un'attività di 4.40 μM (**73**). Inoltre, un altro punto di partenza è rappresentato dal derivato dell'idrazina (**42**) che, secondo gli studi computazionali, sembra conservare la capacità di legare il bersaglio. Sorprendentemente, ha rivelato un IC_{50} di 3.64 μM che denota un netto miglioramento dell'attività. Per delineare il profilo della relazione struttura-attività di questa serie, la porzione di idrazina è stata funzionalizzata con catene lineari e ramificate, nonché gruppi arilici e arilalchilici. Tutti i composti sviluppati si sono dimostrati attivi ad eccezione del derivato etilesile e, in particolare, i candidati isopentilici e benzilici si sono dimostrati i migliori della serie raggiungendo rispettivamente IC_{50} di 0.92 (**98**) e 1.62 (**99**). I derivati finali sono stati caratterizzati dal punto di vista biochimico e biologico. La permeabilità attraverso la BBB utilizzando il test BBB-PAMPA (Parallel Artificial Membrane Permeability Assay) è stata predetta e tutti i composti sintetizzati si sono dimostrati permeabili. Inoltre, il comportamento competitivo sull'ATP e l'effetto di stabilità del legame verso il bersaglio con TSA (Thermal Shift Assay) sono stati eseguiti per il miglior composto della serie. Per esplorare un profilo preliminare di selettività dei candidati, lo screening su GSK3β, un'altra chinasi coinvolta nella neurodegenerazione, è stato eseguito per il riluzolo, il suo metabolita idrossilamminico e i due migliori derivati; Il metabolita N-idrossilamminico ha riportato un IC_{50} di 23.1 μM, nello stesso intervallo per quello registrato per CK1δ. Infine, sono stati eseguiti saggi *in vitro* su linee cellulari di neuroblastoma (SH-SY5Y); il test preliminare MTT (3-(4,5-dimetiltiazol-2-il)-2,5-difeniltetrazolio bromuro) per stabilire se i derivati sono innocui o meno, hanno evidenziato una forte tossicità per il metabolita N-idrossilamminico (**39**). I saggi di

neuroprotezione, condotti per composti che si sono dimostrati non-tossici per le cellule, hanno condotto ad un importante effetto del riluzolo ma contributi non positivi per i migliori derivati della serie. Pertanto, per il riluzolo è stata effettuata un'analisi preliminare di Western Blot ma il farmaco non ha determinato una diminuzione della fosforilazione di TDP-43. In conclusione, risultati preliminari sono stati ottenuti somministrando il riluzolo in modelli di *Drosophila* che sovraesprimono TDP-43: è stato osservato un miglioramento della durata della vita delle mosche. Tuttavia, sono necessari ulteriori risultati per convalidare tutti i dati raccolti.

Riluzole (**34**) IC_{50} = 16.1 μM

39, IC_{50} = 35.1 μM

42, IC_{50} = 3.64 μM

73, IC_{50} = 4.40 μM

99, IC_{50} = 1.62 μM

98, IC_{50} = 0.92 μM

Sviluppo di pirazine tri- e tetra-sostituite: una strategia basata sull'utilizzo di nuovi *scaffolds*

Uno *screening* di routine di molecole interne progettate per scopi completamente diversi ha evidenziato l'attività su CK1δ nell'intervallo alto micromolare per tre 2-amminopirazine tetra-sostituite recanti la 2-fluoro-6-metilpiridina in posizione 6 e il gruppo 4-fluorofenil nella posizione 5. I tre composti si differenziano per la catena alchilica introdotta in posizione 3 dello *scaffold*. Partendo da questi composti, diversi gruppi sono stati inseriti nelle posizioni 3 e 4 del nucleo provando diverse combinazioni al fine di potenziare l'attività verso CK1δ. Alcuni precursori sintetici di derivati 3-alchilici sono stati saggiati sul bersaglio rivelando cruciale la sostituzione in posizione 5 per ottenere l'attività. Questa ipotesi SAR è stata confermata sviluppando derivati 3-amminici funzionalizzati con un 4-fluorofenile in posizione 6: senza sostituenti in posizione 5, questi composti non hanno riportato alcuna attività verso CK1δ. La situazione cambia introducendo il gruppo 4-fluorofenilico in posizione 5 mentre si inserisce un estere in posizione 3: il derivato dell'estere etilico ha mostrato una'IC_{50} di 12.3 μM (**125**). È interessante notare che l'esplorazione della posizione 5 dell'anello ha portato a risultati promettenti: introducendo un doppio anello fluorofenilico in posizione -5 e -6, è stato raggiunta un'IC_{50} di 1.86 μM (**137**) e l'attività migliora quando la frazione 4-fluorofenilica è stato sostituita da una piridina raggiungendo un'IC_{50} di 69.0 nM (**138**), il miglior composto della serie. Quindi, funzionalizzando il bis-fluorofenil derivato con gruppi amminici in posizione 3 come la piperazina, si è raggiunta l'attività di 0.86 μM (**136**). Cambiando la natura del sostituente, inserendo una catena butilica in posizione 3, l'attività migliora (**120,** IC_{50} = 0.20 μM). Dati i risultati promettenti della serie, sono state condotte indagini biochimiche e biologiche. In primo luogo, sono state valutate le permeabilità attraverso la BBB: il derivato 3-piperazinico

così come il composto più potente della serie hanno mostrato valori *borderline* mentre il candidato con un doppio fluorofenile ha mostrato una caratteristica CNS+ secondo il BBB-PAMPA eseguito. Il comportamento ATP-competitivo e la capacità di stabilizzare il bersaglio sono stati valutati per il candidato più potente. Inoltre, i derivati più promettenti sono stati saggiati su GSK3β: è interessante esplorare la selettività di questa nuova serie verso altre chinasi. I derivati si sono dimostrati inattivi su GSK3β. I composti più potenti della serie sono stati testati su linee cellulari di neuroblastoma: si sono dimostrati innocui per le cellule nel test MTT alle concentrazioni di 5 e 10 μM; nel saggio di neuroprotezione, in particolare, il derivato più attivo ha mostrato un effetto neuroprotettivo alla concentrazione di 1 μM. L'esperimento preliminare Western Blot è stato condotto per osservare una diminuzione della fosforilazione di TDP-43; in questo caso sono stati ottenuti due risultati contraddittori che suggeriscono la necessità di ulteriori indagini per confermare i risultati.
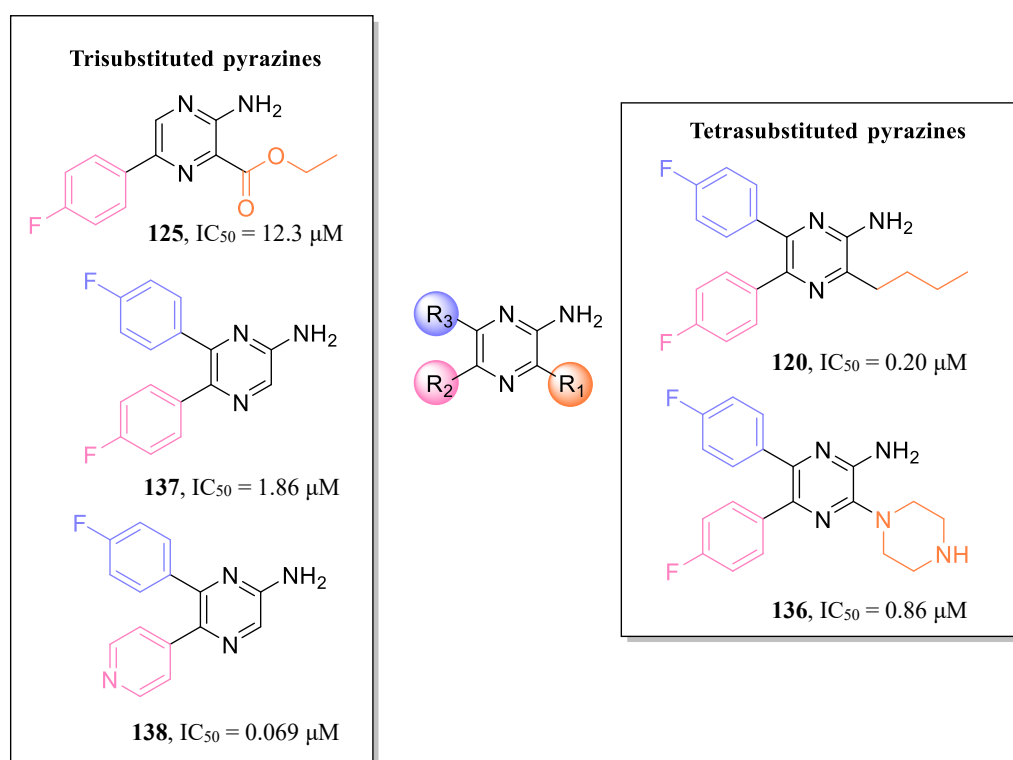
1,3,5-Triazines come inibitori di CK1δ: una strategia di semplificazione

Il derivato biciclico 5-(7-ammino-5-(benzilammino)-[1,2,4]triazolo[1,5-a][1,3,5]triazin-2-il)benzen-1,3- diolo (**35**) ha riportato un'IC$_{50}$ di 0.18 μM su CK1δ. Inoltre, si è dimostrato non citotossico nei confronti di linfociti e delle cellule di neuroblastoma. La strategia sintetica per ottenere derivati [1,2,4]triazolo[1,5-a]triazinici (TT) prevede otto passaggi e, in particolare, la ciclizzazione intramolecolare porta a basse rese. Per semplificare l'approccio sintetico, è stata applicata una semplificazione molecolare funzionalizzando il nucleo 1,3,5-triazinico aprendo la possibilità di sviluppare un profilo SAR rapido e approfondito. Sono stati considerati diversi sostituenti: gruppi amminici sono state inserite in posizione 6 dello *scaffold* mantenendo i gruppi polimetossi e idrossifenilici come R$_2$ collegati da un *linker* di diversa dimensione e natura tra cui un'idrazide, una catena alchilica, un gruppo amminico o ureidico. Alcuni composti della serie si sono dimostrati attivi nell'alto *range* micromolare, il migliore ha mostrato un'IC$_{50}$ di 19.6 μM (**174**). La sua attività suggerisce che si comporti più come frammento che come inibitore completo; pertanto, un ibrido molecolare è stato sviluppato fondendo l'N-benzil-4,6-dicloro-1,3,5-triazin-2-ammina e la 4-fluoro-1H-indazol-3-ammina, molecola eteroaromatica scoperta in un lavoro di *fragment-based* pubblicato dal gruppo di ricerca che ha riportato un'attività di 24.9 μM. L'ibrido molecolare ha determinato un miglioramento dell'IC$_{50}$ (**142**, 3.86 μM) confermando questa strategia come vincente. Questa molecola è stata confermata come un inibitore di CK1δ

Riassunto

ATP-competitivo. Inoltre, lo screening su GSK3β, che permette di ottenere alcune informazioni sull'attività nei confronti di un'altra chinasi coinvolta nella neurodegenerazione, ha portato ad un derivato inattivo su questo *target*. Tuttavia, nonostante la promettente permeabilità del candidato, l'indagine *in vitro* su linee cellulari di neuroblastoma ha evidenziato una forte tossicità del derivato nel saggio dell'MTT. Pertanto, applicando questa strategia, l'ottimizzazione del composto mediante la funzionalizzazione del frammento indazolico può essere condotta per consentire lo sviluppo di una nuova serie di inibitori.
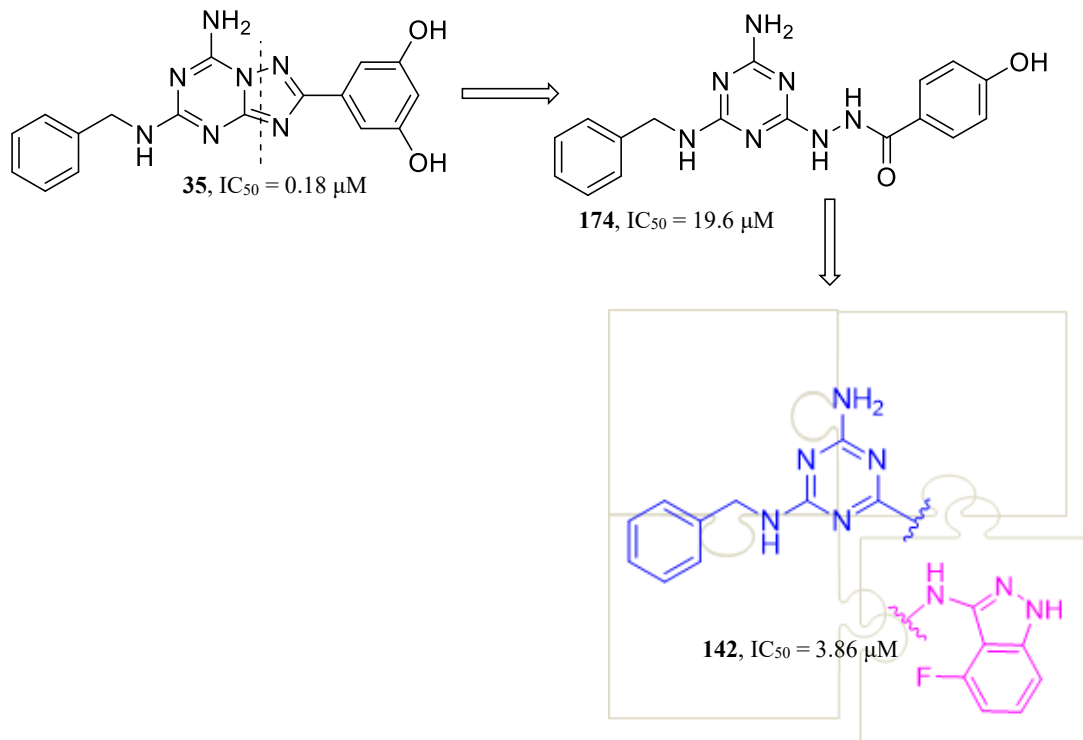
Table of contents

Table of contents

List of abbreviations

AD	Alzheimer's Disease
ADP	Adenosine Diphosphate
AGC	Cyclin nucleotide regulated protein kinases
ALK-5	Activin Receptor-like Kinase 5
ALS	Amyotrophic Lateral Sclerosis
APC	Adenomatous Polyposis
aPKs	Atypical Protein Kinases
APP	Amyloid Precursor Protein
ATP	Adenosine Triphosphate
Aβ	Amyloid β
BBB	Blood Brain Barrier
CAMK	Ca^{++} Modulated Kinases
CDK5	Cyclin Dependent Kinase 5
CHBP2B	Charged Multivesicular Body Protein 2B
CK1	Casein Kinase 1
CK1BP	Casein Kinase 1 Binding Protein
CKBD	Casein Kinase Binding Domain
CLL	Chronic Lymphocytic Leukemia
CMGC	(CDKs, Cyclin Dependent Kinases, GSK3, Glycogen Synthase Kinase 3, MAPKs, Mitogen Active Protein Kinases, CDK, Cyclin Dependent Kinase)
CRY	Cryptocrome
D3Rs	Dopamine Receptors 3
DA	Dopamine
DAAM1	Dishvelled Associated Activator of Morphogenesis
DCM	Dichloromethane
DDX3	RNA helicase
Dhh	Desert Hedgehog
DMAP	4-Dimethylaminopyridine
DMEN	Dulbecco's Modified Eagle Medium
DMF	N,N-Dimethylformamide
DMSO	Dimethylsulfoxide
DNA	Deoxyribonucleic Acid
DVL	Dishvelled
EGFR	Epidermal Growth Factor Receptor
ePKs	Eukaryotic Protein Kinases
ERK	Extracellular Regulated Kinases
EVs	Extracellular Vesicles
FBBD	Fragment- Based Drug Discovery
FBS	Fetal Bovine Serum
FTDL	Frontotemporal Lobar Degeneration
Fzt	Frizzled
GAK	Cyclin G-Associated Kinase
GAPDH	Glyceraldehyde 3-Phosphate Dehydrogenase
GPCR	G-Protein Coupled Receptor
GRCs	G-Protein Coupled Receptor Kinases
GSK3	Glycogen Synthase Kinase 3
GTP	Guanosine Triphosphate
HIF-1α	Hypoxia-Inducible Factor α
Ihh	Indian Hedgehog
JNK	c-Jun N-terminal Kinase

LATS	Large Tumor Suppressor
LBs	Lewy's Bodies
LipE	Lipophilicity Efficiency
LLRK	Leucine-Rich Repeat
LRP	Lipoprotein Receptor-Regulated
MDM2	Murine Double Minute Clone-2
MEK5	Mitogen Activated Protein Kinase 5
MRI	Magnetic Resonance Imagining
MST	Mammalian STE20-like Protein Kinase
mTORs	Mammalian Target of Rapamycin Kinases
MTT	3-[4,5- Dimethylthiazol-2-yl]-2,5-Diphenyltetrazolium Bromide
NBS	N-Bromosuccinimide
NFAT	Nuclear Factor of Activated T-cells
NFTs	Neurofibrillary Tangles
NLS	Nuclear Localization Signal
NMP	N-methyl pyrrolidone
NMR	Nuclear magnetic Resonance
NOESY	Nuclear Over-Hauser Effect Spectroscopy
P53	Tumor Suppressor Protein 53
PAMPA	Parallel Artificial Membrane Permeability Assay
PBL	Peripheral Blood Lymphocytes
PD	Parkinson's Disease
PEG	Polyethylene Glycol
PER	Period Protein
PHA	Phytohematoagglutinin
PHs	Paired Helical Filaments
PINK1	PTEN-Induced Putative kinase 1
PKA	Protein Kinase A
PKB	Protein Kinase B
PKs	Protein Kinases
PLKs	Polo-like Kinases
PS	Presenilin
PTCH	Membrane Receptor Patched
PVA	Polyvinyl Alcohol
R	Repeat
r.t.	Room Temperature
Rfx	Reflux
RGC	Rceptor Guanylyl Cyclase
RNA	Ribonucleic Acid
ROCK	Rho Kinases
RRM	Recognition Motif
SALI	Structure-Activity Landscape Index
sAPPα	Soluble Amyloid Precursor Protein α
SAR	Structure-Activity Relationship
SGs	Stress Granulated
Shh	Sonic Hedgehog
SMAD	SMA/Mothers Against Decapentaplegic
SMO	Membrane Smoothened
STE	(MAPK) Mitogen Activated Protein Kinases
STK39	Serine-threonine 39
SPIONs	Superparamagnetic Iron Oxide Nanoparticles
SUFU	Suppressor of Fused
TAZ	Tafazzin Protein
TBX5	T-box Transcription Factor 5

TCF/LEF	T-cells Factor/Lymphoid Enhancer Factor
TDP-43	Trans Activation Response DNA Binding Protein 43 KDa
TEAD	TEA Domain
TGF-β	Tumor Growth Factor-β
TH	Tyrosine Hydroxylase
THF	Tetrahydrofuran
TK	Tyrosine Kinase
TKL	Tyrosine Kinase-like
TP	[1,2,4]triazolo[1,5-*c*]pyrimidine
TSA	Thermal Shift Assay
TT	[1,2,4]triazolo[1,5-*a*]triazine
TVs	Transcriptions Variants
WW45	Adaptor Protein Salvador
YAP	Yes-Associate Protein
α-CTF	αC-Terminal Fragments
α-Syn	α-Synuclein
τ	Tau protein

Abbreviations of Amino Acids

Ala	Alanine	A
Arg	Arginine	R
Asn	Asparagine	N
Asp	Aspartic acid	D
Cys	Cysteine	C
Gln	Glutamine	Q
Glu	Glutamic acid	E
Gly	Glycine	G
His	Histidine	H
Ile	Isoleucine	I
Leu	Leucine	L
Lys	Lysine	K
Met	Methionine	M
Phe	Phenylalanine	F
Pro	Proline	P
Ser	Serine	S
Thr	Threonine	T
Trp	Tryptophan	W
Tyr	Tyrosine	Y
Val	Valine	V

1. Introduction

1.1. Protein Kinases

The PhD thesis focuses on the development of ATP-competitive Casein Kinase 1 isoform δ (CK1δ) inhibitors. Kinome is partitioned in about 20 lipid kinases and 518 protein kinases. CK1δ is comprised in the superfamily of human Protein Kinases (PKs) that are encoded by 1.7% of human genes. [1] Among cluster of PKs, 478 are eukaryotic PKs (ePKs) and 40 are composed by lack sequences similarity with ePKs but have unknown activity and are called atypical protein kinases (aPK) as represented in **Fig. 1**. [1,2,3]
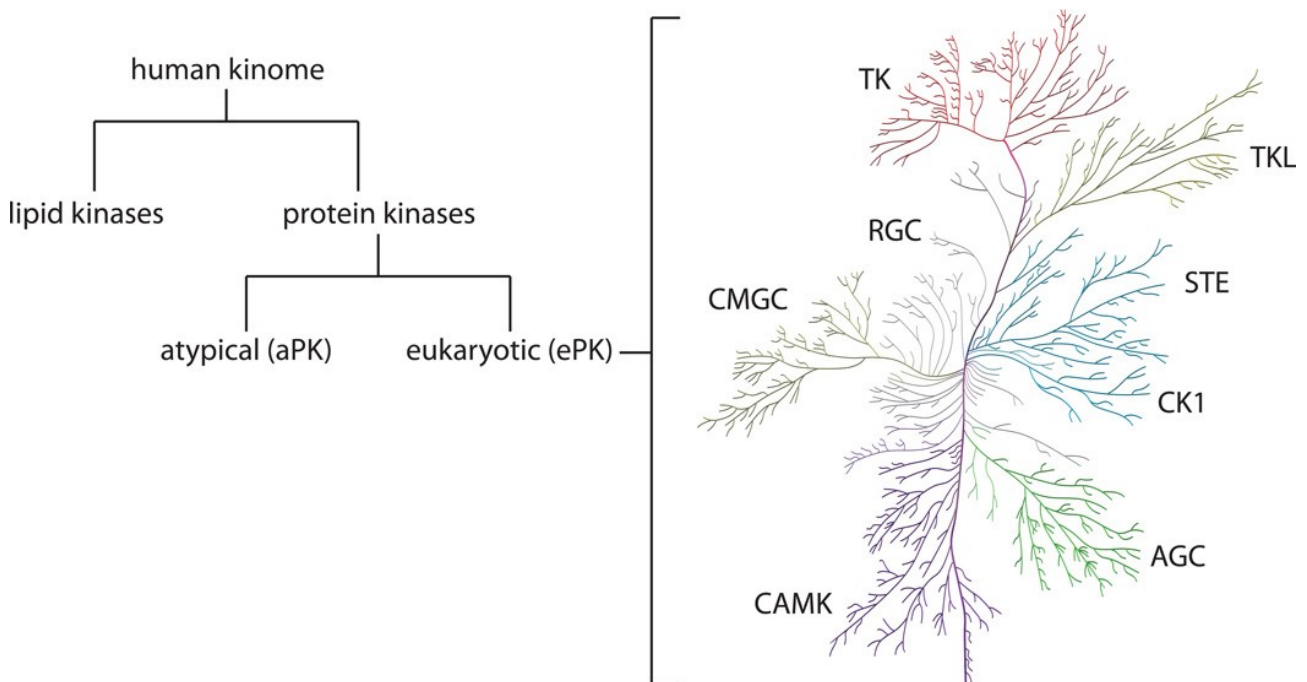
Figure 1: Human kinoma subdivision and ePK tree representation setting out kinase families that share a similarity in kinase domain. Abbreviations are given in specific chapter. [1,2]
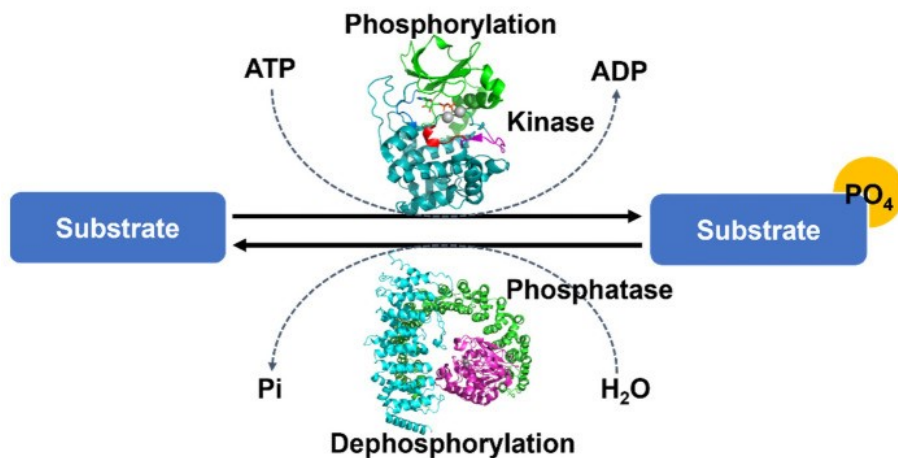
Figure 2: Schematic representation of phosphorylation. [4]

1. Introduction

Protein kinases are able to catalyze the phosphorylation of substrates containing serine, threonine or tyrosine residues (Ser/Thr/Tyr) by transferring the γ-phosphoryl moiety of adenosine triphosphate (ATP) on hydroxy group of a specific aminoacidic residue, therefore it is possible to further divide PKs in Ser/Thr kinases and Tyr kinases (**Fig. 2**). [4]

To understand the mechanism of phosphotransfer reaction several efforts have been carried out summarized in the review of Wang *et al.* [5] The mechanism of this reaction can be concerted or stepwise in the associative or dissociative kinds. The concerted one represented in **Panel A** of **Scheme 1** involves a single transition state, metaphosphate-like, in which the phosphoryl group binds in a non-covalent manner both nucleophile and leaving group. The associative stepwise mechanism consists in addition and elimination phases with the formation of penta-valent phosphorane intermediate while the dissociative one proceeds through the production of non-covalent transition adduct with either nucleophile and monomeric metaphosphate (**Scheme 1, Panel B**). The vast majority of the ATP recruited by kinase as a cofactor in the catalytic process is Mg-bound ATP: the bivalent metal, Mg^{2+} or less frequently Mn^{2+}, helps to stabilize the charge of the ADP (adenosine diphosphate) leaving group. [5]
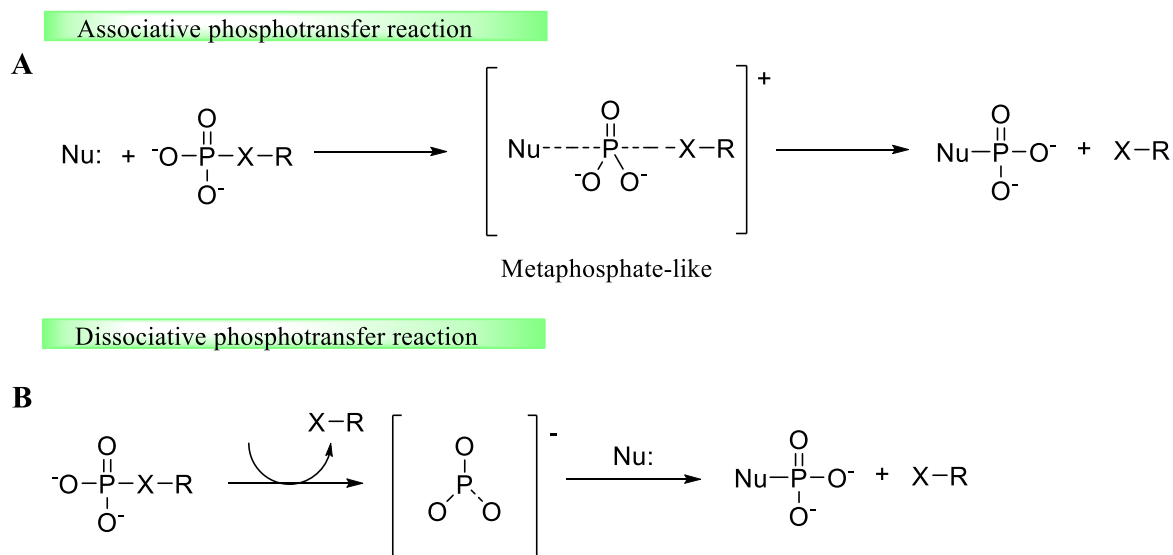
Scheme 1: Associative (Panel A) and dissociative (Panel B) phosphotransfer reactions.

The ubiquitously expression of PKs affects many physiological aspects in cells including proliferation, growth, and death. The capability of kinases to participate in several signaling pathways with complicated and tricky mechanisms in which a plenty of players are involved makes these proteins promising and challenging targets. Dysregulations can lead to the development of pathological conditions such as circadian rhythm disorders, cancer and neurodegenerative diseases. [6]

1.1.3. Architecture of Protein Kinases

PKs have the peculiarity to share common features in their architecture; the typical bilobed structure is composed by N-terminal lobe with five-stranded β-sheets and an α-helix called the C-helix and C-terminal lobe consisting in six α-helices. The two domains are connected by the hinge region that defines the ATP-binding pocket and this site appears to be conserved in kinome representing a limit in the design of selective kinase inhibitors. Thanks to the studies conducted by Hangs and Hunter in 1995 it has been possible to know lots of aminoacidic sequences in kinases, opening the possibility of elucidating key structural elements and crucial functions of these proteins. Several structural components compose the active site of kinases, and they are essential for the enzymatic activity. Among these features the activation loop, catalytic loop, P loop and

C-helix must be mentioned and described in detail in the following part with a mention for CK1δ, the protein kinase of interest (**Fig. 3**). [7,8,9]
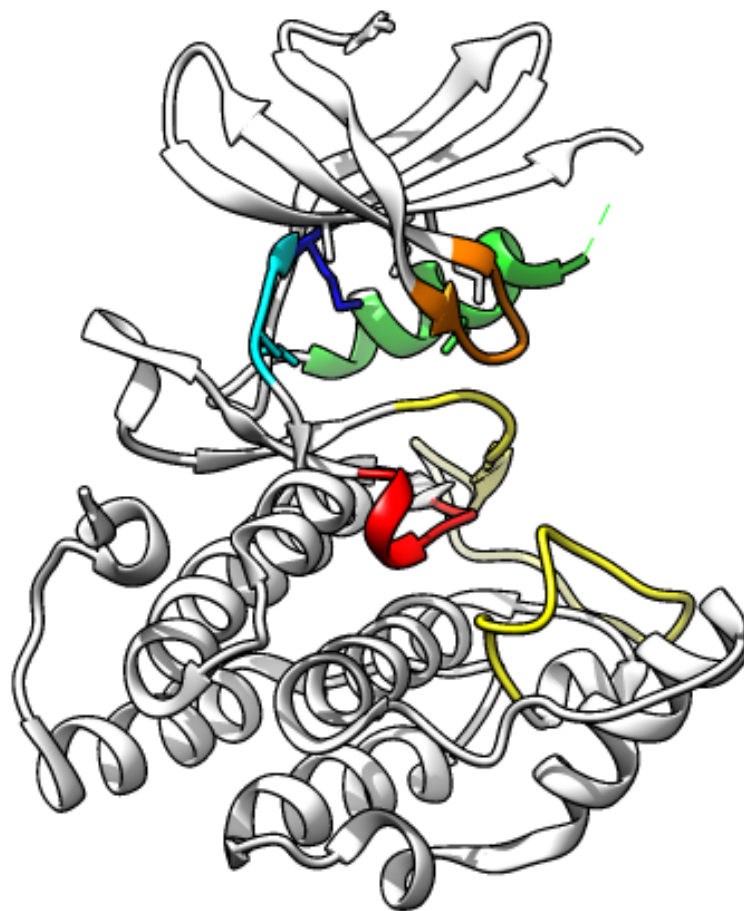
Figure 3: representation of CK1δ and structural key elements crucial for the catalytic activity of kinase: P loop (orange), activation loop (yellow), C-helix (green), catalytic loop (red) and hinge region (light blue) with the "gatekeeper" residue reported in blue. PDB code: 4HNF.

- **P loop**: the phosphate-binding loop (orange in **Fig. 3**) is a glycine-rich domain in N-terminal lobe that is conserved in kinome and defined with the motif Gly-X-Gly-X-X-Gly (Gly-Ser-Gly-Ser-Phe-Gly in CK1δ). This loop helps to stabilize the phosphates of ATP during catalysis. An amino acid of lysine of the P-loop that is located in β-sheet in N-terminal domain (Lys-38 in CK1δ) results attractive residue for the development of selective covalent inhibitors due to its catalytic activity targeted by an appropriate electrophilic portion. [10,11,12,13]
- **Activation loop**: this loop (yellow in **Fig. 3**) is composed by 20 to 30 aminoacidic residues starting from DFG motif (Asp-Phe-Gly), which is highly conserved, extending to the APE cluster (Ala-Pro-Glu) in the C-terminal lobe shaping a cleft for the location of substrate. The Asp residue of DFG in the active conformation of the enzyme ("*in*") is oriented on the side of ATP-binding pocket and it is able to coordinate the magnesium ion allowing its interaction with oxygen of β phosphate of ATP. The activation statement of kinase can switch to the "*out*" conformation: the activation loop collapses into the hinge region by blocking the catalytic activity of the enzyme preventing the binding with substrate. In addition, in this scenario Asp and Phe of DFG motif switch roles and positions allowing Phe to

occupy the ATP-binding site but some evidences are also collected by Modi *et al*. about intermediate situations between activation and inactivation of kinases (**Fig. 4**). [9,14,15,16]
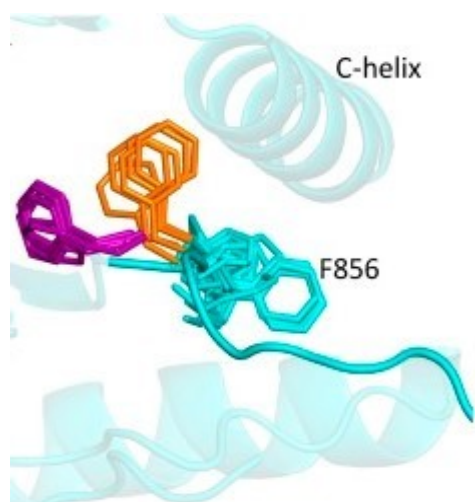
Figure 4: position of Phe chain in DFG "in" (cyan), "out" (purple) and "inter" as intermediate state (orange). The superposition of Phe sidechains is shown for tyrosine kinases EGFR family (Epidermal Growth Factor Receptors) [9]

- **C-helix**: this section (green in **Fig. 3**) is the unique α-helix in N-terminal lobe of kinase. When the enzyme assumes the active conformation, the conserved Glu-91 included in C-helix is able to establish a salt bridge with a Lys-72 in β3-strand of P-loop and this interaction appears conserved in ePK family. [2,8]

- **Catalytic loop**: (red in **Fig. 3**) in the C-terminal lobe is localized the catalytic loop of kinase characterized by the HRD motif (His-Arg-Asp) in which the residue of aspartate plays an important role in the reaction between the enzyme and the substrate: during the transfer of γ-phosphate group, Asp deprotonates the hydroxy moiety of substrate allowing its nucleophilic attack towards ATP. In CK1δ the catalytic loop comprises residues 126-133 with the corresponding *consensus* sequence DVKPDN (Asp-Val-Lys-Pro-Asp-Asn) crucial for the ATP binding. [2,11]

- **Hinge region**: (light blue in **Fig. 3**) is the connection between the two lobes of the kinase and it defines the ATP-binding pocket. In CK1δ it is represented by the sequence M-E-L-L-G (Met82-Glu83-Leu84-Leu85-Gly86). This is a key element in the architecture of the enzyme because lends itself to the housing of ATP-competitive inhibitors. **Figure 5** represents the catalytic pocket for the accommodation of ATP. Met82, called "*gatekeeper*", is a particular residue represented in blue in **Fig. 3** which is a key amino acid for the accessibility at the level of catalytic motif of enzyme. Mutations of gatekeeper residue can influence the affinity and selectivity of small molecule inhibitors and also drug resistance.. [8,11,17,18]

Figure 5: representation of CK1δ with its surface: the cycle highlights the ATP-binding pocket of the kinase. PDB code: 4HGT, CK1δ co-crystallized with ADP.

1.2. Casein Kinase 1 isoform δ (CK1δ)

Protein casein kinase 1 (CK1) gets its name from the capability to phosphorylate *in vitro* casein (milk protein). This enzyme comprises seven isoforms: α, β, γ1, γ2, γ3, δ, ε and their transcription variants (TVs). All the isoforms are expressed in humans except for the β one. They share a high homology of kinase domains (51-98% of conserved residues) schematically represented in **Fig. 6,** while C-terminal domain results in different lengths. The highest similarity has been reported between isoforms δ and ε. [17,19]

Figure 6: schematic alignment of CK1 isoforms (32-52.2 kDa). The light green zone represents the conserved kinase domain while N- and C-termini portions (dark green) differ. [17]

The seven isoforms of CK1δ are ubiquitously expressed even if it is known that α, δ and ε are located in cytoplasm and nucleus while the isoform γ appears to be the bound-membrane component of CK1 family. [20]

The discussion will be focused on the isoform δ whose gene encoding it, CSNK1D, was firstly isolated by Graves *et al.* in 1993 and it consists in a sequence of 1284 nucleotides. Several variants of CK1δ are described in different organisms and three TVs in humans. As shown in **Table 1**, sequences of human TVs appear conserved until residue 399. [7,11]

1. Introduction

Table 1: Partial alignment of sequences of TV1-3 of CK1δ. Residues conserved (372-399) are highlighted in yellow. Adapted by ref. 11.

HomoSapiens_TV1 (1-415)	RLHRGAPVNISSSDLTGRQDTSRMSTSQIPGRVASSGLQSVVHR------------
HomoSapiens_TV2 (1-409)	RLHRGAPVNISSSDLTGRQDTSRMSTSQNSIPFEHHGK-----------------------
HomoSapiens_TV3 (1-427)	RLHRGAPVNISSSDLTGRQDTSRMSTSQRSRDMASLRLHAARQGTRCRPQRPRRTY-

Over the years several crystal structures of CK1δ have been reported and co-crystallized with ligands and inhibitors. The chronological list of structures on *Homo Sapiens* is reported in **Table 2**.

Table 2: crystal structures of CK1δ in chronological order: PDB code, ligands, resolution, year, and reference.

PDB code	Ligands	Resolution (Å)	Year	Reference
3UYS	SO₄	2.30	2012	[21]
4HNF	16W	2.07	2012	[21]
4HGT	15G	1.80	2012	[22]
3UZP	0CK	1.94	2012	[21]
3UYT	0CK, SO₄	2.00	2012	[21]
4TWC	37J, BOG, DMS, GOL, SO₄	1.70	2012	[23]
4KBK	1QG, SO₄	2.10	2013	[24]
4KBC	1QJ, EDO, SO₄	1.98	2013	[24]
4KBA	1QM, SO₄	1.98	2013	[24]
4KB8	1QN, 1QO, SO₄	1.95	2013	[24]
5MQV	D5Q, SO₄	2.15	2017	[25]
5OKT	9XK, ACT, GOL, SO₄	2.13	2018	[26]
6GZM	CIT, GOL, LCI	1.59	2018	[27]
6RU8	ADP, EDO, NA, SO₄	1.92	2020	[28]
6RU7	ADP, EDO, NA	2.08	2020	[28]
6RU6	ADP, EDO, NA, SO₄	2.05	2020	[28]
7P7F	ADN, AMP, EDO, SO₄	1.96	2022	[29]
7P7G	AMP, CIT, EDO	1.70	2022	[29]
7P7H	AMP	2.40	2022	[29]
6RCG	EDO, KOE	1.40	To be published	
6RGH	EDO, KOE, NA, SO₄	1.45	To be published	
4TN6	PFO, SO₄	2.41	To be published	

CK1 is regulated by other protein kinases: it is demonstrated that the isoform δ can be phosphorylated by *c*AMP-dependent protein kinase (PKA), CDC-like kinase 2 (CLK2), protein kinase C α (PKCα). In particular, PKA was found to phosphorylate *in vitro* and *in vivo* Ser-370 of CK1δ and the result provides a decrease in the phosphorylation of substrate. [30] Regarding the isoform α, instead, Clokie and co-workers have reported the interaction with protein 14-3-3. 14-3-3 is an important member that can regulate several physiological functions included intracellular trafficking, modulation of cell cycle and signal transduction. CK1α is phosphorylated by the just discussed protein determining the modulation of different cellular functions. [31] Interestingly, it is well known that CK1δ and ε are less active when the truncation at C-terminal domain occurs and the autophosphorylation of these kinases is an important regulation mechanism studied both *in vitro* and *in vivo*. Maintenance of dephosphorylation status was detected *in vivo*. This evidence suggests that kinases consume ATP in this cycle decreasing their activity confirming the key role of protein phosphatases in the modulation of kinases. [32] CK1 is able to intercalate in several processes and, as reported, can take action downstream of other kinases preferring pre-phosphorylated negative-charged substrates bearing the *consensus*

sequence pS/pT-X-X-S*/T* in which S*/T* represent the amino acid target of phosphorylation. Nevertheless, non-canonical motif such as S-L-S have found to be phosphorylated in well-known substrates including nuclear factor of activated T-cells (NFAT) and β-catenin whose signaling pathway is discussed in the following chapter. [32] Other phosphorylation clusters have been reported, for example sequence K/R-X-K/R-X-X-S/T suggesting that, despite the ability to phosphorylate primed substrates, CK1 family is able to phosphorylate also unprimed substrates. [33,34]

CK1δ results a promising target since it is implied in several signaling pathways including Wnt/β-catenin, Hedgehog, Hippo and p-53 pathways, thus playing an important role in the setting of physiological functions. Its deregulation can lead to the development of several diseases such as circadian rhythm disorders, cancer and neurodegenerative pathological conditions.

1.3. Cellular signaling pathways and development of cancer

Upstream of the development of a disease there is a deregulation of a biochemical pathway and to describe the significant role of Casein Kinase 1; Wnt/β-catenin, Hippo, Hedgehog and p-53 signaling pathways are discussed in following chapter to understand the implication of CK1δ in the development of several types of cancers as well as the complexity of interconnections between the various members implied in these pathways. It appears clear that inhibitors of this target can be useful as tools for the investigation of cancer conditions.

1.3.1. Wnt/β-catenin signaling pathway

Wnt name of the Wnt/β-catenin signaling pathway takes its name from the fusion of "*wingless*", gene encoding for *Drosophila* segment polarity and "*integrated*", the vertebrate homolog [35] and controls lots of biological and physiological functions and it is finely regulated. The crucial role of the perfect coordination of this pathway is reflected in several features including organogenesis, cell determinations and the modulation of primary axis formation. [36] The aberrant counterpart of this pathway could lead to the development of several pathological conditions; the first connection between the deregulation and the development of diseases was discovered in 1990s: the gene encoded for Adenomatous Polyposis Coli (APC) has been traced back to the occurrence of familial adenomatous polyposis, a type of cancer. [37,38] Mutations at the level of β-catenin gene could determine a wide range of tumors including hepatocellular carcinoma, colon cancer, melanoma and sebaceous skin cancer. [37,39,40,41,42] Wnt signaling pathway can be divided into canonical and non-canonical in relation to the β-catenin dependence. [43] In the canonical one, the presence of Wnt signal that binds the Frizzled (Fzd) receptor and Lipoprotein Receptor-Related (LRP) co-receptor determines the turning on of the pathway. [43] The signal leads to the intracellular phosphorylation of LRP6 in its PPPSPxS motif by CK1 and GSK3β, members of the Axin complex. GSK3β-mediated phosphorylation is the primary event in the pathway that primes CK1 to phosphorylate the S (serine) in the PPPSPxS motif of LRP6. [44,45] The double phosphorylation of LRP6 generates the docking site for the recruitment of the Axin complex called "disruption complex" whose members are Axin, APC, GSK3β and CK1α and the induction of Dishevelled proteins that move from the plasma membrane. [45,46] This provides the stabilization of the Axine complex and the accumulation of β-catenin that translocates at the level of nucleus binding several transcription factors including TCF/LEF (T-cells factors/lymphoid enhancer factor), TBX5 (T-box transcription factor 5) and HIF-1α (hypoxia-inducible factor-1α). [47] In the absence of Wnt signal, the β-catenin recruited by the "disruption complex" is phosphorylated in Ser-45 by CK1α and in Ser-33, Ser-37 and Thr-41 by GSK3β determining its recognition by β-Transducin Repeat Containing E3 Ubiquitin Protein Ligase catalyzing the polyubiquitylation at Ser-19. The catalysis of this reaction prompts the degradation of β-catenin by the proteasome system. [46,48,49,50] The canonical Wnt-signaling pathway discussed above in its activation and inactivation phases is represented in **Fig. 7**. Even if the isoform α plays the main role in the pathway, also the other isoforms of Casein Kinase are involved; LRP6

is phosphorylated by CK1γ with a positive regulation and CK1ε with a negative one indicating a very intricate and complicated regulation. [17,51,52] In addition, CK1δ and CK1ε can be activated by Wnt signal traducing it in the phosphorylation of Axin complex in several sites determining the disruption of the complex and, consequently, the degradation of β-catenin even if the signaling pathway is in the active mode. CK1ε also plays a role in the stabilization of β-catenin thanks to the action of DDX3 (RNA helicase) recruited during the Wnt-activation and this isoform is able to phosphorylate TCF3, a transcription factor, mediating its bound to β-catenin. [17,51,53,54]

The non-canonical Wnt-pathway is defined as β-catenin independent. Wnt signal, in this case, can bind Frizzled receptor recruiting Dishevelled. Through an inhibitory effect on DAAM1 (Dishvelled Associated Activator of Morphogenesis 1), Dvl receptor affects the GPTase Rho determining the activation of ROCK (Rho kinase) and JNK (c-Jun N-terminal kinase) leading to the rearrangement of cytoskeleton and transcriptional response. [43,55,56,57] The same response of Wnt signal just described is also given by the triggering of phospholipase C activity via Frizzled GPCR-mediated (G-protein coupled receptors-mediated); the result is provided by the release of intracellular calcium. [43,58,59,60] Finally, isoforms δ and ε are main characters in the positive regulation of non-canonical Wnt pathway phosphorylating DVL (Dishvelled) and, thus, providing the activation of Rho/JNK cascade. [17,51,53,54]
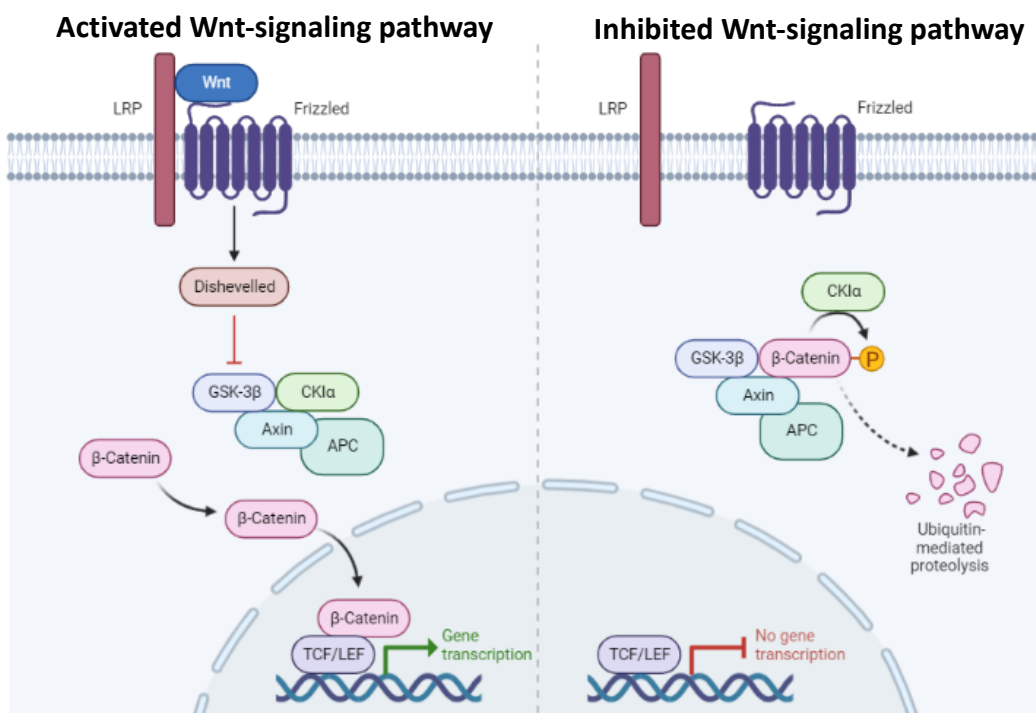
*Figure 7: representation of activated and inhibited Wnt-signaling pathway. In the presence of Wnt signal (activated pathway), the Axin complex is stabilized determining the accumulation and translocation of β-catenin at the level of nucleus switching on the gene transcription. Without Wnt signal (inhibited pathway), instead, the Axin complex leads to the ubiquitylation of β-catenin. [43] The image is created using **BioRender**.*

1.3.2. Hippo pathway

Hippo pathway is involved in several processes including the modulation of cell proliferation and apoptosis. [61] Deregulation of this finely regulated system can lead to the development of pathological conditions, included several types of cancer. The signaling pathway starts with the phosphorylation of large tumor suppressor LATS1/2 by mammalian Ste20-like kinase (MST1/2, ortholog of Drosophila Hippo) helped by adaptor protein Salvador (WW45) and MOB kinase activator 1 A/B (MOB1A/B). LATS1/2 is able to phosphorylate YAP

(Yes-associate protein) and TAZ (Tafazzin protein) and this event triggers the inhibition of YAP/TAZ leading to the failure of nuclear interaction with the targets TEAD (TEA domain) which is a transcription factor and SMAD (SMA/mothers against decapentaplegic) determining the phosphodegron-mediated degradation of YAP/TAZ. [17,62,63,64] The just described mechanism is applied when the signaling pathway is in the "on" mode; in this way the nuclear transcription of cyclin E and diap1, cell-cycle and death regulators, is locked. CK1δ and ε are found as modulators in Hippo pathway since they are able to control several steps of the pathway. LATS phosphorylates on Ser-381 TAZ protein, and this is considered as a trigger event for the CK1δ/ε-mediated phosphorylation of phosphodegron of TAZ protein providing its degradation as a result. In addition, the TAZ phosphorylation on Ser-311 caused by the isoform ε has proved to determine the same consequence: the ubiquitylation of TAZ. [17,62,65] Moreover, Xu *et al.* reported a possible connection between Hippo and Wnt pathways providing an idea of the complexity of interactions and concatenations between several members and effectors of pathways *in vivo*. MST1/2 can bind CK1ε preventing the phosphorylation of DVL and determining the block of Wnt/β-catenin pathway. [11]

1.3.3. Hedgehog pathway

The Hedgehog pathway is predominant in child organism since its role in the organogenesis, while in adults it is important in renewing of epithelia of internal organs. Deregulations associated with this pathway can lead to the development of several cancer types including basal cell carcinoma, medulloblastomas, gliomas and gastrointestinal and prostate cancer. [66,67,68,69,70] Upstream of the pathway there is the activation of PTCH (membrane receptor Patched) by three Hh ligands: Sonic Hedgehog (Shh), Indian Hedgehog (Ihh) and Desert Hedgehog (Dhh). When ligands are absent, PTCH inhibits the activity of 7-pass membrane smoothened (SMO) blocking the signal transmission at the level of nucleus via glioma-associated oncogene transmission factors GLI1, GLI2, GLI3. Consequently, PKA, GSK3β and CK1 are able to phosphorylate GLI factors making them available for the proteolytic degradation by suppressing the activity of SUFU (suppressor of fused), gene negative regulator of Hedgehog pathway. Moreover, SUFU prevents the activation of Hh genes by binding GLI in cytoplasm and nucleus. [17,71] When this cascade is in the "on" modality, instead, Hh ligands can bind PTCH leading to the release of SMO and then activation of GLI factors that translocate at the nuclear level to start the transcription as reported in **Fig. 8**. [17,71] Interestingly, a crucial role of kinases CK1δ and GSK3β have been proved by examining the phosphorylation of Ci-155 of an homolog in *Drosophila* of GLI2 and GLI3 that has resulted the trigger event for the successive degradation of transcription factors and CK1 is also involved in the positive regulation of SMO. [72,73,74,75,76]
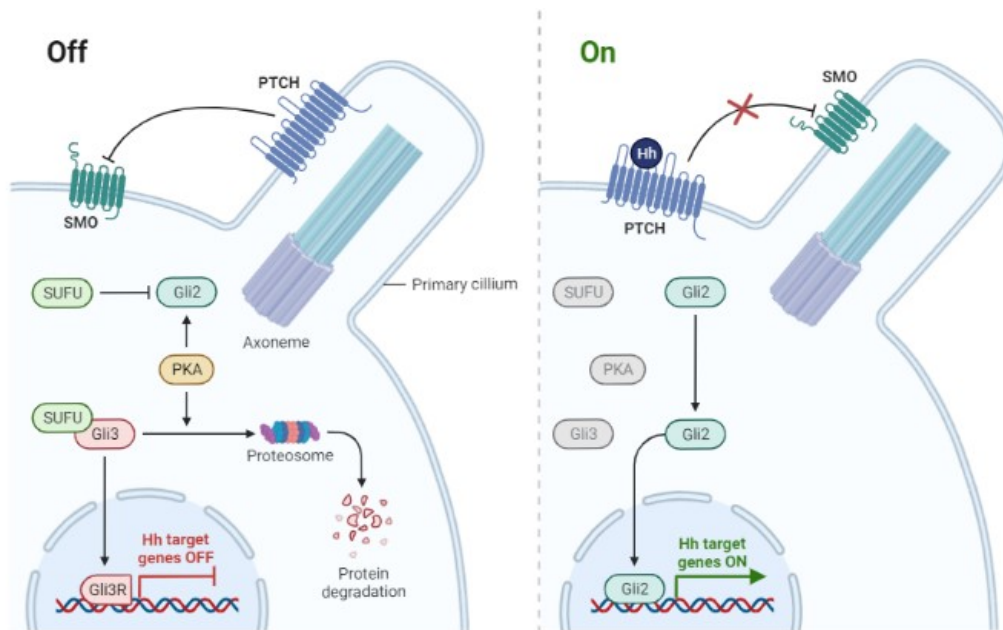
*Figure 8: Hedgehog pathway: when ligands are absent, GLI factors are degraded by proteosome ("off" mode). At the presence of ligand, GLI factors can translocate at nuclear level activating the gene transcription. [17,71] Image created using **BioRender**.*

1.3.4. The response in DNA damage

Tumor suppressor protein p53 is an important member in the regulation of tissue integrity preventing cell damages and proliferation of cells that can lead to the development of cancerogenic conditions. [77] The levels of p53 are finely regulated but, after various stimuli, the increase of activation is reported. Several functions are associated to p53, including apoptosis, autophagy and the repairment of DNA by regulating lots of transcription factors. [77] The regulation of this key effector is carried out by MDM2 (murine double minute clone 2) via negative feedback: p53 is able to activate MDM2 that establishes the ubiquitylation of p53 maintaining basal levels in a physiological condition. [78] Moreover, MDM2 acts with an anti-apoptotic role by switching E2F-1 from negative to a positive regulator of the progression of cell cycle. Subjected to a stress condition that determines a damage at the level of DNA, p53 inhibits MDM2 but the activity of this effector depends also to its phosphorylation state kinases mediated. [79] This suggests that several signaling pathways can modulate p53/MDM2 regulation. Interestingly, CK1 isoforms α, δ and ε are found to phosphorylate p53: in response to a DNA damage, CK1δ can phosphorylate p53 at the level of Thr-18 and Ser-20 determining the impairment of the interaction with MDM2 and providing the binding with p300 resulting in the final activation of p53. Nevertheless, under physiological conditions, isoforms δ and ε are able also to interact directly with MDM2 by phosphorylating several residues suggesting a crucial role of CK1 in the regulation of this signaling pathway. [79]

All the described pathways are involved in the development of several cancer diseases; thus, it appears evident the important role of Casein Kinase 1 that results a promising target for its multifaceted features.

1.4. Circadian rhythm disorders

Circadian rhythm involves all the processes included in the daily setup of cells and their functions in 24 h and deregulation of these factors can lead to the development of sleeping problems, metabolic diseases, and neurological disorders. In this scenario, the main characters are PER (PER1 and PER2), period proteins, and CRY (CRY1 and CRY2) proteins whose expression levels are finely regulated in time-dependent manner

during the day. These effectors can interact with CLOCK-BMALI-responsive circadian gene transcription regulating themselves expression at the nuclear level. CK1δ determines the inhibition of the transcription process by reducing the binding affinity of CLOCK-BMALI on DNA but it is also implied in the phosphorylation of PER and in degradation of this one together with isoform ε thanks to the "phosphoswitch" action. [11,80] The CK1-mediated phosphorylation is explicated at the level of Casein Kinase Binding Domain (CKBD) that resulted conserved in PER proteins. Between the CKBD site there are two important domains: Degron and FASP and they are crucial for the regulation of circadian rhythm functions. [80] The isoforms δ and ε can establish a balance between degradation and stabilization of PER due to the isoform preference of site: this equilibrium is called "phosphoswitch". In particular, as described in **Fig. 9**, CK1δ phosphorylates degron leading to its degradation β-TrCP mediated while the ε isoform prefers the binding with FASP stabilizing PER against the polyubiquitylation. [34]
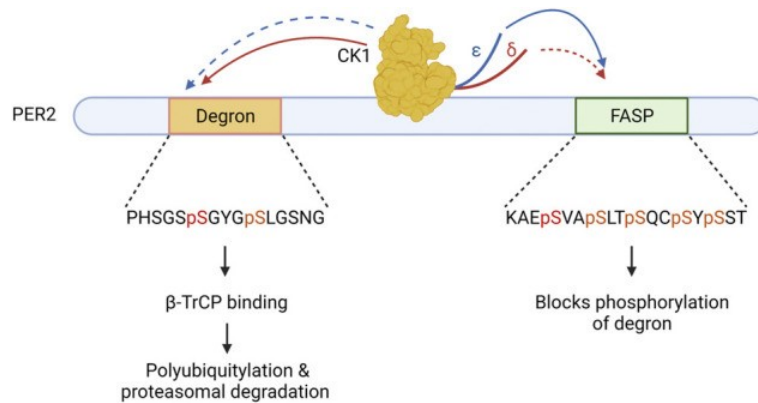
Figure 9: representation of the role of CK1δ and CK1ε in degradation and stabilization of PER protein by interacting with Degron and FASP domains, respectively. The two isoforms can balance their effects in the modulation of PER, the main character in the development of circadian rhythm disorders. [34]

1.5. Neurodegenerative diseases and the role of CK1

CK1δ is involved in neurodegenerative diseases and results an appealing target to investigate for the development of possible candidates for the treatment of these pathological conditions since the poorly commercial results in which the drugs are limited and often directed to treat only symptoms. This kinase is implicated in the pathogenesis of Alzheimer's disease (AD), Parkinson's disease (PD) as well as Amyotrophic Lateral Sclerosis (ALS).

1.5.1. Alzheimer's disease

The disease of Alzheimer is a neurodegenerative disorder characterized by the occurrence of *dementia*. The familial AD is linked by mutations at the level of the amyloid precursor or presenilin genes but also the causes-unknown sporadic AD is widely spread all over the world; it is complicated to establish the origin of this disease's type since there are lots of factors and members interconnecting each other in the development of the pathological condition. [81] AD is characterized by the occurrence of memory deficits, cognitive and language impairments and, consequently, the failure in daily activities. [82,83] Hallmarks of this disease comprise the formation at the microscopic level of senile plaques composed by the aggregation and the accumulation of Amyloid β (Aβ) peptide and neurofibrillary tangles (NFTs) that are the result of the hyperphosphorylation of Tau protein (τ) accompanied by neuronal loss and the insurgence of a neuroinflammatory process (**Fig. 10**). [81]
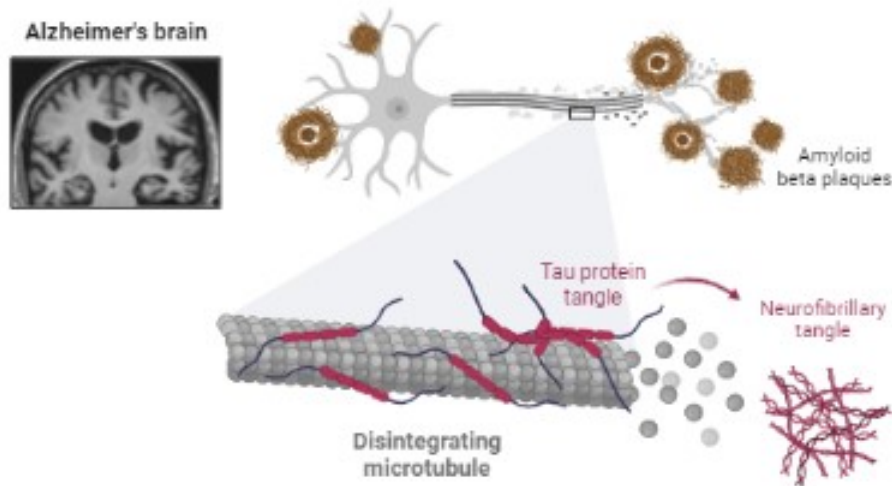
*Figure 10: hallmarks of Alzheimer's disease: accumulation of amyloid β plaques and neurofibrillary tangles (NFTs) composed by amyloid β peptide (Aβ) and disrupted τ protein, respectively. Image created using **BioRender**.*

The starting event that triggers the pathological conditions is debated: in literature an experiment conducted by Lewis *et al.* in two lines of transgenic mice expressing mutant forms of τ protein and Amyloid Precursor Protein (APP) is reported. The result highlights that both the lines have been displayed neurofibrillary tangles. [84] Nevertheless, evidences suggest that Aβ aggregation prompts the impairments linked to the development of NFTs via caspase-3 activation leading to the cleavage of τ protein, In addition, Aβ peptide is able to reduce interactions between τ and microtubules determining the loss of stabilization. [85,86,87,88] APP is a transmembrane protein (**Fig. 11, Panel a)** cleaved by α and β-secretase (BACE-1); the first enzyme triggers the non-amyloidogenic pathway and determines the obtainment of the soluble APPα (sAPPα) and α-CTF (αC-terminal fragment) while β-secretase leads to sAPPβ and β-CTF via amyloidogenic pathway (**Fig. 11**, **Panels b** and **c**). The cleavage-products α and β-CTFs are then processed by γ-secretase obtaining p3 that is rapidly degraded and Aβ peptide of different lengths (Aβ40 and Aβ42) leading to the accumulation and the formation of senile plaques. [89,90,91] All this process is accompanied by chronic neuroinflammation but the real mechanism leading to the Aβ formation is still unknown since it is demonstrated that the release of cytokines from neurons is not able to induce the Aβ production. [92,93] Thus, Li *et* coworkers in 2020 demonstrated an indirect mechanism by which astrocytes, that control neuronal functions via extracellular vesicles (EVs), induce the release of CK1 from the complex with GSK3β and APC described in a previous chapter. β-catenin is free to reach nucleus where it binds the *Hnrnpc* gene providing an increased amount of APP co-localized with BACE-1. [92] Furthermore, Flajolet *et* coworkers have conducted an *in silico* analysis to find putative CK1 phosphorylation sites in proteins connected to the AD. Interestingly, from the computational studies several CK1 *consensus* sites have been discovered in APP, BACE-1 and γ-secretase. [94] This theoretical base has been investigated assaying CK1α, CK1γ, CK1δ and CK1ε in N2A cells expressing APP and results suggest that only the isoform ε is able to increase Aβ40 and Aβ42 and, moreover, the administration of CK1ε inhibitors has proved to reduce the accumulation of Aβ peptide modulating the APP cleavage operated by γ-secretase. Unexpectedly, the isoform δ is not connected to the overproduction of Aβ peptide even if it shares a 97% of homology with the isoform ε. This evidence suggests the presence of several substrates participating in the regulation of β-amyloid cascade and several pathways implied in the development of pathology since it is demonstrated that CK1δ mRNA is strongly present in *post-mortem*. [94] Another hallmark of the AD, especially for familial one, is represented by mutations at the level of genes encoding for Presenilin (PS): PS1 and PS2. PS1 covers the role of being the catalytic subunit of γ-secretase. [95] Mutations at the level of PSEN1, gene encoding for PS1, are common in familial AD that leads to the production of Aβ40 and Aβ42. Another gene involved in the trigger of the pathology is represented by PSEN2 encoding for PS2 that is known as modulators of several signaling

pathways independent to γ-secretase. Regulating the intracellular Ca^{2+} homeostasis, it leads to a disruption in autophagy processes determining the progression of the neurodegenerative disease since the pivotal role of Ca^{2+}. [96] The role of several kinases in the phosphorylation of PS2 leading to the modulation of the caspase-activity is demonstrated but there is no evidence that supports the role of CK1 in PS-regulation. [97]
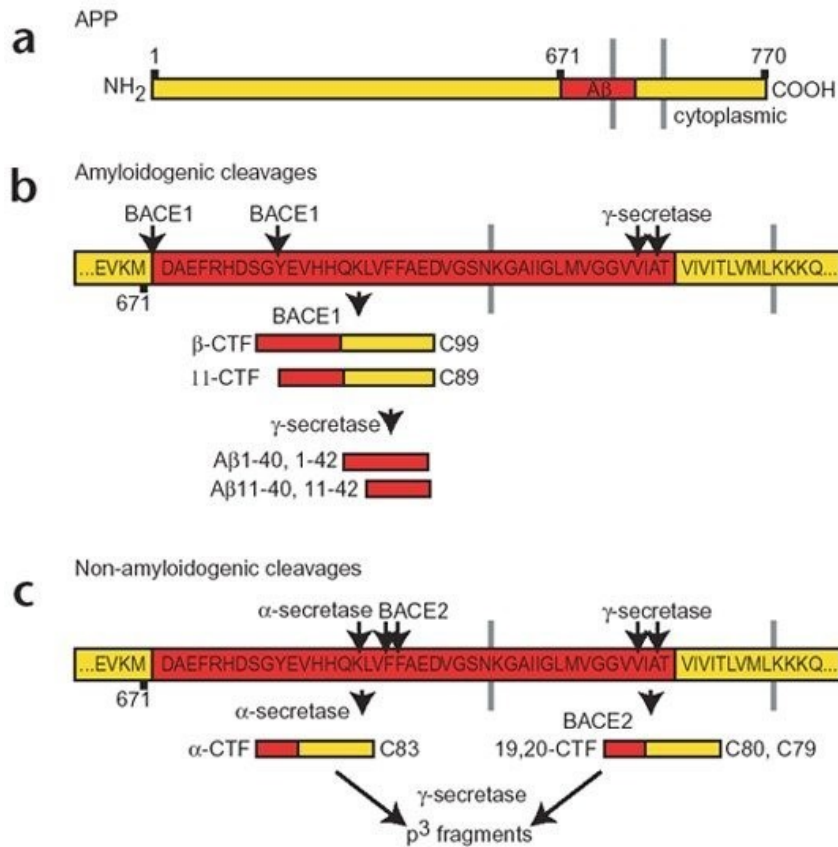
Figure 11: Panel a) representation of APP; Panel b) amyloidogenic pathway with β and γ-secretases cleavage; Panel c) non-amyloidogenic pathway. Image adapted by ref. 93.

An important feature that characterizes the AD as tauopathy is the insurgence of abnormal Tau protein (τ) that, under physiological conditions, contributes to stabilize microtubules preserving physiological cellular functions. The microtubule-associated protein is expressed at the level of neurons and axons and comprises six isoforms that differ each other by the primary structure: three or four repeats (3R, 4R), repetitive sequences of 31-32 amino acids. [98,99,100] The primary structure is composed by 441 residues and it is susceptible to posttranslational modifications including phosphorylation, O-glycosylation, methylation, deamidation, acetylation and ubiquitylation. [99] Interestingly, Tau protein is known as a flexible and disordered structure that, after the binding with microtubule, is structured in stable folds composing fibrils as displayed in **Fig. 12**. [101]
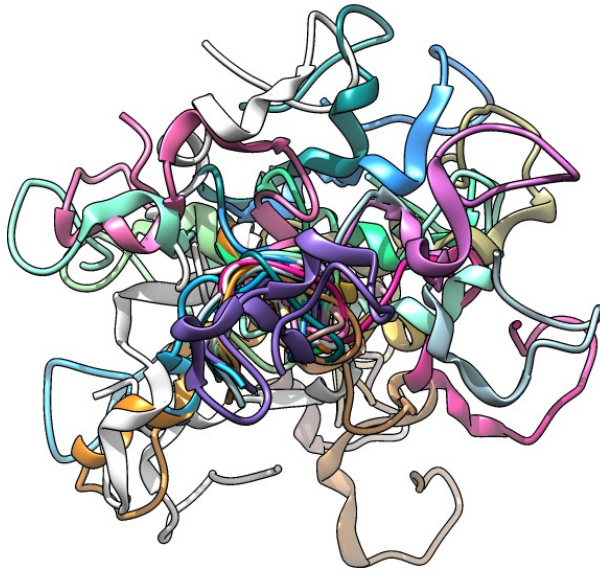
Figure 12: crystal structure of τ protein organized in fibrils bound to the microtubule in two points of view. PDB Code: 2MZ7.

In AD, Tau protein is found mutated with an hyperphosphorylated status leading to the formation of neurofibrillary tangles (NFTs). The pattern of physiological phosphorylation of the protein changes with the development of the disease occurring especially in residues involved in the binding with tubulin to allow the stabilization of microtubule (**Fig. 13**) but also in other regions linked to conformation changes. [102,103]
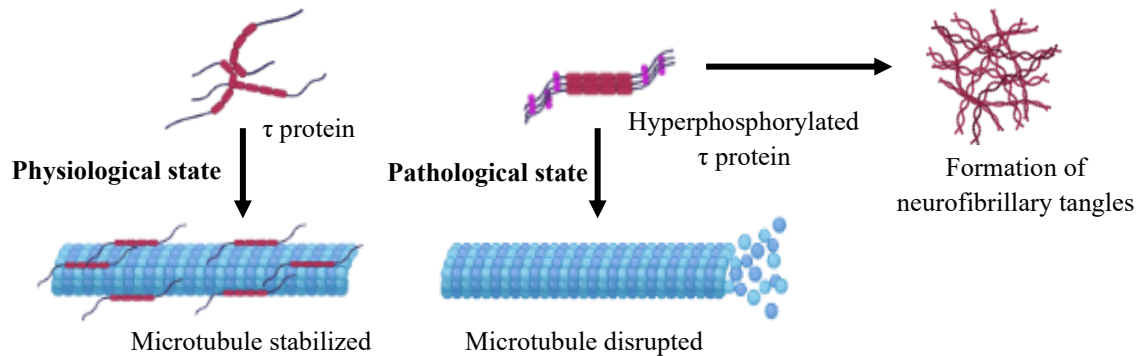
*Figure 13: physiological and pathological states: in the first mentioned, Tau protein stabilizes microtubule. When hyperphosphorylation occurs, microtubule is disrupted, and the result is the accumulation of abnormal Tau forming fibrils and then neurofibrillary tangles. Image created using **BioRender**.*

Moreover, Tau abnormal modifications linked to a mutation of gene encoding for this protein are connected to the occurrence of unusual change in 3R:4R ratio leading to the deposition of hyperphosphorylated Tau. [104] The region assigned to the binding is represented by amino acids S244-S368 in the C-terminal site of the protein. [105] Residues involved in the formation of earliest stage of the development of pathology are Ser-199, Ser 202-205, Thr-231 and Ser-262; hyperphosphorylation at the level of these amino acids is connected to the pre-tangles processes. [102,106] The chain of events suggests that it is complicated to establish the order and the role of each occurrence; the hyperphosphorylations at Ser-422 and Ser-396 represent an advanced pathological condition and these residues appear as the most relevant. [102] The event that determines the aggregation of Tau protein is the cleavage of Asp-421 and curiously, the phosphorylation on residue 422 tends to inhibit this cleavage process suggesting and intricated system of events to determine the development of the AD. [102] The hyperphosphorylated Tau protein at this point becomes inclined to self-assemble obtaining pathological intracellular paired helical filaments (PHFs) leading to the accumulation and, as a result, the development of

1. Introduction

NFTs that determine neuronal loss. [103,107] Since excessive phosphorylation appears as a posttranslational modification occurred in Tau protein in a pathological statement, it is reported that many kinases are involved in this reaction contributing to the trigger of the neurodegeneration. [102] Li and coworkers reported in 2004 the role of CK1δ in phosphorylation of Ser202/Thr205 and Ser396/Ser404 of Tau protein: the use of IC261 as inhibitor determines the decrease of the phosphorylation. [108] Nevertheless, CK1-mediated phosphorylation sites in Tau protein are various; [109] even if its role, in comparison to other kinase in the development of AD is less studied, at least 15 residues are found to be phosphorylated by CK1 in *in vitro* models of Tau. The study carried out together GSK3β suggests that the combination of the two enzymes can lead to the worsening of the hyperphosphorylation statement. [104] The **Table 3** below resumes the studied sites phosphorylated by CK1.

Table 3: phosphorylation sites in Tau protein (abbreviations: S = serine, T = threonine). The asterisks indicate that residues are phosphorylated by CK1 identifying them in AD brain extracts. Symbol ½ indicates that the phosphorylation occurs at two closely-spacer amino-acids. Table adapted by Ref 104.

Site in Tau protein	CK1
S113	*
S184	*
S198	*
S208	*
S210	½
T212	½
S214	*
S237	*
S238	*
S258	*
S262	*
S289	*
S356	*
S396	*
S404	*
S412	*
S413	½
T414	½
S416	*
S433	*
S435	*

Moreover, to validate the role of CK1 in the abnormal prospect of Tau protein, a study of sequences of Syrian hamster Tau and hibernated and not rodents was carried out. It is well established that the hibernated animals show similarities with the AD modifications including the phosphorylation state of Tau protein whose changes are detected in CK1-dependent manner in hibernated rodents. [110] Interestingly, since the real mechanism by which CK1 acts on Tau alterations is not fully understood, the most recent evidence of the role of CK1 in the AD is provided by Roth and coworkers. [111] This study confirms CK1δ, in particular, as a challenging target. Investigating the phosphorylation of recombinant tau441, ten sites and, among them, five linked to AD, were recognized: many of these residues were reported by previously described work of Hanger *et al.* in 2007 while sites Ser-324 and Thr-427 were not detected before. The massive phosphorylation is displayed for residues 243-441, many included in C-terminal region that is involved in the microtubule-binding (**Fig.14**). [105,111]
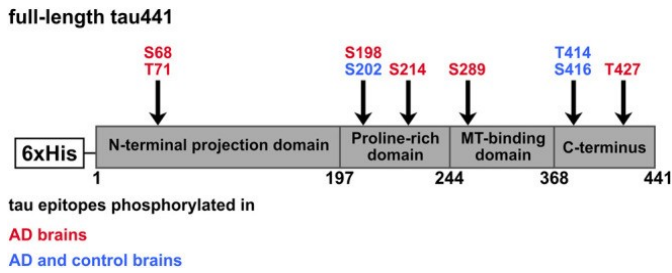
Figure 14: phosphorylation sites in full-length Tau protein. Image is reported in a recent study of 2022 (ref. 105), and it is possible to appreciate residues S68 and T71 in N-terminal domain and T427 in C-terminal region not reported in ref 104 of 2009.

The presence of CK1δ and Tau protein was also explored in neuronal cell anatomy revealing a co-localization of the two proteins at the level of nucleus and cell body. In the same work, as a conclusion, it was reported the role of CK1δ in the formation of Tau aggregates leading to PHFs since the phosphorylation of Ser-441 is attributed to the propensity of Tau to aggregate. [111] Nevertheless, not only the isoform δ is involved in the AD initiating events and progression: in a study of 2006 examining the hippocampal regions of advanced-stage AD brains, CK1δ was localized prevalently in granulovacuolar degeneration bodies while the α one in neurofibrillary regions. [112] CK1ε, as well, has been investigated in cell cultures displaying a massive hyperphosphorylation of Tau protein. [90] All these studies together suggest that CK1 appears as an important member in the development of AD pathology acting at various levels.
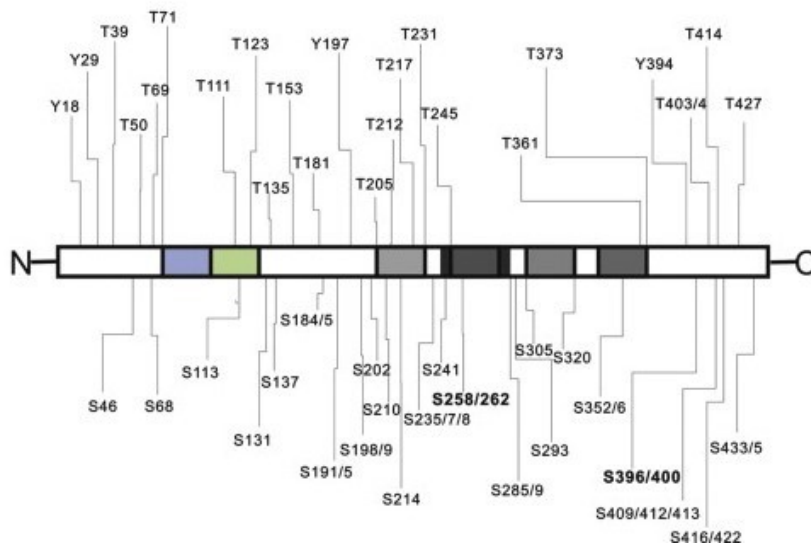
Figure 15: representation of all the CK1-mediated phosphorylation sites in Tau protein. Image adapted by Ref. 109.

1.5.2. Parkinson's disease

Parkinson's disease (PD) is a neurodegenerative disorder characterized by insurgence of several and debilitating symptoms including bradykinesia, instabilities in posture, problems in the coordination of movements as well as in language. This pathological condition is accompanied by the formation of Lewy's bodies (LBs) composed by the accumulation of abnormal α-Synuclein (α-Syn) (**Fig. 16**). [113,114,115]

1. Introduction
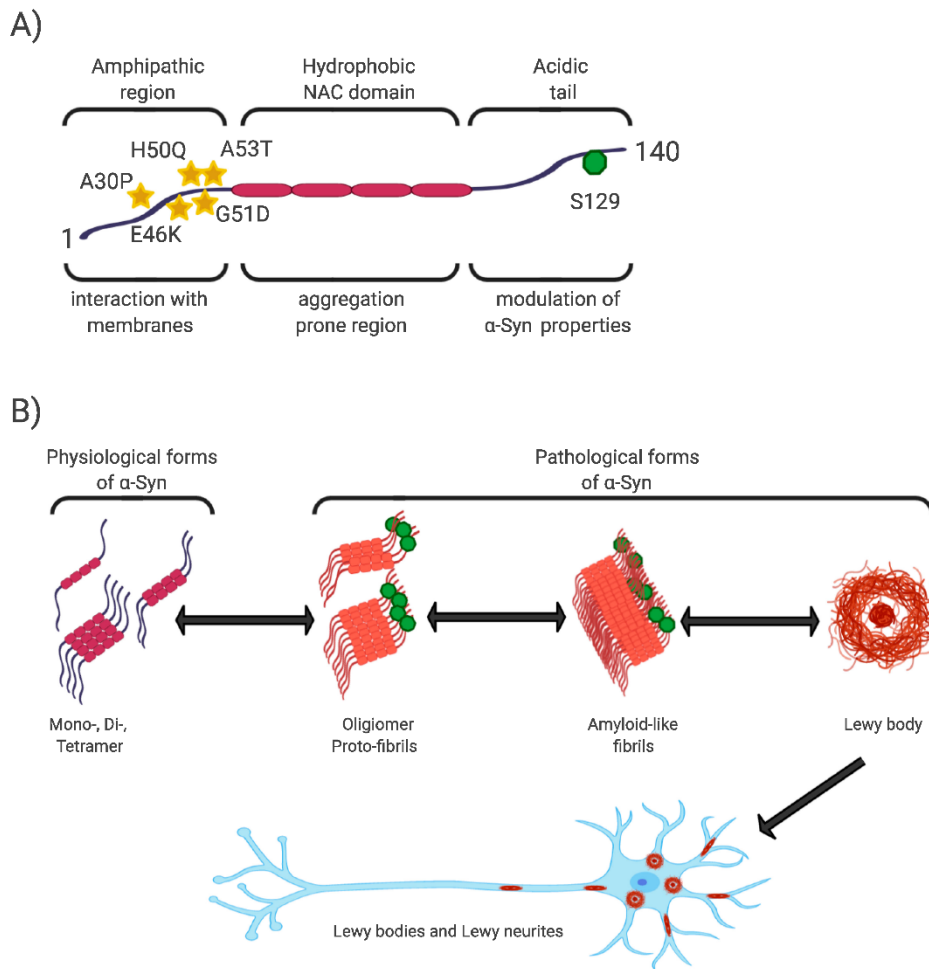
Figure 16: Panel A) schematic representation of α-Syn. Panel B) in a pathological scenario, α-Syn appears hyperphosphorylated and in abnormal form resulting in the accumulation of fibrils and the formation of Lewy bodies (LBs) causing damages at the level of neurons. [115]

The aggregate causes disruption in the dopamine biosynthesis leading to the inhibition of tyrosine hydroxylase (TH), enzyme that determines in normal situations an increase in dopamine production. [116] In a physiological scenario, dopamine (DA) plays an important role as neurotransmitter in neuroprotection: in the DA signaling pathway one byproduct is represented by neuromelanin, a dark insoluble complex, that captures toxic molecules preventing the oxidative stress at the central level. [117] With the progression of the disease, damages and loss of dopaminergic neurons can occur at the central compartment called *substantia nigra*. [118,119] 90% of α-Syn aggregates reported the phosphorylation at Ser-129 and this modification was found related to modulation of dopamine uptake. [120] Nevertheless, also phosphorylation at tyrosine residues has been recovered but less studied. [120] Several kinases have been found to be able to phosphorylate *in vitro* and *in vivo* α-Syn and to be implied in generally in the PD development: Polo-like kinases (PLKs), G protein coupled receptor kinases (GRCs), leucine-rich repeat kinase 2 (LLRK2), PTEN-induced putative kinase 1 (PINK1), cyclin G-associated kinase (GAK), serine-threonine kinase 39 (STK39), c-Jun N-terminal kinase (JNK), extracellular signal-regulated kinase (ERK), protein kinase B (PKB), glycogen synthase kinase 3β (GSK3β), mammalian target of rapamycin kinases (mTORKs) as well as casein kinase 1 and 2 (CK1/2). [121] According to the literature CK1 and CK2 are able to induce *in vitro* the phosphorylation on Ser-129 and, as counterproof, the inhibition of the two kinases has displayed the decrease of α-Syn phosphorylation even if more studies need to demonstrate the role of CK1 in the development of PD. [121,122] Elsholz and co-workers, in a recent work, have confirmed the role of this kinase in the pathology; by overexpressing CK1 binding protein (CK1BP), that is able to inhibit CK1 activity, in HEK293T cells, the Ser-129 phosphorylation as well as the aggregation of α-Syn has been evaluated and results confirm the key role of CK1 in the development of AD. [123] Another implication of this

kinase in the disease is related to the activation of cyclin-dependent kinase 5 (CDK5) CK1-mediated triggered by the activity of dopamine receptors (D3Rs). This action can induce the inhibition of P/Q-type Ca^{2+} channel determining the block of DA release at the synaptic level. [115] Even if symptoms appear different, the disorder shares the formation of NFTs with Alzheimer's disease confirming itself as a tauopathy. [109] There are several connections between Tau protein and the development of Parkinsonism: Lewy was the first that described NFTs in the disease.[84,109,124] In addition, the phosphorylation at Ser-396 of Tau protein is detected in PD-affected brains and the co-localization of abnormal Tau and α-Syn in LBs determined the development of PD. [109,125,126] All the collected evidence highlights the important role of CK1 in the PD and the use of inhibitors can be a promising approach to study all the mechanisms involved in the pathology as well as new tools to be applied in the therapeutic treatment.

1.5.3. Amyotrophic Lateral Sclerosis (ALS)

The Amyotrophic Lateral Sclerosis (ALS) is a neurodegenerative disorder characterized by the injury, damage, and progressive loss of motor neurons. Mutations at the level of TDP-43 (Trans activation response DNA binding protein 43 kDa) provide the possibility of insurgence of the pathological condition. In a physiological situation, this factor can bind DNA and RNA at the nucleus level leading to mRNA modulation. Mutations of TDP-43 cause its localization in cytoplasm in a ubiquitylated and hyperphosphorylated form. It is true that the real function of this factor is exploited at the nuclear level, but it is freely to move at the cytoplasmatic one suggesting that probably an equilibrium is established in the two compartments and the occurrence of mutations and modifications can break this statement determining the mis-localization. [127] The progression of the disease determined by the loss of motor neurons is triggered by the aggregation of this factor in the abnormal aspect that contributes to create stress granulates (SGs), and the resulting oxidative stress determines the development of toxicity at neuronal level. TDP-43 is composed by an N-terminal domain that contains the nuclear localization signal (NLS) and two recognition motifs (RRM1 and RRM2) required for the activity at the level of RNA and DNA, and a C-terminal domain composed by a glycine-rich motif. [127,128] Instead, the real structure of aggregates of TDP-43 was unknown even if a recent work of Arseni and co-workers has reported the structure of these filaments using cryo-EM starting from samples of frontal and motor cortices of ALS-affected patients. [129] Interestingly, TDP-43 with its abnormal aggregates is also recovered in Alzheimer's disease and Parkinson's disorder confirming that possible candidates able to decrease its phosphorylated status can be very useful as tools and for the treatments of different neurodegenerative diseases. [129,130] The two posttranslational modifications hyperphosphorylation and hyperubiquitylation were detected in ALS patients, evidencing that the phosphorylation can be the primary event that triggers the other phenomenon even if the two modifications influence each other in the pathology. The ubiquitin system has an important role in a physiological condition determining the degradation of toxic complexes via proteasome while, in the pathological counterpart, defects and injuries at the level of autophagic system are detected. In ALS models, several phosphorylation sites are reported on TDP-43 including Ser-379, Ser-403, Ser-404, Ser-409, Ser-410 even if lots of sites have been detected in its structure without enough data to support their real existence and role in the development of ALS (**Fig. 17**). [127,131,132,133] The presence of hyperphosphorylated and mis-localized TDP-43 has been found also in FTDL (Frontotemporal lobar degeneration) characterized by atrophy in frontal and temporal lobes. [134]

1. Introduction
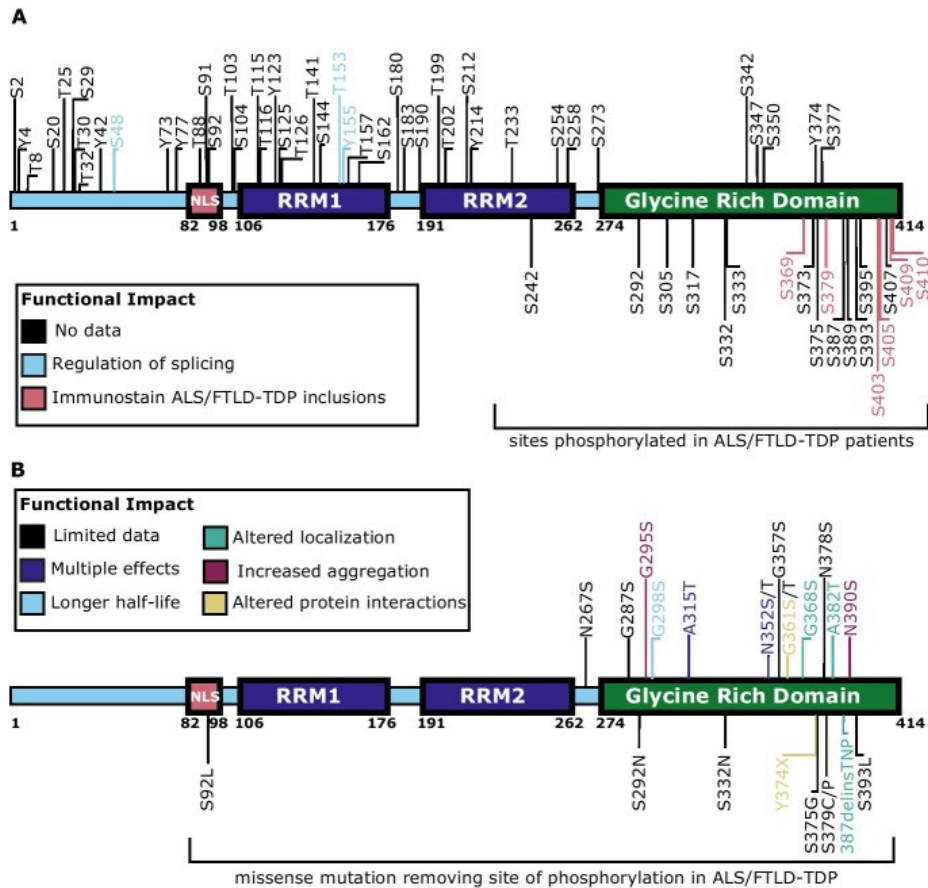
Figure 17: TDP-43 phosphorylation sites. The panel A shows TDP-43 (441 residues) that is composed by NLS (nuclear localization signal) motif in N-terminal domain, two RNA recognition motifs (RRM1 and RRM2) and a glycine rich domain in C-terminal one. 64 phosphorylation sites are detected in ALS/FTLD-TDP patients (reported above the diagram A), many residues were investigated using immunostaining (red residues) or linked to the regulation of TDP-43 splicing (light blue residues). Panel B reports mutations occurred on TDP-43, among them several are connected to mis localization, altered protein interactions, aggregation and longer half-like (reported in the appropriate color according to the box of color code. [127]

Nonaka and colleagues have demonstrated the relationship between this hallmark and CK1δ in neuroblastoma cell lines (SH-SY5Y) reporting that the hyperactivated form of this kinase is able to determine the cytoplasmatic mis-localization as well as the hyperphosphorylation of TDP-43 and it is possible to see in cells the formation of aggregates triggering the neurodegenerative process. [135] The phosphorylation sites of TDP-43 related to the activity of CK1δ have been identified: 29 total residues have been recognized and among them 18 are located in the C-terminal domain of TDP-43 in the glycine-rich zone demonstrating that this is the preferred domain in which the kinase works. [136] Some CK1δ inhibitors bearing benzo[*d*]thiazole scaffold, that will be discussed in the **chapter 3**, have been investigated in neuroprotection with a toxicity induced by ethacrynic acid to simulate the ALS disease and they have displayed good results also in the decrease in the TDP-43 phosphorylation. [137] The performed test using SH-SY5Y cell lines confirmed the role of CK1δ in the development of disease and the importance that new candidates could have in the study of ALS and in its treatment. For this reason, this is the approach that we have applied in this PhD project to investigate the role of the most promising compounds in ALS cell models. Moreover, also the isoform ε has been found to prompt ALS symptoms by enhancing the TDP-43 proteinopathy *in vivo*. [138] Interestingly, CK1 is not only implicated in the development of the disease by phosphorylating TDP-43; mutations at the level of charged multivesicular body protein 2B (CHBP2B) are connected to the development of ALS and its role consists in the modulation of autophagic system and vesicle trafficking. Thus, the pathogenicity is given by disruption of autophagic and endolysosomal pathways determining the accumulation of proteins involved in physiological proteasome systems and this event can determine the aggregation of TDP-43. [139] CHBP2B is able to interfere with the phosphorylation of TDP-43 by regulating the turnover of CK1 mediated by ubiquitin-proteasome system, in

fact the downregulation of CHBP2B has proved to determine the decrease in TDP-43 phosphorylation in *Drosophila* models as well as mammalian cells. [139] In order to demonstrate this CHBP2B activity mediated by the action of CK1, it has been demonstrated that the autophagy system does not interact with TDP-43 phosphorylation and, moreover, the activity of this protein towards CK1. [139] Literature explored suggests that the research is still opened to investigate pathways involved in ALS but is evident the key role of CK1 in different fronts. Thus, the development of potent inhibitors can be the turning point to have new tools for the study and treatment of pathology.

1.6. Kinase Inhibitors

1.6.1. Types of kinase inhibitors

Over the years, kinase inhibitors have been classified in five classes based on the position of molecule within the target.

➢ Type I: small molecules able to bind the ATP-binding site of the kinase in the active conformation (DFG-in). The standard exploration of this class of inhibitors provides a heterocyclic core that occupies the adenine binding region establishing from one to three hydrogen bonds with residues belonging to the ATP cleft. The main scaffold is substituted with different moieties that can exploit the hydrophobic sites of this pocket trying to improve selectivity and potency. [140,141]

The five subregions in which the ATP-binding site can be divided are reported in **Fig. 18**; ATP is represented with its interactions towards the active site of the kinase domain.

- Adenine binding region: the zone occupied by adenine that is able to establish two hydrogen bonds with residues of the hinge region mediated by N1 and N6 nitrogen atoms. [142]
- Sugar pocket: is the hydrophilic region of the ATP-binding site exploited by the sugar ribose of the ATP. [142]
- Hydrophobic region I (HRI): it consists in a site that is not occupied by the ATP molecule; it can be exploited by developed compounds to gain more potency and selectivity trying to achieve the gatekeeper residue presented at the level of the hinge region. [142]
- Hydrophobic region II (HRII): this site is exposed to the solvent, and it can be useful to investigate in the development of more potent inhibitors. [142]
- Phosphate binding region: also this site appears to be exposed to the solvent; it can be explored to develop more selective inhibitors since residues in this region are not conserved among kinases. [142]

1. Introduction
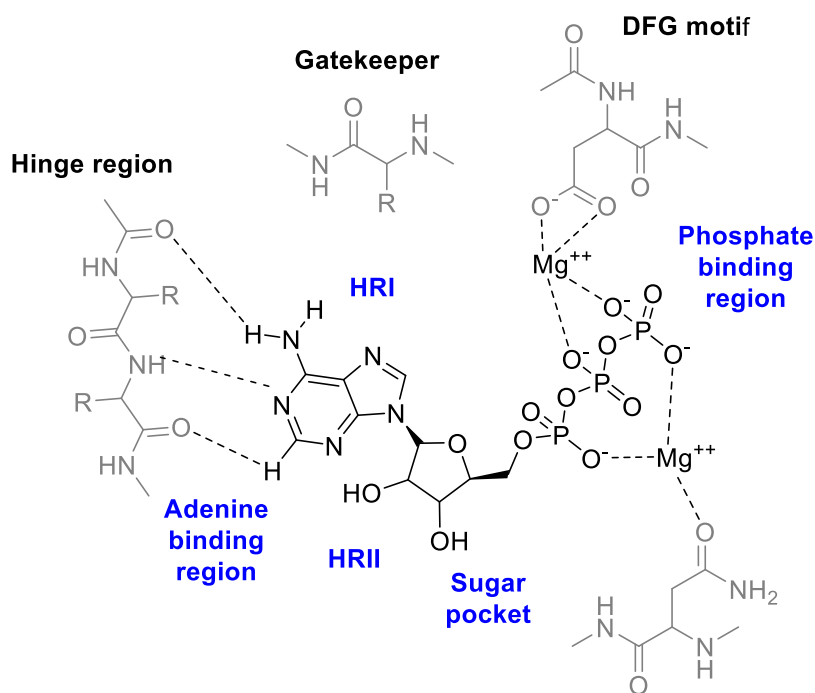
Figure 18: ATP-binding site composed by five sites: adenine binding region, hydrophobic pockets (I and II), sugar pocket and phosphate binding region.

Interestingly, Zuccotto and co-workers have identified a subset of type I inhibitors that bind the adenine site establishing hydrogen interactions with the hinge region of the enzyme but that extend themselves to the back site of ATP cavity giving interactions that are typical of type II inhibitors; for this reason, called type ½ inhibitors. [141]

➤ Type II: small molecules that bind the same ATP pocket but with the kinase in the inactive conformation (DFG-out). Type II inhibitors can occupy the ATP binding site extending to the adjacent allosteric one determining a rearrangement of phenylalanine belonged to the DFG motif out of hydrophobic pocket towards the ATP region. This type of inhibitors present enhanced selectivity in comparison to the just discussed type I. Categories I and II are ATP-competitive inhibitors. [141]

➤ Type III: allosteric inhibitors that can bind adjacent to the ATP-binding pocket between the two lobes where the catalytic site of the kinase is present. Their most representative feature is characterized by a high selectivity since this type of inhibitor can interact with the regulatory mechanisms of enzyme. [143]

➤ Type IV: allosteric inhibitors that bind outside of the catalytic cleft of the kinase. Also in this case, molecules are characterized by selectivity. [144]

➤ Type V: this class is explored by bivalent inhibitors composed by two portions able to interact with different regions of the kinase. It is possible to design type V inhibitor choosing accurately both nucleus and substituent in order to achieve a potent and selective candidate. [145]

➤ Type VI: is represented by covalent inhibitors that have several advantages including the long half-life and the maximized effectiveness even if the toxicity due to the off-target effect is discussed. This type of inhibitor is characterized by a heterocyclic core substituted with an electrophile portion (**Fig. 19**) able to give interaction with a cysteine or lysin of target. [146,147,148]

1. Introduction
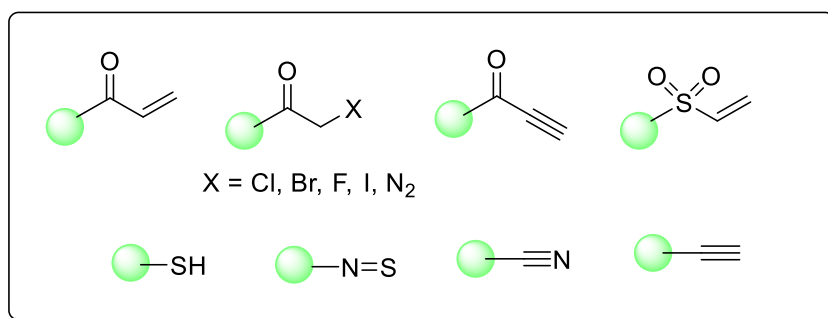
Figure 19: examples of electrophile moieties for the design of covalent inhibitors. [140,141]

1.6.2. CK1 inhibitors

1.6.2.1. IC-261: indol-2-one derivative

IC-261 (**1**) was synthesized in 2000 and displayed an interesting activity towards both the isoforms δ and ε of CK1 due to the high homology of the structures. It showed an IC_{50} of 1.0 μM and selectivity against other kinases including PKA. As showed in **Fig. 20**, this candidate appears as the mixture of E and Z isomers. The crystal structure (PDB code: IEH4) suggests that the main core of the molecule characterized by an oxindole occupies the adenine region of the kinase domain while the trimethoxy phenyl moiety binds the phosphate binding region establishing hydrogen bonds. Interestingly, this compound has been tested *in vitro* in cell lines due to the implication of CK1δ/ε in pancreatic tumors. [149,150]

IC-261, 1
IC_{50} CK1δ/ε = 1.0 μM
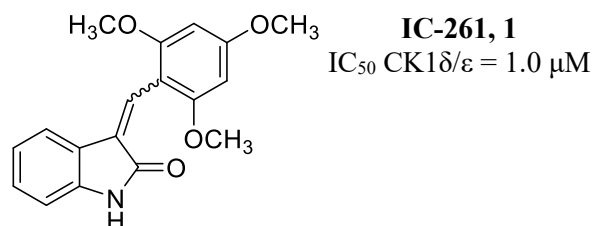
*Figure 20: structure of IC-261 (**1**) and its activity on CK1δ/ε.*

1.6.2.2. Monocyclic system inhibitors: imidazole, pyrazole and isoxazole

Compound D-4476 (**2**), bearing an imidazole scaffold (**Fig. 21**), was developed in the first years of the 2000s as inhibitor of activin receptor-like kinase 5 (ALK-5), enzyme involved in several types of cancer diseases that induce modulations in tumor grown factor β (TGF β). Later, in the screening on the kinome panel, it showed inhibitory activity on CK1δ reporting an IC_{50} of 0.3 μM. [151]

D-4476, 2
IC_{50} CK1δ = 0.3 μM
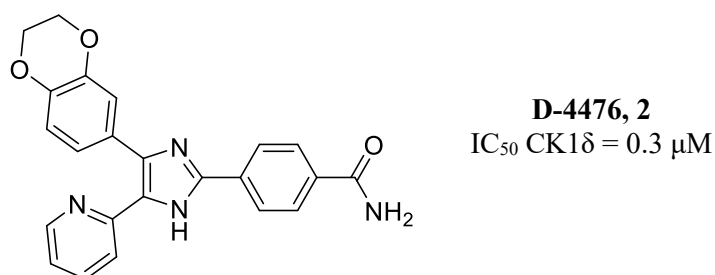
*Figure 21: structure of D-4476 (**2**) and its activity on CK1δ.*

1. Introduction

Successively, the imidazole nucleus has been revaluated: originally this fashionable scaffold was used to the design of p38α inhibitors, then Peifer and co-workers discovered an activity towards CK1δ of compound **3** and **4** (**Fig 22**) in the nanomolar range. [152] Compound **3** displayed an IC_{50} (CK1δ) of 5.0 nM but it inhibited also the isoform ε (IC_{50} = 73 nM). The sulfoxide derivative (**4**), obtained from the precursor **3**, instead, has proved to be more selective reporting an activity on CK1ε of 40-fold related to the isoform δ. [152]

3
IC_{50} CK1δ = 5.0 nM
IC_{50} CK1ε = 73 nM

4
IC_{50} CK1δ = 11 nM
IC_{50} CK1ε = 447 nM
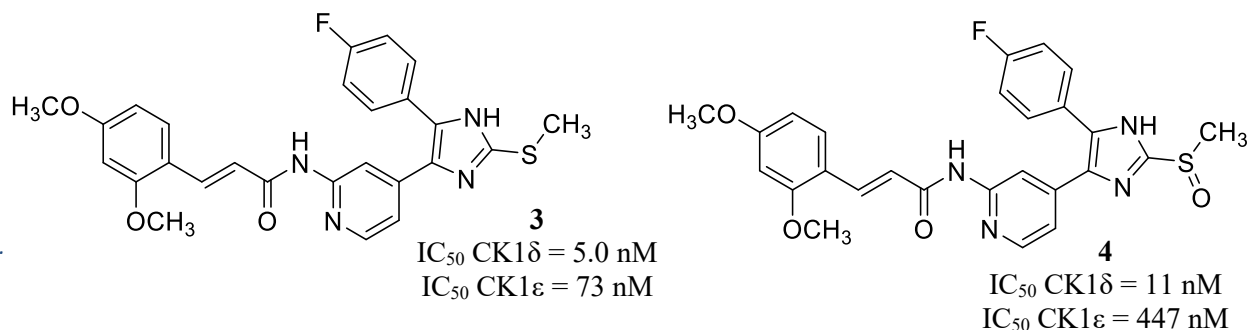
Figure 22: structures of compounds 3 and 4 and their activities on CK1δ and CK1ε.

In the year 2017 Halekotte *et al.* published an interesting series of 4,5-diarylimidazoles as potent CK1δ inhibitors by optimizing the series previously discussed. Due to the chemical instability of cinnamic acid as spacer between dimethoxy phenyl ring and pyridine moiety, other types of chains have been evaluated considering amino, amido, ureido and pyrrole-amido linkers as reported in **Fig. 23**. [25]

5
IC_{50} CK1δ = 386 nM
IC_{50} CK1ε = 6731 nM

6
IC_{50} CK1δ = 20 nM
IC_{50} CK1ε = 129 nM

7
IC_{50} CK1δ = 4.0 nM
IC_{50} CK1ε = 25 nM

8
IC_{50} CK1δ = 8.0 nM
IC_{50} CK1ε = 81 nM
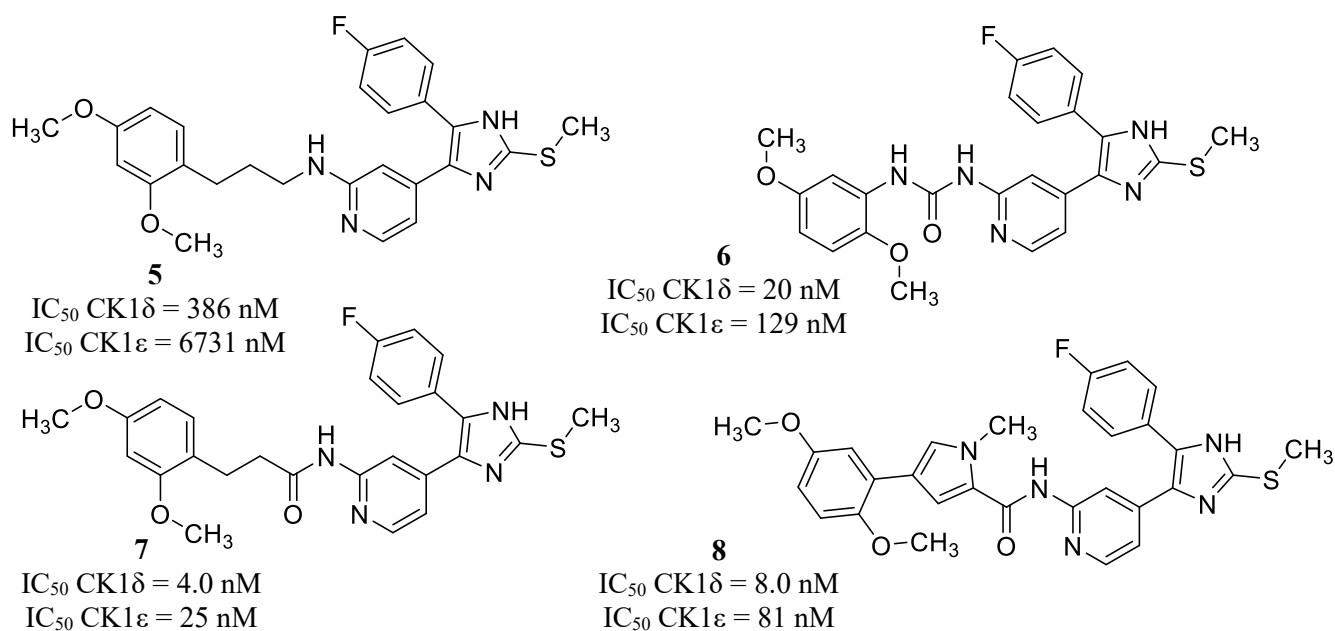
Figure 23: 4,5-diarylimidazole scaffold compounds (5-8) and their IC50s on CK1δ/ε..

Compounds **7** and **8** have resulted the best of the series reporting IC_{50}s (CK1δ) of 4.0 and 8.0 nM, respectively (**Fig. 23**). Derivative **8** displayed also a great selectivity related to the isoform ε, comparable to that exhibited by parent compound **3**. [25]

Interestingly, another potent imidazole inhibitor PF-670462 (**9**) (**Fig. 24**, **Panel A**) was developed reporting IC_{50}s on isoforms δ and ε of 14 nM and 7.7 nM, respectively. The crystal structure of this compounds reported in **Fig. 24 (Panel B)** reveals that it anchors the ATP-binding site of CK1δ establishing a double hydrogen bond

with Leu-85, residue belonged to the hinge region, through the amino-pyridine backbone. The fluorophenyl moiety engages strong hydrophobic interactions with Met-80 and Met-82 (gatekeeper residue) while the -NH of imidazole core can interact with the catalytic Lys-38 and Asp-149 of DFG motif through a water molecule. It is a promising inhibitor: it displayed a good selectivity profile showing binding affinity over few other kinases like PKAα, p38, EGFR, LCK,and MAP4K4. [21]
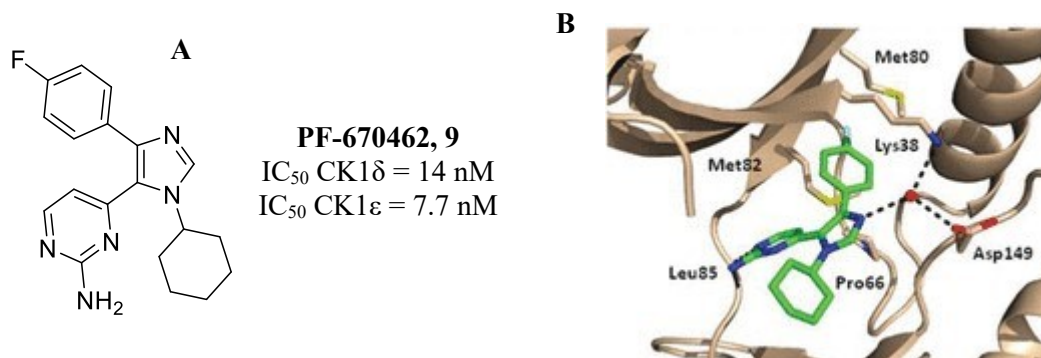
Figure 24: structure (Panel A) and predicted binding pose on CK1δ (B) of compound PF-670462 (9).

PF-670462 (**9**) was used as tool *in vitro* and *in vivo* studies involving the circadian rhythm disorders due to the implication of the isoform ε. [153,154,155] Moreover, Janovska *et al.* demonstrated a role of this inhibitor also in chronic lymphocytic leukemia (CLL) since CK1δ/ε is resulted implying in the Wnt signaling pathway that appears disrupted in this pathologic condition. The study on mouse reveals that the inhibition of this kinase using PF-670462 leads to the decrease of the accumulation of leukemic cells in peripheral blood obtaining a longer survival with the administration of the drug. [156]

According to Mente and co-workers, an optimization of PF-670462 (**9**) has been carried out to develop pyrazole-substituted pyridine compounds able to permeate at the central level gaining a selectivity towards CK1δ. PF-670462 (**9**) binds both the isoform ε as well as the five other kinases mentioned above. Thus, this compound can be optimized from the point of view of druglike properties and selectivity profile. [24]
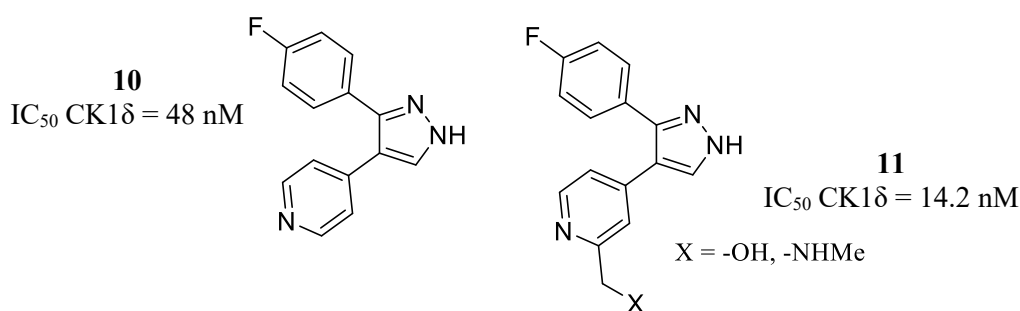
*Figure 25: compounds **10** and **11** and their activities on CK1δ.*

Compounds **10** and **11** (**Fig. 25**) have displayed IC_{50}s (CK1δ) of 48 nM and 14.2 nM, respectively, showing good BBB permeation properties and an excellent selectivity profile considering the kinases that PF-670462 was able to bind. Moreover, these candidates have been tested *in vivo* on mice demonstrating the capability to modulate the circadian rhythm confirming their usefulness as tools for the study of circadian rhythm-related pathological condition. [24]

Starting from the co-crystalized complex of CK1δ and PF-670462 (**9**), a series of isoxazole molecules was developed. Compound **12**, reported in **Fig. 26**, showed an IC_{50} of 33 nM on CK1δ and it is possible to appreciate the analogy of substituents with the 5,6-diarylimadozoles previously discussed. 4-fluorophenyl moiety can bind the hydrophobic pocket I, stabilizing the structure between sidechains of Lys-38, Met-80 and

the gatekeeper residue, while the amino pyridinyl moiety establishes a double hydrogen bond at the level of the hinge region. The main isoxazole core engages another hydrogen bond with a molecule of water; regards the cinnamic portion and the linked polimethoxy phenyl group, this part of the compound can place itself in the hydrophobic pocket II in the ATP-binding site (**Panel B**, **Fig.26**). [157]
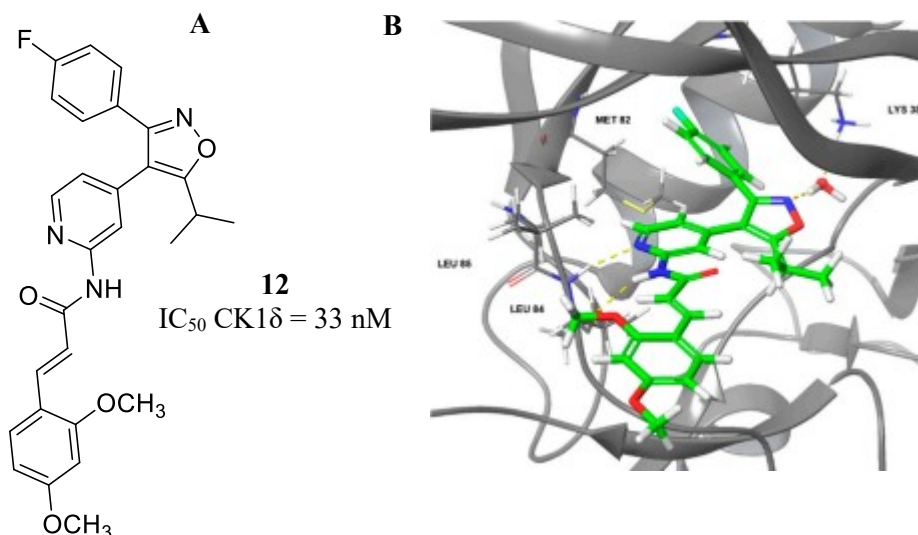
*Figure 26: structure of compound **12** (**Panel A**) and predicted binding pose on CK1δ (**Panel B**). Computational image of Ref. 157.*

To achieve additional interactions occupying the hydrophilic ribose pocket, a pyrrole ring has been inserted to the main scaffold to provide selectivity. Compound **13** (**Fig. 27**, **Panel A**) has reported IC$_{50}$s of 37 nM on CK1δ and 100 nM on CK1ε. Nevertheless, it displayed an excellent selectivity profile against 320 kinases as the dendrograms represented in the **Panel B** of **Fig. 27**. [157]
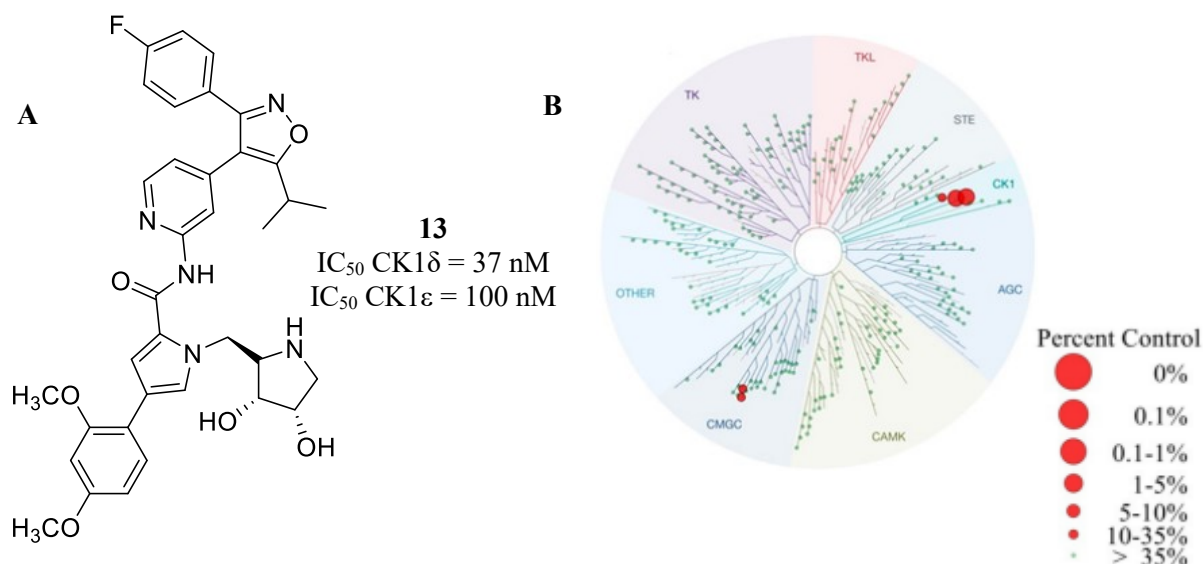
*Figure 27: structure of compound **13** and the screening on 320 kinases, derivative tested at the concentration of 1 μM. The dendrograms is adapted from ref. 157.*

1. Introduction

1.6.2.3. Bicyclic inhibitors: purines

The purine scaffold appears an appealing nucleus for the development of kinase inhibitors. A series of derivatives bearing this type of scaffold has been reported by Oumata *et al.* developing Roscovitine-like candidates. [158] (*R*)-roscovitine and its "second generation" derivative (*S*)-CR8 (**14**, **Fig. 28**), inhibitors of cyclin-dependent kinases (CDKs) are found to be able to also inhibit several kinases, among them CK1δ/ε. [159] Thus, repurposing the same nucleus, several CK1δ inhibitors have been obtained. As reported in **Fig. 29**, compounds **15-17** have proved to be the best of the developed series displaying IC$_{50}$s of 50 nM, 80 nM and 48 nM, respectively. Interestingly, these derivatives displayed antiproliferative properties when tested in neuroblastoma cell lines (SH-SY5Y) and have proved to reduce the formation of β40 peptide. [158] Compounds **15-17** have been tested on CDK1, CDK5 and GSK3α/β and, in particular, derivative **15** has displayed a good selectivity towards CK1δ considering the just mentioned kinases.
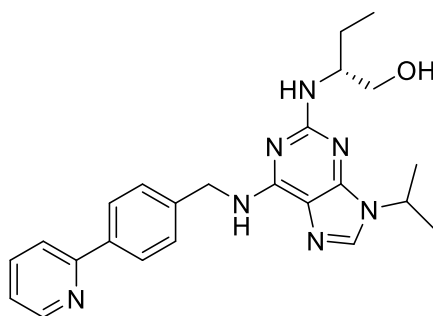
*Figure 28: structure of (S)-CR8 (**14**).*

15
IC$_{50}$ CK1δ = 50 nM

16
IC$_{50}$ CK1δ = 80 nM

17
IC$_{50}$ CK1δ = 48 nM
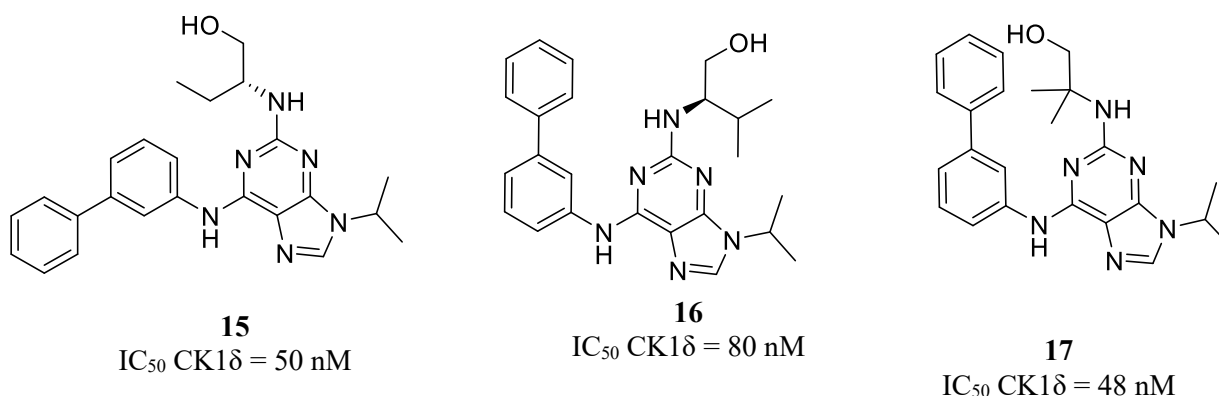
*Figure 29: compounds **15-17** and activities on CK1δ.*

Nevertheless, several series bearing this main bicyclic core have been developed. Compound **18**, reported in **Fig. 30**, with the name of SR-653234 revealed an inhibitory activity on the isoform δ of 160 nM. Using it as a precursor, positions 2 and 3 of benzimidazole have been investigated. The introduction of a nitro group at the 2-position led to compound **15**, which showed an improved IC$_{50}$ of 49 nM. The potency has been increased by substituting this position with methane sulfonic moiety (**20**) and studying the 3-position, trifluoromethyl, cyan, methoxy groups as well as the methane sulfonic one have been inserted achieving potent and promising derivatives (**21-24**). [160]
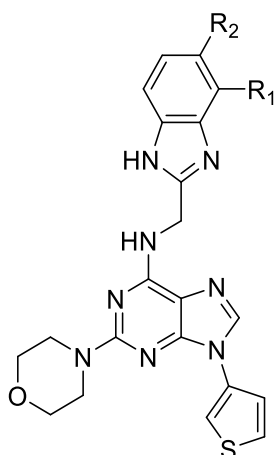
18, SR-653234 $R_1 = $ -H, $R_2 = $ -H
19, SR-1277 $R_1 = $ -NO$_2$, $R_2 = $ -H
20, SR-2805 $R_1 = $ -SO$_2$CH$_3$, $R_2 = $ -H
21, SR-1273 $R_1 = $ -H, $R_2 = $ -CF$_3$
22, SR-1276 $R_1 = $ -H, $R_2 = $ -CN
23, SR-1279 $R_1 = $ -H, $R_2 = $ -OCH$_3$
24, SR-2797 $R_1 = $ -H, $R_2 = $ -SO$_2$CH$_3$

18, IC$_{50}$ CK1δ = 160 nM
19, IC$_{50}$ CK1δ = 49 nM
20, IC$_{50}$ CK1δ = 16 nM
21, IC$_{50}$ CK1δ = 13 nM
22, IC$_{50}$ CK1δ = 11 nM
23, IC$_{50}$ CK1δ = 17 nM
24, IC$_{50}$ CK1δ = 10 nM

*Figure 30: SR-653234 (**18**) and its derivatives **19-24**. Activities on CK1δ are reported.*

More recently, Monastyrskji and co-workers optimized these purine scaffold compounds by substituting morpholine and thiophene moieties of derivatives **18**-**24** as reported in **Fig. 31**. 2 and 3-positions of benzoimidazole ring have been occupied by halogens while morpholine has been replaced by piperazine. Derivatives **25** and **26** have proved to be potent and promising towards CK1δ obtaining IC$_{50}$s of 4 and 5 nM, respectively. [161]

25
IC$_{50}$ CK1δ = 4.0 nM

26
IC$_{50}$ CK1δ = 5.0 nM
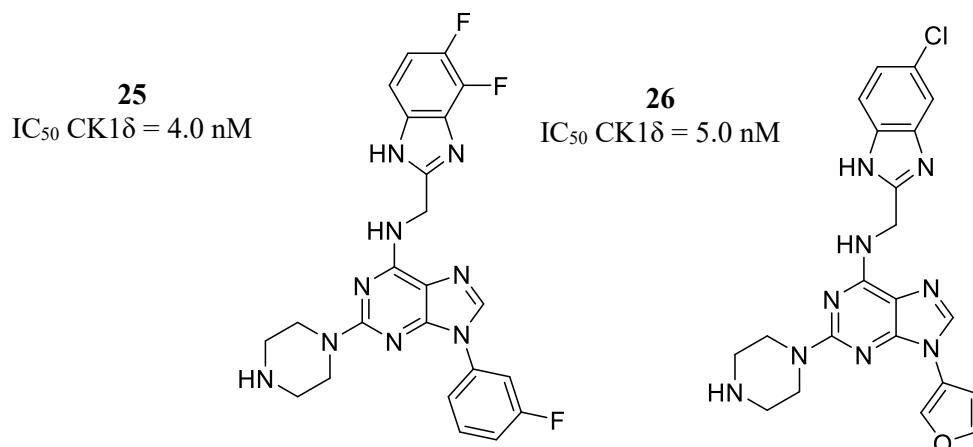
*Figure 31: compounds **25** and **26** and activities on CK1δ.*

1.6.2.4. Bicyclic inhibitors: benzo[*d*]imidazole and benzo[*d*]thiazole derivatives

Bischof and co-workers developed by an in-house screening a series of benzo[*d*]imidazole compounds and among them, in particular, two molecules have proved to be promising tools. Compounds **27** and **28** displayed IC$_{50}$s (CK1δ) of 40 nM and 42 nM, respectively. Moreover, derivative **27** has proved to be selective on a panel of 442 kinases even if an activity on the isoform ε as well as other CK1 isoforms has been detected. The results of the selectivity screening testing compound at the concentration of 10 μM are reported in **Fig. 32** (**Panel B**). The candidate showed an inhibition of proliferative effect in cancer cell lines. [23]
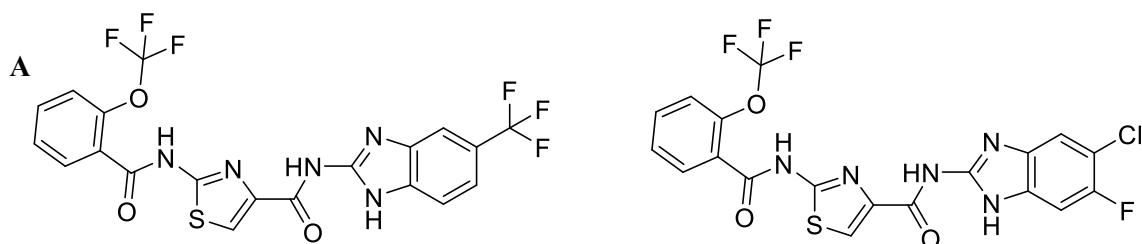
Bischof-5, 27
IC$_{50}$ CK1δ = 40 nM
IC$_{50}$ CK1ε = 199 nM

Bischof-6, 28
IC$_{50}$ CK1δ = 42 nM
IC$_{50}$ CK1ε = 33 nM

KINOMEscan Gene Symbol	%Ctrl @ 10 µM
CLK1	2.6
CLK2	10
CLK3	20
CLK4	7.2
CSNK1A1	3
CSNK1A1L	1
CSNK1D	2
CSNK1E	0.35
CSNK1G2	9.9
CSNK1G3	31
DYRK1A	4.1
DYRK1B	6.6
DYRK2	17
FLT3(D835H)	25
FLT3(D835Y)	10
FLT3(ITD)	24
IRAK3	27
PIP5K2C	9.6
SLK	12
TAOK1	24
TAOK3	20

0 ≤ x < 1   1 ≤ x < 10   10 ≤ x < 35
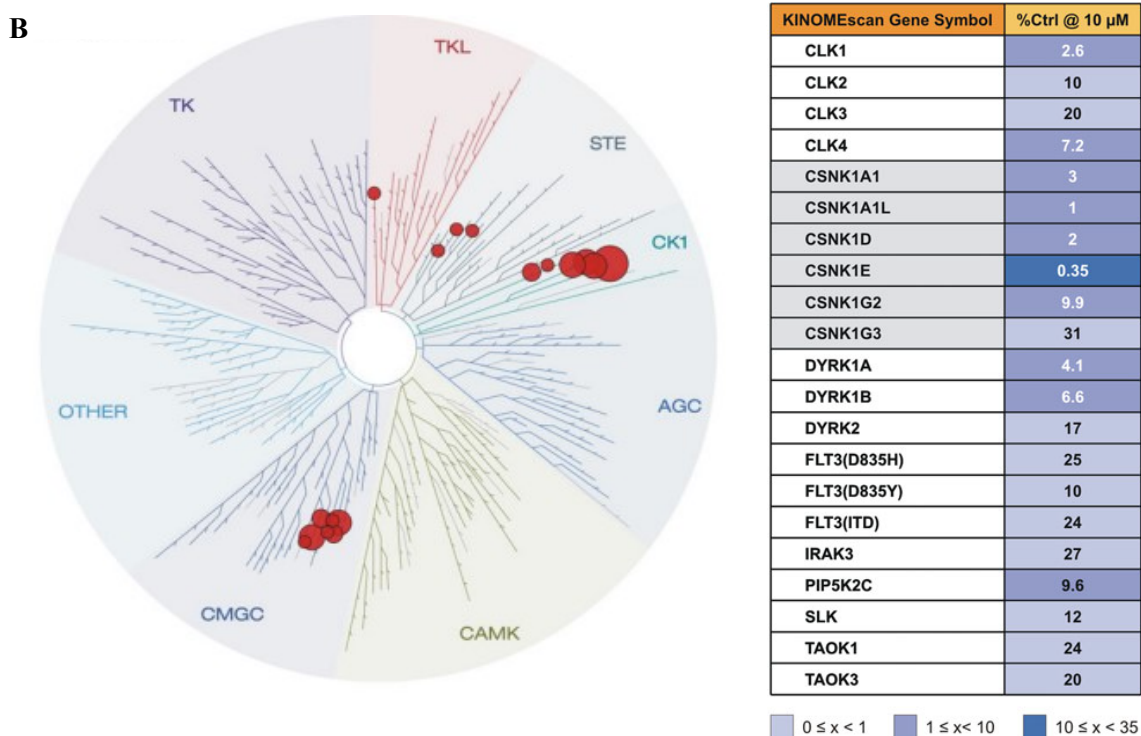
Figure 32: structures and activities of compounds 27 and 28 (Panel A) and selectivity profile of compound 27, ref. 23 (Panel B). The table reports the % binding on kinases in which an activity was detected testing compound 27 at the concentration of 10 µM.

These promising compounds are then modified to improve the selectivity towards the other isoforms of CK1, especially the ε one. The benzo[*d*]imidazole scaffold has been functionalized with difluoro-dioxolo moiety and the developed derivatives have shown not only a good selectivity, but they revealed important efficacy in several tumor lines. [162]

Compounds **29-31** reported in **Fig. 33** have displayed interesting activities on CK1δ of 20 nM, 140 nM and 570 nM, respectively, and they reported a good selectivity towards CK1ε.

29
IC$_{50}$ CK1δ = 20 nM
IC$_{50}$ CK1ε = 210 nM

30
IC$_{50}$ CK1δ = 140 nM
IC$_{50}$ CK1ε = 520 nM

31
IC$_{50}$ CK1δ = 570 nM
IC$_{50}$ CK1ε = 999 nM
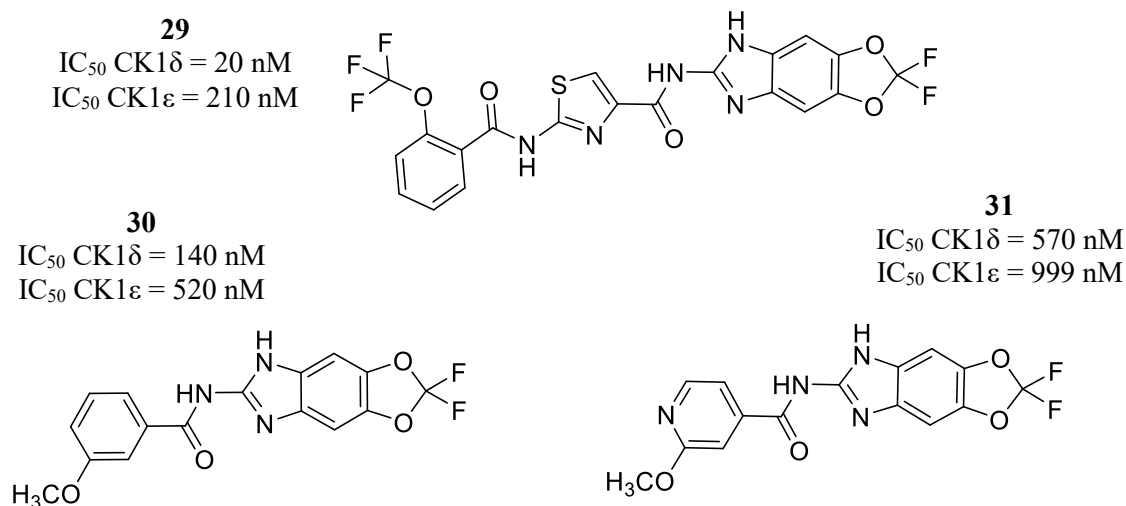
Figure 33: structures of compounds 29-31 and activities on CK1δ/ε.

Interestingly, the predicted binding pose reported in **Fig. 34** suggests that compound **29** can bind the ATP-binding site in the same manner of Bischof-5 (**27**); the imidazole main nucleus establishes a double hydrogen bond with Glu-83 and Leu-85 of the hinge region while additional hydrophobic interactions are reported with Ile-23, Leu-84, Leu-85 and Pro-87. [162]
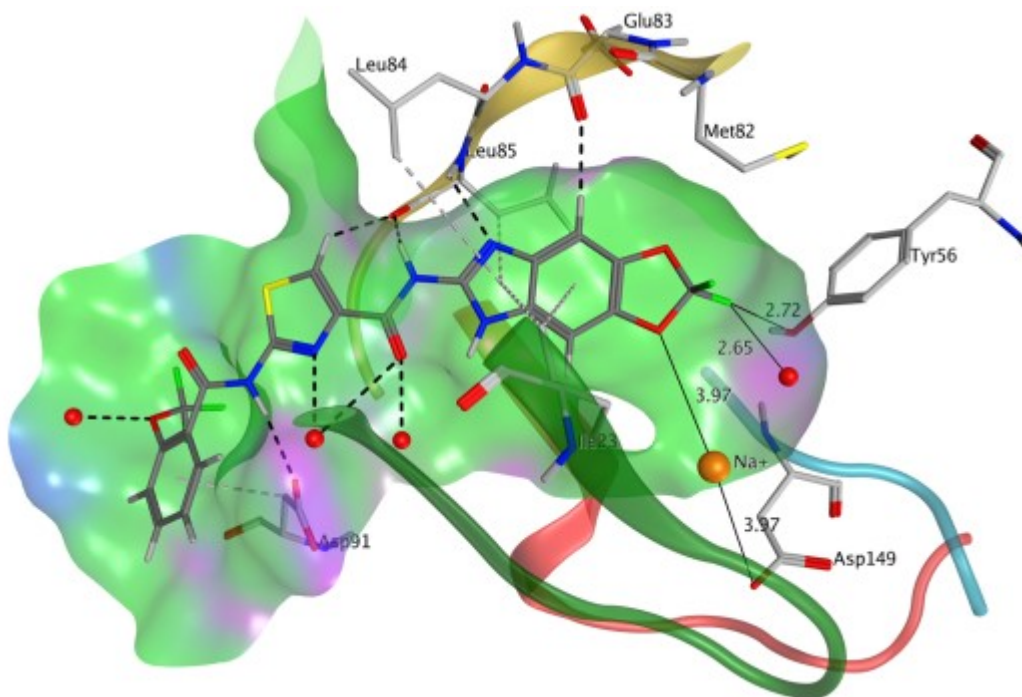
Figure 34: predicted binding pose of compound 29. [162]

Moving to another type of bicyclic scaffold, benzo[*d*]thiazole nucleus was widely used for the development of CK1δ inhibitors. Salado and co-workers starting from a virtual screening of in-house compounds have synthesized potent and selective inhibitors applying structural modifications to achieve several lead derivatives, the best ones are reported in **Fig. 35**. [163]

IGS-2.7, 32
IC$_{50}$ CK1δ = 23 nM

33
IC$_{50}$ CK1δ = 10 nM
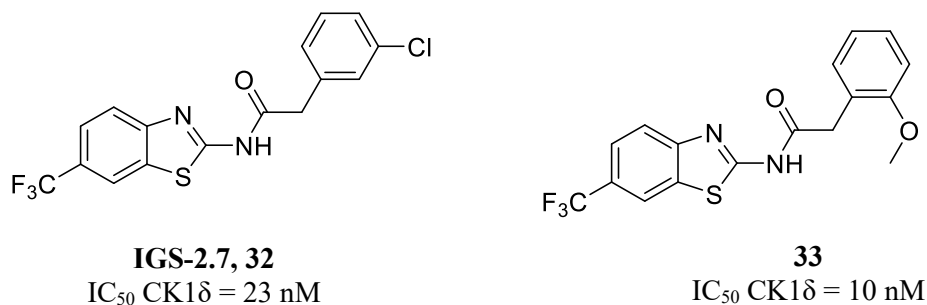
Figure 35: compounds 32 and 33 and their activities.

Compounds **32** displayed excellent selectivity profiles: it has been screened in a panel of 456 kinases at the concentration of 10 μM denoting a marked difference in percentages of binding (**Fig. 36**). [163]
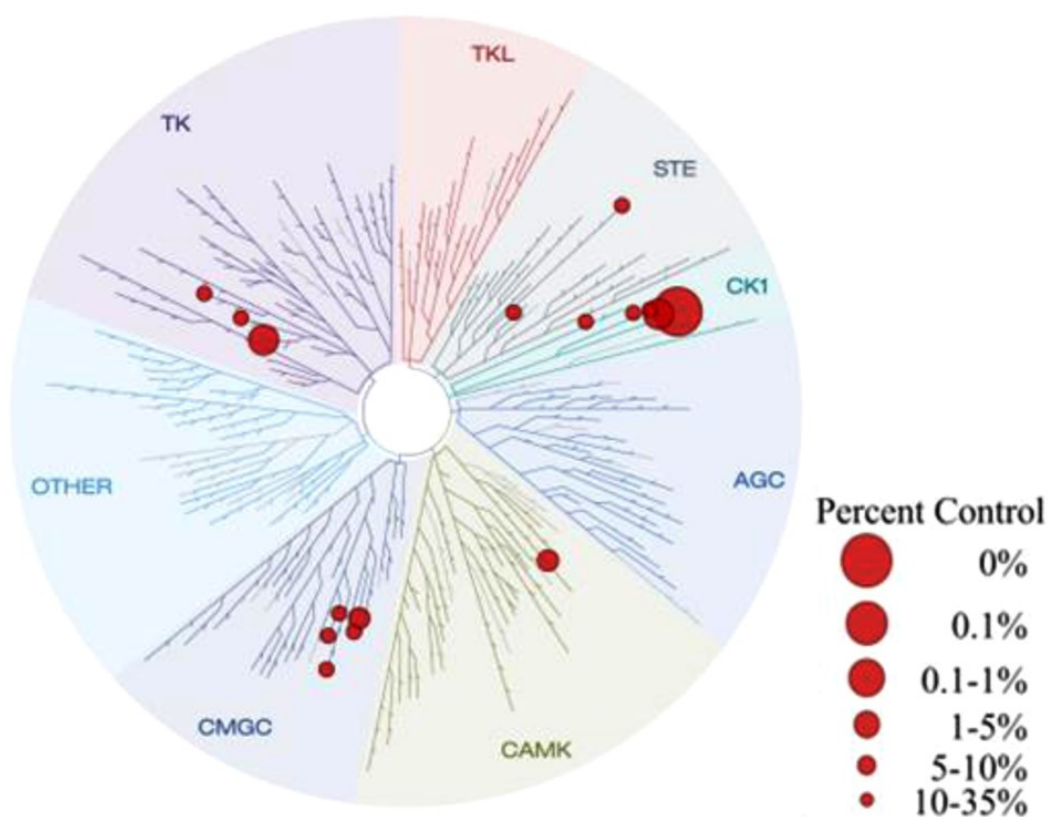
Figure 36: selectivity profile of compound 32 in a panel of 456 kinases. Data are shown in kinome tree; according to the legend, size of dots agrees with the % binding. The derivative was tested at the concentration of 10 μM. [163]

Moreover, compounds **32** and **33** have displayed druglike properties demonstrating to be able to cross BBB *in vitro* by conducting the BBB-PAMPA (BBB-Parallel Artificial Membrane Permeability Assay). Moreover, they test of compounds on HEK293 cell lines showed an increase in the prevention of TDP-43 phosphorylation and, to support the *in vitro* experiment, these two molecules have proved to be neuroprotective in transgenic Drosophila models of TDP-43 proteinopathies. [163]

Interestingly, the same research group of Martinez has published in 2021 the biological investigations on IGS-2.7 (**32**) as CK1δ inhibitor assaying it in human neuroblastoma cells and in transgenic mice. A decrease in pTDP-43 was detected in both *in vitro* and *in vivo* systems showing neuroprotective effects confirming IGS-2.7 (**32**) as a promising candidate for the study of ALS. [164]

1.6.3. Development of compounds with CNS-druglike properties

1.6.3.1. Estimation of passive transport through the blood brain barrier: Parallel Artificial Membrane Permeability Assay (PAMPA)

The development of CK1δ inhibitors for the potential treatment of neurodegenerative diseases implies the possibility to exploit their function at the central level. The blood brain barrier (BBB) separates brain from the rest of organism, and it is composed by endothelial cells and tight junctions. Transport mechanisms to overcome BBB comprise paracellular diffusion of water-soluble agents, transcellular diffusion that allows the passage through phospholipid barrier in favor of lipid soluble small molecules and carrier-mediated transport of molecules (active influx and active efflux carriers) applying suitable gradient concentration to support transporters. [165,166,167] BBB allows the preservation of the integrity of physiological conditions of central nervous system (CNS); when the homeostasis of BBB appears altered, commercial drugs and neurotoxic agents can enter at the central level determining injury progression, neuronal impairments and loss of central functions leading to damages of the BBB integrity and concomitant increase of CNS permeability. The result implies the exposition of BBB to pro-inflammatory cytokines contributing to determine neuroinflammation. To predict a possible passive transport through the BBB, Parallel Artificial Membrane Permeability Assay (PAMPA) can be performed: this test consists in an *in vitro* technique that simulates BBB using porcine lipids brain containing phosphatidylcholine and phosphatidylserine solved in inert organic solvent. The experiment is performed using a bicompartmental system and data are validated testing in the same plate 10 known commercial drugs whose results allow also to establish the cut-off values to categorize BBB permeable and BBB not permeable compounds. The solution of desired compound from the donor compartment permeates at the level of the acceptor one during the incubation time and the absorbance at the appropriate wavelengths is detected to obtain, after the elaboration, permeability coefficients of compounds (**Fig. 37**).[168,169,170,171]
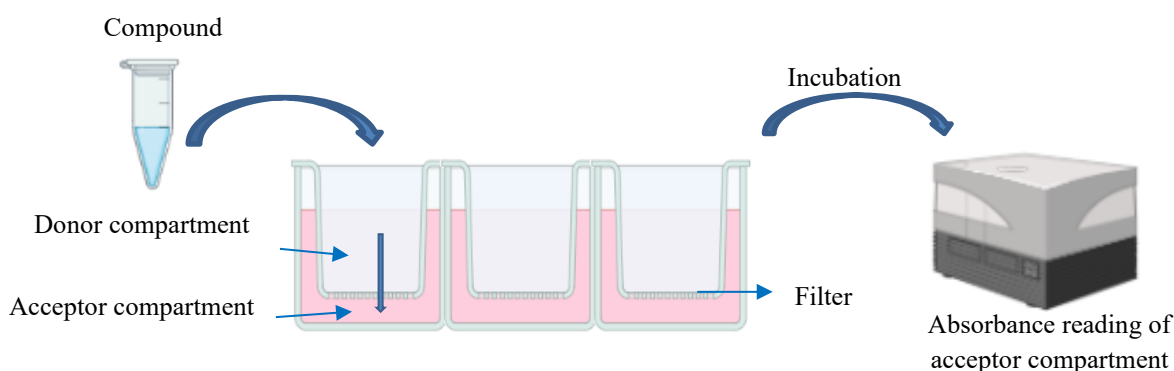
*Figure 37: schematic representation of PAMPA assay; compound inserted in the donor compartment permeates at the level of the acceptor one where buffer is present. The amount of compound is detected after the incubation time using absorbance mode. Image is made using **BioRender**.*

1.6.3.2. Druglike properties of compounds

Most of small molecules can enter at the level of CNS *via* passive diffusion across BBB. To allow brain uptake, the designed compounds must respect some parameters including molecular weight, lipophilicity, hydrogen bonding, polar surface area and charge and molecular flexibility. [166]

- Molecular weight: the passive diffusion is allowed at considerable small size molecules. Molecular mass could be settled in the range of 400-500 Da. [166]
- Lipophilicity: to across the BBB, small molecules must have lipophilic behavior. LogP, partition coefficient between *n*-octanol and water at pH of 7.4, is considered as an excellent indicator of BBB-permeation. The great majority of commercial drugs provides a value of log P in the range between -

0.05 and 6.0, consequently optimal values of logP to estimate lipophilicity stand between 1.5 and 2.7.
[166,172]

- Hydrogen bonding: the capability of a compound to establish hydrogen bonds should also be considered to predict a passive diffusion through the BBB. CNS+ drug candidates calculate a number <5 of H-bond donor and <10 of H-bond acceptor. [166]
- Polar surface area and charge: other chemical and physical properties result significant to the central permeation: generally, a high polar surface does not allow the CNS diffusion while the accepted range comprise molecules in the range of 60-90 Å. The charge of the candidate also results important an anionic charge is proved to be thermodynamically unfavorable to across the phospholipid barrier while interestingly, the presence of a tertiary amine with cationic charge in the small molecule improves the BBB-permeation. [166]
- Molecular flexibility: to predict a possible passive transport through the BBB, the number of rotatable bonds can be a useful filter. CNS+ candidates present five or less rotatable single bonds not connected to the main scaffold or to a non-terminal heavy atom. [166]

All the above discussed requirements provide an important framework for the design of druglike compounds from the point of view of solubility and absorption. The crucial parameter included is the lipophilicity, feature that presents a substantial linker with ADME properties, not only with absorption, but also with distribution, metabolism, and excretion and CNS permeation as attractive feature. [173,174] LogP or LogD are the parameters that express the property of lipophilicity: *c*logP or logD are the mostly used. *C*logP is a calculated (*c*) and predicted value evaluating properties of the molecules while logD is the measured parameter by partitioning compound in *n*-octanol and water at pH of 7.4. Arnott and co-workers have been resumed (**Table 4**) relationships between lipophilicity and ADME properties [175]:

Table 4: relationships between lipophilicity (ClogP and logD parameters) and ADME properties. [175] The highlighted values represent the CNS penetration property; - = not reported.

ADME properties	*C*logP values	logD values
Solubility	<3	-
Permeability	-1-5.9	<better
Bioavailability	0-3	1-3
Distribution	>better	-
CNS penetration	>better	1-3
>clearance	3-5	-
Toxicity	>3	-
CYP inhibition	<better	.

It is possible to correlate potency and lipophilicity using lipophilic ligand efficiency (LipE) as a parameter to estimate the druglikeness of a candidate:

$$LipE = -log\,(K_i \; or \; IC_{50}) - logD\,(or\,clogP)$$

where K_i or IC_{50} are expressed in molar units.

This parameter can be taken in account in the early phase of drug discovery trying to focus on the design potent and druglike compounds but also in the optimization phase searching for the lead derivative. It is clear that maintaining ideal values of *c*logP or logD of 1-3, LipE is increased for most potent compounds: the overview that provides an higher LipE represents the optimal situation for the druglike features of a candidate [173]

2. Aim of the work

The previous chapters have highlighted the key role of CK1δ in several pathological conditions and, in particular, in neurodegenerative diseases such as Alzheimer's and Parkinson's disorders and Amyotrophic Lateral Sclerosis. Over the course of years only a few candidates have succeeded in reaching clinical phases and for this reason the development of potent and druglike CK1δ inhibitors take on crucial importance to study deeply the target and to obtain steps forward in the design of potential candidates for the treatment of these pathologies. According to the literature, kinase domain appears to be conserved in kinome, therefore the current challenge is represented by the achievement of selective inhibitors; however, the ATP-binding site proves to be the most exploited region for the development of potential inhibitors.

This PhD research project is focused on the design of ATP-competitive CK1δ small molecules based both on new and known scaffolds to study a possible implication in the treatment of neurodegenerative diseases. Series of heteroaromatic derivatives has been developed exploiting three main strategies: metabolic-based design, simplification-based and new scaffold development.

1) **Metabolism-based**. The first series with benzo[*d*]thiazole (BT) as main nucleus has been achieved starting from riluzole (**34**), approved drug for ALS. Riluzole, whose complete mechanism of action is still unknown, has demonstrated to be active on CK1δ reporting an IC$_{50}$ of 16.1 μM. Since this candidate is subjected to a strong hepatic metabolism, the first purpose is the achievement of its N-hydroxylamine metabolite: the activity towards the target can establish an additional link between **34** and CK1δ corroborating the hypothesis linked to a possible mechanism of action of the candidate **34**. Another interesting precursor is the hydrazine derivative that, according to the computational studies, seems to be able to maintain the capability of binding the kinase. Therefore, a series of functionalized hydroxylamines has been developed to modify phase II metabolism given by the glucuronoconjugation of the riluzole's main metabolite. To outline a structure-activity relationship profile, also the corresponding hydrazine derivatives have been obtained (series **I**, **Panel A** of **Fig. 38**). **Synthesis and characterization of benzo[*d*]thiazole derivatives: a metabolism-based strategy**, reported in **chapter 3**.

2) **New scaffold-based**. A screening of in-house pyrazine compounds developed for completely different purposes has been conducted allowing to explore this new scaffold for the achievement of ATP-competitive CK1δ inhibitors. The versatility of the pyrazine scaffold allows to explore different substituents at the four positions of the nucleus (**II**, **Panel B** of **Fig. 38**), **Development of tri- and tetra-substituted pyrazines: new scaffold-based strategy**, reported in **chapter 4**.

3) **Simplification-based**. Applying a molecular simplification strategy, starting from [1,2,4]triazolo[1,5-*a*]triazine compound **35** (discussed in the **Appendix** of this thesis), a series of 1,3,5 triazine has been developed and the SAR profile has been outlined exploring different types of substituents (series **III**, **Panel C** of **Fig. 38**). The applied approach allows to simplify the synthetic pathway to obtain a quick achievement of SAR. **1,3,5-triazines as CK1δ inhibitors: a simplification strategy**, reported in **chapter 5**.

All compounds have been accompanied by biochemical and biological characterization considering the possible passive transport through the blood brain barrier as a requisite for the development of potential candidates exploiting their functions at the central level and neuroprotection assay using SH-SY5Y as cell line.
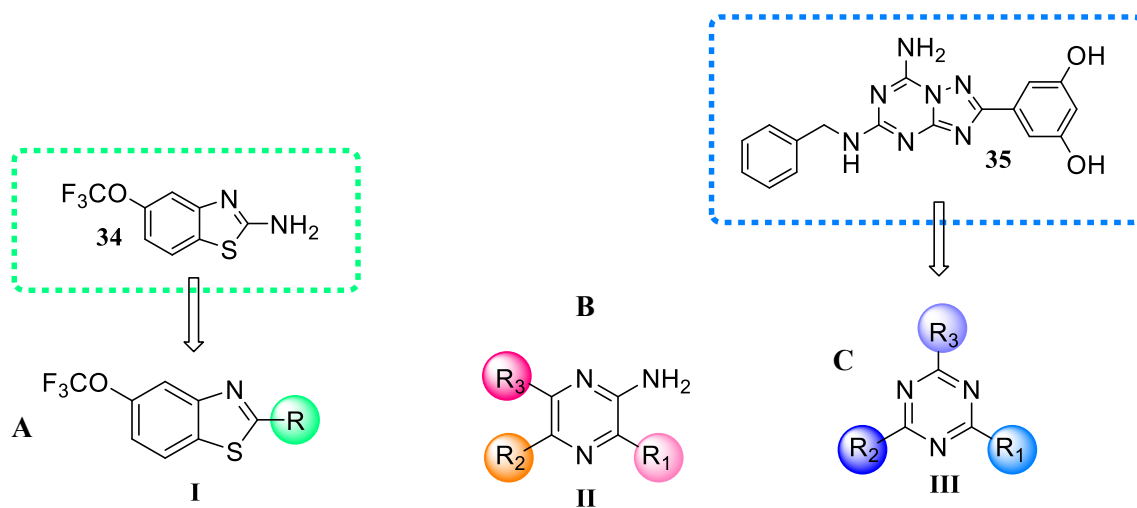
*Figure 38: heteroaromatic nuclei discussed in related chapters of this thesis: benzo[d]thiazole (**I**, **Panel A**), pyrazine (**II**, **Panel B**) and 1,3,5-triazine 2,4,6-trisubstituted (**III**, **Panel C**), respectively.*

3. Synthesis and characterization of benzo[d]thiazole derivatives: a metabolism-based strategy

3.1. Introduction

Riluzole (**Fig. 39**, compound **34**), approved by FDA in 1995 for ALS treatment, demonstrated to be able to reduce the excitotoxic effects of glutamate in brain, mitigating the disease progression given by depolarization and cell death. [176,177,178] Curiously, even if a lot of *in vitro* and *in vivo* studies were performed to fully explore how this drug works, the exact mechanism of action results still unclear. [176,179] Bissaro *et al*. in collaboration with our research group postulated using computational tools (predicted binding pose is reported in **Fig. 40**) and experimentally demonstrated a riluzole's activity on CK1δ finding an IC$_{50}$ value of 16.1 μM and, thus opening the possibility of elucidating the therapeutic profile of this hit compound. [180,181] Riluzole was found to interfere with the glutamatergic transmission by antagonizing the acetylcholine-induced release by N-methyl-D-aspartate (NMDA) *in vitro* even if it is not an antagonist of NMDA receptor. Moreover, it is able to block inactivated Na$^+$-channel inhibiting the glutamate release and the candidate has shown an *in vivo* improvement in ALS progression and the decrease of motoneuron loss. Nevertheless, the experimentally validated effects do not provide the trigger point, therefore the demonstration of its activity on CK1δ allows not only to deepen the mechanism of action but also to highlight the role of the kinase in ALS.
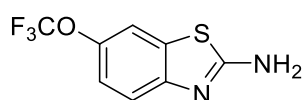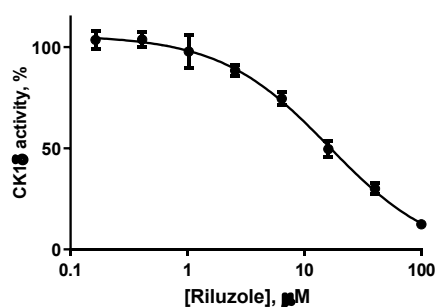
*Figure 39: structure of riluzole (**34**) and its activity on CK1δ (concentration/activity curve on the right).*

Riluzole (**34**) underwent strong liver and extrahepatic metabolism by cytochromes P450 CYP1A2 and CYP1A1 decreasing the bioavailability of the drug. The main metabolic pathways involve the hydroxylation of the phenyl ring of benzo[d]thiazole leading to compounds **36-38** and N-hydroxylation of nucleus at achieving metabolite RPR 112512 (**39**) that is subjected to quick glucuronoconjugation (**41**) by UDPG-T (Uridine 5'-diphospho-glucuronosyltransferase) (**Fig. 41**). Other phase I reactions can occur to a lesser extent resulting in the formation of oxidized dealkylated compound (**40**), ureido metabolite and cleavage product not reported in the figure but also unidentified metabolites are suspected. [177,179,182,183,184] Nowadays steps forward in understanding riluzole's mechanism of action would represent a big challenge since it is confirmed as a turning point in the ALS treatment.

3. Synthesis and characterization of benzo[d]thiazole derivatives: a metabolism-based strategy
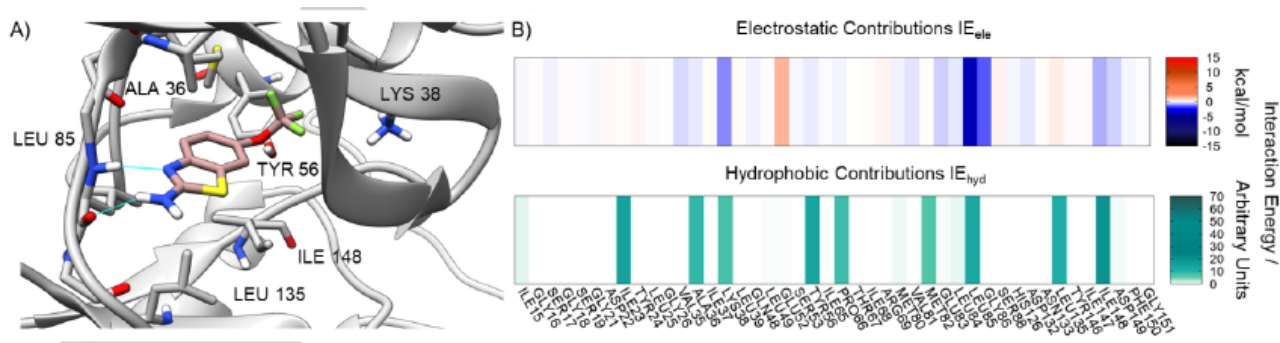
Figure 40: the panel A shows the predicted binding pose of riluzole (34) on CK1δ (PDB Code: 5OKT). Panel B displays the interaction energy fingerprint in which the electrostatic as well as hydrophobic contributions for each residue in the binding site of the kinase are reported. [180]
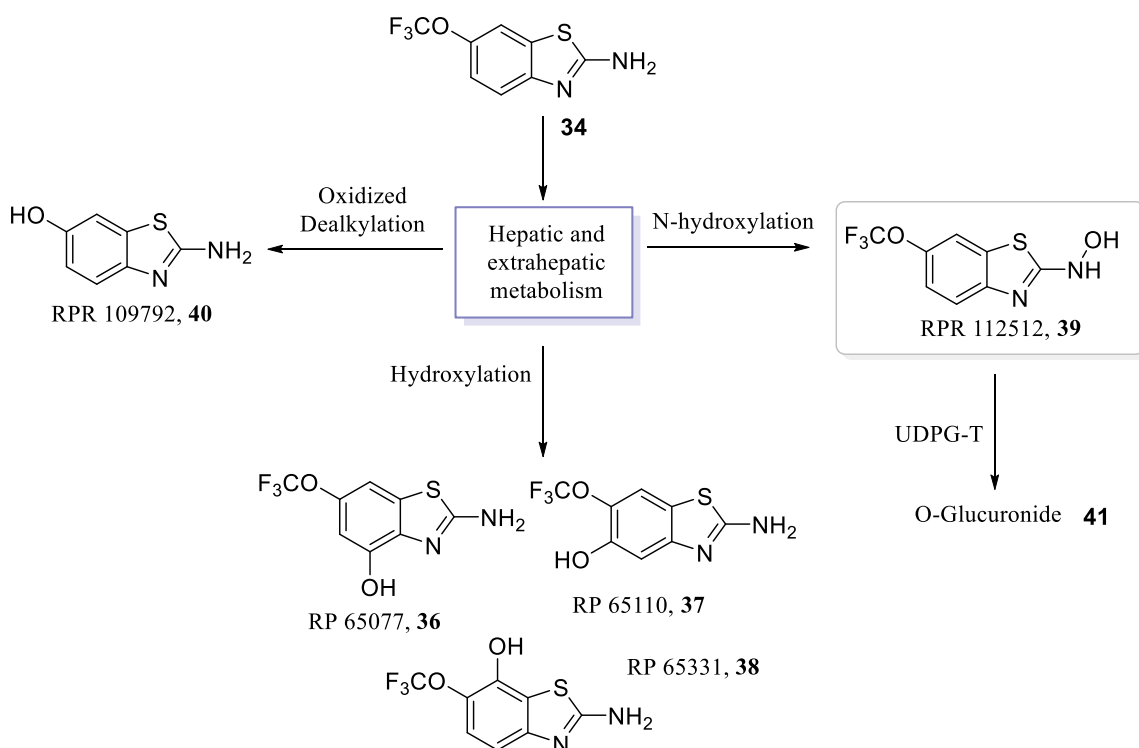
Figure 41: main phase I reactions underwent by riluzole (34) at the hepatic and extrahepatic levels leading to hydroxylated metabolites (36-38), N-hydroxylated one (39) and dealkylated metabolite (40).

3.2.   Aim of the work

The first goal is represented by the achievement of 2-hydroxylamino-benzo[d]thiazole (**39**), the main metabolite of riluzole, that from computational studies performed by University of Padua seems to conserve the capability of binding CK1δ (**Fig. 42**) and the validation of this hypothesis can establish an additional link between riluzole (**34**) and the kinase contributing to explain the mechanism of action of candidate **34** hypothesizing a CK1δ-mediated effect on SLA of candidate **34** and its metabolite **39**.
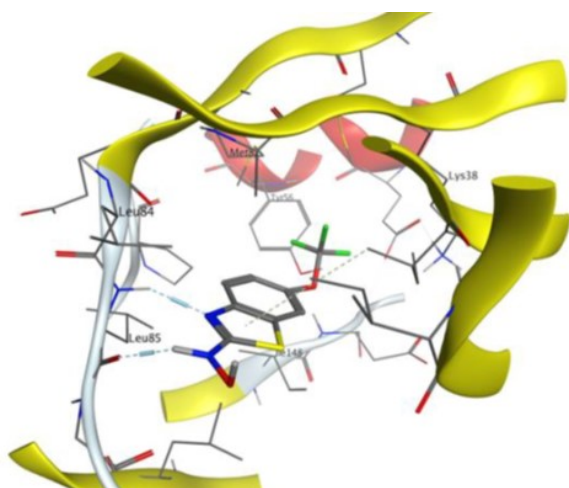
*Figure 42: predicted binding pose of hydroxylamine metabolite (**39**) of riluzole (**34**). The main nucleus seems to be able to establish interactions with Leu-84 and Lys-38 while the -NH establishes a hydrogen bond with Leu-85. PDB Code: 4HNF.*

In addition, a series of functionalized derivatives has been developed to modify the phase II metabolism of compound **39**; several evidences, in fact, were reported concerning the O-glucuronidation of this metabolite (**Scheme 2**) determining a quick elimination. [182] Thus, a series of 6-(trifluoromethoxy)benzo[d]thiazoles substituted at the 2-position with alkyloxylamino moiety has been developed with alkyl or arylalkyl groups with different size with the idea to modify the phase II metabolism and to obtain new potent candidates on CK1δ. Another focus involves the 2-hydrazineyl-6-(trifluoromethoxy)benzo[d]thiazole (**42**), the hydrazine derivative of riluzole, which is synthesized since, in accordance with the computational prediction, seems to maintain the capability of binding CK1δ (**Fig. 43**).

Several functionalized derivatives have been developed by substituting benzo[d]thiazole nucleus with different types of groups. Firstly, some substitutions to functionalize hydrazine, hydroxylamine or amino groups have been conducted to observe the activity of methyl-derivatives when the possibility of establishing hydrogen bonds is excluded (left side of **Fig. 44**). Then, different types of alkyl chains including linear and branched moieties and arylalkyl moieties have been inserted on main scaffold to functionalize hydroxylamine and hydrazine groups. Moreover, aromatic phenyl derivative has been developed for hydrazine series that has led to most promising results to study the optimal distance of the spacer between the hydrazine and phenyl ring (right side of **Fig. 44**). Some riluzole-like derivatives developed for this series have been reported in literature to obtain an "anti-glutamate" activity; in this work they have been investigated on CK1δ. [185] Therefore, a structure activity relationship profile has been outlined for functionalized derivatives. All the developed compounds have been tested on CK1δ and a biochemical and biological characterization has been carried out. The biological investigation has been conducted in CSIC of Madrid in Prof. Martinez group to establish a possible neuroprotective behavior of developed inhibitors and the detection of decreasing p-TDP-43 that is the main hallmark of the ALS in neuroblastoma cells (SH-SY5Y).

3. Synthesis and characterization of benzo[d]thiazole derivatives: a metabolism-based strategy
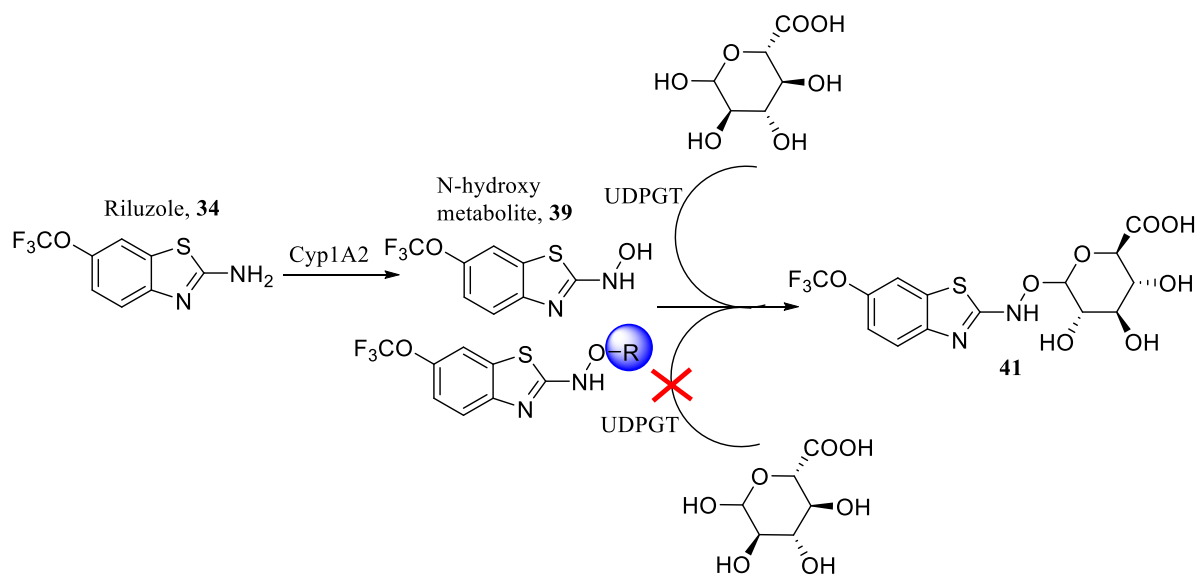
Scheme 2: O-glucuronidation of N-hydroxylamine metabolite (39) of riluzole (34).
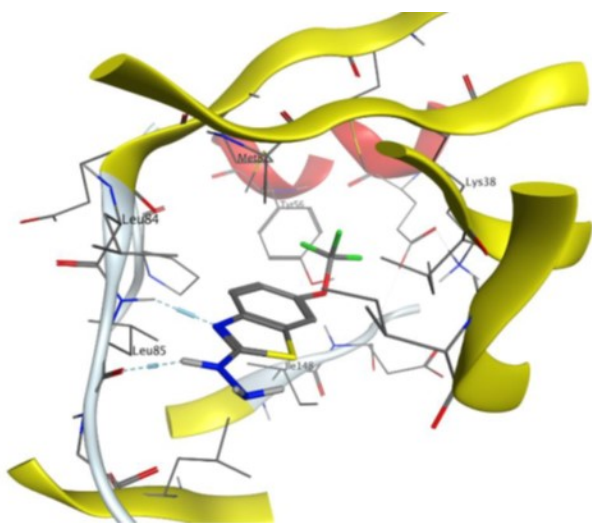
Figure 43: predicted binding pose of 2-hydrazineyl-6-(trifluoromethoxy)benzo[d]thiazole (42). Same interaction of the predicted binding pose of 39 are reported. PDB Code: 4HNF.
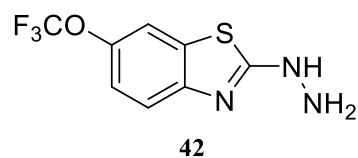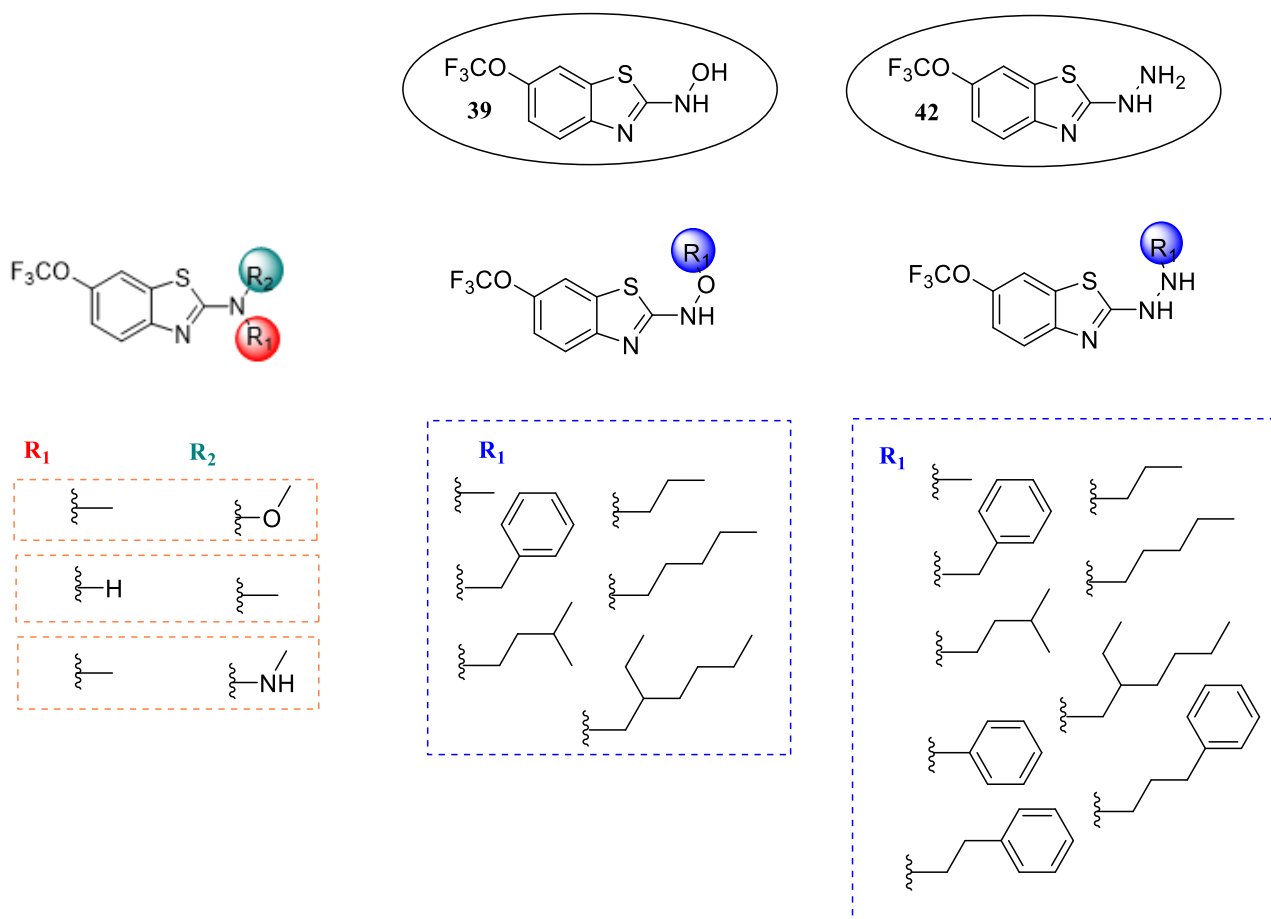
Figure 44: overview of substitutions conducted on benzo[d]thiazole nucleus.

3.3. Discussion

3.3.1. Chemistry

When hydroxylamine, hydrazine and amino moieties are commercially available, a simple nucleophilic substitution is conducted leading to the final products **39**, **42**, **44-47**. To explore different types of substituents, not commercial hydroxylamine chains were synthesized by a Gabriel reaction followed by hydrazinolysis (**53-58**). Regards the hydrazine moieties, the desired alkyl chain was inserted at di-*tert*-butyl hydrazine-1,2-dicarboxylate (**78**) leading to compounds **79-86**. The Boc-protected hydroxylamine and hydrazine alkyl chains were then reacted with 2-chloro-6-(trifluoromethoxy)benzo[d]thiazole (**43**) in a Buchwald-Hartwig Pd-catalyzed reaction (**65-70**, **87-94**). For compound **47** bearing an aryl hydrazine substituent, a nucleophilic substitution is conducted.

3.3.1.1. Synthesis of N-substituted-6-(trifluoromethoxy)benzo[d]thiazol-2-amine derivatives (39, 42, 44-47).

The synthesis of N-substituted-6-(trifluoromethoxy)benzo[d]thiazol-2-amine derivatives **39**, **42, 44-47** was performed according to **Scheme 3**. [186,187,188]
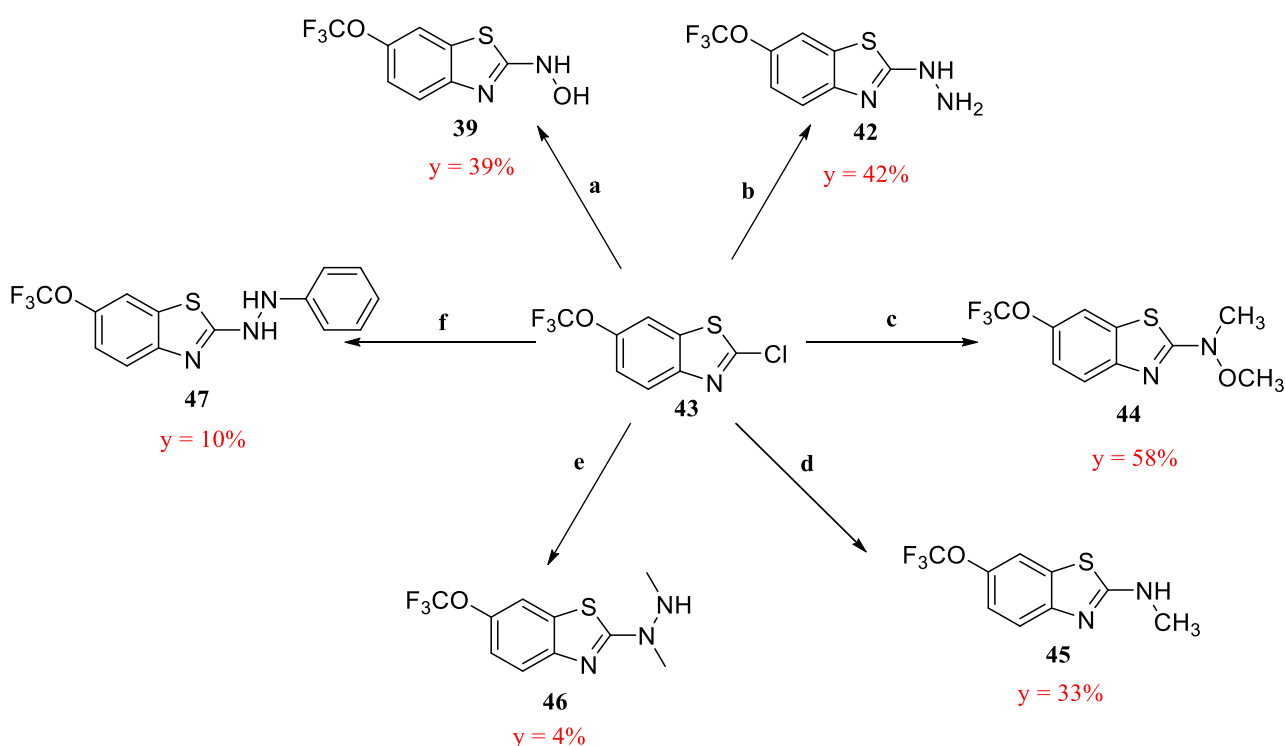
*Scheme 3: synthesis of N-substituted-(6-(trifluoromethoxy)benzo[d]thiazol-2-amine derivatives **39**, **42**, **44-47**. Reagents and conditions. **a**: NH₂OH·HCl, K₂CO₃, MeOH, 65°C, 4h, Ar; **b**: NH₂NH₂·H₂O, MeOH, rfx, 2h; **c**: NH(CH₃)OCH₃·HCl, Et₃N, BuOH, rfx, 24h; **d**: NH₂OCH₃·HCl, Et₃N, BuOH, MW, 150°C, 1h; **e**: CH₃NHNH₂, EtOH, rfx, 24h; **f**: NH₂NH₂Ph, BuOH, rfx, 3h; y = yield.*

Compounds **39**, **42**, **44-47** were obtained through a nucleophilic substitution between 2-chloro-6-(trifluoromethoxy)benzo[d]thiazole (**43**) and the corresponding hydroxylamino or hydrazino derivatives in alcohol (e.g. BuOH or MeOH) in the presence, when required, of a base. The achievement of compound N-(6-(trifluoromethoxy)benzo[d]thiazol-2-yl)hydroxylamine (**39**) appeared difficult since this derivative is unstable: for this reason, the reaction was performed applying specific conditions including carrying out the reaction under argon atmosphere and performing hydrochloride salt as fast as possible.

3. Synthesis and characterization of benzo[d]thiazole derivatives: a metabolism-based strategy

3.3.1.2. Synthesis of O-substituted-N-(6-(trifluoromethoxy)benzo[d]thiazol-2-yl)hydroxylamine hydrochloride derivatives (71-76)

O-alkylhydroxylamine derivatives were obtained starting from the Gabriel reaction between alkylhalides and N-hydroxyphthalimide (**48**), commercially available, in the presence of potassium carbonate as a base in dry DMF (N,N-dimethylformamide) to achieve 2-alkyloxyisoindoline-1,3-dione derivatives (**49-52**) that underwent hydrazinolysis *via* Ing-Manske procedure in THF (tetrahydrofuran) (**53-58**). [189] Given the volatility of alkylhydroxylamines, hydrochloride acid in 1,4-dioxane was then used to provide hydrochloride salts of previous mentioned compounds. To avoid the possibility of the formation of O-alkyl-N,N-bis(6-(trifluoromethoxy)benzo[*d*]thiazol-2-yl)hydroxylaminederivatives, the amino moiety of alkylhydroxylamines was protected with *tert*-butyloxycarbonyl group in acetonitrile using di-*tert*-butyl carbonate and triethylamine affording compounds **59-64**. [190] Coupling between *tert*-butyl alkyloxycarbamates (**59-64**) and 2-chloro-6-(trifluoromethoxy)benzo[*d*]thiazole (**43**), commercially available, was performed through a Buchwald-Hartwig amination using Pd$_2$(dba)$_3$ (bis(dibenzylideneacetone)palladium(0)) and DPPF (1,1'(bis(diphenylphosphino)ferrocene) as ligand in dry acetonitrile using cesium carbonate as base (**65-70**). [191,192] *Tert*-butyl alkyloxy(6-(trifluoromethoxy)benzo[*d*]thiazol-2-yl)carbamate derivatives were than deprotected *via* the development of *in situ* hydrochloride acid from acetyl chloride and methanol or using hydrochloride acid in 1,4-dioxane to provide the hydrochloride salts of final compounds **71-76 (Scheme 4)** to try different conditions for the Boc-deprotection.
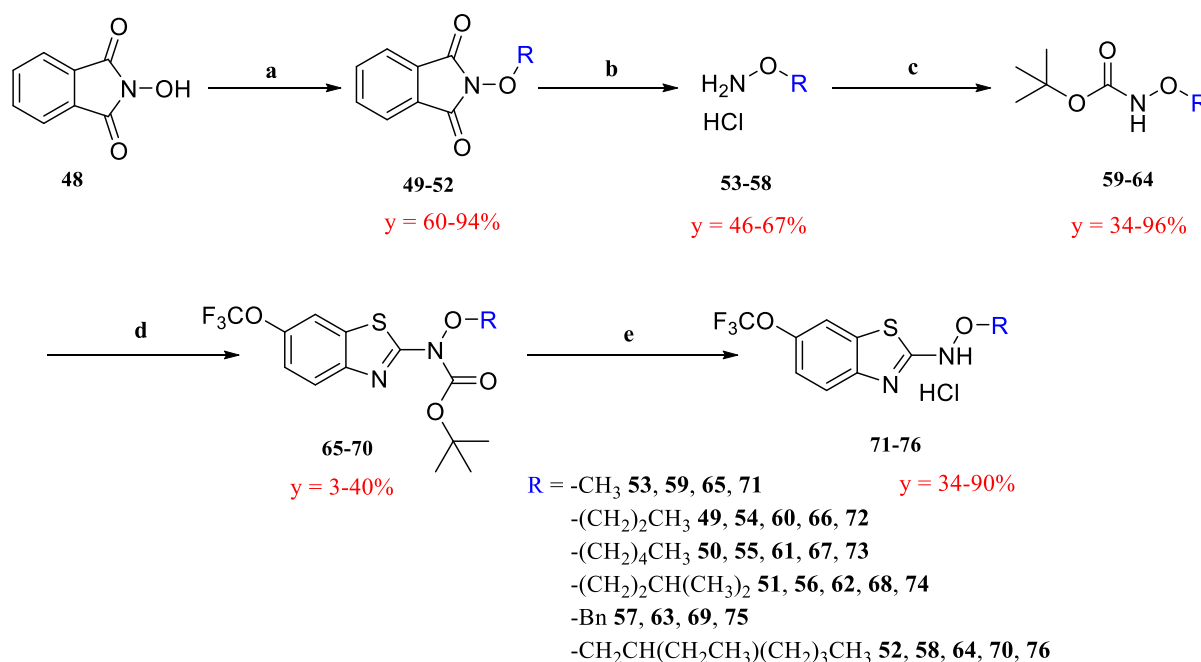
*Scheme 4: synthesis of O-substituted-N-(6-(trifluoromethoxy)benzo[d]thiazol-2-yl)hydroxylamine hydrochloride derivatives **71-76**. Reagents and conditions. **a**: RBr, K$_2$CO$_3$, dry DMF, Ar, rt, 72 h; **b**: NH$_2$NH$_2$·H$_2$O, THF, rt, 12 h; HCl in 1,4-dioxane, rt, 5 min; c: Et$_3$N, CH$_3$CN, rt, 90 min; Boc$_2$O, Et$_3$N, CH$_3$CN, rt, 12 h; **d**: 2-chloro-6-(trifluoromethoxy)benzo[d]thiazole (**43**), Pd$_2$(dba)$_3$, DPPF, Cs$_2$CO$_3$, dry CH$_3$CN, 40°C, 12h; **e**: AcCl, MeOH, EtOAc, 0°C to rt, 12h (compounds **71, 73-76**) or HCl in 1,4-dioxane, rt, 1h (compound **72**); y = yield.*

3.3.1.3. Synthesis of 2-(2-alkylhydrazineyl)-6-(trifluoromethoxy)benzo[d]thiazole hydrochloride derivatives (95-102)

Di-*tert*-butyl hydrazine-1,2-dicarboxylate (**78**) was obtained from the protection of *tert*-Butyl carbazate (**77**) using di-*tert*-butyl carbonate. The α-branching di-substituted hydrazines were then performed through a

nucleophilic reaction from alkyl halide in the presence of cesium carbonate as a base in dry DMF affording compounds **79-86**. [193] To introduce alkyl hydrazine moiety in 6-(trifluoromethoxy)benzo[d]thiazole nucleus (**43**) a Palladium-catalyzed Buchwald-Hartwig was conducted using Pd$_2$(dba)$_3$ and DPPF as ligand with toluene increasing the temperature (**87-94**). [192] The 2-(2-alkylhydrazineyl)-6-(trifluoromethoxy)benzo[d]thiazole hydrochloride derivatives **95-102** were obtained using the same conditions described above *via* HCl-mediated removal of *tert*-butoxy carbonyl group (**Scheme 5**).
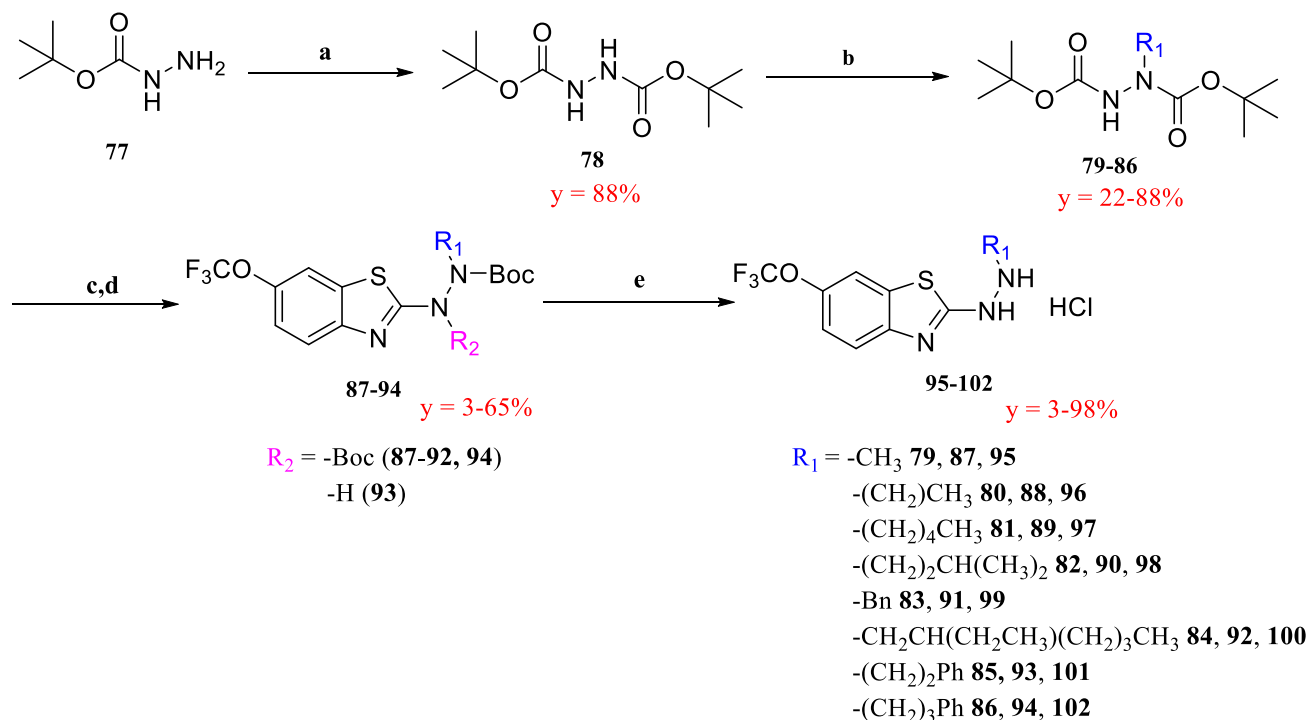
Scheme 5: *Synthesis of 2-(2-alkylhydrazineyl)-6-(trifluoromethoxy)benzo[d]thiazole hydrochloride derivatives* **95-102**. *Reagents and conditions.* **a**: *Boc$_2$O, neat, rt, 10 min;* **b**: *R$_1$X, Cs$_2$CO$_3$, dry DMF, rt, 12 h, Ar;* **c**: *2-chloro-6-(trifluoromethoxy)benzo[d] thiazole (**43**), Pd$_2$(dba)$_3$, DPPF, Cs$_2$CO$_3$, dry CH$_3$Ph, 110°C, 12 h, Ar;* **d**: *2-chloro-6-(trifluoromethoxy)benzo[d]thiazole (**43**), Pd$_2$(dba)$_3$, DPPF, Cs$_2$CO$_3$, dry CH$_3$Ph, 60°C, 12 h, Ar;* **e**: *AcCl, MeOH, EtOAc, 0°C to rt, 12 h **or** HCl in Et$_2$O, rt, 1 h; y = yield.*

3.3.2.   Structure-activity relationship (SAR) studies

An immediate SAR representation can be given by the SALI (Structure Activity Landscape Index) plot: a correlation between potency of molecules and their structure similarity. It appears as a graphical representation of a dataset of molecules in which changes in activity are reflected in structural variation. In this SAR landscape, pairwise analysis leads to edges that indicate structure-activity cliffs and each edge connects molecules with chemical similarity represented by nodes. Therefore, the correlation of SALI values of a dataset of compounds allows to create a relationship between the diversity of substituents introduced in the main scaffold and changes in the activity. SALI values are calculated as reported below [194]:

$$SALI_{i,j} = |Ai - Aj| / 1 - sim_{i,j}$$

where A indicates the activities of molecules i-j and sim the Tanimoto coefficient of similarity between the compounds. The Tanimoto coefficient (Tc) is calculated as follows: Tc = C/ (A+B-C) in which A and B are bit sets of two molecules evaluating their fingerprints and C represents bits appearing in both the fingerprints. Values are given in a range of 0 (no bits in common) -1 (all bits are common). [194]

3. Synthesis and characterization of benzo[d]thiazole derivatives: a metabolism-based strategy

It is possible to appreciate in **Figure 45** the change in IC$_{50}$ introducing different size and nature of substituents. In this case, the edges are colored according to the activity of compound and the size changes in agreeing with the LipE (lipophilicy efficiency) value discussed in the following section. The upper left side of the plot is represented by more active and similar compounds indicating the achievement of homogeneous SAR profile exploring similar alkyl chains and substituents. In this part of the graph best compounds **98-99** are displayed and, moreover pentyl derivatives **73** and **97** as well as propyl hydrazine compound **96** and phenyl and arylalkyl candidates **47**, **101-102** are reported. Observing the plot, it is possible to note a correlation between the precursors (**39**, **42**) of the series disconnected to the main group of the representation and the Boc-protected derivatives (**69**, **91**) in the upper right side of the graph depicted with smaller edges, therefore with negative LipE, thus with non-druglike properties, and lower potency.
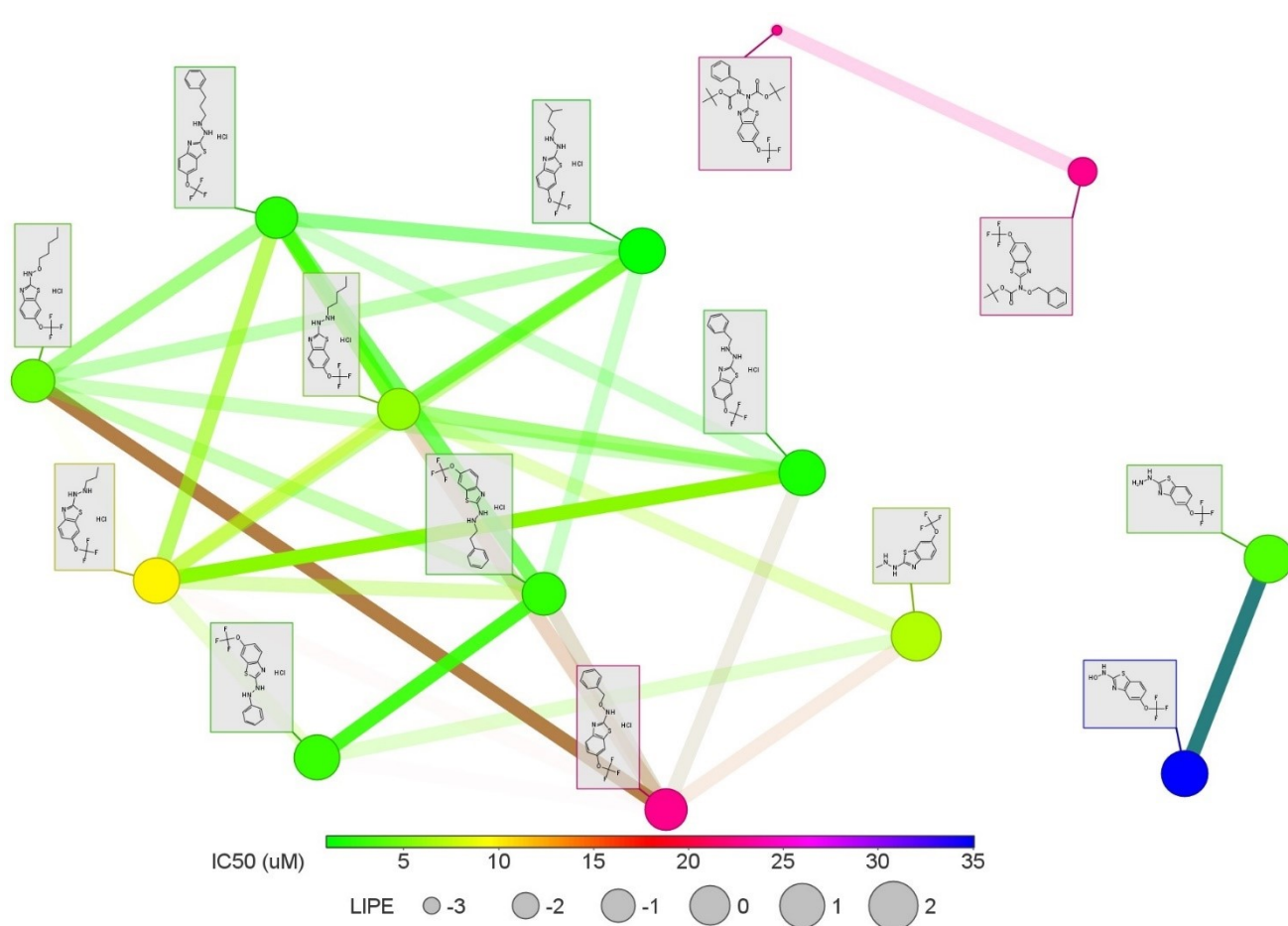
Figure 45: SALI representation of active compounds of the series. Colors of edges agree with IC$_{50}$ values of derivatives while the size of dots changes according to LiPE values. Image created using DataWarrior 3.5.0.

Synthesized compounds have been firstly tested on truncated CK1δ (aa 1-294) at fixed concentration of 40 μM by using luminescence kinase assay that exploits a coupled reaction: the ATP that has not been consumed by kinase is proportional to the luminescence signal detected. For compounds that displayed an activity percentage less than 50% at the concentration of 40 μM, IC$_{50}$s have been performed. Thus, alkyl chains, linear and branched, as well as arylalkyl and phenyl moieties have been inserted at the main scaffold to develop functionalized derivatives. As reported in the **Table 4**, the N-hydroxy metabolite **39** has showed an IC$_{50}$ value of 35.1 μM: this inhibitory activity in the micromolar range agrees with the reported one for riluzole (**34**) (IC$_{50}$ = 16.1 μM). [180] According to the computational studies, the 2-hydrazineyl-6-(trifluoromethoxy)benzo[*d*]thiazole derivative (**42**) maintains the capability to inhibit CK1δ, surprisingly it

exhibited a higher inhibitory potency compared to compound **39**, showing an IC$_{50}$ of 3.64 μM. The substitution of the hydroxy group of compound **39** with a methyl moiety (compound **45**) has resulted in non-active derivative towards CK1δ at the concentration of 40 μM. The substitution of both -NH and -OH in hydroxylamino series with alkyl moieties like in N,O-dimethyl compound **44** or like N,N-dimethyl hydrazino compound **46** has determined inactive derivatives.
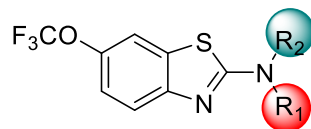
39, **42**, **44-47**

*Table 4: IC$_{50}$s of compounds **39, 42, 44-46**.*

Cmpd	R$_1$	R$_2$	IC$_{50}$ μM^a (% activity at 40 μM)^b
39	-H	-OH	35.1 ± 4.0
42	-H	-NH$_2$	3.64 ± 0.58
44	-CH$_3$	-OCH$_3$	n.d. (102% ± 9)
45	-H	-CH$_3$	n.d. (52.3% ± 0.9)
46	-CH$_3$	-NCHCH$_3$	n.d. (68.2% ± 4.4)

^{a} *Data represent the mean ± SD of three independent experiments performed in technical duplicate.* ^{b} *Data represent the % of activity at 40 μM concentration expressed as a mean ± SD of two independent experiments performed in technical duplicate; n.d.: not determined.*

As showed in **Tables 5** and **6**, maintaining free amino groups, linear chains such as methyl or propyl inserted at the hydroxylamino moiety led to inactive compounds (**71-72**) while the same substitutions at the hydrazine group determined IC$_{50}$s in the micromolar range, IC$_{50}$ = 6.77 μM (**95**) and 9.89 μM (**96**), respectively. Increasing the number of carbon atoms with pentyl chain, both hydroxylamine and hydrazine derivatives resulted active: compound **73** displayed an IC$_{50}$ of 4.40 μM and compound **97** a similar activity of 5.81 μM. Changing the size of substituent, a branched alkyl chain was inserted; ethylhexyl moiety proved to be too bulky revealing inactive derivatives (**76**, **100**) as well as with *tert*-butyloxycarbonyl moiety as R$_1$ substituent in precursors **70** and **92**. On the contrary, the introduction of isopentyl chain on hydrazine group gave the best potent compound of the series with an IC$_{50}$ in the submicromolar range of 0.92 μM (**98**), while the same substitution for hydroxylamino series in compound **74** led again to an inactive compound. To asses if arylalkyl group affected a possible result in terms of potency, benzyl was introduced in 6-(trifluoromethoxy)benzo[*d*]thiazol nucleus and again it is possible to observe a low micromolar activity of 1.62 μM for hydrazine derivative (**99**), while substitution at hydroxylamine compound with the same arylalkyl chain (**75**) revealed an IC$_{50}$ of 22.6 μM. Surprisingly, intermediates of compounds **75** and **99**, containing one or two *tert*-butyloxycarbonyl protecting group on nitrogen atoms, derivatives **69** and **91**, respectively, preserved inhibitory activity against kinase, even if potency was low, about 22 μM.

3. Synthesis and characterization of benzo[d]thiazole derivatives: a metabolism-based strategy

*Table 5: inhibitory activities of compounds **69-76** on CK1δ.*

Cmpd	R_1	R_2	IC_{50} µM [a] (% activity at 40 µM)[b]
71	-H	-CH$_3$	n.d. (52.6% ± 2.8)
72	-H	-propyl	n.d. (95.9% ± 9.5)
73	-H	-pentyl	4.40 ± 0.21
74	-H	-isopentyl	n.d. (96.9% ± 3.2)
75	-H	-Bn	22.6 ± 12.4
76	-H	-ethylhexyl	n.d. (60.8% ± 10.4)
69	-Boc	-Bn	22.8 ± 5.3
70	-Boc	-ethylhexyl	n.d. (95.9% ± 5.2)
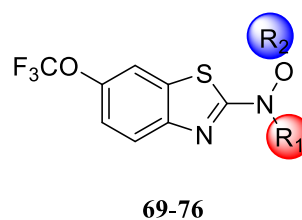
69-76

[a] Data represent the mean ± SD of three independent experiments performed in technical duplicate. [b] Data represent the % of activity at 40 µM concentration expressed as a mean ± SD of two independent experiments performed in technical duplicate; n.d.: not determined.

*Table 6: inhibitory activities of compounds **91-92**, **95-102** on CK1δ.*

Cmpd	R_1	R_2	R_3	IC_{50} µM [a] (% activity at 40 µM)[b]
95	-H	-H	-CH$_3$	6.77 ± 1.21
96	-H	-H	-propyl	9.89 ± 2.83
97	-H	-H	-pentyl	5.81 ± 0.74
98	-H	-H	-isopentyl	0.92 ± 0.09
99	-H	-H	-Bn	1.62 ± 0.29
100	-H	-H	-ethylhexyl	n.d. (85.5% ± 6.2)
91	-Boc	-Boc	-Bn	22.70 ± 5.40
92	-Boc	-Boc	-ethylhexyl	n.d. (85.4% ± 4.7)
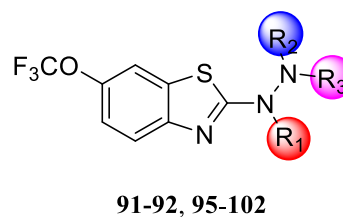
91-92, 95-102

[a] Data represent the mean ± SD of three independent experiments performed in technical duplicate. [b] Data represent the % of activity at 40 µM concentration expressed as a mean ± SD of two independent experiments performed in technical duplicate; n.d.: not determined.

Concentration-inhibition curves of most promising compounds (**98-99**) are reported in **Fig.46 (Panel A** and **B**, respectively)**.
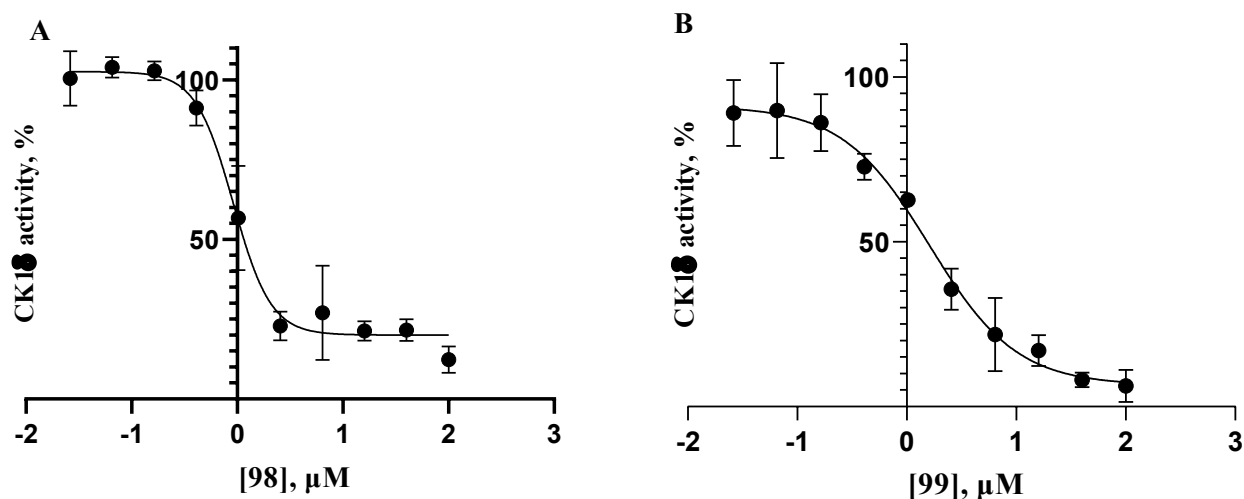
*Figure 46: concentration-inhibition curves of compounds **98** (**Panel A**) and **99** (**Panel B**).*

Giving the promising activity of compound **99** that reported IC_{50} of 1.62 µM, the investigation of the optimal distance of the spacer between phenyl ring and hydrazine moiety has been established developing the phenylethyl (**101**) as well as phenylpropyl (**102**) and the direct substitution with the simple phenyl giving compound **47**. As reported in **Table 7**, compounds **47, 101-102** displayed comparable IC_{50}s in the range of 2 µM, for comparison, also the already reported compound **99** has been inserted in this table, suggesting that the optimal distance between main nucleus and phenyl ring was reached with compound **99** that provided 1C-spacer showing the activity of 1.62 µM even if the reported IC_{50}s for derivatives **47, 101-102** are comparable.

*Table 7: inhibitory activities of compounds **47, 101-102** on CK1δ.*

Cmpd	R_1	IC_{50} µM [a]
47	-Ph	2.67 ± 1.10
99	-(CH₂)Ph	1.62 ± 0.29
101	-(CH₂)₂Ph	2.52 ± 0.59
102	-(CH₂)₃Ph	2.30 ± 0.32
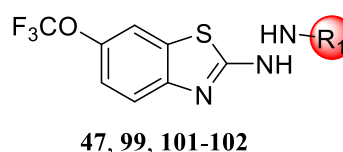
47, 99, 101-102

[a] *Data represent the mean ± SD of three independent experiments.*

3.3.3.   Evaluation of LipE profile of the series

The designed compounds were analyzed considering their LipE values discussed in the introductive chapter trying to estimate druglike properties. The plot reported in **Fig. 47** enclosed all the active compounds of the series with benzo[*d*]thiazole nucleus. In x and y axis, *C*log P and pIC$_{50}$ are indicated, respectively while in z axis LipE values are given, and the labeled dots are colored agreeing with the activity.
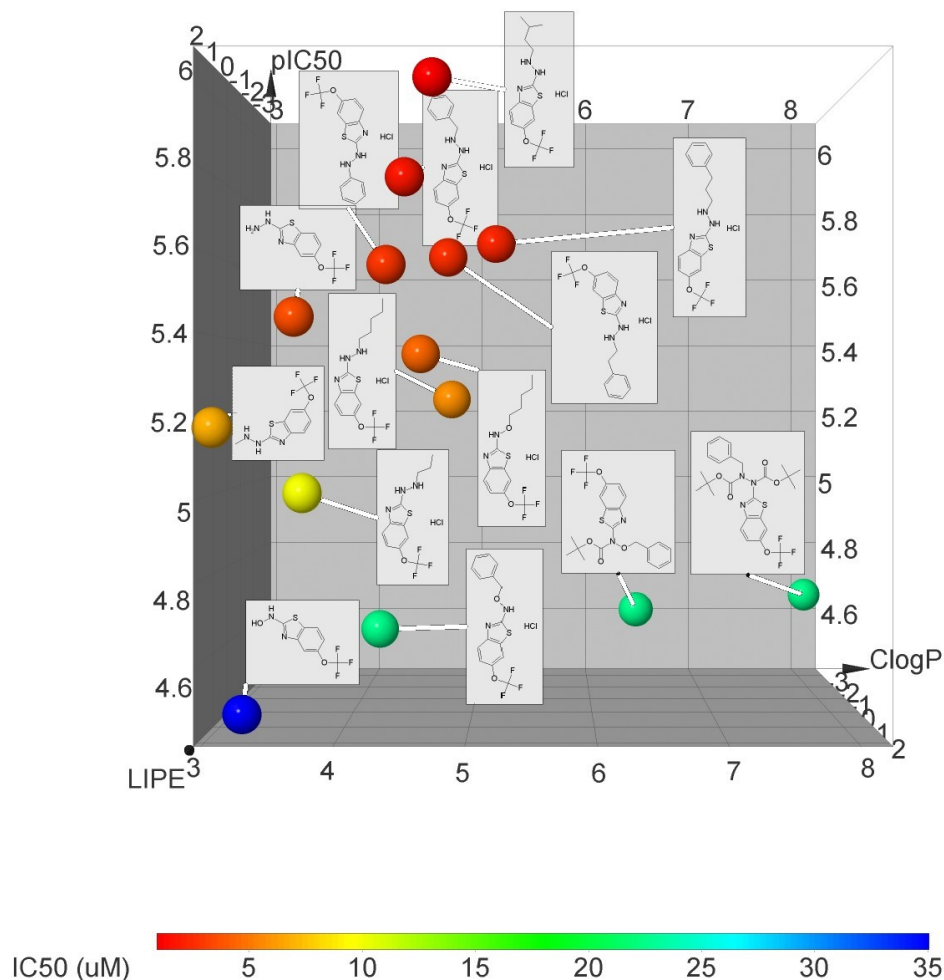
Figure 47: LiPE plot made using DataWarrior 3.5.0; in x and y axis ClogP and pIC$_{50}$ are reported while in z axis LiPE values of compounds are given. According to IC$_{50}$s of derivatives, colors of the labeled dots are chosen as represented in the color code below the figure.

In the upper left side of the graph compounds with best activity and higher LipE (z axis of the graph, reported in the **Panel A** of **Fig. 48**) are located; among them, hydrazine precursor **42** and isopentyl derivative **98** appear as well as compounds **47**, **99**, **101** and **102** just discussed. Considering their location in the 3D plot, these derivatives provide the best LipE values of the series. Nevertheless, LipE is obtained assuming both potency and ClogP that must be included in the range 1-3 to obtain desired druglike features. [175] Observing the **Panel B** of **Fig. 48**, all of the mentioned derivatives report a high value of *C*logP but, considering their potency, they achieve good LipE values. Interestingly, the light blue highlighted derivatives **39** and **95**, the hydroxylamine metabolite of riluzole (**39**) and the methylhydrazine compound, respectively, that report a poor potency towards CK1δ, display great *C*logP, thus great LipEs providing promising druglike properties. On the contrary, the opposite part of the graph is characterized by Boc-protected derivatives with negative LipE values given by a too high *C*logP and low potency.

A

LiPE plot

B

Cmpd	ClogP
39	3.2
42	3.7
47	4.3
73	4.6
95	3.1
96	3.7
97	4.8
69	6.4
75	4.3
98	4.7
91	8.1
99	4.5
101	4.8
102	5.2
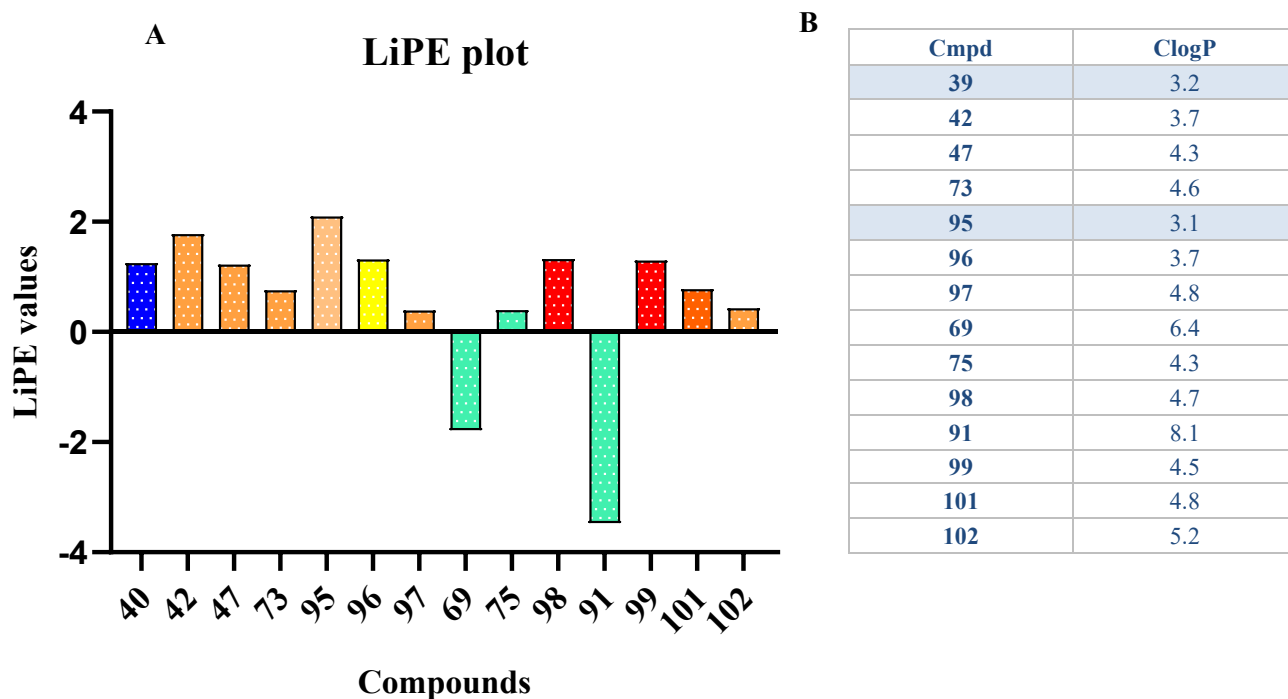
*Figure 48: LiPE values of active compounds are reported in panel A. Histogram made with GraphPad Prism 8.0. Panel B shows ClogP values, calculated with ChemDraw Professional of compounds **40, 42, 47, 69, 73, 75, 95-102**.*

3.3.4. Stability tests

Compounds **39** and **98**, in the view of performing a biological characterization, were investigated about their stability in solution since, mainly hydroxylamine candidate **39** has proved to be very unstable. Runs in HPLC-MS of derivatives **39** and **98** were performed every hour for the first day, every day for a week and then every week for a month maintaining compounds in DMSO, which is the solvent more suitable for biological assays, at room temperature and diluting with water for the injection. The first run carried out displayed a purity of 95.70% and 100.00% for compounds **39** and **98**, respectively, as reported in **Fig. 49** and **50**.
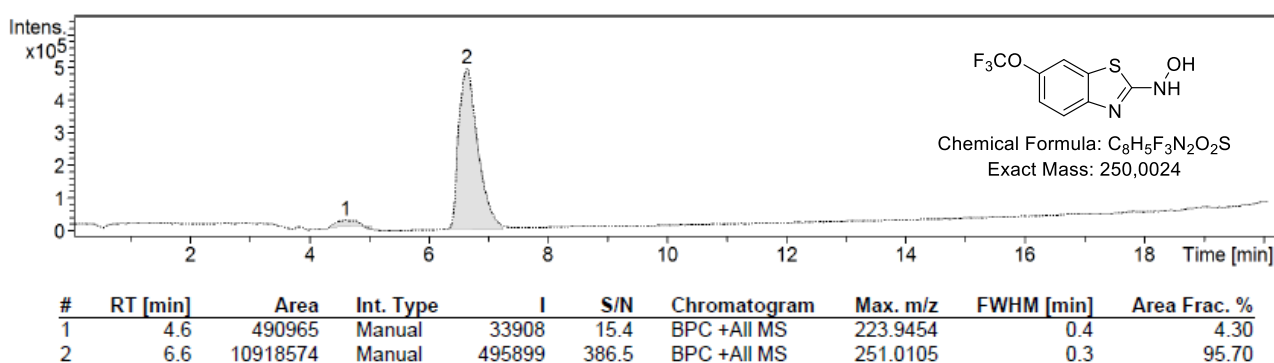
Chemical Formula: $C_8H_5F_3N_2O_2S$
Exact Mass: 250,0024

#	RT [min]	Area	Int. Type	I	S/N	Chromatogram	Max. m/z	FWHM [min]	Area Frac. %
1	4.6	490965	Manual	33908	15.4	BPC +All MS	223.9454	0.4	4.30
2	6.6	10918574	Manual	495899	386.5	BPC +All MS	251.0105	0.3	95.70
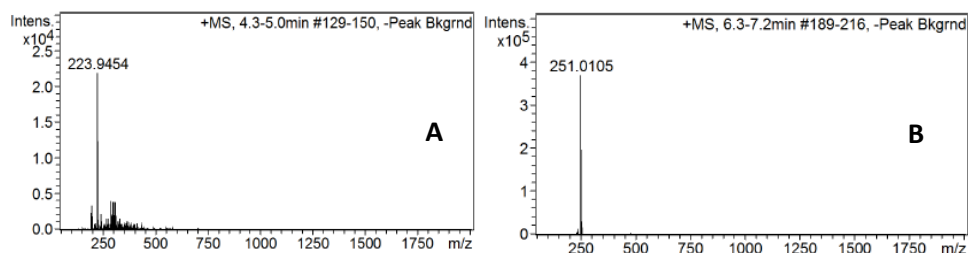
*Figure 49: HPLC-MS chromatogram of compound **39** at t = 0. Purity reported of 95.70%. Below the chromatograms, masses of the two peaks observed are given (overview **B** reports the mass of the candidate **39**). Specific conditions of the experiment are given in the experimental chapter.*

#	RT [min]	Area	Int. Type	I	S/N	Chromatogram	Max. m/z	FWHM [min]	Area Frac. %
1	15.2	247533104	Manual	6554707	3485.4	BPC +All MS	320.1033	0.6	100.00
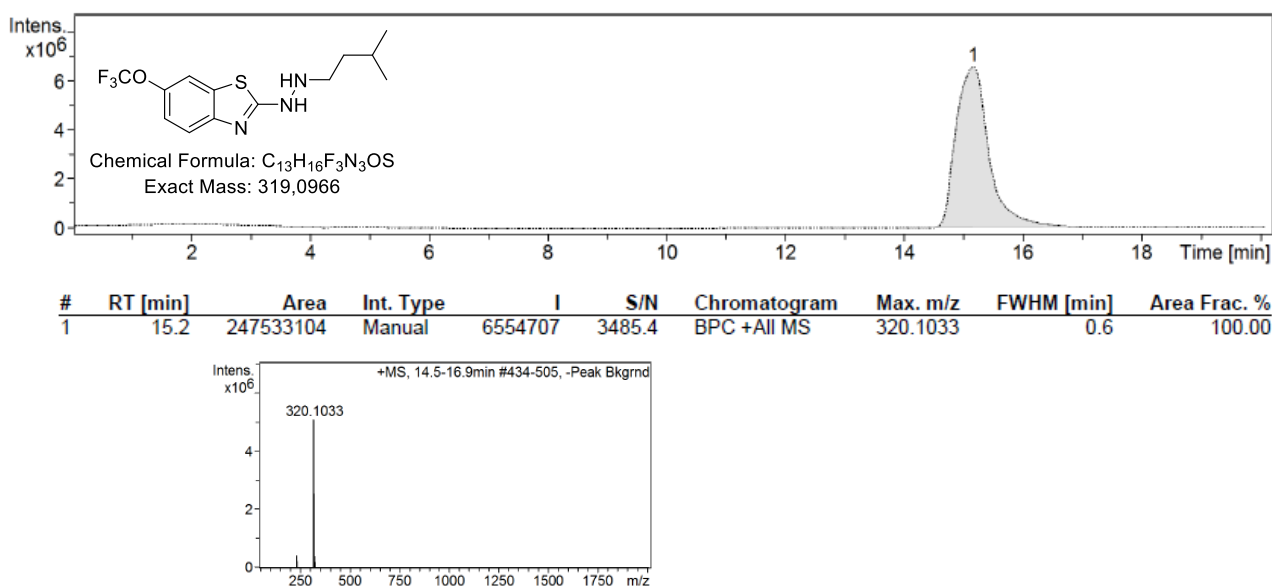
*Figure 50: HPLC-MS chromatogram of compound **98** at t = 0. Purity reported of 100.00%. Below the chromatogram, the mass of peak observed is given and agrees with the molecular weight of the candidate.*

During the time, compound **39** is subjected to changes in the color; curiously not appreciated by the UV spectrum of the sample registered at the initial time (T_0) and final time (T_f) (**Fig. 51**, **Panels A** and **B**).

A UV-spectrum compound 39 T$_0$

B UV-spectrum compound 39 T$_f$
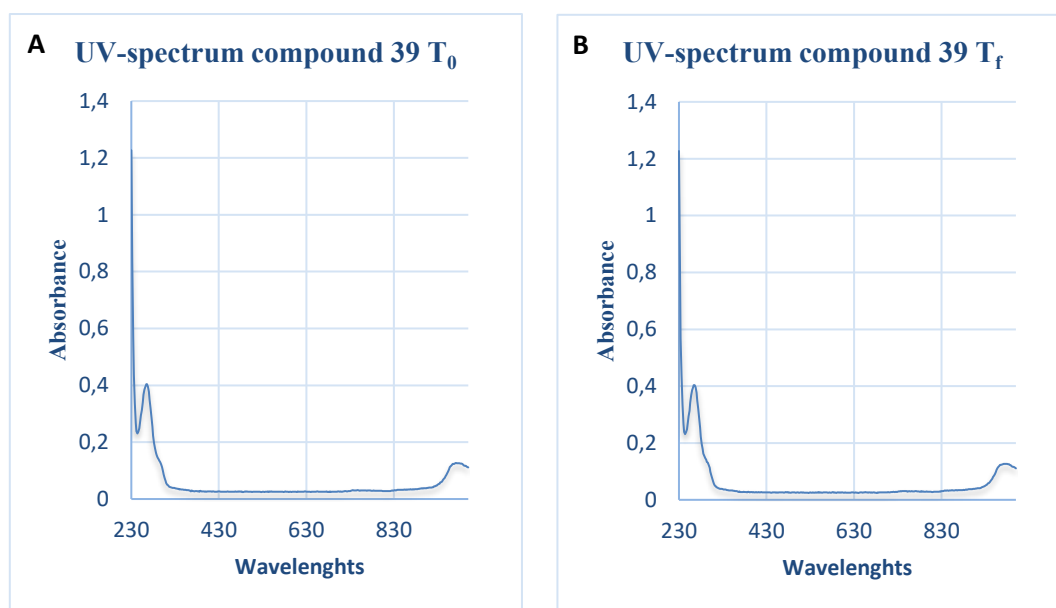
*Figure 51: UV-spectra of compound **39** over the time: T$_0$ = initial time (Panel A) and T$_f$ = final time, 28 days (Panel B)*

Compounds underwent degradation during the month of investigation. In fact, in **Fig. 52** and **53,** which report the final runs registered after a month in solution, the hydroxylamine candidate (**39**) has reported a purity of 81.67%, significantly decreased in comparison to the first registered but conditions must take in consideration since the unstable compound has been stored in solution at room temperature. Instead, compound **98** has proved to be more stable, its purity decreased to 93.77% after one months under the same conditions.
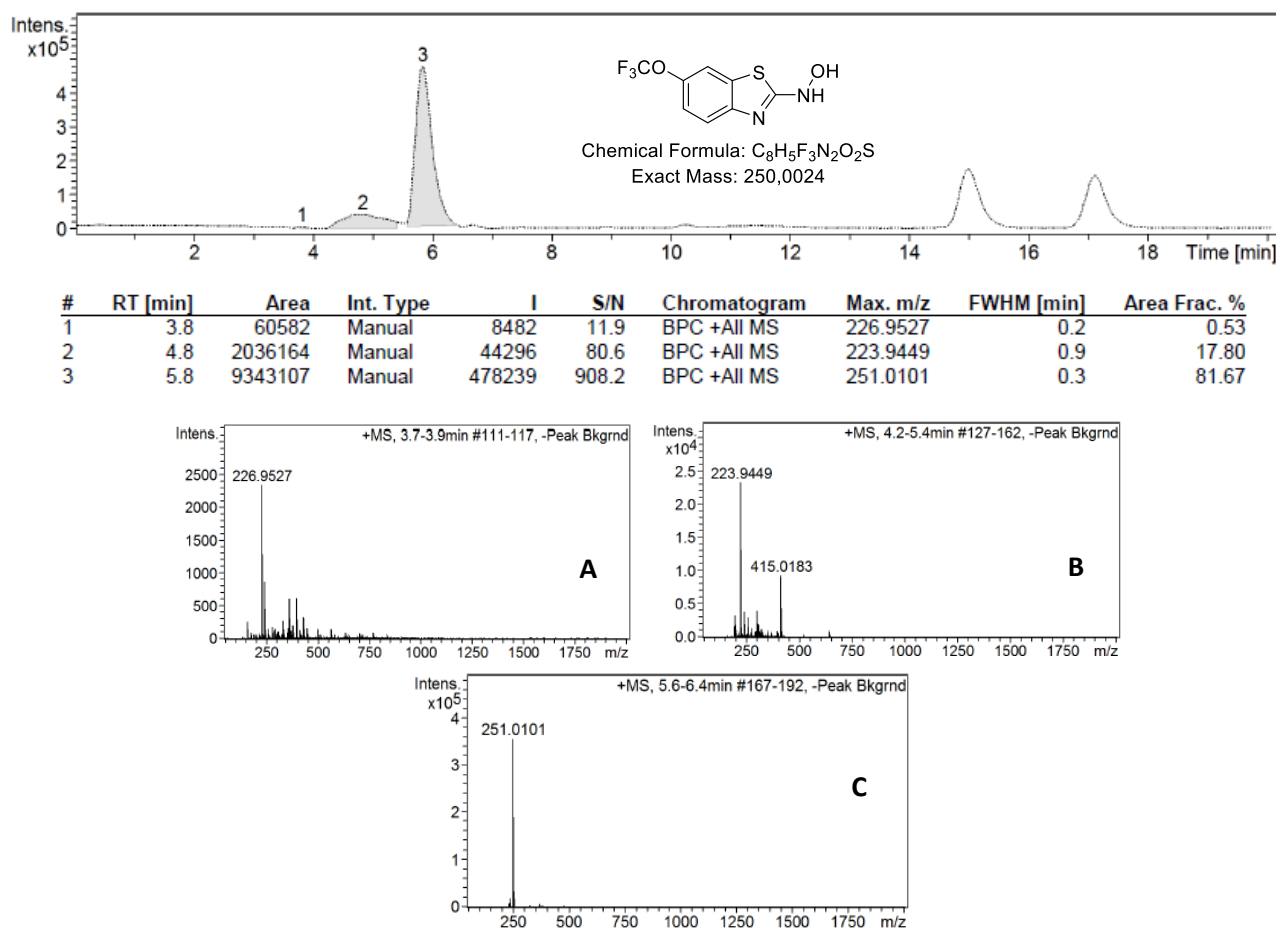
Chemical Formula: $C_8H_5F_3N_2O_2S$
Exact Mass: 250,0024

#	RT [min]	Area	Int. Type	I	S/N	Chromatogram	Max. m/z	FWHM [min]	Area Frac. %
1	3.8	60582	Manual	8482	11.9	BPC +All MS	226.9527	0.2	0.53
2	4.8	2036164	Manual	44296	80.6	BPC +All MS	223.9449	0.9	17.80
3	5.8	9343107	Manual	478239	908.2	BPC +All MS	251.0101	0.3	81.67

#	RT [min]	Area	Int. Type	I	S/N	Chromatogram	Max. m/z	FWHM [min]	Area Frac. %
1	16.2	174217824	Manual	4915071	16675.4	BPC +All MS	320.1030	0.5	93.77
2	18.3	11571374	Manual	595669	1807.1	BPC +All MS	318.0881	0.4	6.23

*Figure 53: HPLC-MS chromatogram of compound **98** at t = 28 days. Purity reported of 93.77%. Below the chromatogram, masses of the two peaks observed are given (overview **A** reports the mass of compound **98** in agreeing with its molecular weight).*

3.3.5. Biochemical and biological characterization

3.3.5.1. *In vitro* evaluation of BBB-permeability

Developed compounds must cross the BBB to explicate their function at the central level. To predict a possible passive transport, the BBB-Parallel Artificial Membrane Permeability Assay (BBB-PAMPA) technique has been performed assaying derivatives that have reported best IC_{50} values. A general view of the technique is reported in the introductive chapter. A correlation between experimental and bibliographic permeabilities (Pe) of ten well-known drugs is required to obtain cut-off values of permeable and non-permeable molecules according to the equation of the calibration lines. Compounds of the series have been split in two experiments; thus two calibration lines have been determined with their corresponding limits [168,169,170] (**Fig. 54, A** and **B**).
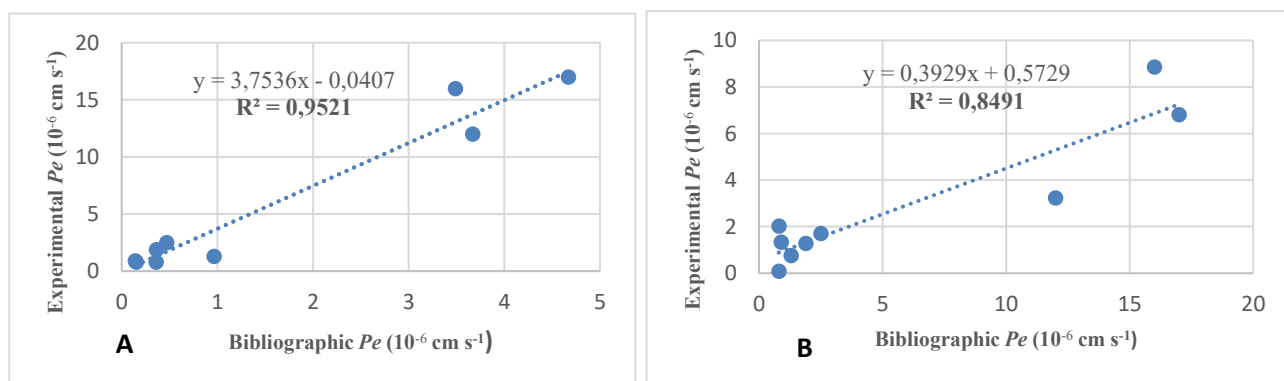
*Figure 54: calibration lines given by the correlation between experimental and bibliographic permeabilities (Pe) of ten known drugs to obtain cut-off values. **A** and **B** represent the two batches, respectively.*

3. Synthesis and characterization of benzo[d]thiazole derivatives: a metabolism-based strategy

The experimentally permeability values for ten commercially available drugs and the active compounds of the series are described in the following **Table 8** (Sections **A** and **B**) and summarized in **Fig. 55** (**A** and **B**). Obtained Pe have been filtered according to the literature: the BBB permeability in humans is predicted as positive if it is higher than $4 \cdot 10^{-6}$ cm/s and negative if it is lower than $2 \cdot 10^{-6}$ cm/s. Therefore, applying these limits to the equation of calibration line it is possible to establish cut-off values: in this case compounds with Pe higher than $1.1 \cdot 10^{-6}$ cm/s and $2.1 \cdot 10^{-6}$ cm/s, experiment 1 and 2 respectively, are classified as CNS+ while Pe permeations below $0.6 \cdot 10^{-6}$ cm/s and $1.4 \cdot 10^{-6}$ cm/s represent CNS- derivatives. Giving the range of distant values, some compounds can obtain a borderline Pe and they are categorized as CNS+/-.

As represented in **Table 8** (panels **A** and **B**), most of the developed compounds are able, according to the prediction, to across BBB. In the experiment also the riluzole (**34**) was included even though is it well established its role as a substrate of P-glycoprotein, therefore subjected to the activity of efflux transporters at the level of BBB. [195] The permeability of the two precursors of hydroxylamine (**39**) and hydrazine (**42**) series results crucial to demonstrate the hypothesis of a possible activity of metabolite **39** on CK1δ to better understand the mechanism of action of the riluzole (**34**) and, as reported in **Table 8**, they seem to be able to permeate at the central level. All the other substitutions on hydrazine moiety with an arylalkyl chains as well as methyl group and hydroxylamine compound **73** have provided CNS+ derivatives.
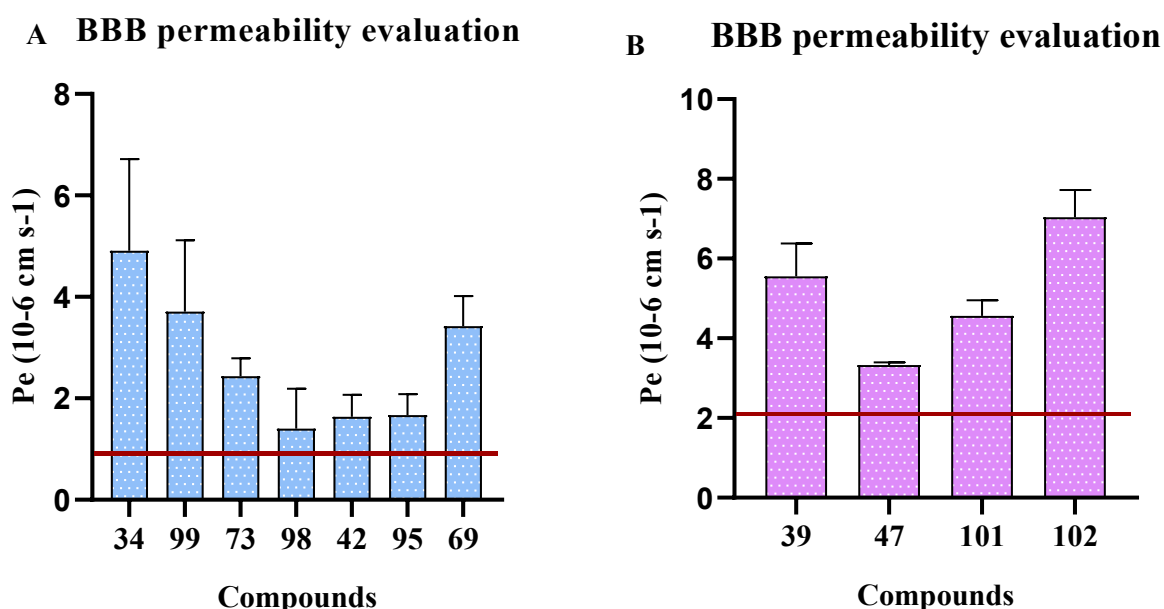
*Figure 55: histograms reporting Pe values of compounds obtained from the two BBB-PAMPA experiments (**A** and **B** represent the two batches).*

*Table 8: experimental Pe of compounds **34, 42, 69, 73, 95, 98-98** in section **A** and Pe of compounds **39, 47, 101-102** in section **B**.*

A

Cmpd	Bibl.	Pe (10^{-6} cm/s)	Prediction
Atenolol	0.8	0.4 ± 0.6	
Caffein	1.3	1.0 ± 0.1	
Desipramine	12	3.7 ± 1.3	
Enoxacin	1.6	0.1 ± 0.2	
Hydrocortisone	2.4	0.4 ± 0.1	
Ofloxacine	0.8	0.2 ± 0.3	
Piroxicam	2.5	6.8 ± 1.4	
Promazine	8.8	0.5 ± 0.1	
Testosterone	17	4.7 ± 2.2	
Verapamil	16	3.3 ± 3.0	
Riluzole (34)		4.9 ± 2.2	CNS+
42		1.6 ± 0.4	CNS+
98		1.4 ± 0.9	CNS+
99		4.3 ± 1.7	CNS+
73		2.4 ± 0.4	CNS+
95		1.7 ± 0.4	CNS+
69		3.4 ± 0.6	CNS+

B

Cmpd	Bibl.	Pe (10^{-6} cm/s)	Prediction
Atenolol	0.8	0.1 ± 1.2	
Caffein	1.3	0.8 ± 0.9	
Desipramine	12	2.7 ± 3.2	
Enoxacin	1.6	1.3 ± 0.4	
Hydrocortisone	2.4	1.3 ± 0.3	
Ofloxacine	0.8	2.1 ± 0.7	
Piroxicam	2.5	1.7 ± 0.3	
Promazine	8.8	13.8 ± 10.2	
Testosterone	17	6.8 ± 2.1	
Verapamil	16	8.9 ± 2.8	
39		5.6 ± 0.8	CNS+
47		3.3 ± 0.1	CNS+
101		4.6 ± 0.4	CNS+
102		7.0 ± 0.7	CNS+

3.3.5.2. ATP-competition

To demonstrate the ATP-competitive behavior of this series of CK1δ inhibitors, the experiment has been conducted for compound **98** that has proved to be the best of the series, the kinetic ATP-competition assay has been performed by reporting the reciprocal consumed ATP in x axis and the reciprocal of consumed ATP divided for total volume of the reaction (40 µL) in y axis. Enzymatic activity has been determined using the same luciferase-based assay (Kinase Glo®) used to determine potency of compounds. The elaboration has been carried out by assaying compound **98** at the concentrations of 1.0 µM and 2.0 µM, corresponding to about 1x and 2x the IC_{50} value of compound on CK1δ ($IC_{50} = 0.92$ µM), using increasing ATP concentrations (1 µM, 2 µM, 10 µM, 50 µM). In **Fig. 56** the Lineweaver-Burk graph is reported: it is possible to appreciate the span between the line of control and lines of the two concentrations of derivative **98**. The CK1δ inhibitor **98** has been confirmed as ATP-competitive since the intercept (e.g. $1/V_{max}$) is common between the three lines reported as it is possible to see looking the zoom reported in the right part of the **Fig. 56**, so V_{max} was constant. The y-intercept values are reported in **Table 9**.

*Table 9: y-intercept values of the Lineweaver-Burk plot reported in Fig.54 for compound **98**.*

Cmpd	y-intercept
[98] 1.0 µM	0.07
[98] 2.0 µM	0.07
Control	0.07
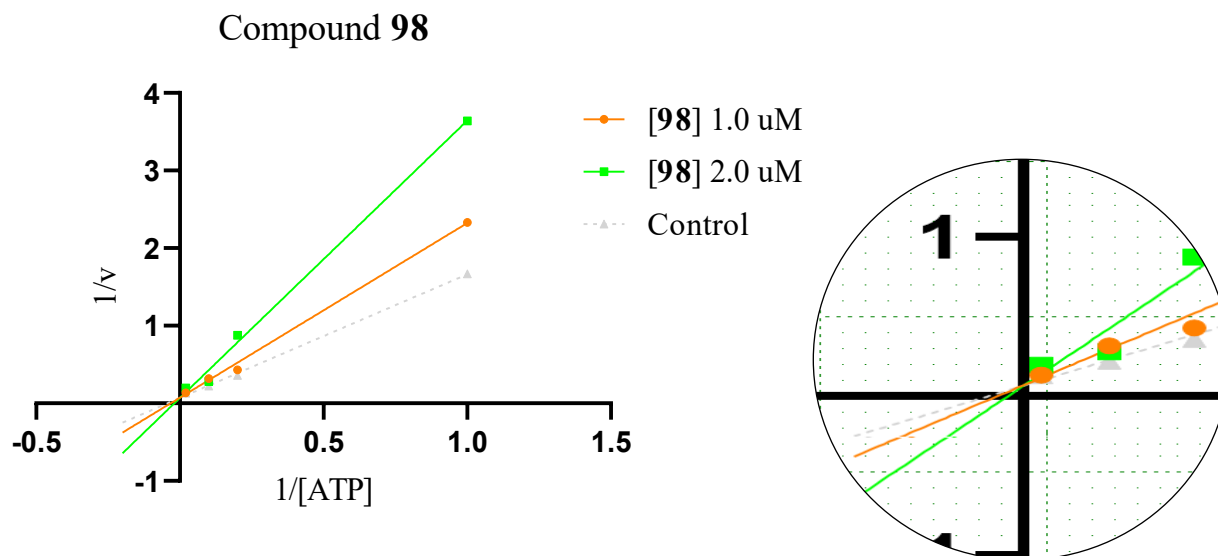
*Figure 56: Double-reciprocal Lineweaver graph of compound **98** assaying at concentrations of 1 and 2 μM. The zoom of the intercept is reported on the right.*

3.3.5.3.   Thermal Shift Assay (TSA)

Thermal shift assay (TSA) is a qualitative technique used to detect the binding of a ligand-protein complex by measuring the thermal stability of the protein. [196] Protein stability *in vitro* is a fundamental parameter in protein biochemistry. Historically, Differential Scanning Calorimetry (DSC) has been the method of choice for characterizing the thermal stability *in vitro*. Although, due to its low throughput and expensive instrumentation that is dedicated to this study, a fluorescence-based thermal shift assay has been replacing DSC. [197] The usage of a hydrophobic fluorophore can be used to distinguish between folded and unfolded state of proteins. More precisely, in an ideal case, at low temperatures water quenches the fluorescence of the dye, observing a basal fluorescence signal. Heating the system, the protein starts to melt exposing hydrophobic patches which could be bound by the fluorescent dye thus giving rise to a fluorescence signal. When finally, proteins aggregate due to the denaturation induced by the increasing temperature, the dye dissociates from the protein giving a decrease of fluorescence signal (**Fig. 57**). [198] The high-throughput and small-scale nature of the TSA makes them an excellent platform for screening of small ligand, such as organic compounds.
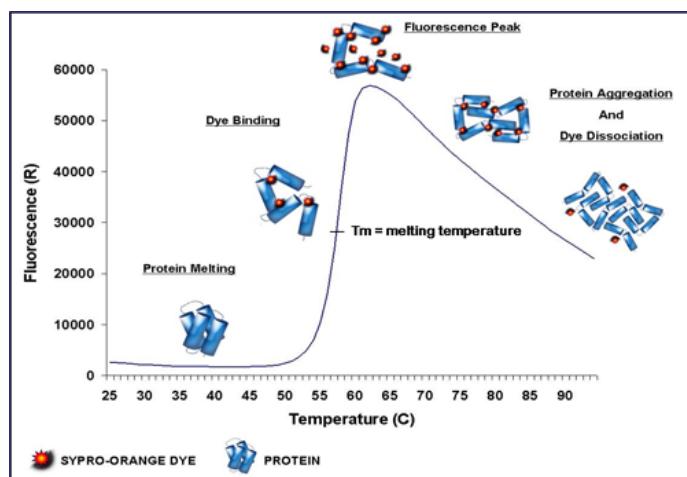
Figure 57: schematic representation of protein state in TSA experiment. Temperature is reported in x axis and fluorescence in y axis.

3. Synthesis and characterization of benzo[d]thiazole derivatives: a metabolism-based strategy

The protein stability is related to Gibbs free Energy (DG_u), which decreases to zero at the equilibrium between folded and unfolded state. The temperature measured at this point is considered the melting temperature (Tm). If a ligand binds to the protein, the free energy contribution of the binding in most cases results in an increase in DG_u which may be observed with an increase of the Tm. [198] The resulting DTm can give a solid and useful information about the binding, considering also that the stabilizing effect of the binding is often proportional to concentration and affinity of the ligand.

Therefore, to qualitative appreciate an active compound, a positive shift of the melting curve of protein in the presence and in the absence of the derivative could be detected. The TSA experiment has been conducted for the most potent compound of the series (**98**). As reported in **Fig. 58**, a positive shift of the melting point curve is registered increasing the concentrations of compound **98** (**Table 10**).
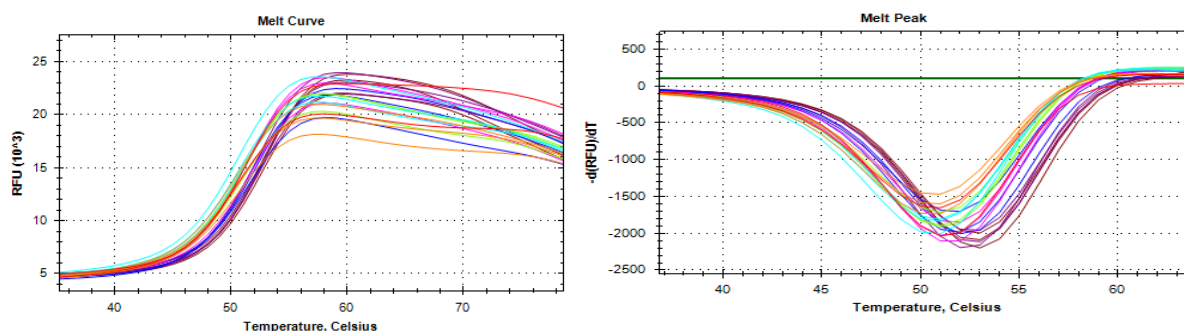
Colour code: red protein; orange DMSO; cyan 0.5x; green 1x; pink 3x; blue 5x; purple 10x; brown 15x

*Figure 58: melting curves of compound **98**. The first graph (melt curve) reports the temperature (C°) in x axis and RFU (relative fluorescence unit) in y axis. The second graph (dissociation curve) reports the temperature in x axis and the negative derivate of RLU in the y one.*

*Table 10: table of shift values for TSA performed for compound **98**. The "condition" reports concentrations of compound (multiples of protein concentration), the "average" column indicates the mean of temperature of technical triplicate accompanied by the standard deviation ("SD") while the "DT°C" (difference of temperature) column reports the temperature shift.*

Condition	Tm	DT°C	SD triplicates
CK1d	51.0		0
DMSO 2,5%	51.0	(0)	0
93 0.5x	51.0	0	0
93 1x	51.0	0	0
93 3x	51.7	+0.7	0.6
93 5x	52.0	+1	0
93 10x	52.7	+1.7	0.6
93 15x	53.0	+2	0

3. Synthesis and characterization of benzo[d]thiazole derivatives: a metabolism-based strategy

The TSA data of most promising compounds were performed by Eleonora Cescon, in collaboration with Paola Storici's group at BioLab of Elettra Sincrotrone of Trieste.

3.3.5.4. Screening on GSK3β

For the most promising compounds of the series the screening on GSK3β has been conducted during the Erasmus+ program in the Prof. Martinez' group (CSIC-Madrid-ES) to obtain useful information about the selectivity of developed derivatives. Glycogen Synthase Kinase 3 (GSK3), in fact, is another kinase involved in several physiological and pathological processes including cancer and neurodegenerative diseases. [48] Compounds have been tested on full-length GSK3β (1 ng/μL) taking advantage from luminescence reaction by using GS-2 as substrate (0.2 μg/μL) and ATP at the final concentration of 1 μM. Firstly, compounds **39**, **98-99** have been tested 10 μM as inhibitor concentration and for derivatives that display an activity percentage less than 50% at the concentration, IC_{50}s are performed. Activity percentages and IC_{50}s are reported in **Table 11**. Compound **39** has displayed an IC_{50} on GSK3β of 23.1 μM suggesting that the hydroxylamine metabolite of riluzole appears not selective towards CK1δ. Regards derivatives **98-99**, the most promising of the series, compound **98** functionalized with isopentyl chain has proved to be inactive while benzyl-derivative **99** has reported IC_{50} of 16.4 μM highlighting an acceptable span considering the IC_{50} value of 1.62 μM on CK1δ. Thus, the selectivity for best derivatives, taking into consideration only GSK3β, has been reached. IC_{50}s concentration-inhibition curve of compounds **39** and **99** are reported below (**Fig. 59**).

Table 11: IC_{50}s of compounds 39, 98-99 and activity percentages.

Cmpd	IC_{50} μM [a] (% activity at 40 μM)[b]
39	23.1 ± 1.0 (45.7 % ± 2.6)
98	n.d. (100% ± 0)
99	16.4 ± 1.1 (29.4 % ± 5.8)

[a] Data represent the mean ± SD of three independent experiments performed in technical duplicate. [b] Data represent the % of activity at 10 μM concentration expressed as a mean ± SD of two independent experiments performed in technical duplicate; n.d.: not determined.
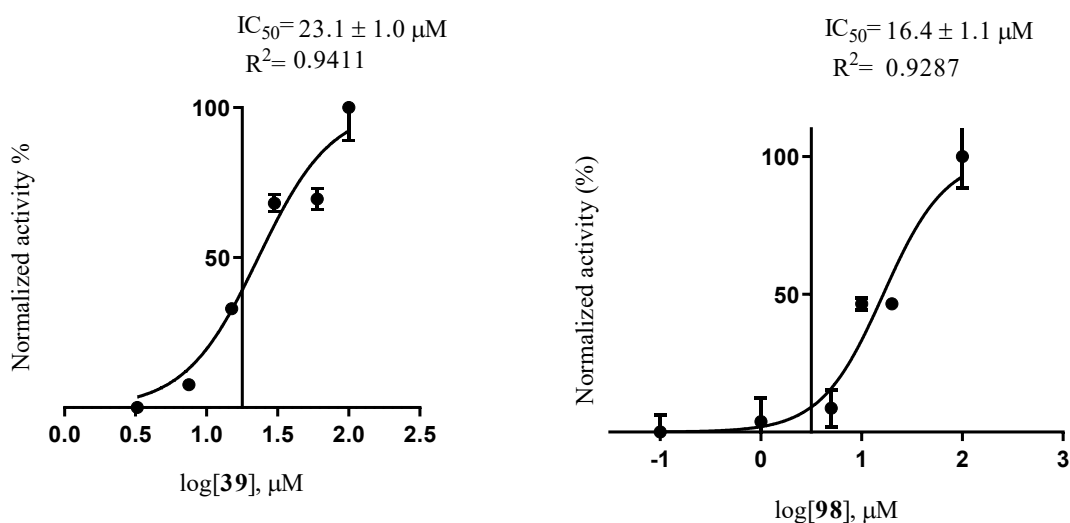
Figure 59: IC_{50} concentration-inhibition curves of compounds 39 and 98 on GSK3β, respectively.

3.3.5.5.   Biological characterization *in vitro* of riluzole and most promising derivatives in neuroblastoma cell lines

Riluzole (**34**), N-hydroxylamine metabolite (**39**) and most promising derivatives **98** and **99** have been tested *in vitro* in neuroblastoma cell lines (SH-SY5Y) during the Erasmus+ program in Prof. Martinez' group (CSIC-Madrid-ES) to evaluate the capability of candidates to mediate neuroprotection and to decrease the phosphorylated TDP-43. Firstly, compounds have been assayed at the concentrations of 5 μM and 10 μM on SH-SY5Y cells to evaluate the toxicity of derivatives. As reported in **Fig. 60**, firstly, cells have been split using trypsin and medium and when they have achieved the right confluence, they are considered ready to use. After collecting them, 80000 cells/well have been plated and incubated. At this point, compounds have been added and, after another 24 h of incubation, MTT (3-(4,5-dimethylthiazol-2-yl)-2,5-diphenyltetrazolium bromide) has been inserted and plate has been red using the absorbance mode (detailed procedures are reported in the experimental chapter). MTT assay is widely used to determine cell viability and the cytotoxic effect of the drugs; living mitochondrial cells are able to convert MTT in formazan crystal and, since the mitochondrial activity is referred to the number of viable cells, the viability percentage can be calculated by the absorbance detection of formazan. [199]
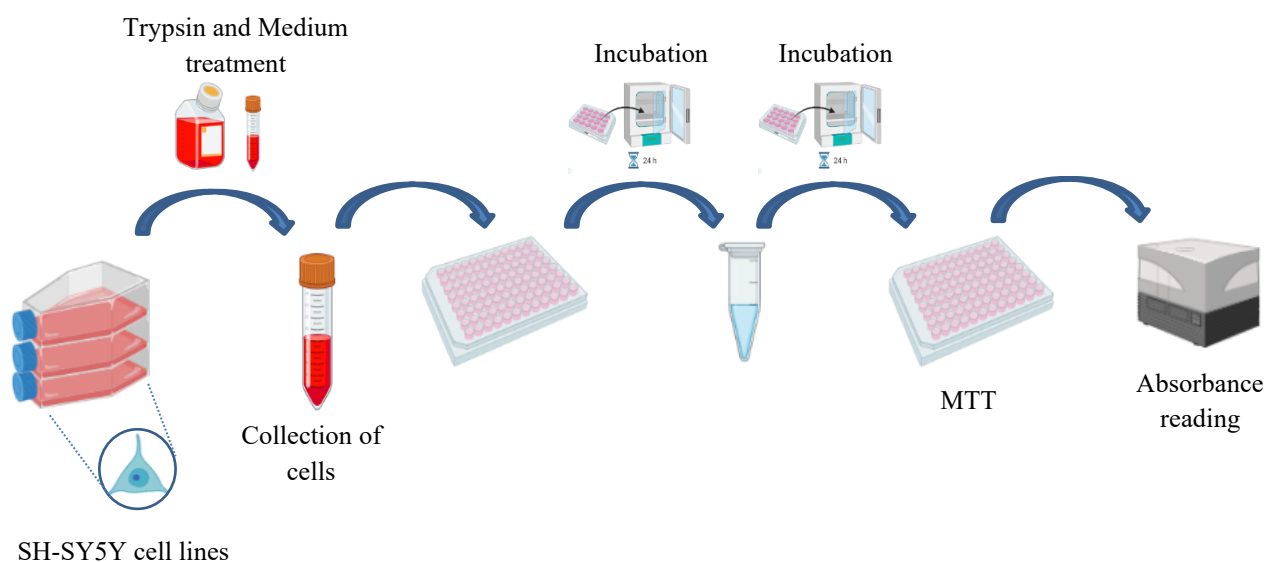
Figure 60: steps in MTT assay: trypsin and medium treatment to collect pellet, the disposition of 80000 cells/well in the plate, incubation of 24 h, adding of compounds, MTT treatment after 24h of incubation and absorbance reading of the plate. Image created using ***BioRender****.*

As displayed in histogram reported in **Fig. 61**, riluzole (**34**) and compounds **98-99** have shown to be harmless for cells while N-hydroxylamine metabolite (**39**) has demonstrated a percentage of cell availability of 61.0% after 24 h, denoting its toxicity at the concentration of 5 μM. The same derivatives have been assayed also at the concentration of 10 μM (**Fig. 62**) and it is possible to observe a worsening in the behavior of compound **39** achieving the 47% of cell viability and a toxicity for compound **98** reporting a value of 77.3%. Regards derivative **98** that has displayed an IC_{50} on CK1δ of 0.92 μM, the reported toxicity at 10 μM results an important information but not relevant for the neuroprotection assay in which the chosen concentration to test this compound is 5 μM.
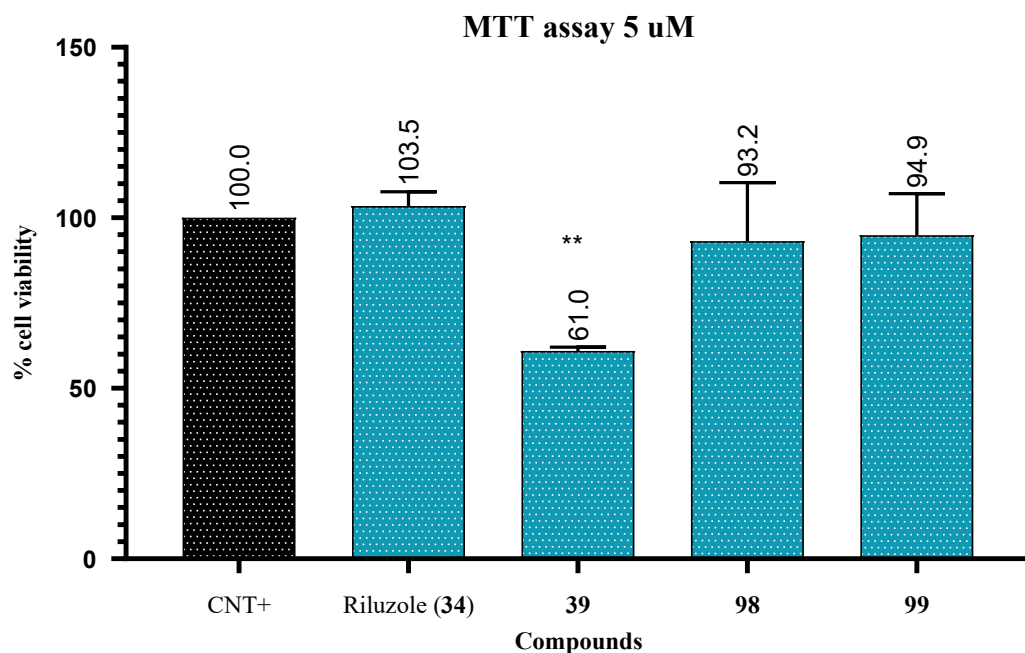
*Figure 61: MTT assay of compounds **34**, **39**, **98-99** at the concentration of 5 μM. In y axis the cell viability percentage is reported. The elaboration performed with GraphPad Prism 8.0 in "Anova" mode is the result of three independent experiments and each experiment is conducted using the mean of six wells per compound Results are expressed as the mean of three data ± standard error (error bars); ****p<0.0001 significantly different from control cells, ***p<0.001 significantly different from control cells, **p<0.01 significantly different from control cells, *p<0.1 significantly different from control cells.*
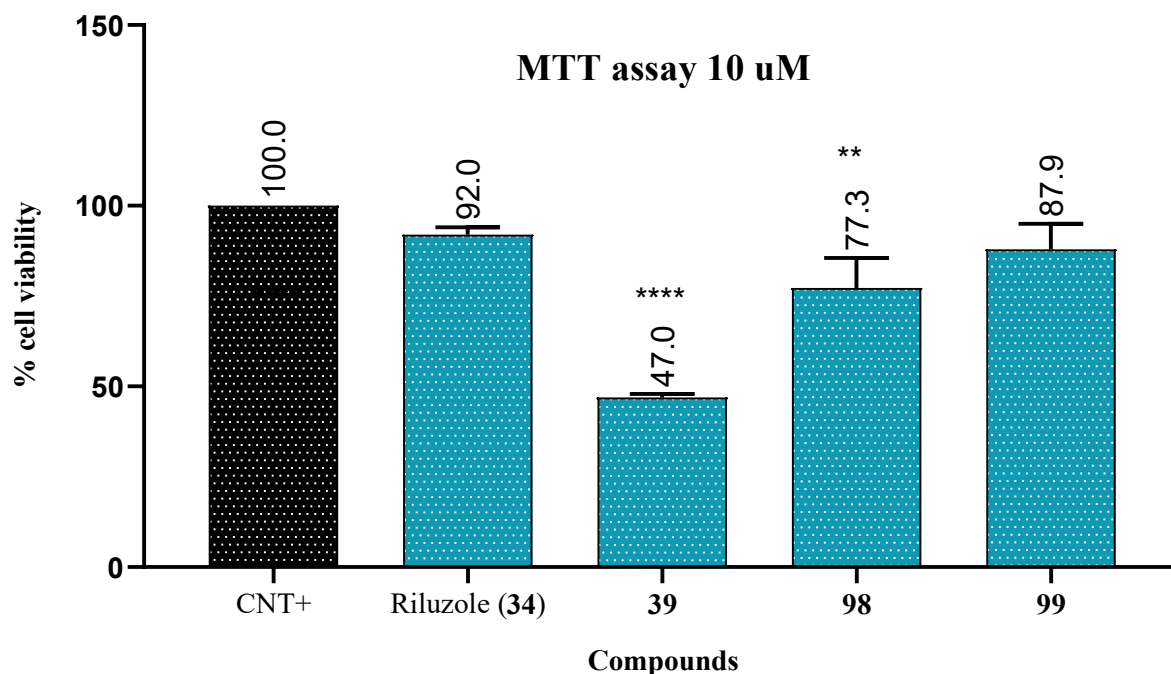
*Figure 62: MTT assay of compounds **34**, **39**, **98-99** at the concentration of 10 μM. In y axis the cell viability percentage is reported. The elaboration performed with GraphPad Prism 8.0 in "Anova" mode is the result of three independent experiments and each experiment is conducted using the mean of six wells per compound. Results are expressed as the mean of three data ± standard error (error bars); ****p<0.0001 significantly different from control cells, ***p<0.001 significantly different from control cells, **p<0.01 significantly different from control cells, *p<0.1 significantly different from control cells.*

Compounds that have been resulted harmless for cells have been tested in the neuroprotection assay to assess if the administration of derivative increases the cell viability percentage in comparison to the negative control using ethacrynic acid (EA) as neurotoxic agent to simulate neuronal death increasing oxidative stress and the glutathione depletion. [200] The protocol as well as the detection method are similar to the previous described MTT assay; the unique difference is represented by adding ethacrynic acid to cells previous treated with compounds. To establish the right concentration of EA, several attempts have been carried out using this toxic agent at 40 μM, 45 μM, 50 μM and 60 μM. The highest concentrations have denoted a more toxic affect with the administration of compounds, thus the use of EA at 45 μM has been resulted the best condition plating 60000 cells/well. Regards the concentrations of inhibitors, riluzole (**34**) has been assayed at 10 μM considering its IC_{50} on CK1δ while other compounds (**98-99**) at 5 μM. As **Fig. 63** displays, the neuroprotection assay has revealed non-significant data for compounds **98-99** while an important neuroprotective effect, as expected, has been detected for riluzole (**34**).
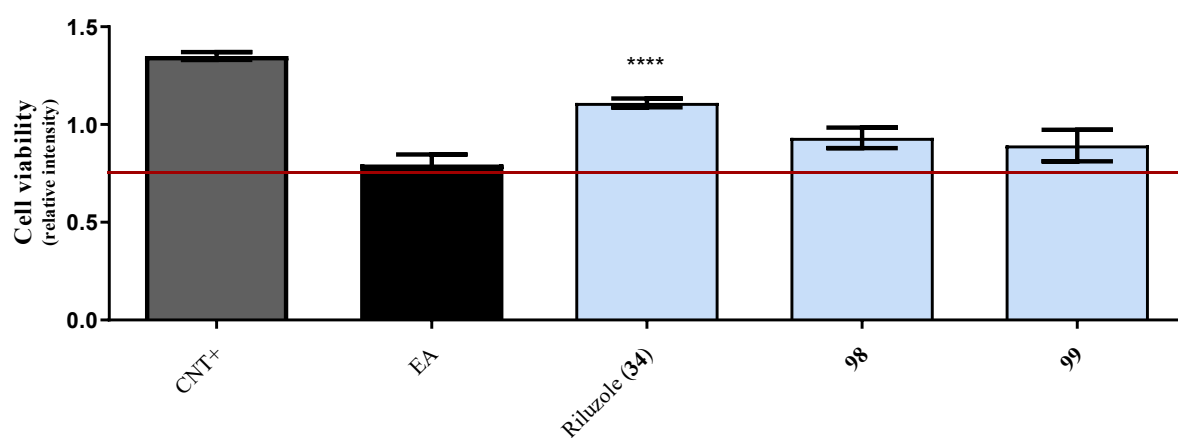
Figure 63: neuroprotection assay's results. Three independent experiments have been conducted and the elaboration has been performed with GraphPad Prism 8.0 using the "Anova" mode with the mean of eight wells per compounds for each plate and then final data have been obtained with "T test" mode to compare the three experiments. EA has been used at 45 μM while chosen concentrations for compounds 34, 98 and 99 are 10 μM, 5 μM and 5 μM, respectively. Results are expressed as the mean of three data ± standard error (error bars); ****p<0.0001 significantly different from control cells, ***p<0.001 significantly different from control cells, **p<0.01 significantly different from control cells, *p<0.1 significantly different from control cells.

Riluzole (**34**) that has displayed neuroprotective properties has been then investigated using Western Blot to detect the effect p-TDP-43 levels (phospho TDP-43). To conduct the experiment 2000000 of cells/well are plated and, after the 24 h of incubation, the introduction of compounds and ethacrynic acid is required and after another incubation, protein extraction occurred using lysis buffer. The soluble fraction has been separated from the insoluble one that has been treated with Sarkosyl hypertonic buffer, more aggressive than lysis one, to evaluate the presence of proteins not only in supernatant with the cytoplasmatic content but also in the collected pellet after the lysis of nucleus. To establish right conditions to perform Western Blot analysis, the calibration line of increasing concentrations of albumin is required registering the absorbance at different concentrations. (**Fig. 64**).

3. Synthesis and characterization of benzo[d]thiazole derivatives: a metabolism-based strategy
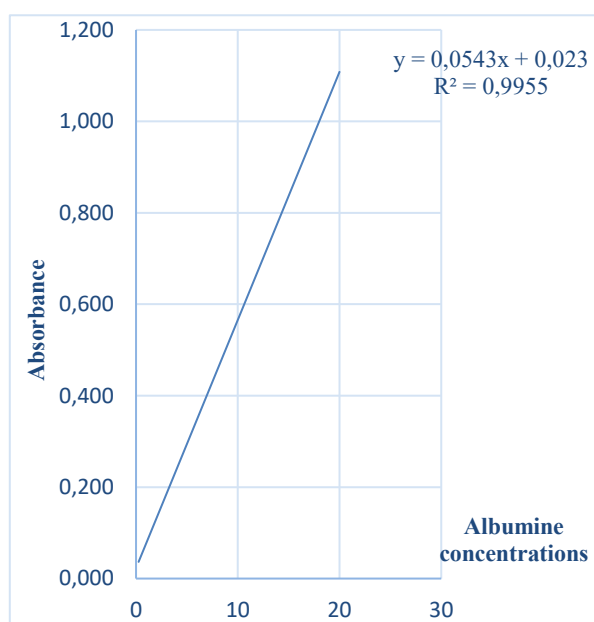
Figure 64: calibration line of albumin. In x axis eight increasing concentrations are reported, in y axis the absorbance values are given (each value has been subtracted previously for the negative control). The linear correlation is ensured by the R^2.

All values related to each condition (soluble and insoluble fractions) have been subtracted by the mean of negative controls and then substituted in the line's equation to find the conditions for performing the electrophoresis separation. Once the runs have been conducted as well as the transfer of gel on methanol-activated membrane, incubated with primary antibody anti TDP-43 phosphorylated at Ser-409/Ser-410 (phospho TDP-43 mouse) is required. After 24 h of incubation, membrane has been washed and incubated with secondary antibody labeled with Alexa Fluor 488 to give signal amplification (anti-mouse). As a conclusion, the reaction has been detected in luminescence mode. The schematic procedure has been represented in **Fig. 65**.
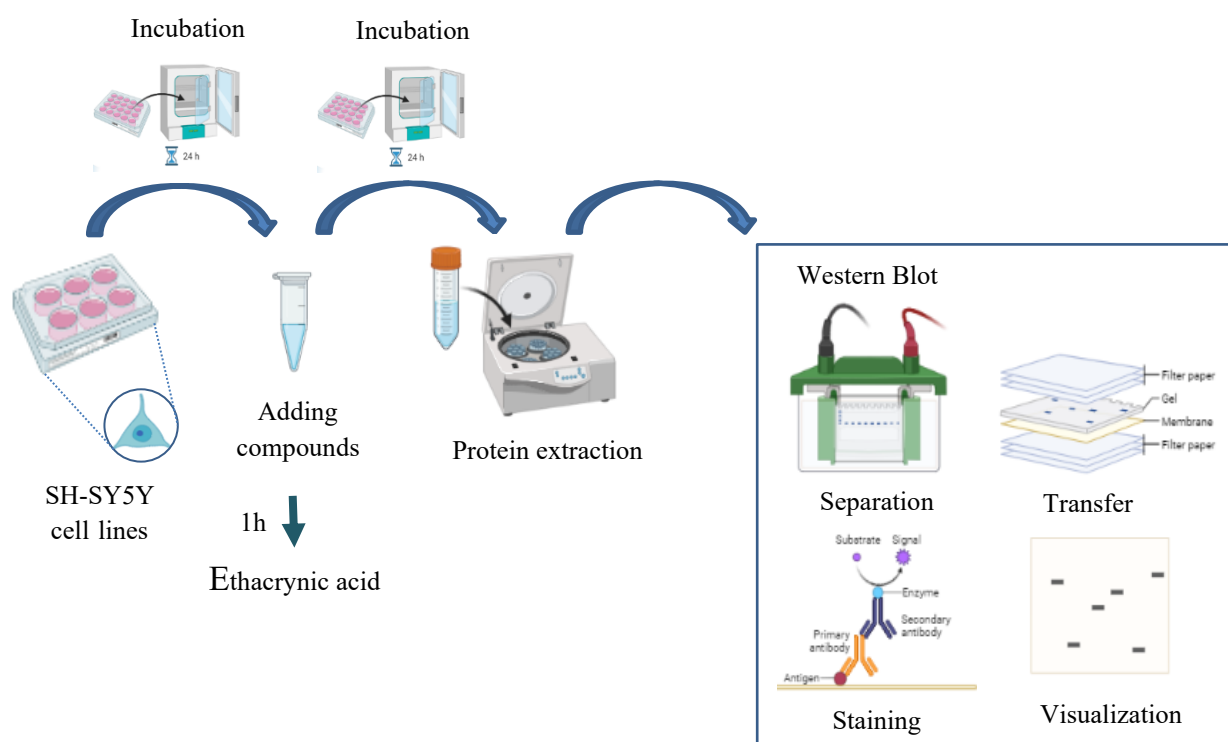
*Figure 65: schematic representation of cell collection, protein extraction and immunoblotting. Image created using **BioRender**.*

In order to obtain also a quantitative result, it is important to know the precise amount of total TDP-43 in each condition; thus, after several washes to remove antibodies primary and secondary pospho TDP-43, membrane has been incubated with another primary antibody (TDP-43 rabbit) and the staining reaction has been carried out with secondary antibody labeled with Alexa Fluor 488 (anti rabbit). This second incubation has been accompanied by another luminescence detection. In this way, it is possible to elaborate data in a normalization mode by plotting pTDP-43 data in relation to TDP-43. Moreover, membrane has also been incubated with glyceraldehyde 3-phosphate dehydrogenase (GAPDH, rabbit) and the secondary antibody. GAPDH is an enzyme that is present in equal amount in each cell, therefore another normalization can be available to establish if obtained results can be reliable or not.

Two separated Western Blot experiments have been conducted, nevertheless a third one is required to confirm and adjust preliminary data obtained and showed in **Fig. 66** and **67** below. Phosphorylated TDP-43 has been detected as it is possible to see in the first window of Western Blot results of the first experiment conducted (**Fig. 66**); the 25 kDa fragment has been displayed instead of 43 KDa and it is quite common in a strong degradation process during the protein extraction. Inserting in the same experiment also the marker pTDP43 the recognition of fragmentation's spots is available. In the histogram reported in the **Panel B** of **Fig. 66** the normalization of phospho TDP-43 against total TDP-43 ha been displayed**;** considering riluzole (**34**), the percentage of intensity is the same of the control (absence of ethacrynic acid). Nevertheless, the difference between control and ethacrynic acid is minimal, therefore it is difficult to establish it the results for riluzole are significative or not.
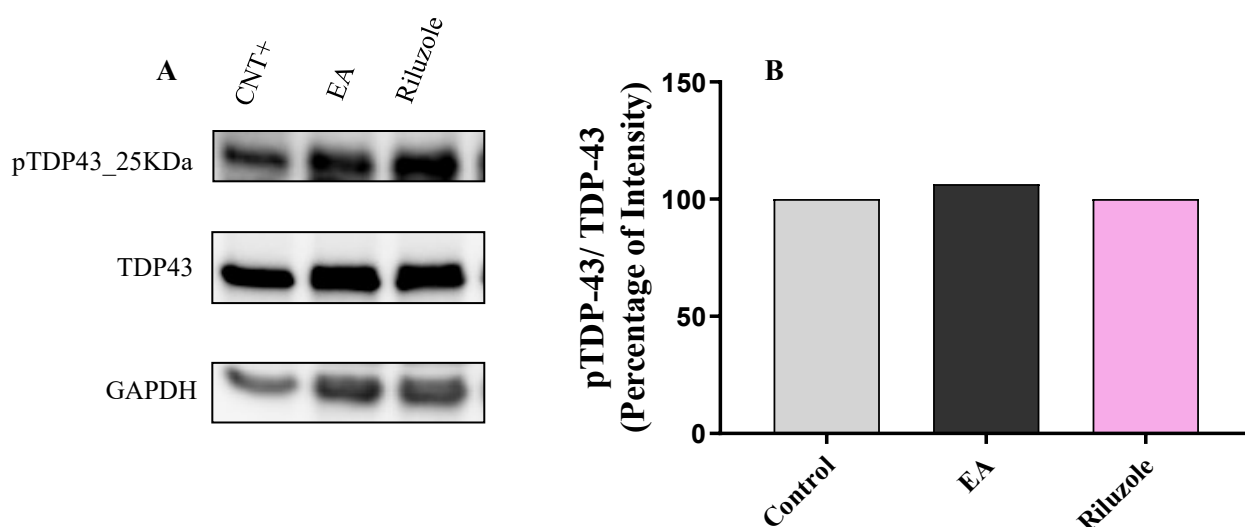
*Figure 66: **Panel A**) Western Blot results of the first experiments: the three windows report the pTDP43 (25 KDa) overview, TDP-43 and GAPDH, respectively. **Panel B**) the histogram displays quantitative results of Immunoblotting. There is not a decrease in pTDP-43 administrating riluzole at the concentration of 10 μM. Quantitative results of Western Blot analysis are elaborated using ImageLab as program.*

Interestingly, pTDP-43 (25 kDa fragment) has been detected also in the insoluble fraction as reported in **Fig. 67**. It is evident, in this case, a stronger qualitative difference between control and treatment with ethacrynic acid even if there is not a homogeneous amount of total TDP-43 in the three conditions. Moreover, considering riluzole an improvement in the situation has not been detected. Data registered are too low to classify them in the normalized histogram.
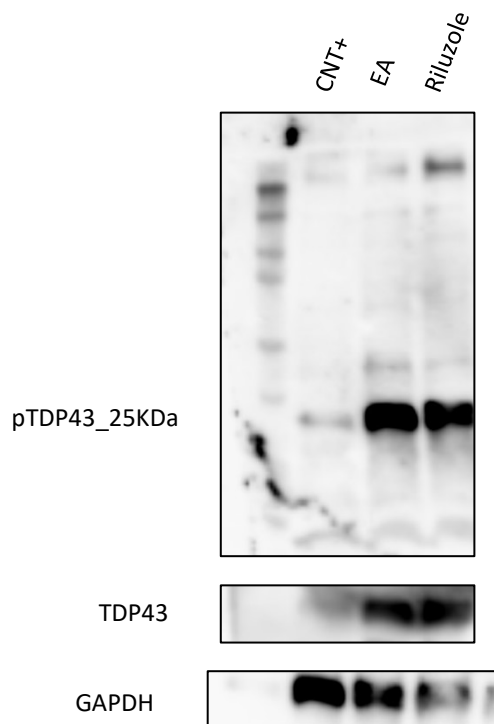
Figure 67: Western Blot result of the first experiment for the insoluble fraction. In the three windows, pTDP-43 (25 kDa fragment), TDP-43 and GAPDH are reported, respectively.

In the second experiment represented in **Fig. 68** a marked difference between control and ethacrynic acid has been detected in the first overview. In this situation, the 37 kDa fragment of pTDP-43 has been recovered. Nevertheless, riluzole (**34**) has proved to be not efficient in the decrease of pTDP-43 as showed in the **Panel B** of **Fig. 68** in which histogram of quantitative results can be appreciated.
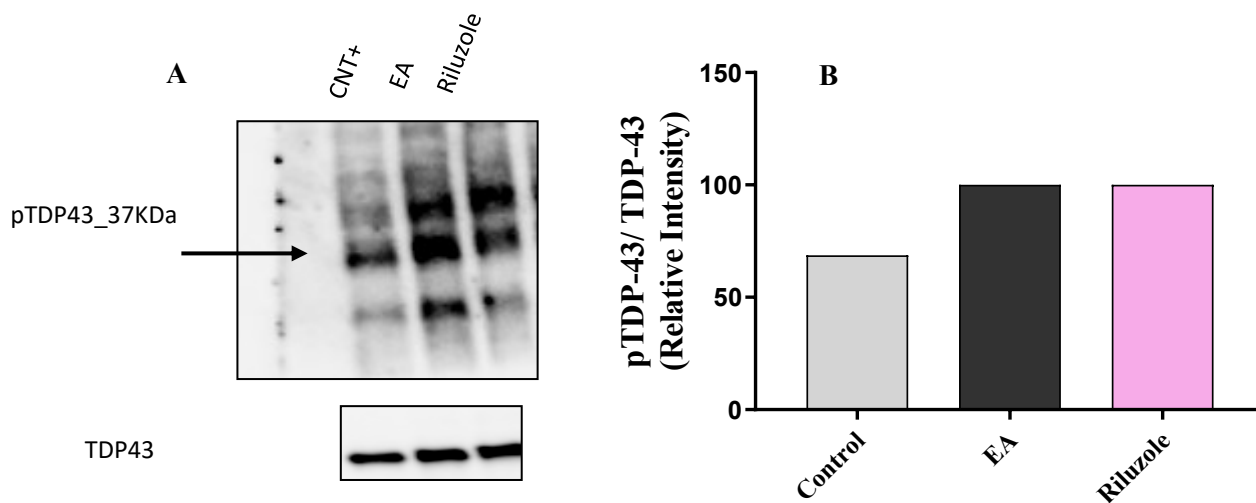
*Figure 68: **Panel A)** Western Blot results of the second experiment: the two windows report the pTDP43 (37 KDa) overview and TDP-43, respectively. **Panel B)** the histogram displays quantitative results of Immunoblotting. There is not a decrease in pTDP-43 administrating riluzole at the concentration of 10 µM. Quantitative results of Western Blot analysis are elaborated using ImageLab as program.*

From these preliminary results it is clear that at least a third experiment is needed in order to validate if riluzole has or not an effect in decreasing of TDP-43 phosphorylation even if it has displayed a neuroprotective effect on neuroblastoma cell lines. Considering its IC$_{50}$ on CK1δ in the high micromolar range, it is evident that

several pathways and mechanisms of action cooperate in the neuroprotective behavior of riluzole. The activity of 16.1 µM on CK1δ has been demonstrated for this candidate, nevertheless hypothesis including the glutamatergic one has been reported. Further studies will be conducted to better understand real mechanism of action.

3.3.5.6. Assays of riluzole on *Drosophila* overexpressed TDP-43

To confirm the hypothesis that one of the possible mechanisms of riluzole (**34**) can be connected to its activity on CK1δ, this candidate has been tested in *vivo* on *Drosophila* specie that overexpress TDP-43 in glial cells considered "astrocyte-like" in collaboration with Prof. Marco Bisaglia of University of Padua. From preliminary results the compound administrating at the concentration of 1 mM shows, as reported in **Fig. 69**, the increase of lifespan of *Drosophila* achieving 37 days in comparison to control (31 days).
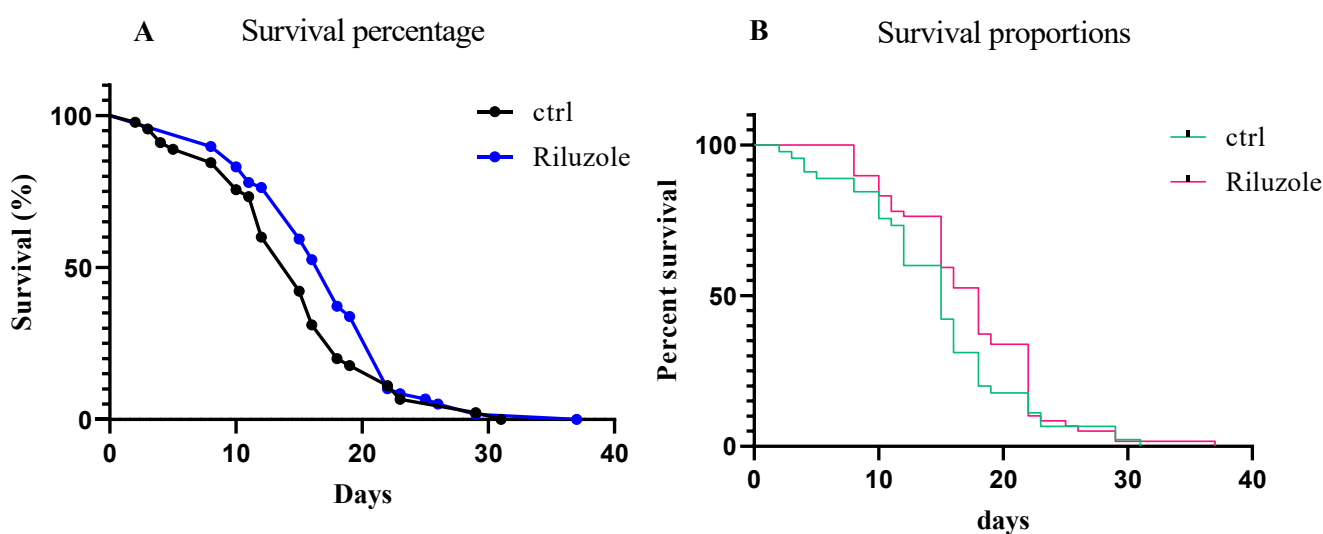
*Figure 69: survival percentage (**Panel A**) and survival proportions (**Panel B**) on Drosophila testing riluzole (**34**) at the concentration of 1 mM.*

Nevertheless, overexpressing TDP-43 selectively in specific cell populations, some experiments have been conducted in D42-Gal4 and Repo-Gal4 transgenic *Drosophila*. D42-Gal4 results (**Fig. 70**) overexpressing Gal4 in motoneurons opening the possibility to explore the behavior of riluzole (testing at the concentration of 5 mM) in flies bearing the specific localization of TDP-43 in motoneurons do not allow to observe changes in comparison to the control. The same experiment has been conducted by overexpressing Gal4 in glial cells (Repo-Gal4, **Fig.71**) and no significant increase in survival percentage has been detected. Thus, further experiments are required to confirm the activity of riluzole in *Drosophila* prolongation of lifespan when TDP-43 is overexpressed.

3. Synthesis and characterization of benzo[d]thiazole derivatives: a metabolism-based strategy

D42-Gal4
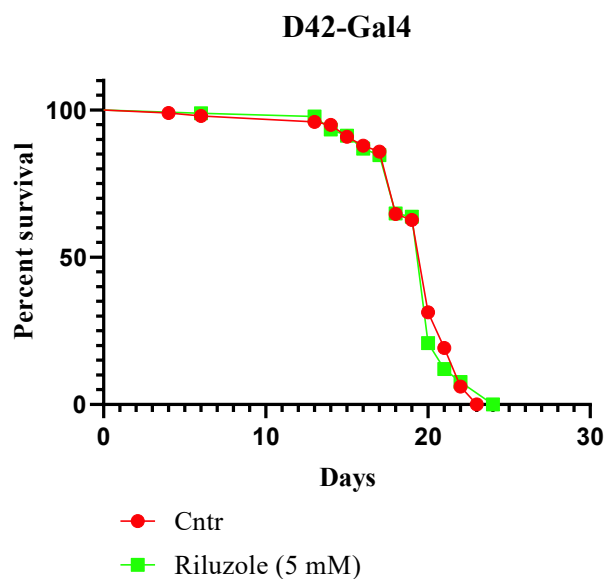
*Figure 70: from the left to the right, the survival percentage on Drosophila assaying riluzole (**34**) at the concentration of 5 mM is reported when TDP-43 is overexpressed on motoneurons.*

Repo-Gal4
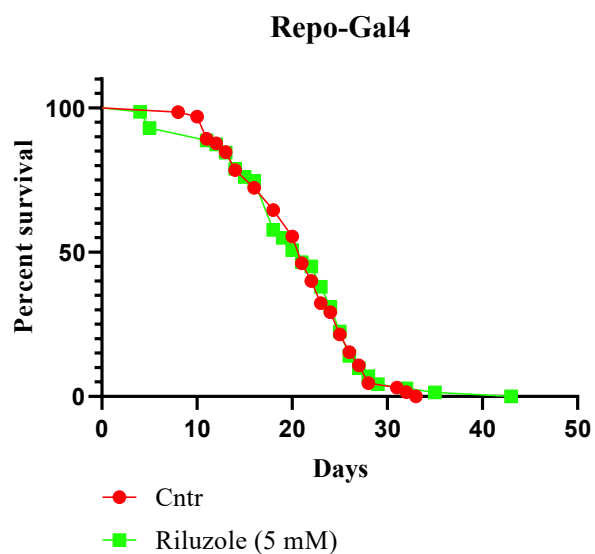
*Figure 71: from the left to the right, the survival percentage on Drosophila assaying riluzole (**34**) at the concentration of 5 mM is reported when TDP-43 is overexpressed on glial cells.*

3.4.   Conclusions and future perspectives

In this chapter the N-hydroxylamine metabolite (**39**) of riluzole (**34**) has been synthesized to support the validated hypothesis of the activity of riluzole on CK1δ displaying an IC$_{50}$ of 16.1 μM. This represents an important achievement since the real mechanism of action of candidate **34** is still obscure. Compound **39** has revealed an IC$_{50}$ on CK1δ of 35.1 μM, in the high micromolar range, nevertheless this activity agrees with the reported one for riluzole. Candidate **39** has been functionalized developing a series of alkyl derivatives to modify phase I metabolism strongly featured for riluzole. Moreover, the hydrazine precursor (**42**) has been developed; from the computational studies conducted by the University of Padua (group of Prof. Stefano Moro), the predicted binding pose of compound **42** appears the same as the reported one for hydroxylamine metabolite **39**. Surprisingly, hydrazino derivative **42** has revealed an IC$_{50}$ of 3.64 μM opening the possibility of obtaining functionalized derivatives to outline a structure activity relationship profile. Several compounds have been developed with different types of linear and branched chains, as well as arylalkyl and aromatic moieties. Most of hydroxylamine derivatives has proved to be inactive on CK1δ except for compound **73** that bears a pentyl chain. The situation changes with the hydrazino derivatives: all the synthesized compounds have resulted active excepting the ethylhexyl one denoting a too bulky substituent (**100**). Benzyl and isopentyl hydrazino compounds, instead, have proved to be the best derivatives reporting IC$_{50}$s of 1.62 μM and 0.92 μM, respectively (**99**, **98**). The predicted passive transport through the BBB has been explored using BBB-PAMPA: results have highlighted that all the derivatives are able to cross BBB to arrive at the central level. Nevertheless, since riluzole (**34**) is a well-known substrate of P-glycoprotein, all the functionalized derivatives will be evaluated from this point of view. Moreover, the ATP-competition behavior has been assessed for the best derivative of the series (**98**) with Lineweaver-Burk plot; Vmax has proved to be constant, thus the compound has demonstrated to be ATP-competitive, and the same feature can be applied for the other analogues. To obtain some information about the selectivity, the screening on GSK3β, another kinase involved in neurodegeneration, has been conducted for derivatives **39**, **98** and **99**. Metabolite **39** has reported an activity of 23.1 μM while **98** and **99** have displayed good selectivity considering GSK3β. Finally, the most promising derivatives **98** and **98** as well as compounds **34** and **39** have been further investigated. N-hydroxylamine candidate (**39**) has displayed a strong toxicity on neuroblastoma (SH-SY5Y) cell lines denoting possible additional reactions in physiological environment. For derivatives that have proved to be harmless, neuroprotection assay on the same cells has been conducted and riluzole (**34**) has demonstrated itself as neuroprotective candidate allowing the investigation *via* Western Blot analysis to detect a decrease in pTDP-43. Results suggest that a third experiment will be required but riluzole seems to be not able to improve the situation. Also, a preliminary test on a pTDP-43 *Drosophila* model showed a protective effect of riluzole (**34**) denoting an increased in lifespan of flies, even if assaying **34** with the selectively overexpression of TDP-**43** in motoneurons and glial cells on transgenic *Drosophila* models (D42-Gal4 and Repo-Gal4, respectively) no significant results have been reported, therefore further investigation will be conducted. Despite these non-positive achievements, considering riluzole (**34**) it is possible to observe that it can act in a non-direct way in the decrease of TDP phosphorylation determining an improvement in ALS pathology's symptoms. Several mechanisms can cooperate in the neuroprotective action and further investigations can contribute to better explain and deepen the therapeutic profile of riluzole. Regards functionalized derivatives, they have reported promising activities on CK1δ, nevertheless the structure-activity relationship profile has been deeply explored, consequently, the series can be deemed to be completed.

3.5.   Experimental Section

3.5.1.   General chemistry

Reagents were obtained from commercial suppliers and used without further purification. Reactions were monitored by TLC, on precoated silica gel plates (Macherey-Nagel, 60FUV254). Final compounds and intermediates were purified by flash chromatography using as stationary phases silica gel (Macherey-Nagel, silica 60, 240-400 mesh) or preparative TLC (stationary phase silica gel, Mechery-Nagel, silica 60, 240-400 mesh, 0.25 mm). When used, light petroleum ether refers to the fractions boiling at 40-60°C. Melting points were determined with a Stuart SMP10 melting point apparatus, and they were not corrected. The ^{1}H NMR, ^{13}C NMR and gHSQCAD bidimensional spectra were determined in CDCl$_3$ or DMSO-d_6 and recorded on Varian 400 MHz or Varian 500 MHz spectrometers; chemical shifts (δ scale) are reported in parts per million (ppm) and referenced to residual solvent peak, with splitting patterns abbreviated to: s (singlet), d (doublet), dd (doublet of doublets), dt (doublet of triplets), t (triplet), m (multiplet) and bs (broad signal). Coupling constants (*J*) are given in Hz. MS-ESI analysis was performed using ESI Bruker 4000 Esquire spectrometer or microTOF-Q – Bruker, used also for the recording of accurate mass. Compound purities were determined by HPLC using the instrument SHIMADZU CBM-20A, column Gemini® 5 μm NX-C18 (Phenomenex®). Elution gradient was performed for 30 min at the flow of 1 ml/min from water-methanol 55:45 to 15:85. The detector was set at 254 nm. Stability tests were conducted by HPLC-MS using the instrument Bruker micrOTOF-Q coupled with HPLC Agilent (procedures are described in dedicated following section).

3.5.2.   Synthesis of N-substituted-6-(trifluoromethoxy)benzo[*d*]thiazol-2-amine derivatives (**39**, **42**, **44-47**).

3.5.2.1.   Synthesis of N-(6-(trifluoromethoxy)benzo[*d*]thiazol-2-yl)hydroxylamine hydrochloride (**39**)

A solution of 84.9 mg (1.22 mmol) of hydroxylamine hydrochloride, commercially available, and 70.8 mg (0.512 mmol) of K$_2$CO$_3$ was refluxed under argon atmosphere for 30 min. Once completed, 50.0 mg (0.197 mmol) of 2-chloro-6-(trifluoromethoxy)benzo[*d*]thiazole (**43**), commercially available, were added and the mixture was stirred at 65°C for 3 h. The mixture was then filtered to eliminate the base and the solvent was removed under reduced pressure. The crude product was purified with preparative TLC (light petroleum 60% - EtOAc 40%), washed with EtOAc 90% - MeOH 10% and stirred with hydrogen chloride in 1,4-dioxane for 30 min. The solvent was removed under reduced pressure and the crude was filtered with EtOAc to give 22.0 mg of white solid. Yield 39%; mp 176°C d. ^{1}H NMR (499 MHz, DMSO-d_6) δ 10.72 (s, 1H), 9.89 (d, *J* = 28.2 Hz, 1H), 7.71 (s, 1H), 7.26 – 7.07 (m, 1H), 6.95 (d, *J* = 7.2 Hz, 2H). ^{13}C NMR (101 MHz, DMSO-d_6) δ 173.86 (d, *J* = 4.2 Hz), 158.42, 154.42 (d, *J* = 1.4 Hz), 137.02, 135.89, 120.28 (s, *J* = 42.4, 33.0 Hz), 116.13, 109.56 (d, *J* = 1.7 Hz). ES-MS (methanol) *m/z*: 250.9 [M+H]$^+$, 249.2 [M-H]$^+$. HRMS (ESI-TOF) *m/z*: C$_8$H$_6$ClF$_3$N$_2$O$_2$S (hydrochloride compound), C$_8$H$_5$F$_3$N$_2$O$_2$S experimental 251.0095 [M+H]$^+$, theoretical 251.0097 [M+H]$^+$, Δ = 0.0002. Purity HPLC: 99.2%.

3.5.2.2.   Synthesis of 2-hydrazineyl-6-(trifluoromethoxy)benzo[*d*]thiazole (**42**)

To a solution of 0.500 mL (10.0 mmol) of monohydrate hydrazine in 3.00 mL of methanol, 100 mg (0.394 mmol) of 2-chloro-6-(trifluoromethoxy)benzo[d]thiazole (**43**), commercially available, were added. The mixture was refluxed for 2h. The solvent was then removed under reduced pressure and the residue was purified with flash chromatography (light petroleum 70% – EtOAc 30%) to give 42.0 mg of white solid. Yield 42%; mp 202°C. ^{1}H NMR (400 MHz, DMSO-d_6) δ 9.20 (s, 1H), 7.78 (d, *J* = 2.4 Hz, 1H), 7.34 (d, *J* = 8.7 Hz, 1H), 7.27-7.09 (m, 1H), 5.11 (s, 2H). ^{13}C NMR (101 MHz, DMSO-d_6) δ 175.15, 152.72, 141.61 (q, *J* = 1.8 Hz), 131.43, 120.30 (q, *J* = 255.1 Hz), 118.83 (CH), 118.10 (CH), 114.46 (CH). ES-MS (methanol) *m/z*: 250.0

[M+H]$^+$. HRMS (ESI-TOF) *m/z*: C$_8$H$_6$F$_3$N$_3$OS experimental 250.0258 [M+H]$^+$, theoretical 250.0256 [M+H]$^+$, Δ = 0.0002. Purity HPLC: 98.4%.

3.5.2.3. Synthesis of N,O-dimethyl-N-(6-(trifluoromethoxy)benzo[d]thiazol-2-yl)hydroxylamine (44)

To a solution of 100 mg (0.394 mmol) of 2-chloro-6-(trifluoromethoxy)benzo[d]thiazole (**43**), commercially available, in 10 mL of buthanol, 154 mg (1.58 mmol) of N-methyl methoxylamine and 0.274 mL (1.97 mmol of triethylamine were added and the mixture was refluxed overnight. Then the crude product was concentrated under reduced pressure and purified with flash chromatography (light petroleum 95% – EtOAc 5%) to give 63.0 mg of white solid. Yield 58%; mp 53°C. ^{1}H NMR (400 MHz, DMSO-*d$_6$*) δ 8.02 (dd, *J* = 2.3, 0.8 Hz, 1H), 7.68 (d, *J* = 8.8 Hz, 1H), 7.39 –7.27 (m, 1H), 3.82 (s, 3H), 3.35 (s, 4H). ^{13}C NMR (101 MHz, DMSO-*d$_6$*) δ 173.30, 151.06, 143.16 (d, *J* = 1.9 Hz), 132.78, 120.77 (CH), 120.21 (q, *J* = 255.8 Hz), 119.71 (CH), 115.12 (CH), 61.54 (CH$_3$), 39.01 (CH$_3$). ES-MS (methanol) *m/z*: 279.0 [M+H]$^+$. HRMS (ESI-TOF) *m/z*: C$_{10}$H$_9$F$_3$N$_2$O$_2$S experimental 279.0410 [M+H]$^+$, theoretical 279.0410 [M+H]$^+$, Δ = 0.0000. Purity HPLC: 99.9%.

3.5.2.4. Synthesis of N-methyl-6-(trifluoromethoxy)benzo[d]thiazol-2-amine (45)

In a microwave test-tube 100 mg (0.394 mmol) of 2-chloro-6-(trifluoromethoxy)benzo[d]thiazole (**43**), commercially available, 83.0 mg (1.58 mmol) of methoxyamine hydrochloride and 0.274 mL (1.97 mmol) of triethylamine were suspended in 2.00 mL of buthanol. The mixture was stirred in the microwave reactor at 150°C for 1 h. Once completed the solvent was removed under reduced pressure and the residue was purified with flash chromatography (Light petroleum 60% – EtOAc 40%). The product was then filtered with EtOEt collecting 32.0 mg of white solid. Yield 33%; mp 112°C. ^{1}H NMR (400 MHz, DMSO-*d$_6$*) δ 8.09 (d, *J* = 4.7 Hz, 1H), 7.78 (d, *J* = 2.0 Hz, 1H), 7.42 (d, *J* = 8.7 Hz, 1H), 7.19 (dd, *J* = 8.7, 2.0 Hz, 1H), 2.94 (d, *J* = 4.7 Hz, 3H). ^{13}C NMR (101 MHz, DMSO-*d$_6$*) δ 167.96, 151.85, 142.08, 131.41, 120.27 (q, *J* = 255.2 Hz), 119.06 (CH), 118.19 (CH), 114.50 (CH), 30.52 (CH$_3$). ES-MS (methanol) *m/z*: 249.0 [M+H]$^+$. HRMS (ESI-TOF) *m/z*: C$_9$H$_7$F$_3$N$_2$OS experimental 249.0305 [M+H]$^+$, theoretical 249.0304 [M+H]$^+$, Δ = 0.0001. Purity HPLC: 99.3%.

3.5.2.5. Synthesis of 2-(1,2-dimethylhydrazineyl)-6-(trifluoromethoxy)benzo[d]thiazole (46)

To a solution of 100 mg (0.364 mmol) of 2-chloro-6-(trifluoromethoxy)benzo[d]thiazole (**43**), commercially available, in 10 mL of ethanol 42.0 μL (1.19 mmol) of methylhydrazine were added. La reaction was refluxed overnight and once completed, the crude was purified with flash chromatography (light petroleum 60% – EtOAc 40%) to give 5.00 mg of white compound. Yield 4%; mp 152°C. ^{1}H NMR (400 MHz, CDCl$_3$) δ 7.57 (d, *J* = 8.8 Hz, 1H), 7.50 (dd, *J* = 5.5, 5.0 Hz, 1H), 7.21 – 7.13 (m, 1H), 7.09 (q, *J* = 5.3 Hz, 1H), 3.57 (s, 3H), 2.11 (d, *J* = 5.3 Hz, 3H). ^{13}C NMR (101 MHz, CDCl$_3$) δ 170.02, 150.70, 143.93 (q, *J* = 1.8 Hz), 137.83 (CH), 132.83, 120.63 (q, *J* = 256.4 Hz, CH), 120.01, 119.34, 113.94 (CH), 31.99 (CH$_3$), 18.74 (CH$_3$). ES-MS (methanol) *m/z*: 290.1 [M+Na]$^+$. HRMS (ESI-TOF) *m/z*: C$_{10}$H$_{10}$F$_3$N$_3$OS experimental 290.0567 [M+Na]$^+$, theoretical 290.0569 [M+Na]$^+$, Δ = 0.0002. Purity HPLC: 89.2%.

3.5.2.6. Synthesis of 2-(2-phenylhydrazineyl)-5-(trifluoromethoxy)benzo[d]thiazole hydrochloride (47)

To a solution of 150 mg (0.590 mmol) of 2-chloro-6-(trifluoromethoxy)benzo[d]thiazole (**43**), commercially available, in 7.5 mL of butanol, 145 μL of phenylhydrazine were added. The reaction was refluxed under argon atmosphere for 3 h; once completed the solvent was removed under reduced pressure and the crude product was purified with flash chromatography (light petroleum 90% - EtOAc 10%). Hydrochloride salt of the compound was then formed by adding hydrochloride acid in 1,4-dioxane at room temperature for 30 minutes. Solvent was then eliminated under vacuum and the crude was then filtered using EtOAc to provide 21.0 mg of white compound. Yield 10%; mp 134°C. ^{1}H NMR (400 MHz, DMSO-*d$_6$*) δ 9.78 (s, 1H), 7.83 (d, *J* = 1.3 Hz, 1H), 7.81 – 7.75 (m, 1H), 7.45 (dd, *J* = 5.1, 2.1 Hz, 1H), 7.21 – 7.11 (m, 5H), 3.99 (s, 1H). ^{13}C NMR (101

MHz, DMSO-d_6) δ 186.13, 169.80, 158.27, 143.26, 128.84, 128.72 (d, J = 1.5 Hz), 126.56, 126.41, 119.41, 118.78, 111.40, 110.00 (d, J = 1.3 Hz), 102.66. ES-MS (methanol) m/z: 326.0 [M+H]$^+$. HRMS (ESI-TOF) m/z: $C_{14}H_{11}ClF_3N_3OS$ (hydrochloride compound) experimental 326.0568 [M+H]$^+$, theoretical 365.0569 [M+H]$^+$, Δ = 0.0001. Purity HPLC: 93.5%.

3.5.3. Synthesis of O-substituted-N-(6-(trifluoromethoxy)benzo[*d*]thiazol-2-yl)hydroxylamine hydrochloride derivatives (**71-76**).

3.5.3.1. General procedure for the synthesis of 2-(alkyloxy)isoindoline-1,3-dione (**42-52**)

To a solution of 4.00 g (29.4 mmol) of N-hydroxy phthalimide (**48**), commercially available, and 1.5 equivalents of the desired 1-bromoalcane in 106 mL of anhydrous DMF, 8.10 g (58.8 mmol) of K_2CO_3 were added under argon atmosphere. The mixture was stirred at room temperature for 48 h. Once completed, the reaction was quenched dropwise at 0°C using 60.0 mL of saturated solution of Na_2CO_3 and the mixture was extracted with DCM (90.0 mL x 3). The organic layer was then washed with 90.0 mL of $NaHCO_3$, 90.0 mL of H_2O and 90.0 mL of brine and finally dried over anhydrous sodium sulfate.

3.5.3.1.1. 2-propoxyisoindoline-1,3-dione (**49**)

Yield 60% (3.00 g). White solid; mp 76°C. ^{1}H NMR (499 MHz, DMSO-d_6) δ 7.86 (s, 4H), 4.09 (t, J = 6.6 Hz, 2H), 1.74 – 1.63 (m, 2H), 0.99 (t, J = 7.4 Hz, 3H). ESI-MS (methanol) m/z $C_{11}H_{11}NO_3$: 206.0 [M+H]$^+$, 228.0 [M+Na]$^+$.

3.5.3.1.2. 2-(pentyloxy)isoindoline-1,3-dione (**50**)

Yield 94% (2.70 g from 2.00 g of starting material). White solid; mp 40°C. ^{1}H NMR (400 MHz, CDCl$_3$) δ 7.83 (td, J = 5.2, 2.0 Hz, 2H), 7.75 (td, J = 5.2, 2.0 Hz, 2H), 4.20 (t, J = 6.8 Hz, 2H), 1.90 – 1.71 (m, 2H), 1.52 – 1.30 (m, 4H), 0.93 (t, J = 7.2 Hz, 3H).

3.5.3.1.3. 2-(isopentyloxy)isoindoline-1,3-dione (**51**)

Yield 74% (4.00 g). White solid; mp 47°C. ^{1}H NMR (400 MHz, DMSO-d_6) δ 7.85 (s, 4H), 4.16 (t, J = 6.6 Hz, 2H), 1.81 (dt, J = 13.5, 6.7 Hz, 1H), 1.57 (q, J = 6.7 Hz, 2H), 0.92 (d, J = 6.7 Hz, 6H). ESI-MS (methanol) m/z $C_{13}H_{15}NO_3$: 334.0 [M+H]$^+$.

3.5.3.1.4. 2-((2-ethylhexyl)oxy)isoindoline-1,3-dione (**52**)

Yield 70% (1.93 g). Transparent liquid. ^{1}H NMR (400 MHz, DMSO-d_6) δ 7.85 (s, 4H), 4.04 (d, J = 5.6 Hz, 2H), 3.55 (dd, J = 4.7, 1.4 Hz, 2H), 1.70 – 1.59 (m, 1H), 1.54 – 1.39 (m, 4H), 0.89 (dt, J = 10.0, 5.3 Hz, 8H).

3.5.3.2. General procedure for the synthesis of O-alkylhydrazine hydrochloride (**54-56**, **58**)

1 equivalent (10.0 mmol) of 2-(alkyloxy)isoindoline-1,3-dione (**42-52**) was solved in 11 mL of THF. 3 equivalents (30.0 mmol) of monohydrate hydrazine were added dropwise to the mixture and the reaction was covered and stirred at room temperature overnight. Once completed, the mixture was filtered and washed with THF and with 60.0 mL of NaOH 0.1 M and extracted with 30.0 mL of EtOAc (2 x 30.0 mL). The organic layer was dried over anhydrous sodium sulfate and the resulting mixture was acidified with 25.0 mL of HCl in 1,4-dioxane for 5 minutes. The solvent was removed under reduced pressure and the resulting crude product was filtered with diethyl ether at 0°C to collect white solid compounds **54-56**, **58**.

3.5.3.2.1. O-propylhydroxylamine hydrochloride (**54**)

Yield 66% (1.05 g). White solid; mp 127°C. ^{1}H NMR (400 MHz, DMSO-d_6) δ 11.03 (s, 3H), 3.96 (t, J = 6.5 Hz, 2H), 1.66 – 1.52 (m, 2H), 0.88 (t, J = 7.4 Hz, 3H). ESI-MS (methanol) m/z $C_3H_{10}ClNO$ (hydrochloride compound): 76.1 [M+H]$^+$, 113.9 [M+K]$^+$.

3.5.3.2.2. O-pentylhydroxylamine hydrochloride (**55**)

Yield 46% (741 mg). White solid; mp 139°C. ^{1}H NMR (400 MHz, DMSO-d_6) δ 11.08 (bs, 2H), 4.00 (t, $J =$ 6.5 Hz, 2H), 1.72 – 1.47 (m, 2H), 1.37 – 1.23 (m, 4H), 0.86 (t, $J =$ 6.9 Hz, 3H).

3.5.3.2.3. O-isopentylhydroxylamine hydrochloride (**56**)

Yield 67% (1.63 g). White solid; mp 121°C. ^{1}H NMR (400 MHz, DMSO-d_6) δ 10.82 (s, 3H), 4.00 (t, $J =$ 6.6 Hz, 2H), 1.64 (dt, $J =$ 13.5, 6.7 Hz, 1H), 1.45 (q, $J =$ 6.7 Hz, 2H), 0.88 (d, $J =$ 6.6 Hz, 6H). ESI-MS (methanol) *m/z* $C_5H_{14}ClNO$ (hydrochloride compound): 104.0 [M+H]$^+$.

3.5.3.2.4. O-(2-ethylhexyl)hydroxylamine hydrochloride (**58**)

Yield 67% (740 mg). White solid; mp 138°C. ^{1}H NMR (400 MHz, DMSO-d_6) δ 10.97 (s, 3H), 3.92 (d, $J =$ 5.7 Hz, 2H), 1.37 – 1.17 (m, 9H), 0.92 – 0.79 (m, 6H). ESI-MS (methanol) *m/z* $C_8H_{20}ClNO$ (hydrochloride compound: 146.0 [M+H]$^+$.

3.5.3.3. General procedure for the synthesis of tert-butyl alkyloxycarbamate (**59-64**)

1 equivalent of synthesized O-alkylhydrazine hydrochloride (**54-56**, **58**) or commercially available **53**, **57** was solved in CH_3CN (0.75 mL/mmol) and 1.1 equivalents of Et$_3$N was added to the mixture that was stirred at room temperature for 1.30 h. Once completed, the reaction was filtered and washed with CH_3CN and the resulting solution was cooled at 0°C. To this mixture a solution of 2 equivalents of Boc$_2$O in CH_3CN (3 mL/mmol) was added dropwise at 0°C. The reaction was then stirred overnight at room temperature. Once completed, the solvent was removed under reduced pressure, the crude product was solved in 75 mL of DCM and washed with water. The organic layer was dried over anhydrous sodium sulfate and the solvent was eliminated under vacuum to collect white solid.

3.5.3.3.1. *Tert*-butyl methoxycarbamate (**59**)

Yield 51% (1.80 g). White solid; mp 63°C. ^{1}H NMR (400 MHz, CDCl$_3$) δ 7.18 (s, 1H), 3.71 (s, 3H), 1.48 (s, 9H).

3.5.3.3.2. *Tert*-butyl propoxycarbamate (**60**)

Yield 96% (1.50 mg). White solid; mp 49°C. ^{1}H NMR (400 MHz, DMSO-d_6) δ 9.89 (s, 1H), 3.63 (t, $J =$ 6.6 Hz, 2H), 1.51 (dd, $J =$ 14.2, 6.8 Hz, 2H), 1.40 (s, 9H), 0.88 (t, $J =$ 7.4 Hz, 3H). ESI-MS (methanol) *m/z* $C_8H_{17}NO_3$: 197.9 [M+H]$^+$.

3.5.3.3.3. *Tert*-butyl (pentyloxy)carbamate (**61**)

Yield 58% (612 mg). White solid; mp 56°C. ^{1}H NMR (400 MHz, CDCl$_3$) δ 7.12 (s, 1H), 3.83 (t, $J =$ 6.7 Hz, 2H), 1.66 – 1.53 (m, 2H), 1.47 (s, 9H), 1.41 – 1.28 (m, 4H), 0.98 – 0.81 (m, 3H).

3.5.3.3.4. *Tert*-butyl (isopentyloxy)carbamate (**62**)

Yield 95% (1.40 g). White solid; mp 67°C. ^{1}H NMR (499 MHz, DMSO-d_6) δ 9.88 (s, 1H), 3.70 (t, $J =$ 6.6 Hz, 2H), 1.67 (dt, $J =$ 13.4, 6.7 Hz, 1H), 1.47 (s, 11H), 0.87 (d, $J =$ 6.7 Hz, 6H). ESI-MS (methanol) *m/z* $C_{10}H_{21}NO_3$: 226.0 [M+Na]$^+$.

3.5.3.3.5. *Tert*-butyl (benzyloxy)carbamate (**63**)

Yield 34% (788 mg). White solid; mp 48°C. ^{1}H NMR (400 MHz, CDCl$_3$) δ 7.42-7.32 (m, 5H), 7.07 (s, 1H), 4.86 (s, 2H), 1.48 (s, 9H).

3.5.3.3.6. *Tert*-butyl ((2-ethylhexyl)oxy)carbamate (**64**)

Yield 82% (821 mg). White solid; mp 74°C. ^{1}H NMR (400 MHz, DMSO-d_6) δ 9.85 (s, 1H), 3.56 (d, $J =$ 5.8 Hz, 2H), 1.46 (s, 2H), 1.45 (s, 9H), 1.28 (ddd, $J =$ 27.8, 16.1, 6.0 Hz, 7H), 0.88 – 0.80 (m, 6H). ESI-MS (methanol) *m/z* $C_{13}H_{27}NO_3$: 268.1 [M+Na]$^+$, 284.1 [M+K]$^+$.

3.5.3.4. General procedure for synthesis of tert-butyl alkyloxy(6-(trifluoromethoxy)benzo[d]thiazol-2-yl)carbamate (**65-70**)

Under argon atmosphere 0.15 equivalents of Pd$_2$(dba)$_3$ and 0.20 equivalents of dppf were added to 15 mL of anhydrous CH$_3$CN. The mixture was heated at 40°C. Then, 2.0 equivalents of *tert*-butyl alkyloxycarbamate (**59-64**) were added to the reaction. After 10 minutes 1.0 equivalent of 2-chloro-6-(trifluoromethoxy)benzo[*d*]thiazole, commercially available, and 1.6 equivalents of Cs$_2$CO$_3$ were added and the mixture was stirred at 40°C overnight. Once completed, the catalyst was removed by filtration through a Celite pad. The filtered solution was then washed with brine (2 x 20 mL) and dried over anhydrous sodium sulfate. The solvent was removed under reduced pressure and the crude was purified with flash chromatography (light petroleum 95% – EtOAc 5%) to obtain pale yellow solid.

3.5.3.4.1. *Tert*-butyl methoxy(6-(trifluoromethoxy)benzo[*d*]thiazol-2-yl)carbamate (**65**)

Yield 23% (98.3 mg). Pale yellow solid; mp 56°C. ^{1}H NMR (400 MHz, CDCl$_3$) δ 7.87 (d, *J* = 8.9 Hz, 1H), 7.61 (d, *J* = 1.5 Hz, 1H), 7.30 – 7.26 (m, 1H), 4.04 (s, 3H), 1.65 (s, 9H).

3.5.3.4.2. O-propyl-N-(6-(trifluoromethoxy)benzo[*d*]thiazol-2-yl)hydroxylamine (**66**)

Preparative TLC was performed after the flash chromatography (light petroleum – EtOAc 95:5). Yield 4% (15.0 mg). HRMS (ESI-TOF) *m/z*: C$_{11}$H$_{11}$F$_3$N$_2$O$_2$S experimental 293.0560 [M+H]$^+$, theoretical 293.0566 [M+H]$^+$, Δ = 0.0006. The compound was treated with HCl *in situ* without ^{1}H and ^{13}C characterization because of its instability.

3.5.3.4.3. *Tert*-butyl (pentyloxy)(6-(trifluoromethoxy)benzo[*d*]thiazol-2-yl)carbamate (**67**)

Yield 19% (122 mg). Pale yellow solid; mp 77°C. ^{1}H NMR (400 MHz, CDCl$_3$) δ 7.85 (d, *J* = 8.6 Hz, 1H), 7.61 (d, *J* = 1.3 Hz, 1H), 7.27 (d, *J* = 6.8 Hz, 1H), 4.21 (d, *J* = 3.6 Hz, 2H), 1.80 (d, *J* = 7.7 Hz, 2H), 1.64 (s, 9H), 1.54 – 1.46 (m, 2H), 1.46 – 1.31 (m, 2H), 0.94 (t, *J* = 7.2 Hz, 3H). ESI-MS (metanolo) *m/z* C$_{18}$H$_{23}$F$_3$N$_2$O$_4$S: 443.0 [M+Na]$^+$, 459.0 [M+K]$^+$.

3.5.3.4.4. *Tert*-butyl (isopentyloxy)(6-(trifluoromethoxy)benzo[*d*]thiazol-2-yl)carbamate (**68**)

Yield 3% (17.0 mg). Pale yellow solid; mp 68°C. ^{1}H NMR (499 MHz, DMSO-*d$_6$*) δ 8.43 (d, *J* = 1.3 Hz, 1H), 8.33 (d, *J* = 8.9 Hz, 1H), 7.65 (dd, *J* = 8.6, 2.1 Hz, 1H), 3.86 (t, *J* = 6.4 Hz, 2H), 1.71 (dt, *J* = 13.4, 6.7 Hz, 1H), 1.46 (s, 9H), 1.44 – 1.40 (m, 2H), 0.89 (d, *J* = 6.7 Hz, 6H). ESI-MS (methanol) *m/z* C$_{18}$H$_{23}$F$_3$N$_2$O$_4$S: 443.2 [M+Na]$^+$.

3.5.3.4.5. *Tert*-butyl (benzyloxy)(6-(trifluoromethoxy)benzo[*d*]thiazol-2-yl)carbamate (**69**)

Yield 40% (300 mg). Pale yellow solid; mp 64°C. ^{1}H NMR (400 MHz, CDCl$_3$) δ 7.90 (d, J = 8.7 Hz, 1H), 7.63 (d, J = 1.3 Hz, 1H), 7.53 (dd, J = 6.4, 2.9 Hz, 2H), 7.45 – 7.37 (m, 3H), 7.30 (d, J = 7.5 Hz, 1H), 5.23 (s, 2H), 1.55 (s, 9H). ESI-MS (methanol) *m/z* C$_{20}$H$_{19}$F$_3$N$_2$O$_4$S: 463.0 [M+Na]$^+$.

3.5.3.4.6. *Tert*-butyl ((2-ethylhexyl)oxy)(6-(trifluoromethoxy)benzo[*d*]thiazol-2-yl)carbamate (**70**)

Yield 22% (142 mg). Pale yellow solid; mp 82°C. ^{1}H NMR (499 MHz, DMSO-*d$_6$*) δ 8.27 (d, *J* = 1.9 Hz, 1H), 8.08 (d, *J* = 8.9 Hz, 1H), 7.57 (dd, *J* = 10.0, 2.1 Hz, 1H), 4.09 (s, 2H), 1.68 – 1.38 (m, 18H), 0.97 (t, *J* = 7.4 Hz, 3H), 0.90 (t, *J* = 7.1 Hz, 3H). ESI-MS (methanol) *m/z*: 486.1 [M+Na]$^+$. HRMS (ESI-TOF) *m/z*: C$_{21}$H$_{29}$F$_3$N$_2$O$_4$S experimental 485.1693 [M+Na]$^+$, theoretical 485.1692 [M+Na]$^+$, Δ = 0.0001. Purity HPLC: 99.2%.

3.5.3.5. General procedure for the synthesis of O-alkyl-N-(6-(trifluoromethoxy)benzo[*d*]thiazol-2-yl)hydroxylamine (**71-76**)

Method A: 2.5 mmol of acetyl chloride was added dropwise at 0°C to 11 mL of MeOH. Once completed, a solution of 0.5 mmol of **65, 67-70** in 3 mL of EtOAc was added dropwise to the first solution. The reaction

was stirred at room temperature overnight. Then, the solvent was removed under reduced pressure and the crude was filtered using EtOAc to collect white solid.

Method B: 4 mL of HCl in 1,4-dioxane were added to 1 mmol of compound **66**. The mixture was stirred at room temperature overnight. Once completed, the solvent was removed under reduced pressure and the crude was filtered using EtOAc to collect white solid of final products **72**.

3.5.3.5.1. O-methyl-N-(6-(trifluoromethoxy)benzo[d]thiazol-2-yl)hydroxylamine hydrochloride (71)

Method A. Yield 34% (26.0 mg). White solid; mp 135°C. ^{1}H NMR (400 MHz, DMSO-d_6) δ 7.65 (d, J = 1.7 Hz, 1H), 7.16 (dd, J = 8.7, 1.6 Hz, 1H), 7.03 (d, J = 8.7 Hz, 1H), 3.72 (s, 3H).^{13}C NMR (101 MHz, DMSO-d_6) δ 142.15, 125.20, 124.44, 121.90, 120.21 (CH), 119.35, 116.31 (CH), 111.78 (CH), 62.25 (CH$_3$). ESI-MS (methanol) m/z: 264.9 [M+H]$^+$. HRMS (ESI-TOF) m/z: C$_9$H$_8$ClF$_3$N$_2$O$_2$S (hydrochloride compound) experimental 265.0256 [M+H]$^+$, theoretical 265.0253 [M+H]$^+$, Δ = 0.0003. Purity HPLC: 96.9%.

3.5.3.5.2. O-propyl-N-(6-(trifluoromethoxy)benzo[d]thiazol-2-yl)hydroxylamine hydrochloride (72)

Method B. Yield 67% (10.0 mg). White solid; mp 157°C. ^{1}H NMR (400 MHz, DMSO-d_6) δ 7.89 (s, 1H), 7.69 (dd, J = 12.1, 2.9 Hz, 1H), 7.19 (s, 1H), 1.61 (dd, J = 14.2, 6.6 Hz, 4H), 0.95 – 0.89 (m, 3H). HRMS (ESI-TOF) m/z: C$_{11}$H$_{12}$ClF$_3$N$_2$O$_2$S (hydrochloride compound) experimental 293.0560 [M+H]$^+$, theoretical 293.0566 [M+H]$^+$, Δ = 0.0006. Purity HPLC: 93.8%.

3.5.3.5.3. O-pentyl-N-(6-(trifluoromethoxy)benzo[d]thiazol-2-yl)hydroxylamine hydrochloride (73)

Method A. Yield 90% (72.0 mg). White solid; mp 139°C. ^{1}H NMR (400 MHz, DMSO-d_6) δ 7.65 (s, 1H), 7.16 (d, J = 8.1 Hz, 1H), 7.04 (d, J = 8.6 Hz, 1H), 6.55 (bs, NH salt), 3.89 (t, J = 6.4 Hz, 2H), 1.72 – 1.52 (m, 2H), 1.40 – 1.24 (m, 4H), 0.87 (t, J = 6.7 Hz, 3H). ^{13}C NMR (101 MHz, DMSO-d_6) δ 158.72, 141.75, 141.22, 125.12, 120.23 (q, J = 255.4 Hz), 119.78 (CH), 115.86 (CH), 111.65 (CH), 73.75 (CH$_2$), 28.11 (CH$_2$), 27.75 (CH$_2$), 22.00 (CH$_2$), 13.97 (CH$_3$). ESI-MS (methanol) m/z: 321.0 [M+H]$^+$, 353.3 [M+Na]$^+$. HRMS (ESI-TOF) m/z: C$_{13}$H$_{16}$ClF$_3$N$_2$O$_2$S (hydrochloride compound) experimental 321.0880 [M+H]$^+$, theoretical 321.0879 [M+H]$^+$, Δ = 0.0001. Purity HPLC: 99.6%.

3.5.3.5.4. O-isopentyl-N-(6-(trifluoromethoxy)benzo[d]thiazol-2-yl)hydroxylamine hydrochloride (74)

Method A. Yield 60% (14.5 mg). White solid; mp 141°C. ^{1}H NMR (400 MHz, DMSO-d_6) δ 8.43 (s, 1H), 8.33 (d, J = 8.8 Hz, 1H), 7.66 (dd, J = 8.3, 2.3 Hz, 1H), 1.57 – 1.44 (m, 1H), 1.34 – 1.27 (m, 2H), 1.16 (d, J = 7.3 Hz, 2H), 0.89 – 0.83 (m, 6H). ^{13}C NMR (101 MHz, DMSO-d_6) δ 160.85 (d, J = 5.7 Hz), 153.43 (d, J = 3.4 Hz), 149.45 – 144.56 (m), 134.85 (d, J = 5.1 Hz), 122.69 (CH), 120.38 (CH), 115.27 (d, J = 3.5 Hz, CH), 109.99, 81.50 (d, J = 100.8 Hz), 48.45 (CH$_2$), 29.46 – 27.35 (CH$_2$), 22.32 (d, J = 10.9 Hz, CH), 14.28 (CH$_3$). ESI-MS (methanol) m/z: 321.2263 [M+H]$^+$, 344.0860 [M+Na]$^+$. HRMS (ESI-TOF) m/z: C$_{13}$H$_{16}$ClF$_3$N$_2$O$_2$S (hydrochloride compound) experimental 320.0890 [M+H]$^+$, theoretical 320.0801 [M+H]$^+$, Δ = 0.0089. Purity HPLC: 96.1%.

3.5.3.5.5. O-benzyl-N-(6-(trifluoromethoxy)benzo[d]thiazol-2-yl)hydroxylamine hydrochloride (75)

Method A. Yield 86% (206 mg). White solid; mp 195°C. ^{1}H NMR (400 MHz, DMSO-d_6) δ 7.62 (s, 1H), 7.40 – 7.28 (m, 5H), 7.15 (d, J = 8.7 Hz, 1H), 7.00 (d, J = 8.7 Hz, 1H), 4.95 (s, 2H). ^{13}C NMR (101 MHz, DMSO-d_6) δ 158.48, 141.76, 140.57, 137.88, 128.30 (CH), 128.07 (CH), 127.80 (CH), 124.71, 119.86 (CH), 115.93 (CH), 111.26 (CH), 75.54 (CH$_2$). ESI-MS (methanol) m/z: 341.0 [M+H]$^+$. HRMS (ESI-TOF) m/z:

$C_{15}H_{12}ClF_3N_2O_2S$ (hydrochloride compound) experimental 341.0565 [M+H]$^+$, theoretical 341.0566 [M+H]$^+$, Δ = 0.0001. Purity HPLC: 98.0%.

3.5.3.5.6. O-(2-ethylhexyl)-N-(6-(trifluoromethoxy)benzo[d]thiazol-2-yl)hydroxylamine hydrochloride (76)

Method A. Yield 48% (10.0 mg). White solid; mp 154°C. ^{1}H NMR (499 MHz, DMSO-d_6) δ 12.10 (s, 1H), 7.87 (d, J = 8.8 Hz, 1H), 7.49 (d, J = 8.9 Hz, 1H), 7.18 (d, J = 8.7 Hz, 1H), 1.66 – 1.31 (m, 8H), 1.03 (t, J = 7.4 Hz, 1H), 0.90 (dt, J = 35.0, 7.0 Hz, 8H). ^{13}C NMR (101 MHz, DMSO-d_6) δ 170.30 (d, J = 11.4 Hz), 161.38 , 149.21 (d, J = 34.7 Hz), 134.38 (d, J = 257.6 Hz), 124.43 (d, J = 97.8 Hz, CH), 119.96 (d, J = 15.9 Hz), 117.01 – 114.74 (CH), 112.51 (CH), 76.57 (CH$_2$), 38.83 – 38.18 (CH), 29.96 (d, J = 6.8 Hz, CH$_2$), 28.60 (d, J = 6.8 Hz, CH$_2$), 22.62 (CH$_2$), 22.55 (CH$_2$), 14.12 (d, J = 9.4 Hz, CH$_3$), 11.15 (d, J = 17.5 Hz, CH$_3$). ESI-MS (methanol) *m/z* $C_{16}H_{24}ClF_3N_2O_2S$ (hydrochloride compound): 363.13 [M+H]$^+$. Purity HPLC: 74.1%.

3.5.4. Synthesis of 2-(2-alkylhydrazineyl)-6-(trifluoromethoxy)benzo[d]thiazole hydrochloride derivatives (95-102)

3.5.4.1. Synthesis of di-*tert*-butyl hydrazine-1,2-dicarboxylate (78)

A mixture of 3.63 g (16.6 mmol) of di-*tert*-butyl dicarbonate, commercially available (77), and 2.00 g (15.0 mmol) of di-*tert*-butyl carbazate was allowed to react at room temperature for 20 min. Once completed, the porous solid was crystallized using chloroform – light petroleum 1:4 and filtered collecting 3.06 g of white solid. Yield 88%; mp 120-122°C. ^{1}H NMR (400 MHz, DMSO-d_6) δ 8.56 (s, 2H), 1.37 (s, 18H).

3.5.4.2. General procedure for the synthesis of di-*tert*-butyl 1-alkylhydrazine-1,2-dicarboxylate (79-86)

A mixture of 1.00 g (4.30 mmol) of di-*tert*-butyl decarbonate (78) and 2.80g (8.60 mmol) of cesium carbonate in 20 mL of anhydrous DMF was allowed to react at room temperature for 1 h. Then, 4.73 mmol of the desired alkyl bromide were added. The reaction was stirred at room temperature for 12 h. The mixture was diluted with water and extracted with EtOAc (3 x 20 mL). The organic layers were washed with water and brine and dried over anhydrous sodium sulfate. The solvent was concentrated under reduced pressure and the crude was purified with flash chromatography.

3.5.4.2.1. Di-*tert*-butyl 1-methylhydrazine-1,2-dicarboxylate (79)

Flash chromatography eluent: light petroleum 93%– EtOAc 7%. Yield 50% (666 mg). White solid; mp 53-58°C. ^{1}H NMR (400 MHz, CDCl$_3$) δ 6.40 (s, 1H), 3.11 (s, 3H), 1.47 (d, J = 5.9 Hz, 18H).

3.5.4.2.2. Di-*tert*-butyl 1-propylhydrazine-1,2-dicarboxylate (80)

Flash chromatography eluent: light petroleum 93%– EtOAc 7%. Yield 64% (1.67 g). White solid; mp 55°C. ^{1}H NMR (400 MHz, DMSO-d_6) δ 9.01 (s, 1H), 3.23 (s, 2H), 1.38 (d, J = 15.7 Hz, 20H), 0.81 (t, J = 7.1 Hz, 3H). ES-MS (methanol) *m/z* $C_{13}H_{26}N_2O_4$: 297.1 [M+Na]$^+$, 313.1 [M+K]$^+$.

3.5.4.2.3. Di-*tert*-butyl 1-pentylhydrazine-1,2-dicarboxylate (81)

Flash chromatography eluent: light petroleum 93%– EtOAc 7%. Yield 88% (1.37 g). White solid; mp 54-55°C. ^{1}H NMR (400 MHz, DMSO-d_6) δ 9.01 (s, 1H), 3.31 (s,23H), 1.38 (d, J = 16.3 Hz, 20H), 1.26 (dd, J = 13.5, 6.9 Hz, 4H), 0.85 (t, J = 6.8 Hz, 3H). ES-MS (methanol) *m/z* $C_{15}H_{30}N_2O_4$: 325.1 [M+Na]$^+$, 341.1 [M+K]$^+$.

3.5.4.2.4. Di-*tert*-butyl 1-isopentylhydrazine-1,2-dicarboxylate (82)

Flash chromatography eluent: light petroleum 90%– EtOAc 10%. Yield 62% (1.22 g). White solid; mp 70-74°C. ^{1}H NMR (400 MHz, CDCl$_3$) δ 6.43 – 5.91 (m, 1H), 3.44 (s, 2H), 1.60 – 1.35 (m, 21H), 0.90 (d, J = 6.6 Hz, 6H).

3.5.4.2.5. Di-*tert*-butyl 1-benzylhydrazine-1,2-dicarboxylate (**83**)

Flash chromatography eluent: light petroleum 90%– EtOAc 1%. Yield 62% (1.30 g). White solid; mp 108°C. ^{1}H NMR (400 MHz, CDCl$_3$) δ 7.43 –7.17 (m, 5H), 6.20 (s, 1H), 4.63 (s, 2H), 1.46 (s, 18H).

3.5.4.2.6. Di-*tert*-butyl 1-(2-ethylhexyl)hydrazine-1,2-dicarboxylate (**84**)

Flash chromatography eluent: light petroleum 90% – EtOAc 10%. Yield 39% (1.15 g). Transparent liquid. ^{1}H NMR (400 MHz, DMSO-d_6) δ 9.04 (s, 1H), 3.10 (d, J = 66.5 Hz, 2H), 1.58 – 1.10 (m, 27H), 0.82 (dt, J = 14.4, 6.8 Hz, 6H). ES-MS (methanol) m/z C$_{18}$H$_{36}$N$_2$O$_4$: 367.2 [M+Na]$^+$.

3.5.4.2.7. Di-*tert*-butyl 1-phenethylhydrazine-1,2-dicarboxylate (**85**)

Flash chromatography eluent: light petroleum 93% – EtOAc 7%. Yield 22% (760 mg). ^{1}H NMR (400 MHz, DMSO-d_6) δ 9.16 (s, 1H), 7.32 – 7.15 (m, 5H), 3.49 (s, 2H), 2.80 – 2.68 (m, 2H), 1.53 – 1.13 (m, 18H). ES-MS (methanol) m/z C$_{18}$H$_{28}$N$_2$O$_4$: 359.1 [M+Na]$^+$.

3.5.4.2.8. Di-*tert*-butyl 1-(3-phenylpropyl)hydrazine-1,2-dicarboxylate (**86**)

Flash chromatography eluent: light petroleum 93% – EtOAc 7%. Yield 31% (590 mg). ^{1}H NMR (400 MHz, DMSO-d_6) δ 9.08 (s, 1H), 7.26 (t, J = 7.4 Hz, 2H), 7.17 (dd, J = 18.1, 7.1 Hz, 3H), 3.25 (d, J = 38.4 Hz, 2H), 2.56 (t, J = 7.0 Hz, 2H), 1.71 (d, J = 5.7 Hz, 2H), 1.39 (d, J = 16.1 Hz, 18H). ES-MS (methanol) m/z C$_{19}$H$_{30}$N$_2$O$_4$: 373.1 [M+Na]$^+$.

3.5.4.3. General procedure for the synthesis of 2-di-*tert*-butyl 1-alkyl-2-(6-(trifluoromethoxy)benzo[*d*]thiazol-2-yl)hydrazine-1,2-dicarboxylate (**87-94**)

To a solution of 1.00 equivalent (2.00 mmol) of 2-chloro-6-(trifluoromethoxy)benzo[*d*]thiazole (**43**) in 5 mL of toluene, 3.00 equivalents (6.00 mmol) of di-*tert*-butyl 1-alkylhydrazine-1,2-dicarboxylate (**78-86**), 2.50 (5.00 mmol) equivalents of cesium carbonate, 0.20 equivalents (0.40 mmol) of dppf and 0.15 equivalents (0.30 mmol) of Pd$_2$(dba)$_3$ were added to the mixture under argon atmosphere and the reaction was refluxed overnight. Once completed, the catalyst was removed by filtration through a Celite pad. The filtered solution was then washed with brine (2 x 20 mL) and dried over anhydrous sodium sulfate. The solvent was removed under reduced pressure and the crude was purified with flash chromatography (light petroleum 95% – EtOAc 5%).

3.5.4.3.1. Di-*tert*-butyl 1-methyl-2-(6-(trifluoromethoxy)benzo[*d*]thiazol-2-yl)hydrazine-1,2-dicarboxylate (**87**)

Yield 65% (154 mg). White solid; mp 101°C. ^{1}H NMR (400 MHz, CDCl$_3$) δ 7.82 (t, J = 9.5 Hz, 1H), 7.61 (dd, J = 8.7, 1.4 Hz, 1H), 7.29 (dd, J = 2.1, 1.2 Hz, 1H), 1.60 (d, J = 4.9 Hz, 9H), 1.53 (s, 3H), 1.34 (s, 9H). ESI-MS (methanol) m/z C$_{19}$H$_{24}$F$_3$N$_3$O$_5$S: 486.1 [M+Na]$^+$.

3.5.4.3.2. Di-*tert*-butyl 1-propyl-2-(6-(trifluoromethoxy)benzo[*d*]thiazol-2-yl)hydrazine-1,2-dicarboxylate (**88**)

Yield 19% (110 mg). Pale yellow solid; mp 193°C. ^{1}H NMR (400 MHz, DMSO-d_6) δ 8.11 (s, 1H), 7.90 – 7.83 (m, 1H), 7.40 (d, J = 8.8 Hz, 1H), 3.81 – 3.34 (m, 2H), 1.82 – 1.33 (m, 20H), 0.90 (q, J = 7.5 Hz, 3H). ESI-MS (methanol) m/z C$_{21}$H$_{28}$F$_3$N$_3$O$_5$S: 514.2 [M+Na]$^+$, 530.1 [M+K]$^+$, 392.1 [(M-Boc)+H]$^+$, 314.0 [(M-Boc)+Na]$^+$, 292.0 [(M-2Boc)+H]$^+$.

3.5.4.3.3. Di-*tert*-butyl 1-pentyl-2-(6-(trifluoromethoxy)benzo[*d*]thiazol-2-yl)hydrazine-1,2-dicarboxylate (**89**)

Yield 8% (47.0 mg). White solid; mp 239°C. ^{1}H NMR (499 MHz, DMSO-d_6) δ 8.15 – 8.10 (m, 1H), 7.86 (dd, J = 13.6, 8.8 Hz, 1H), 7.41 (d, J = 8.2 Hz, 1H), 3.87 – 3.67 (m, 2H), 1.42 – 1.37 (m, 22H), 1.30 (d, J = 6.8 Hz, 4H), 0.87 (t, 3H). ^{13}C NMR (101 MHz, DMSO-d_6) δ 165.63 (s), 155.32 (d, J = 33.0 Hz), 154.63 (s), 144.96 (s), 134.82 (s), 132.03 (d, J = 4.8 Hz), 121.87 (s, J = 38.6 Hz), 121.48 (s), 109.99 (s), 80.16 (s), 49.20 (s), 28.98 (d, J = 2.9 Hz), 28.76 – 27.70 (m), 27.31 (d, J = 5.3 Hz), 22.61 – 22.11 (m), 14.28 (d, J = 1.2 Hz). ESI-MS

(methanol) *m/z*: 520.21 [M+H]$^+$, 542.19 [M+Na]$^+$, 558.17 [M+K]$^+$, 420.16 [(M-Boc)+H]$^+$, 442.14 [(M-Boc)+Na]$^+$, 458.11 [(M-Boc)+K]$^+$, 320.10 [(M-2Boc)+H]$^+$. HRMS (ESI-TOF) *m/z*: C$_{23}$H$_{32}$F$_3$N$_3$O$_5$S experimental 542.1910 [M+Na]$^+$, theoretical 542.1907 [M+Na]$^+$, Δ = 0.0003. Purity HPLC: 99.7%.

3.5.4.3.4. Di-*tert*-butyl 1-isopentyl-2-(6-(trifluoromethoxy)benzo[d]thiazol-2-yl)hydrazine-1,2-dicarboxylate (**90**)

Yield 15% (161 mg). Yellow oil. ^{1}H NMR (400 MHz, DMSO-*d$_6$*) δ 8.13 (s, 1H), 7.87 (dd, *J* = 11.5, 8.9 Hz, 1H), 7.44 – 7.39 (m, 1H), 3.90 – 3.38 (m, 2H), 1.66 (dt, *J* = 19.9, 6.6 Hz, 1H), 1.54 (d, *J* = 13.4 Hz, 9H), 1.45 – 1.37 (m, 2H), 1.24 (s, 9H), 0.88 (td, *J* = 6.6, 3.2 Hz, 6H). ^{13}C NMR (101 MHz, DMSO-*d$_6$*) δ 171.31, 167.27 (d, *J* = 1.1 Hz), 153.39, 144.70, 136.19, 122.72 (CH), 120.40 (CH), 115.29 (d, *J* = 1.3 Hz, CH), 109.99, 81.04, 46.77 (d, *J* = 1.6 Hz, CH$_2$), 36.30 (CH$_2$), 28.05 (dd, *J* = 22.7, 13.7 Hz, CH$_3$), 25.44 (d, *J* = 16.6 Hz, CH), 23.07 – 22.37 (CH$_3$). ESI-MS (methanol) *m/z* C$_{23}$H$_{32}$F$_3$N$_3$O$_5$S: 542.2 [M+Na]$^+$, 442.1 [(M-Boc)+Na]$^+$, 558.1 [M+K]$^+$.

3.5.4.3.5. Di-*tert*-butyl 1-benzyl-2-(6-(trifluoromethoxy)benzo[d]thiazol-2-yl)hydrazine-1,2-dicarboxylate (**91**)

Yield 36% (118 mg). Yellow oil. ^{1}H NMR (400 MHz, DMSO-*d$_6$*) δ 8.14 (d, *J* = 1.5 Hz, 1H), 7.93 (dd, *J* = 10.2, 8.9 Hz, 1H), 7.49 – 7.18 (m, 6H), 4.79 (ddd, *J* = 58.7, 42.6, 14.4 Hz, 2H), 1.43 – 1.15 (m, 18H). ESI-MS (methanol) *m/z* C$_{25}$H$_{28}$F$_3$N$_3$O$_5$S: 562.0 [M+Na]$^+$, 462.0 [(M-Boc)+Na]$^+$.

3.5.4.3.6. Di-*tert*-butyl 1-(2-ethylhexyl)-2-(6-(trifluoromethoxy)benzo[d]thiazol-2-yl)hydrazine-1,2-dicarboxylate (**92**)

Yield 3% (25.0 mg). White solid; mp 211°C. ^{1}H NMR (400 MHz, DMSO-*d$_6$*) δ 8.11 (d, *J* = 13.2 Hz, 1H), 7.90 – 7.81 (m, 1H), 7.41 (d, *J* = 8.9 Hz, 1H), 3.75 – 3.61 (m, 2H), 3.37 (ddd, *J* = 22.3, 15.2, 7.5 Hz, 2H), 1.60 – 1.05 (m, 25H), 0.80 (dt, *J* = 16.1, 6.9 Hz, 6H). HRMS (ESI-TOF, methanol) *m/z* C$_{26}$H$_{38}$F$_3$N$_3$O$_5$S: 562.2519 [M+H]$^+$, 584.2341 [M+Na]$^+$, 600.2072 [M+K]$^+$, 462.1981 [(M-Boc)+H]$^+$.

3.5.4.3.7. Di-*tert*-butyl 2-phenethyl-1-(6-(trifluoromethoxy)benzo[d]thiazol-2-yl)hydrazine-1-carboxylate (**93**)

Obtained the mono-Boc product. Yield 8% (50.0 mg). White solid; mp 215°C. ESI-MS (methanol) *m/z* C$_{25}$H$_{30}$F$_3$N$_3$O$_5$S: 454.1 [M+H]$^+$, 476.1 [M+Na]$^+$, 354.9 [(M-Boc)+H]$^+$, 376.8 [(M-Boc)+Na]$^+$.

3.5.4.3.8. Di-*tert*-butyl 1-(3-phenylpropyl)-2-(6-(trifluoromethoxy)benzo[d]thiazol-2-yl)hydrazine-1,2-dicarboxylate (**94**)

Yield 6% (31.0 mg). White solid; mp 231°C. ESI-MS (methanol) *m/z* C$_{27}$H$_{32}$F$_3$N$_3$O$_5$S: 490.2 [M+Na]$^+$, 468.5 [(M-Boc)+H]$^+$, 490.4 [(M-Boc)+Na]$^+$.

3.5.4.4. General procedure for the synthesis of 2-(2-alkyl hydrazineyl)-6-(trifluoromethoxy)benzo[d]thiazole hydrochloride (**95-105**)

Method A: 2.5 mmol of acethyl chloride was added dropwise at 0°C to 11 mL of MeOH. Once completed, a solution of 0.5 mmol of **87-89**, **92** in 3 mL of EtOAc was added dropwise to the first solution. The reaction was stirred at room temperature overnight. Then, the solvent was removed under reduced pressure and the crude was filtered using EtOAc to collect white solid.

Method B: 4 mL of HCl in diethyl ether were added to 1 mmol of compounds **90-91**, **93-94**. The mixture was stirred at room temperature overnight. Once completed, the reaction was filtered using diethyl ether and DCM to collect white solid of final products **98-99**, **101-102**.

3.5.4.4.1. 2-(2-methylhydrazineyl)-6-(trifluoromethoxy)benzo[d]thiazole hydrochloride (**95**)

Method A. Yield 36% (14.0 mg). White solid; mp 138°C. ^{1}H NMR (400 MHz, DMSO-*d$_6$*) δ 7.96 (bs, 1H), 7.55 (d, *J* = 8.6 Hz, 1H), 7.33 (dd, *J* = 8.7, 1.7 Hz, 1H), 2.75 (s, 3H). ^{13}C NMR (101 MHz, DMSO-*d$_6$*) δ 143.61, 121.89, 120.35 (d, *J* = 3.4 Hz, CH), 119.35 (CH), 115.99 (CH), 112.89, 109.99, 37.13 (CH$_3$). ESI-MS

(methanol) *m/z*: 264.0 [M+H]$^+$. HRMS (ESI-TOF) *m/z*: C$_9$H$_9$ClF$_3$N$_3$OS (hydrochloride compound) experimental 264.0417 [M+H]$^+$, theoretical 264.0413 [M+H]$^+$, Δ = 0.0004. Purity HPLC: 96.3%.

3.5.4.4.2. 2-(2-propylhydrazineyl)-6-(trifluoromethoxy)benzo[*d*]thiazole hydrochloride (**96**)

Method A. Yield 5% (42.4 mg). White solid; mp 180°C. ^{1}H NMR (400 MHz, DMSO-*d$_6$*) δ 10.66 (s, 1H), 7.92 (s, 1H), 7.49 (d, *J* = 8.6 Hz, 1H), 7.30 (d, *J* = 7.8 Hz, 1H), 3.79 (s, 2H), 2.91 (d, *J* = 6.0 Hz, 2H), 1.53 (d, *J* = 7.1 Hz, 2H), 0.91 (t, *J* = 7.4 Hz, 3H). ^{13}C NMR (101 MHz, DMSO-*d$_6$*) δ 177.11, 160.57, 143.32 (CH), 121.88 (CH), 120.29 (CH), 115.81 (CH$_2$), 52.59 (CH$_2$), 11.83 (CH$_3$). ESI-MS (methanol) *m/z*: 292.0 [M+H]$^+$. HRMS (ESI-TOF) *m/z*: C$_{11}$H$_{13}$ClF$_3$N$_3$OS (hydrochloride compound) experimental 242.0726 [M+H]$^+$, theoretical 242.0726 [M+H]$^+$, Δ = 0.0000. Purity HPLC: 95.4%.

3.5.4.4.3. 2-(2-pentylhydrazineyl)-6-(trifluoromethoxy)benzo[*d*]thiazole hydrochloride (**97**)

Method A. Yield 72% (9.00 mg). Pale yellow solid; mp 174°C. ^{1}H NMR (400 MHz, DMSO-*d$_6$*) δ 10.23 (s, 1H), 7.90 (s, 1H), 7.48 (d, *J* = 8.7 Hz, 1H), 7.29 (dd, *J* = 8.8, 1.4 Hz, 1H), 3.05 (qd, *J* = 7.3, 4.8 Hz, 2H), 1.39 – 1.25 (m, 4H), 1.20 (t, *J* = 7.3 Hz, 2H), 0.87 (t, *J* = 7.1 Hz, 3H). ^{13}C NMR (101 MHz, DMSO-*d$_6$*) δ 179.80, 176.58, 157.76, 153.08, 120.08 (CH), 119.38 (CH), 115.72 (CH), 109.99, 45.80 (CH$_2$), 29.02 (CH$_2$), 22.36 (CH$_2$), 14.32 (CH$_2$), 8.89 (CH$_3$). ESI-MS (methanol) HRMS (ESI-TOF) *m/z*: C$_{13}$H$_{17}$ClF$_3$N$_3$OS (hydrochloride compound) experimental 320.1033 [M+H]$^+$, theoretical 320.1039 [M+H]$^+$, Δ = 0.0006. Purity HPLC: 96.6%.

3.5.4.4.4. 2-(2-isopentylhydrazineyl)-6-(trifluoromethoxy)benzo[*d*]thiazole hydrochloride (**98**)

Method B. Yield 65% (72.0 mg). White solid; mp 166°C. ^{1}H NMR (400 MHz, DMSO-*d$_6$*) δ 7.96 (s, *J* = 1.7 Hz, 1H), 7.54 (d, *J* = 8.7 Hz, 1H), 7.34 (dd, *J* = 8.7, 1.7 Hz, 1H), 3.02 (t, *J* = 6.8 Hz, 2H), 1.67 (m, 1H), 1.45 (dd, *J* = 14.6, 6.8 Hz, 2H), 0.88 (d, *J* = 6.6 Hz, 6H). ^{13}C NMR (101 MHz, DMSO-*d$_6$*) δ 143.80, 124.41, 121.86, 120.61 (CH), 119.91, 119.32 (CH), 116.77, 116.23 (CH), 48.72 (CH$_2$), 34.94 (CH$_2$), 25.74 (CH), 22.81 (CH$_3$). ESI-MS (methanol) *m/z*: 320.0 [M+H]$^+$. HRMS (ESI-TOF) *m/z*: C$_{13}$H$_{17}$ClF$_3$N$_3$OS (hydrochloride compound) experimental 320.1036 [M+H]$^+$, theoretical 320.1039 [M+H]$^+$, Δ = 0.0003. Purity HPLC: 98.4%.

3.5.4.4.5. 2-(2-benzylhydrazineyl)-6-(trifluoromethoxy)benzo[*d*]thiazole hydrochloride (**99**)

Method B. Yield 67% (42.0 mg). White solid; mp 184°C. ^{1}H NMR (400 MHz, DMSO-*d$_6$*) δ 7.92 (s, 1H), 7.63 – 7.12 (m, 7H), 4.07 (s, 2H).^{13}C NMR (101 MHz, DMSO-*d$_6$*) δ 143.42, 137.11, 129.51, 128.99 (CH), 128.68 (CH), 127.99 (CH), 124.41, 121.87, 120.42, 119.32 (CH), 117.48 (CH), 116.02 (d, *J* = 2.0 Hz, CH), 54.77 (CH$_2$). ESI-MS (methanol) *m/z*: 340.0 [M+H]$^+$. HRMS (ESI-TOF) *m/z*: C$_{15}$H$_{13}$ClF$_3$N$_3$OS (hydrochloride compound) experimental 340.0727 [M+H]$^+$, theoretical 340.0726 [M+H]$^+$, Δ = 0.0001. Purity HPLC: 99.5%.

3.5.4.4.6. 2-(2-(2-ethylhexyl)hydrazineyl)-6-(trifluoromethoxy)benzo[*d*]thiazole hydrochloride (**100**)

Method A. Yield 3% (7.00 mg). Yellow solid; mp 216°C. ^{1}H NMR (400 MHz, DMSO-*d$_6$*) δ 7.24 (s, 1H), 7.11 (s, 1H), 6.98 (s, 1H), 4.16 (dd, *J* = 4.7, 3.2 Hz, 2H), 2.70 – 2.63 (m, 6H), 1.15 (dd, *J* = 15.0, 7.7 Hz, 4H), 0.85 (dt, *J* = 12.5, 6.7 Hz, 6H). ESI-MS (methanol) *m/z*: 362.1304 [M+H]$^+$. HRMS (ESI-TOF) *m/z*: C$_{15}$H$_{13}$ClF$_3$N$_3$OS (hydrochloride compound) experimental 362.1509 [M+H]$^+$, theoretical 362.1508 [M+H]$^+$, Δ = 0.0001. Purity HPLC: 99.6%.

3.5.4.4.7. 2-(2-phenethylhydrazineyl)-6-(trifluoromethoxy)benzo[*d*]thiazole hydrochloride (**101**)

Method B. Yield 98%. Yellow solid; mp 236°C. ^{1}H NMR (400 MHz, DMSO-*d$_6$*) δ 10.45 (s, 1H), 7.90 (s, 1H), 7.48 (d, *J* = 8.8 Hz, 1H), 7.36 – 7.15 (m, 6H), 4.82 (s, 2H), 3.23 – 3.07 (m, 2H), 2.90 – 2.75 (m, 2H). ^{13}C NMR (101 MHz, DMSO-*d$_6$*) δ 176.57, 170.90, 155.55, 143.02, 139.64, 130.19, 129.00 (2CH), 128.80 (2CH$_2$), 126.55 (CH), 120.06 (CH), 118.06 (CH), 115.62 (CH), 52.68 (CH$_2$), 33.92 (CH$_2$). ESI-MS (methanol) *m/z*: 354.0 [M+H]$^+$, 376.0 [M+Na]$^+$. HRMS (ESI-TOF) *m/z*: C$_{16}$H$_{15}$ClF$_3$N$_3$OS (hydrochloride compound) experimental 354.0822 [M+H]$^+$, theoretical 354.0822 [M+H]$^+$, Δ = 0.0000. Purity HPLC: 98.4%.

3.5.4.4.8.   2-(2-(3-phenylpropyl)hydrazineyl)-6-(trifluoromethoxy)benzo[*d*]thiazole   hydrochloride **(102)**

Method B. Yield 47%. Yellow solid; mp 242°C. ^{1}H NMR (400 MHz, DMSO-d_6) δ 10.40 (s, 1H), 7.90 (s, 1H), 7.83 – 7.77 (m, 1H), 7.51 – 7.44 (m, 1H), 7.32 – 7.14 (m, 5H), 2.97 – 2.86 (m, 2H), 2.73 – 2.57 (m, 2H), 1.89 – 1.72 (m, 2H). ^{13}C NMR (101 MHz, DMSO-d_6) δ 180.79, 167.05, 160.36, 153.00, 142.14, 138.03, 129.44 (CH), 128.99 (CH), 128.83 (CH), 128.72 (d, 3.0 Hz, 2CH), 128.78-128.72 (m, 2CH), 126.22 (CH), 109.99 (CH), 47.71 (CH$_2$), 32.54 (CH$_2$), 29.41 (CH$_2$). HRMS (ESI-TOF) *m/z*: $C_{17}H_{17}ClF_3N_3OS$ (hydrochloride compound) experimental 368.1037 [M+H]$^+$, theoretical 368.1039 [M+H]$^+$, Δ = 0.0002. Purity HPLC: 95.2%.

3.5.5.   Stability tests

Stability tests have been conducted with micrOTOF (Bruker) instrument coupled with HPLC (Agilent Technologies 1260 Infinity II) using column InfinityLab Poroshell 120 EC-C18 (4.6 x 100 mm, 2.8 μm). Samples have been prepared starting from a stock solution in DMSO at the concentration of 10 mM diluted with CH$_3$CH for the injection. Runs have been performed with al elution gradient of 70% CH$_3$CN/ 30% H$_2$O to 90% CH$_3$CN/ 10% H$_2$O returning to the initial condition in 20 minutes with a flow of 0.2 ml/min. Chromatograms have been elaborated using OtofControl (Bruker software).

3.5.6.   Computational procedures

3.5.6.1.   Docking studies

Docking studies were performed by the group of Prof. Stefano Moro (University of Padua, Molecular Modelling Section. Three-dimensional structures of the ligands were built by the MOE-builder tool. Ionization states were predicted using the MOEprotonate 3D tool and structures were minimized by the MMFF94x until the root mean square (RMS) gradient fell below 0.1 kcal mol_1Å_1. PLANTS docking protocol was selected as a conformational search program and ChemPLP as a scoring function. For each compound investigated, 20 docking simulation runs were performed, searching on a sphere of 10 Å radius, build around the coordinates of ligand 16W center of mass (PDB ID:4HNF).

3.5.6.2.   LiPE plot

Smiles of compounds' structures as well as Clog P (calculated by ChemDraw Professional), pIC$_{50}$ (M) and LiPE values obtained according to the formula reported in the **chapter x** were inserted in a Database converted into ".txt" format. The file was loaded in Osiris DataWarrior Software 3.5.0. to achieve a 3D representation. pIC50s were used in y axis, Clog P in x axis and LiPE value in z ones.

3.5.6.3.   SALI plot

Structure-activity Landscape Index (SALI) was calculated, as described in chapter x, to evaluate the similarity between molecules observing the change of IC$_{50}$ values. The dataset used in the previous procedure was loaded in Osiris DataWarrior Software 3.5.0. SALI 3D representation was prepared by settling the software the "fingerprint" descriptor; fingerprints of molecules were processed to obtain the correlation between compounds related to their structure similarity.

3.5.7.   Biochemistry

3.5.7.1.   CK1δ activity assays

Assays with truncated (1-294 aa) CK1δ. Compounds were tested on commercially available CK1δ (Merck Millipore, recombinant human, amino acids 1e294, GST-tagged N-terminal) with KinaseGlo® luminescence kit (Promega). Experiments were performed in 96-well plate (white, flat bottom) using buffer prepared as follow: 50 mM HEPES (pH 7.5), 1 mM EDTA, 1 mM EGTA and 15 mM magnesium acetate. Compound PF-

670462 (IC$_{50}$ CK1δ 0.014 μM) was used as a positive control at the concentration of 40 μM while a solution of DMSO/buffer as negative control. Firstly, 10 μL of inhibitor solution was inserted in the well (10 mM stock solution in DMSO was diluted with buffer) followed by 10 μL of enzyme (16 ng of CK1δ) and 20 μL of casein substrate 0.1% and 2 μM ATP (final concentration) (to perform ATP-competition increasing concentrations were chosen: 1, 2, 10, 50 μM). The final DMSO concentration in the mixture did not exceed 1-2%. After 60 minutes of incubation at 30°C, the enzymatic reaction was stopped with 40 μL of KinaseGlo reagent (Promega). Luminescence signal (RLU) was recorded after 10 minutes at 25°C using Tecan Infinite M100. The inhibitory activities were calculated in relation to the maximal activity (absence of inhibitor). As preliminary screening, each compound was assayed at the concentration of 40 μM, consequently, for derivative that reported an activity percentage less than 50% at the concentration, IC$_{50}$s were performed in triplicate and reported as mean ± standard error. Results were elaborated with Excel and GraphPad Prism 8.0.

ATP-competition assays were performed following the just described procedure by firstly performed the ATP calibration line to obtain the slope. The two chosen inhibitor's concentrations agree with the IC$_{50}$ of the compound (the concentration at its IC$_{50}$ and the double) and the experiment was conducted at the presence of increasing ATP concentrations: 1, 2, 10, 50 μM. The mean of the RLU value was divided for the slope of the calibration line and the mean of negative controls were subtracted by the ATP consumed; the reciprocal characterizes the x axis of the Lineweaver-Burk plot. The ATP consumed divided for volume of reaction (40 μL) provides the y value. Results were elaborated using Excel and GraphPad Prism 8.0.

3.5.7.2. GSK3β activity assays

GSK3β of most promising compounds was developed during the Erasmus program in the research group of Prof. Ana Martinez (CSIC-Madrid-ES). Compounds were tested on commercially available full-length GSK3β (Thermo-Scientific) with KinaseGlo® luminescence kit (Promega). Experiments were performed in 96-well plate (white, flat bottom) using buffer prepared as follow: 40 mM Tris pH 7.5, 20 mM magnesium chloride, 0.1% mg/mL BSA and 50 μM DTT. As a positive control, the reaction mixture without enzyme was used while the solution with enzyme, ATP and substrate as negative control. Firstly, 10 μL of inhibitor solution was inserted in the well (10 mM stock solution in DMSO has been diluted with buffer) followed by 10 μL of GS-2 as substrate (0.2 μg/μL), 10 μL of ATP (starting from a stock solution at 8 mM, it was diluted with buffer to achieve an initial concentration of 4 μM) and 10 μL of enzyme (1 ng/μL). The final DMSO concentration in the mixture did not exceed 1-2%. After 60 minutes of incubation at 25°C, the enzymatic reaction was stopped with 40 μL of KinaseGlo reagent (Promega). Luminescence signal (RLU) was recorded after 10 minutes at 25°C using Tecan Promega. The inhibitory activities were calculated in relation to the maximal activity (absence of inhibitor). As preliminary screening, each compound was assayed at the concentration of 10 μM, consequently, for derivative that reported an activity percentage less than 50% at the concentration, IC$_{50}$s were performed in triplicate and reported as mean ± standard error. Results were elaborated with Excel and GraphPad Prism 8.0.

3.5.7.3. CNS permeation prediction: BBB-PAMPA

CNS prediction of most promising derivatives was evaluated using Parallel Artificial Membrane Permeability Assay (PAMPA). Ten commercial drugs with known permeability were included in the experiment to obtain cut-off values (2-6 mg of Caffeine, Enoxacine, Hydrocortisone, Desipramine, Ofloxacine, Piroxicam, Testosterone and 12-15 mg of Promazine, Verapamil and 23 mg of Atenolol dissolved in 1000 μL of ethanol, then diluted with buffer when it is required). Compounds were dissolved in a 70/30 PBS pH 7.4 buffer/ethanol solution in the appropriate concentration determining absorbance values in the UV-VIS light spectrum. 5 mL of solutions were filtered with PVDF memnrane filters (diameter 30 mm, pore size 0.45 mm). The acceptor 96-well plate (MultiScreen 96-well Culture Tray clear, Merck Millipore) was filled with 180 μL of buffer (70/30). In the donor 96-well plate ((Multiscreen® IP Sterile Plate PDVF membrane, pore size is 0.45 mM, Merck Millipore) 4 μL/well of porcine lipid brain (Merck Millipore) in dodecane (20 mg/ml) were added and,

after 5 minutes, 180 μL of inhibitor solutions were inserted. Once completed, the donor plate was carefully located on the acceptor one to make a "sandwich" and, after 2.5h of incubation at 25°C, the dolor plate was removed. The absorbance values at dedicated wavelengths were red using Tecan Infinite M1000. Experiment was conducted in duplicate. The permeability coefficient (Pe) of each compound was established in centimeter per second.

$$Pe = \frac{Vd \cdot Vr}{(Vd - Vr) \cdot S \cdot t} \quad \frac{100 \cdot Vd}{100 \cdot Vd - \%T(Vd - Vr)}$$

$$\%T = \frac{Vr \cdot Ar}{Ad \cdot Vd} 100$$

Where Vd and Vr are volumes of donor and acceptor solution (0.18 cm^3), S is the membrane area (0.266 cm^2), time of incubation (2.5 h ¼ 9000 s), Ar is the absorbance of the receptor plate after the experiment and Ad0 is the absorbance in the donor compartment before incubation. Results are given as the mean and the average of the two runs ± standard deviation (SD) is reported. Obtained results for quality control drugs were then correlated to permeability data found in the literature. The linear correlation between experimental and literature permeability values was used for the classification of compounds in those able to cross the BBB by passive permeation (CNS+ which correlate with a bibliographic Pe > 4) and those not (CNS- which correlate with a bibliographic Pe < 2). Compounds correlating with reported Pe values from 2 to 4·10^{-6} cm s^{-1} are classified as CNS+/-.

3.5.7.4. Thermal Shift Assay

Thermal Shift Assays for the best compound was performed by Elelonora Cescon in the group of Prof. Paola Storici (BioLab-Elettra Sincrotrone-Trieste). All TSA experiments were conducted in triplicates. Recombinant CK1d 1-294, representing the catalytic core domain of the protein, was produced at Elettra Protein Facility in Elettra Synchrotron. Optimal concentration of protein and dye were tested from preliminary TSA in order to establish the most advantageous set up. Samples were prepared in white 96-multiwell plate (Biorad®) with a final volume of 20 mL into each well. A 5x stock of buffer and a 5x stock of protein solution were prepared hence 4 mL of both were added into the wells. Tested inhibitors were dissolved in 100% DMSO and a 40x stock of each concentration tested was prepared to keep a final concentration of DMSO at 2.5% in each condition tested. Thermal shift assay was performed in assay buffer containing 20 mM Tris pH 7.5, 180 mM NaCl and 0.5 mM TCEP as final concentrations, while protein was kept at 3 mM in all conditions of the analysis. Compounds were tested at final concentrations of 1.5, 3, 9, 15, 30 and 45 mM (0.5x, 1x, 3x, 5x, 10x, 15x). Once added buffer, protein and compounds stocks plus a proper volume of water to reach 20 mL, the multi-well plate was centrifugated at 100 xg, 4°C for 1 min to spin down and stir the components. Protein and inhibitors were then incubated at room temperature for 30 min. After incubation, SyproOrange dye (Protein Thermal shift dye, Thermo Fisher Scientific®) was added into each well to a final concentration of 0.5x from 1000x stock in 100% DMSO. The multiwell plate was centrifuged again and measurement was started. Measures were performed in a real-time PCR machine (CFX96, Biorad®), registering emission of the dye at 560-580 nm every 30 sec, with a temperature gradient of 2°C/min. Each analysis was executed in comparison to a negative control represented by the only buffer or the compounds with SyproOrange, and a positive control consisted of the protein or protein with 2.5% of DMSO plus the fluorophore.

3.5.8. *In vitro* experiments on neuroblastoma cell lines (SH-SY5Y)

Biological investigation of most promising derivatives was conducted during the Erasmus program in the group of Prof. Ana Martinez (CSIC-Madrid-ES).

3.5.8.1. MTT assays

The human neuroblastoma SH-SY5Y cell line was propagated in Dulbecco's Modified Eagle Medium (DMEM) containing L-glutamine (2mM), 1% non-essential amino acids, 1% penicillin/streptomycin and 10%

fetal bovine serum (FBS) under humidified 5% CO_2. Once semiconfluence was achieved, cells were countered using TC10™ Automated Cell Counter Bio-Rad Laboratories (CSIC-Madrid) and 80000 cells/well were plated in 96-well plate. After 24h of incubation, compounds were inserted at the concentrations of 5 and 10 μM (the stock solution in DMSO was diluted with DMEM to obtain the right final concentration) and, after another 24h of incubation, DMEM was removed and MTT reactive (3-[4,5- Dimethylthiazol-2-yl]-2,5-Diphenyltetrazolium Bromide) was added at the concentration of 20 mg/mL. After 2h, absorbance was recorded, and cell survival was estimated as percentage of value of untreated control (mean of six wells). Three independent experiments were carried out.

3.5.8.2. Neuroprotection assays

The human neuroblastoma SH-SY5Y cell line was propagated in Dulbecco's Modified Eagle Medium (DMEM) containing L-glutamine (2mM), 1% non-essential amino acids, 1% penicillin/streptomycin and 10% fetal bovine serum (FBS) under humidified 5% CO_2. Once semiconfluence was achieved, cells were countered using TC10™ Automated Cell Counter Bio-Rad Laboratories (CSIC-Madrid) and 60000 cells/well were plated in 96-well plate. After 24h of incubation, compounds were inserted at the concentrations of 5 and 10 μM (the stock solution in DMSO was diluted with DMEM to obtain the right final concentration) and, after 1h ethacrynic acid (45 μM starting from stock solution of 100 mM diluted in DMEM) was added. As negative control, a solution of DMSO 1% in DMEM was used while as positive control ethacrynic acid without compound. After 24h of incubation, DMEM was removed and MTT reactive (3-[4,5- Dimethylthiazol-2-yl]-2,5-Diphenyltetrazolium Bromide) was added at the concentration of 20 mg/mL. After 2h, absorbance was recorded, and cell survival was estimated as the mean of relative absorbance of six wells/compound. Three independent experiments were conducted, and statistical analysis of data was conducted using GraphPad Prism 8.0 one-way ANOVA for each plate and T-TEST to compare the three experiments.

3.5.8.3. Immunoblotting analysis

In a 6-well plate, 2000000 of cells were plated per well and, after 24h of incubation, compounds were inserted at the chosen concentration (starting from stock solution in DMSO diluted with DMEM). Ethacrynic acid was added at the concentration of 45 μM after 1h of incubation. To prepare the cell extraction, cells were harvested and washed with PBS and then they were lysed in ice-cold lysis buffer. The number of proteins in the extract was detected by the Pierce BCA Protein Assay kit (Thermo Scientific). 20-50 μg of protein of protein were fractionated on SDS poly-acrylamide gel and transferred to poly-vinylidene fluoride (PVDF) membranes (Millipore, Billerica, MA, USA). Membranes were blocked with 5% bovine serum albumin (BSA) (Sigma) for 1h and then they were incubated overnight at 4°C with primary antibodies (pTDP-43 mouse, BioRad) diluting 3μL in 3 mL of BCA. Signal from the primary antibody was amplified using species-specific secondary antibody (pTDP-43 anti-mouse, BioRad) to obtain the "sandwich" detected with a chemiluminescent substrate detection system ECL. Protein band densities were quantified using ChemiDoc station with Quantity One 1D analysis software (Bio-Rad Laboratories, Madrid, Spain).

3.5.9. *In vivo* experiments on *Drosophila*

Riluzole was tested on *Drosophila* that overexpresses TDP-43 at the concentration of 1 mM. Experiments were conducted overexpressing selectively TDP-45 in glial cells and motoneurons testing riluzole at the concentration of 5 mM. *In vivo* assays were performed by Prof. Marco Bisaglia (University of Padua).

4. Synthesis and characterization of tri- and tetra-substituted pyrazines: new scaffold-based strategy

4.1. Aim of the work

A routinely screening of in-house molecules towards CK1δ identified pyrazines **103**-**105**, reported in **Fig. 72**, as hit compounds for the target. Pyrazine represents a versatile scaffold widely used in medicinal chemistry but, according to the literature, not still reported for the development of CK1δ inhibitors. Activities were in the high micromolar range. Thus, they provided a promising starting point for the development of a new series of CK1δ derivatives.

103, $IC_{50} = 21.9\ \mu M \pm 8.8$ **104**, $IC_{50} = 12.5\ \mu M \pm 4.8$ **105**, $IC_{50} = 7.20\ \mu M \pm 3.37$
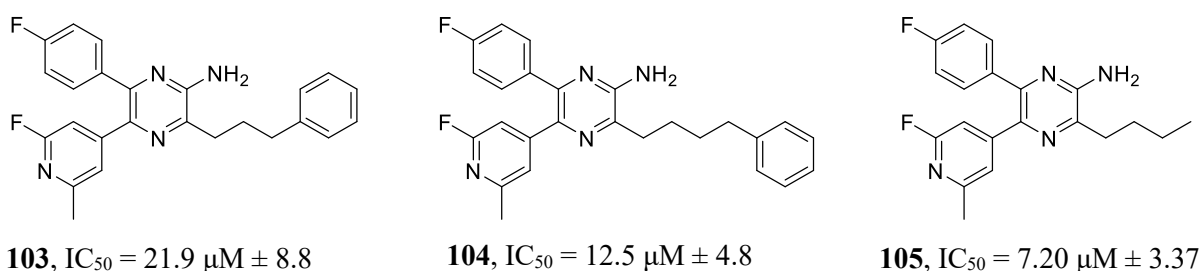
*Figure 72: pyrazine-scaffold compounds (**103-105**) designed for different purpose and their activity on CK1δ.*

Compounds **103**-**105** share the main 2-amino-pyrazine nucleus substituted by a 2-fluoro-6-methylpyridine at the 5 position and a 4-fluorophenyl moiety at the 6-location. The three molecules, that differ by the alkyl chain introduced at the position 3, have the peculiarity to be substituted in all the 4 free positions of the scaffold and the tetra-substitution represented a challenge since the reactivity of the halogens inserted to perform desired reactions resulted decreased after each substitution, especially when an ester or amino moieties are inserted at the 3-position of the ring. Tetra substitution can be performed in several ways, according to the review of Ong *et al.* [201] through condensation reactions refined over the years, nevertheless there is literature that reports the possibility to perform 4 substitutions starting from the commercially available pyrazine ring even if the success of this strategy depends on the reactivity of the substituents. [202]

Aim of this project was the development of series of 2,3,5,6-tetrasubstituted and 2,5,6-trisubstituted pyrazines to investigate the SAR profile of this nucleus. In particular, as reported in **Fig. 73**, different types of substituents were investigated for the study of the 3-position (R_1) including butyl chain, ethyl ester and saturated cycles like morpholine and functionalized and not piperazine. Several aryl moieties were explored to substitute 5-position (R_2): simple phenyl ring, substituted and not pyridine as well as 4-functionalized phenyl groups with fluorine, methoxy and hydroxy moieties were inserted. Finally, some attempts to insert 4-fluorophenyl group and piperazine were carried out to substitute the 6-position of the main scaffold (R_3).
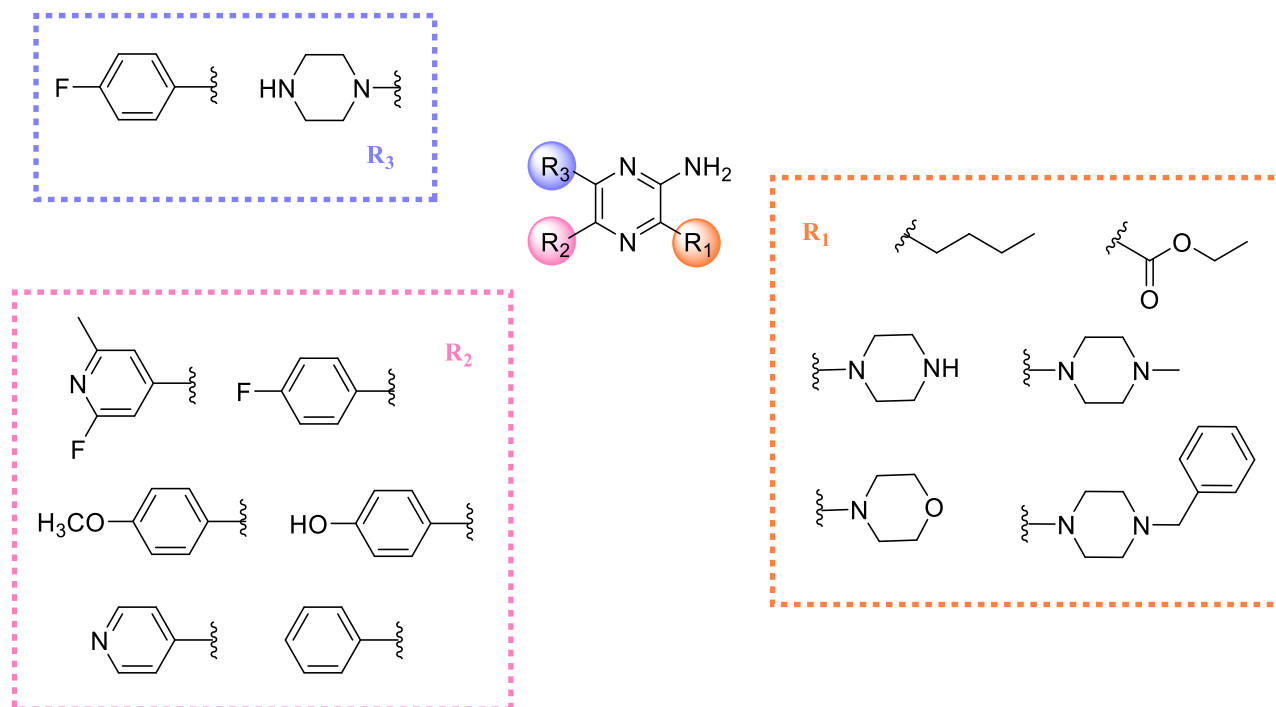
Figure 73: pyrazine nucleus and substituents inserted at positions 3 (R₁), 5 (R₂) and 6 (R₃).

4.2.   Discussion

4.2.1.   Chemistry

In order to develop 3-alkyl derivatives, a series of bromination and catalyzed reactions occurred. Starting from 6-chloro-2-amino pyrazine (**106**), commercially available, firstly the chlorine atom at 6-position was substituted with 4-fluorophenyl ring *via* Suzuki-Miyaura followed by the bromination of the 3-position. Obviously the two regio-isomers were obtained, and the synthetic strategy takes into account the order of substitutions determined by the main bromo-derivative achieved. A modified Kumada coupling was conducted, after the di-Boc protection of the amino group at the 2-location, to insert the alkyl moiety at the 3-position. Finally, the last bromination and Suzuki-Miyaura were carried out to functionalize the 6-position. The bromination performed at the last position of the scaffold trisubstituted appears challenging; in this case, it was successful by increasing the number of equivalents but when the ring is strongly deactivated it can fail like with 3-ester derivatives. The synthetic strategy was adjusted according to the substituent to insert at the 3-position, considering ester moieties, the starting molecule 3-aminopyrazine-2-carboxylic acid (**121**) was esterificated, then brominated at the 5-position to insert *via* Suzuki-Miyaura the desired aromatic group. As previously mentioned, the last bromination appears impracticable. Regards the 3-amino compounds, two different synthetic pathways were considering; one strategy involved the nucleophilic substitution at the brominated compound **109** to obtain trisubstituted pyrazines, the other is characterized by synthesizing 3,5-dibromo-6-chloropyrazin-2-amine (**131**) to firstly proceed with the nucleophilic substitution at the 3-position followed by Suzuki reaction to functionalize -5 and -6 positions. Also, derivatives without substituents at the 3-location were developed; in this case, taking advantage from the 3-bromo derivative obtained in the first mentioned synthetic pathway, compound **108** was reacted with desired boronic acid or ester leading to final derivatives **137-141**.

4.2.1.1.   Synthesis of 3-alkyl-5-substituted-6-(4-fluorophenyl)pyrazin-2-amino derivatives (**103-105**, **120**)

Compound **120** has been synthesized as reported in **Scheme 6**, according to procedures reported in literature [202,203,204]Also the already tested compounds **103-105** were synthetized in this way, and are reported here because some intermediates were tested to complete the SAR of the series. . First step concerns the reaction of 6-chloro-2-amino pyrazine (**106**), commercially available, with 4-fluoro phenyl boronic acid *via* Suzuki reaction.

This reaction has been tried using different types of palladium catalysts 0 or II with PPh$_3$ to obtain the best conditions. [205] Both Pd(PPh$_3$)$_4$ and PdCl$_2$(PPh$_3$)$_2$ have provided semi-quantitative yields in the reaction. Derivative **107** has been then brominated using N-bromo succinimide (NBS) obtaining the two regio-isomers, 3-bromo (**109**) and 5-bromo (**108**) derivatives, in a ratio of 4/1, respectively. The two isomers have been characterized using ^{1}H-^{1}H NOESY (Nuclear Over-Hauser Effect Spectroscopy) NMR bidimensional technique allowing to identify cross-peaks of vicinal protons that are not directly linked in the space. In **Fig. 74** it is possible to appreciate cross-peaks related to singlet of proton at the 5-position at 8.12 ppm and 4-fluorophenyl moiety at 8.03 ppm confirming the achievement of 3-bromo derivative (**109**).
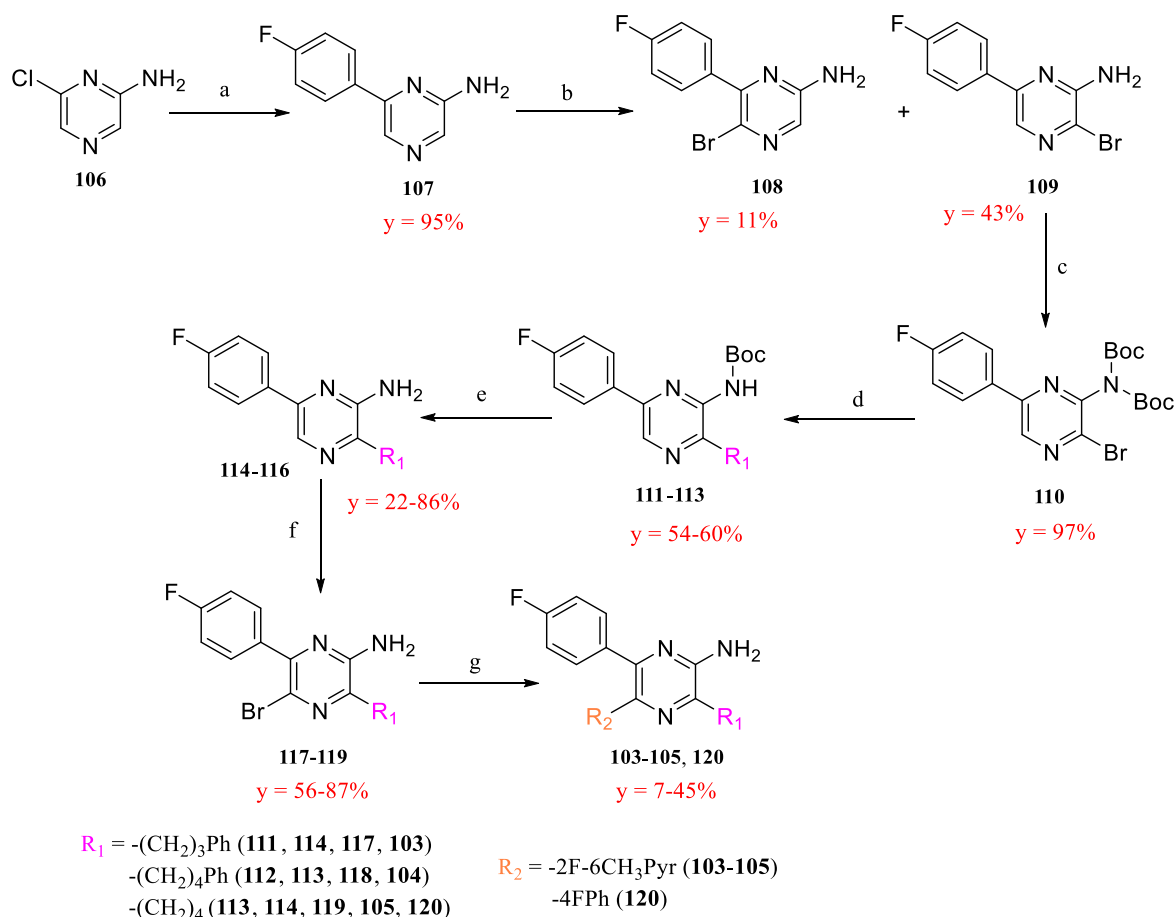
*Scheme 6: synthetic pathway for the development of 3-alkyl-5-substituted-6-(4-fluorophenyl)pyrazin-2-amino derivatives (**103-105**, **120**). Reagents and conditions. **a**: (4-fluorophenyl)boronic acid, Pd(PPh₃)₄, Na₂CO₃, PhMe, EtOH, 110°C, 4h, Ar; **b**: NBS, DCM, r.t., 1h, Ar; **c**: Boc₂O, DMAP, THF, rfx, 2h; **d**: R₁Br, Mg, THF, 60°C, 3-4h, Ar/ R₁MgBr, Fe(acac)₃, THF, NMP, 0°C-r.t., 4h, Ar; **e**: 1,4-dioxane, r.t., overnight; f: NBS, DCM, r.t., 1h, Ar; g: 2-fluoro-6-methyl-4-(4,4,5,5-tetramethyl-1,3,2-dioxaborolan-2-yl)pyridine, PdCl₂(PPh₃)₂, Na₂CO₃, PhMe, EtOH, H₂O, 130°C, MW, 1h; y = yield.*
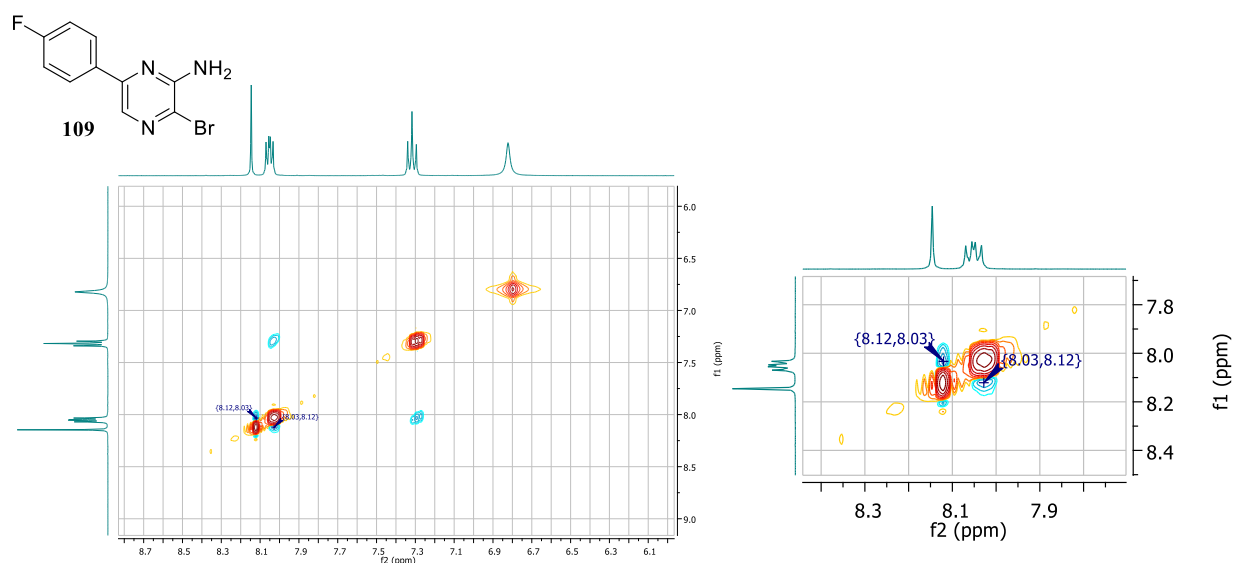
*Figure 74: ¹H-¹H NOESY NMR (DMSO-d₆) of compound **109**. The zoom representing the cross-peaks between free proton at the 5-position and the 4-fluorophenyl moiety is reported.*

4. Synthesis and characterization of tri- and tetra-substituted pyrazines: new scaffold-based strategy

To have the certainty to have obtained compound **109**, the other regio-isomer (**108**) has been characterized with the same NMR technique. In **Fig. 75** is possible to appreciate the cross-peak between the amino group at the position 2 of the scaffold, 6.78 ppm, and the proton at the position 3 of pyrazine (7.68 ppm).
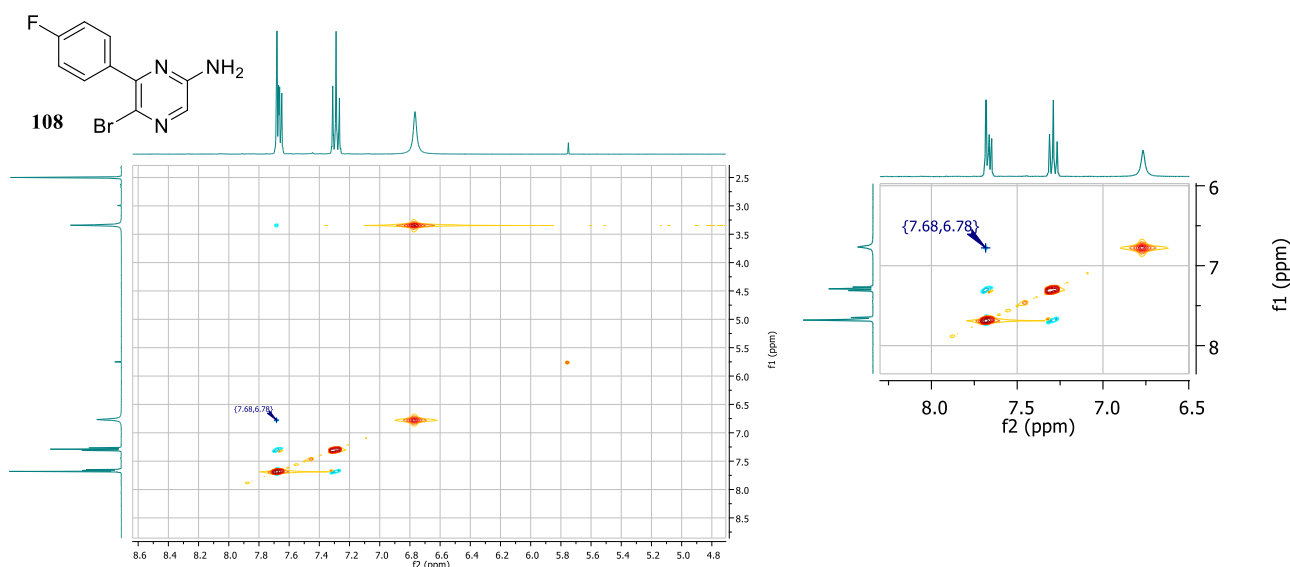
*Figure 75: ^1H-^1H NOESY NMR (DMSO-d$_6$) of compound **108**. The zoom representing the cross-peaks between free proton at the 3-position and the amino group at the 2-position is reported.*

The protection of the amino group at the 2-position (**110**) of the scaffold results mandatory for the success in the next reaction that is provided by a Fürstner-modified Kumada coupling reaction, starting from the synthesis of the Grignard reagent of the appropriate alkylhalide in dry THF using a catalytic amount of iodine. Kumada has been performed in THF and (N-methyl-2-pyrrolidone) NMP 10/1 in the presence of Fe(acac)$_3$ (iron acetyl acetonate) affording compounds **111**-**113**; this catalyst is easy to synthesize applying green procedure starting from FeCl$_3$ and acetylacetonate in H$_2$O and KOH. The Fürstner variant has been developed in order to bypass the limitations given by the Ni-complexes, this Fe(III)-catalyst has the advantages of being economic, efficient and not toxic. [206,207] The Fürstner hypothesized mechanism of this reaction, schematically represented in **Scheme 7**, assumed the formation of a kind of "Inorganic Grignard reagent" [Fe(MgX)$_2$] obtained by the reaction of FeCl$_3$ and the Grignard reagent. Through the reduction process, a zerovalent Fe(0) specie is formed that is subjected to alkylation and finally, in the reductive coupling phase, the desired product is given with the re-obtainment of Fe(II) specie of the initial state. [206]
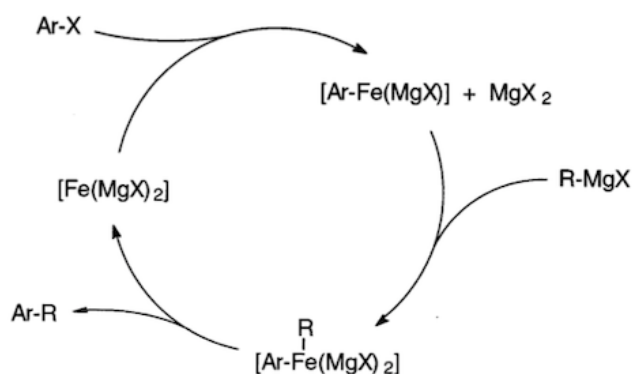
Scheme 7: Fürstner hypothesized mechanism of the modified Kumada coupling.

The following reaction involved the deprotection of Boc-amino group using hydrochloric acid in organic solvent (**114-116**), the bromination of the last free position of the scaffold (**117-119**) and then the Suzuki reaction with the boronic ester commercially available of the 2-fluoro-6-methylpyridine or with the boronic acid of 4-fluorophenyl ring, represent the last steps of the reaction pathway to obtain final desired compounds (**103-105**, **120**)

4.2.1.2. Synthesis of 3-ester-5-substituted-6-(4-fluorophenyl)pyrazin-2-amino derivatives (**124-125**)

The first attempt in the development of 3-ester derivatives has been conducted by substituting the 5-position with 2-fluoro-6-methylpyridine; since an activity in the high micromolar range has been recorded, the correspondent compound with 4-fluorophenyl group has been developed. The commercially available starting material 3-aminopyrazine-2-carboxylic acid (**121**) has been allowed to react, according to the **Scheme 8**, with ethanol to obtain the ethyl ester derivative (**122**). Then a bromination is required at the 5-position of the scaffold affording compound **123**. In this case, the reaction provided a selectivity for the introduction of bromide atom since the 6-location is less reactive and difficult to substitute. As a final reaction, 4-fluorophenyl moiety as well as 2-fluoro-6-methylpyridine were introduced *via* Suzuki to obtain compounds **124-125**.

R_2 = -6CH$_3$-2F-Pyr (**124**)
-4F-Ph (**125**)
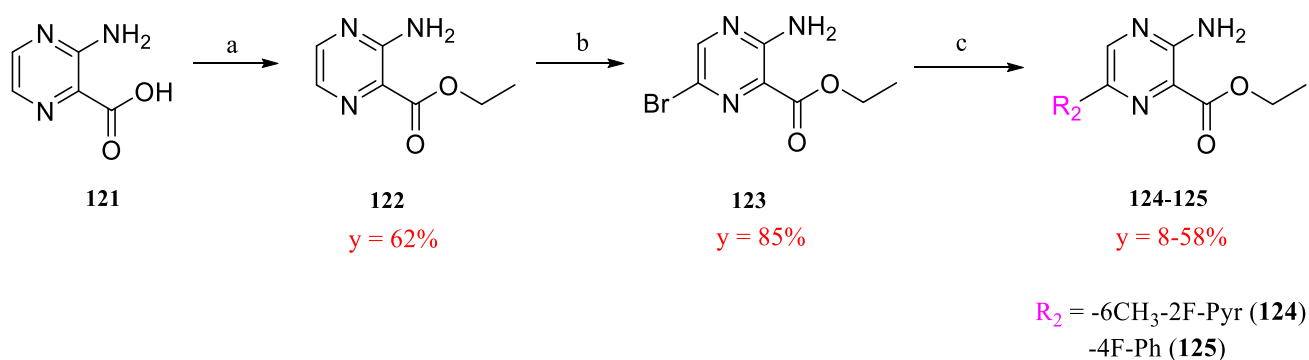
*Scheme 8: synthetic pathway for the development of 3-ester-5-substituted-6-(4-fluorophenyl)pyrazin-2-amine derivatives (**124-125**). Reagents and conditions. **a**: EtOH, SOCl$_2$, rfx, overnight; **b**: NBS, DCM, 0°C to r.t., 1h, Ar; **c**: 2-fluoro-6-methyl-4-(4,4,5,5-tetramethyl-1,3,2-dioxaborolan-2-yl)pyridine or (4-fluorophenyl)boronic acid, PdCl$_2$(PPh$_3$)$_2$, Na$_2$CO$_3$, PhMe, EtOH, H$_2$O, 130°C, MW, 1h; y = yield.*

4.2.1.3. Synthesis of 6-aminopyrazin-2-piperazine derivative (**127**)

The commercially available starting material 6-chloro-2-aminopyrazine (**106**) has been reacted with N-BOC piperazine, previously synthesized using *tert*-buthyloxycarbonate and piperazine, *via* nucleophilic substitution, to achieve compound **126** followed by the BOC removal using hydrochloric acid in 1,4-dioxane obtaining derivative **127** (**Scheme 9**).

4.2.1.4. Synthesis of 3-amino-6-substituted 2-aminopyrazine derivatives (**128-130**, **136**)

According to the **Scheme 10**, two strategies have been used to obtain trisubstituted derivatives (**strategy A**) and tetrasubstituted pyrazines (**strategy B**). Following the first synthetic strategy, starting material 6-chloro-2-amino pyrazine (**106**) has been subjected to Suzuki reaction to insert 4-fluorophenyl moiety at the position 6 of the ring followed by the bromination of compound **107** using NBS leading to 3-bromo derivative (**109**). At this point the desired amine has been inserted applying a nucleophilic substitution in butanol (BuOH) to achieve final derivatives **128-130** (**strategy A**). Proceeding in the **Scheme 10** with the **strategy B**, the direct bromination of **106** with an excess of NBS has led to the obtainment of 3,5-dibromo compound (**131**), 3-bromo and 5-bromo derivatives (**132-133**). The bis-bromo derivative (**131**) has been allowed to react with N-BOC piperazine to obtain compound **134** that has been reacted with two equivalents of 4-fluorophenyl boronic acid to achieve compound **135** with the double fluorophenyl group at 5 and 6-positions. The last reaction involved the deprotection of N-BOC piperazine derivative obtaining compound **136**.
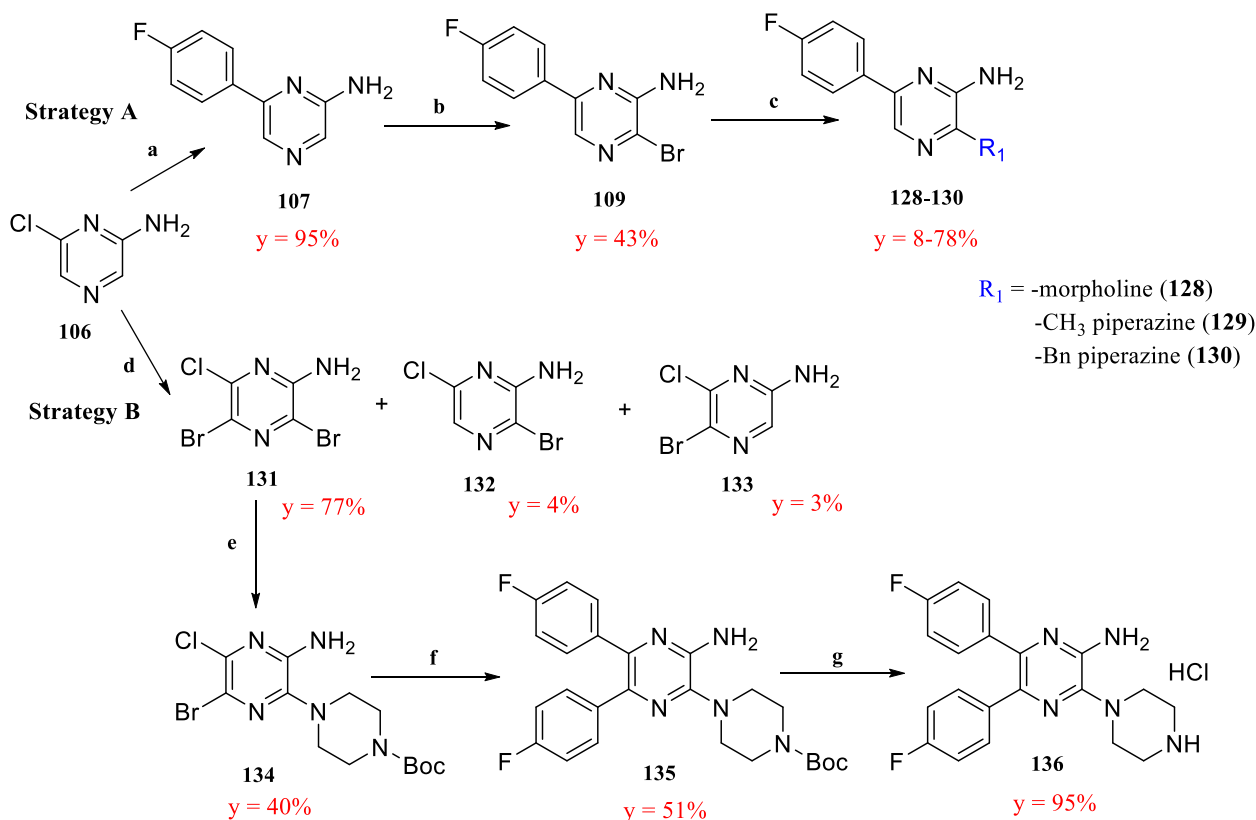
*Scheme 10: synthetic pathways to obtain 3-amino-6-substituted-2-aminopyrazines **128-130**, **136**. Reagents and conditions. **a**: (4-fluorophenyl)boronic acid, Pd(PPh₃)₄, Na₂CO₃, PhMe, EtOH, 110°C, 4h, Ar; **b:** NBS, DCM, 0°C to r.t., 1h, Ar; **c**: R₁, BuOH, 130°C, MW, 6h; **d:** NBS, DCM, 0°C to r.t., 1h, Ar; **e**: piperazine, Boc₂O, DIEA, DCM, r.t., overnight/ **131**, Boc-piperazine, BuOH, rfx, overnight; **f**: (4-fluorophenyl)boronic acid, Pd(PPh₃)₄, Na₂CO₃, PhMe, EtOH, 110°C, 4h, Ar; **g**: HCl in 1,4-dioxane, r.t.; 1h. y = yield.*

4. Synthesis and characterization of tri- and tetra-substituted pyrazines: new scaffold-based strategy

The bromination showed as reaction **d** in the synthetic **Scheme 10** has led to the formation of 3 products: the 3,5-dibromo (**131**), 3-bromo (**132**) and 5-bromo (**133**) derivatives. The characterization has been conducted with ^{1}H-NMR and ^{1}H-^{1}H NOESY NMR.
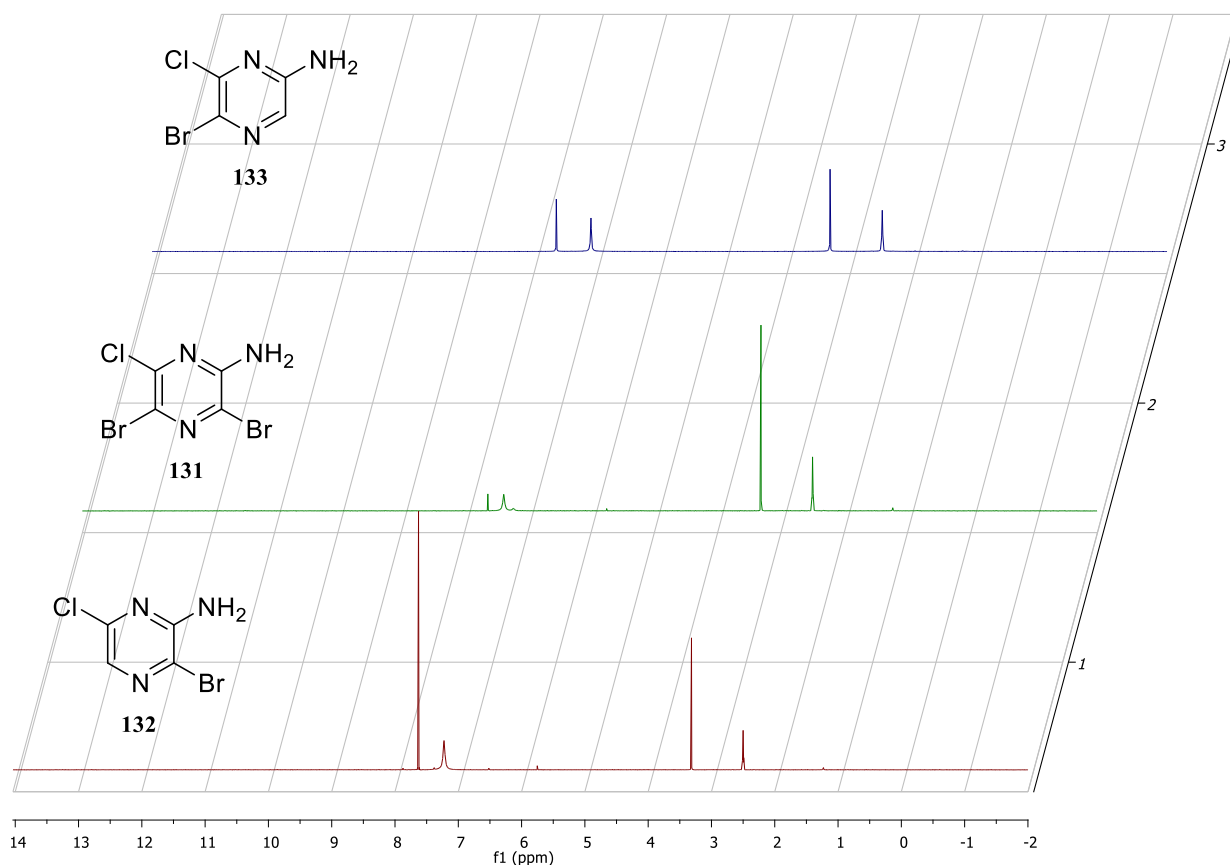
Figure 76: superimposition of ^{1}H-NMR of compounds 132 (red), 131 (green), 133 (blue).

The superimposition of ^{1}H-NMR spectra (**Fig. 76**) of compounds **131-133** does not allow to establish the right assignment of isomers according to the chemical shift of protons in the 3- or 5-locations and amino group at the 2-position. Bis-bromo derivative (**131**) reports a unique signal in ^{1}H-NMR spectrum assigned to amino group and does not register cross-peaks in ^{1}H-^{1}H NOESY NMR (**Fig. 77**). In order to assign the other two regio-isomers, ^{1}H-NMR spectra and the NOESY bidimensional one are given in **Fig. 77**; from the top to the bottom, ^{1}H NMR of the two mono-bromo derivatives have been recorded displaying the presence of the singlet related to the free proton, **132** and **133**, respectively. To assess the location of the proton, NOESY NMR of compound **133** has been registered: cross peaks between amino group (7.08 ppm) and proton at the 3-position (7.63 ppm) have been identified (right side of the **Fig. 78**) confirming the obtainment of the 5-bromo isomer (**133**) allowing to confirm its identity, thus, for exclusion, structure of compound **132** could be also confirmed.
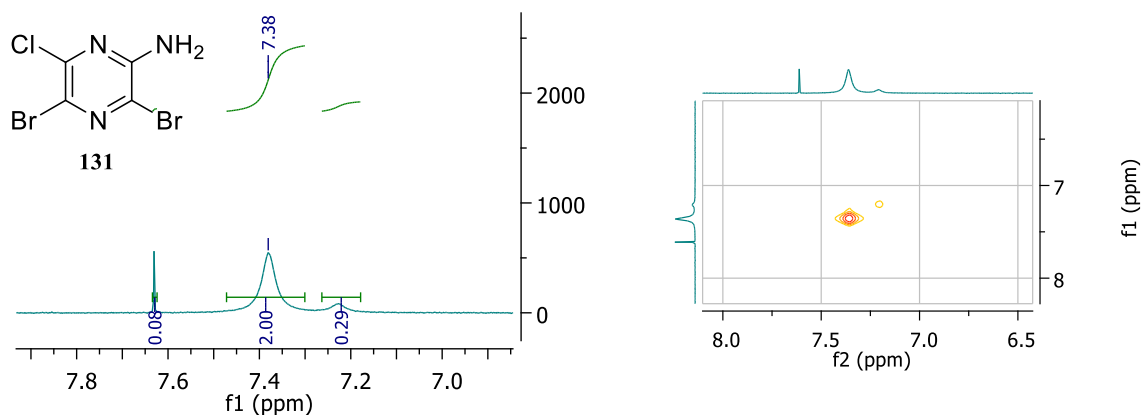
*Figure 77: ^{1}H-NMR (DMSO-d$_6$) and NOESY NMR spectra of compound **131** (3,5-bis bromo derivative).*
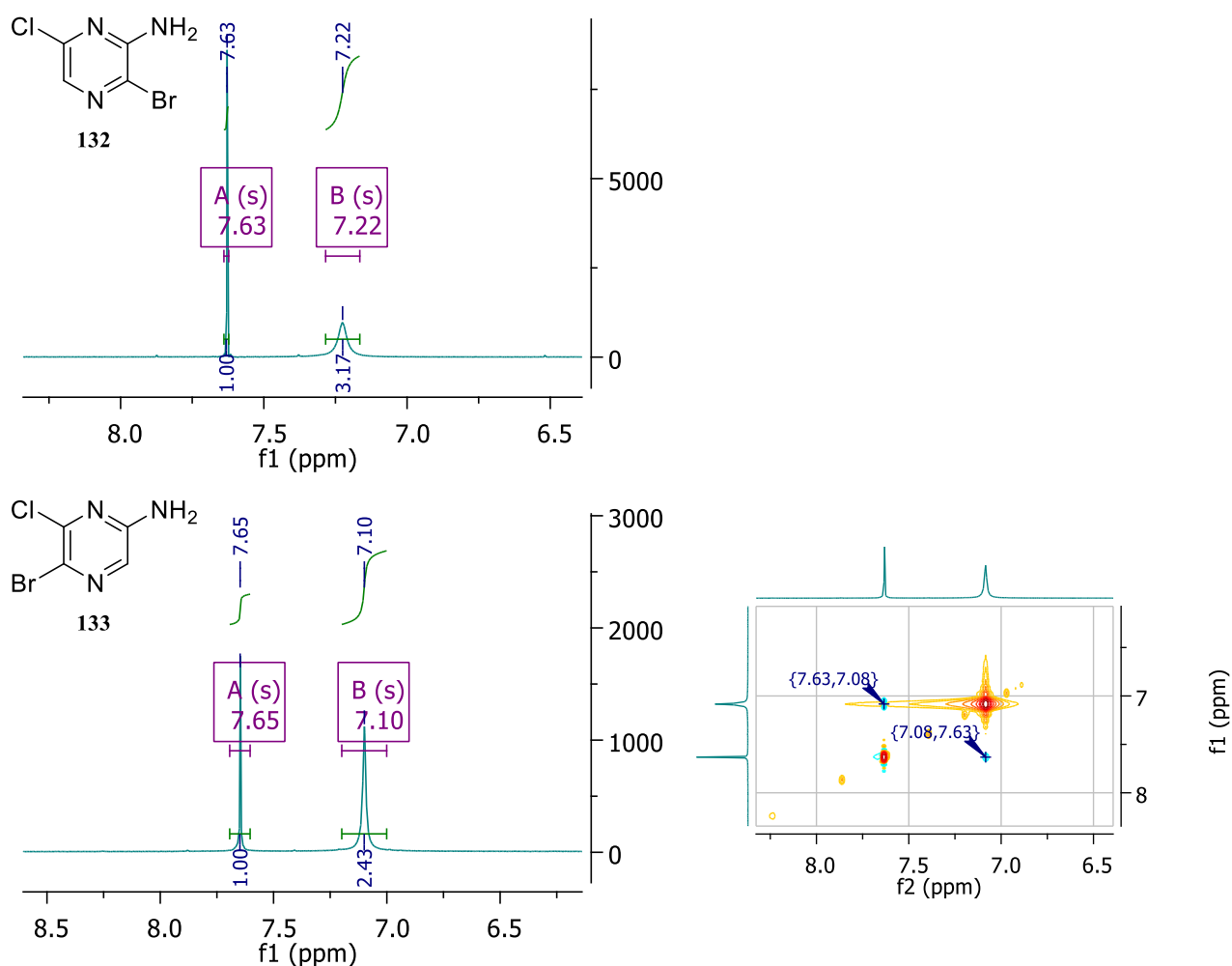
*Figure 78: from the top to the bottom, ^{1}H-NMR (DMSO-d$_6$) of isomers **132** and **133** are reported. In the right side the NOESY NMR of derivative **133** is recorded.*

Following the **strategy B** of the **Scheme 10**, 3-piperazine derivative with double fluorophenyl moiety at 5- and 6-positions has been developed. In order to establish the right structure of compound **136**, the position of piperazine inserted has been investigated. The ^{1}H-NMR (**Fig. 79**) has displayed all the signals of derivatives: singlets of the NH·HCl of piperazine and 2-amino group at 9.24 and 6.48 ppm, respectively, signals of the

double fluoro phenyl moiety at 7.09 and 7.29 ppm and the multiplet of the four -CH₂ related to piperazine at 3.45-3.20 ppm closed to the signal of the residue water in the sample.
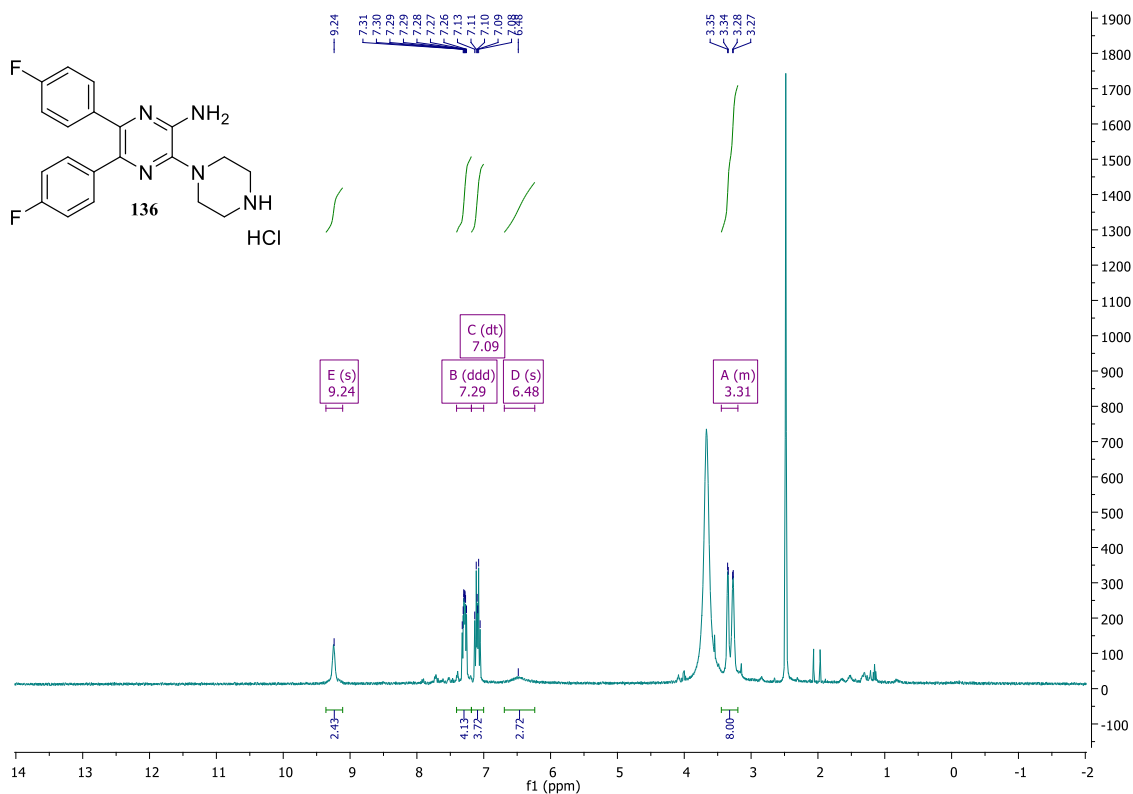
*Figure 79: ¹H-NMR (DMSO-d₆) of compound **136**.*
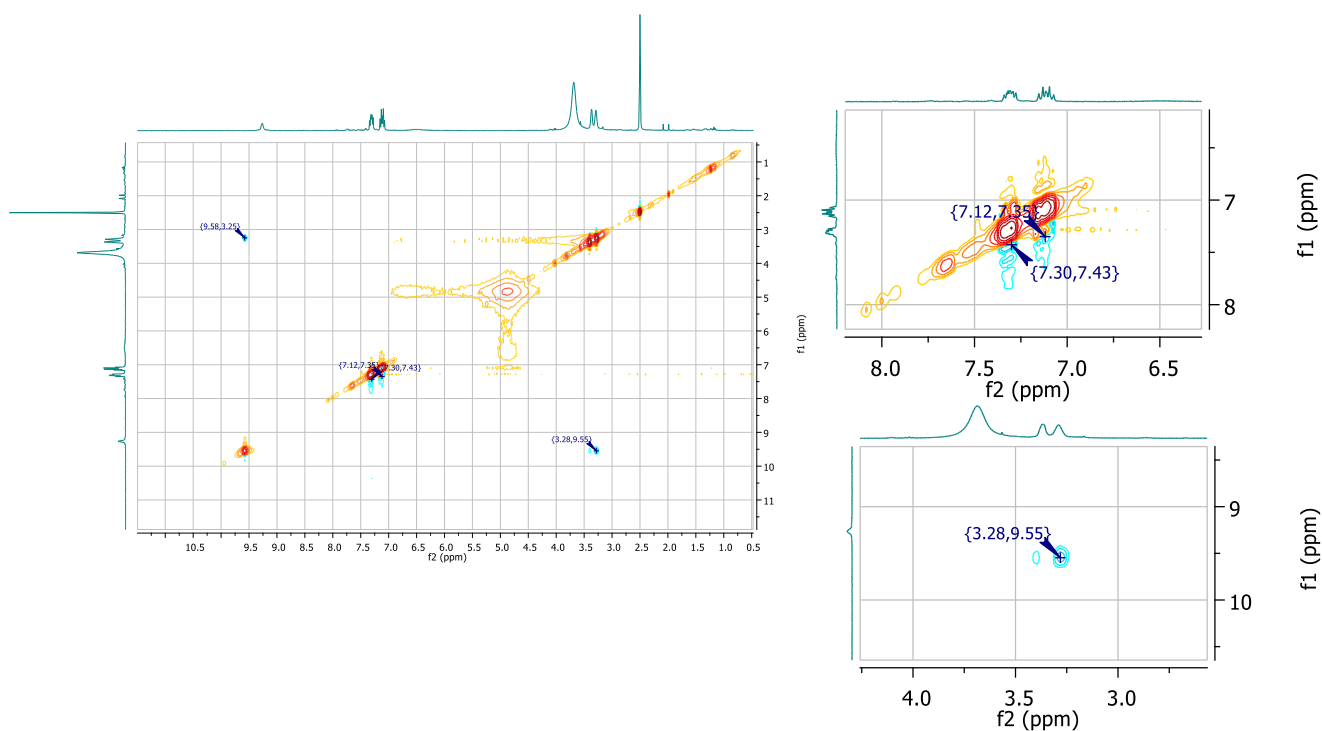
*Figure 80: NOESY NMR (DMSO-d₆) of compound **136**. In the right part zooms related to cross peaks of fluorophenyl ring and between methylenes of piperazine and its amino group, respectively, are given.*

4. Synthesis and characterization of tri- and tetra-substituted pyrazines: new scaffold-based strategy

In **Fig. 80**, that represents the ¹H-¹H NOESY NMR registered of compound **136**, it is possible to appreciate (upper zoom in the right side of the figure) cross peaks related to aromatic protons of fluorophenyl moiety, nevertheless they appear closed to signals of 1D spectrum reported in diagonal: results difficult to understand if cross peaks belong to the effect of protons of a single fluorophenyl group or a double. In the second zoom, another cross peak between methylenes of piperazine and amino moiety of piperazine has been reported. Thus, in the NOESY characterization cross peaks have not been appreciated nor between fluorophenyl ring and piperazine cycle, nor between 2-amino group and piperazine. HRMS characterization confirms that compound **136** has a double fluoro phenyl moiety and a piperazine. To have the absolute validation for the correct positioning of these substitutions the X-ray structure should be performed. Another confirm can be provided by changing the synthetic pathway: starting from 5-bromo derivative **108** with 4-fluorophenyl moiety inserted at the 6-position, it is possible to proceed with the substitution at 5-location and finally, after bromination, piperazine can be inserted as last reaction at 3-position; in this way all the precursors can be confirmed by ¹H-NMR and bidimensional NOESY to establish the right structure of final compound **136**.

4.2.1.5.   Synthesis of 6-(4-fluorophenyl)-5-substituted pyrazin-2-amine (**137-141**)

The 5-bromo derivative (**108**), obtained according to **paragraph 4.2.1,** has been subjected to a Palladium-catalyzed Suzuki to introduce the desired aryl moieties obtaining compounds **137-140**. Most of substituents inserted can be found commercially available in the form of boronic acids excluding compound **139** for which the boronic ester was obtained using 4-bromo anisole, 4,4,4',4',5,5,5',5'-octamethyl-2,2'-bi(1,3,2-dioxaborolane), Pd(PPh₃)₄ as a catalyst and K₂CO₃ as a base. In this reaction the correspondent derivative demethoxylated has been obtained since it is reported the occurrence of demethoxylation at the presence of metals including Pd; [208] therefore, compound **140** has been isolated and tested to deepen the SAR investigation. 4-(5-Amino-3-(4-fluorophenyl)pyrazin-2-yl)phenol (**141**) has been achieved after the deprotection of the methoxy-derivative using boron tribromide (**Scheme 11**).
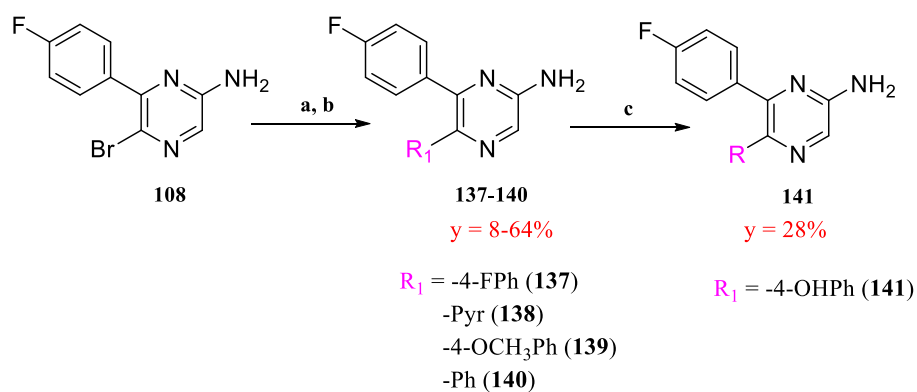
*Scheme 11: synthetic pathway for the development of 6-(4-fluorophenyl)-5-substituted pyrazine-2-amines (137-141). Reagents and conditions. **a**: 115, pyridine-4-ylboronic acid, PdCl₂(PPh₃)₂, Na₂CO₃, 1,4-dioxane, EtOH, H₂O, 130°C, MW, 1h, Ar; **b**: for compounds 138-139: 1-bromo-4-methoxybenzene, 4,4,4',4',5,5,5',5'-octamethyl-2,2'-bi(1,3,2-dioxaborolane), Pd(PPh₃)₂, K₂CO₃, 1,4-dioxane, rfx, overnight/ 2-(4-methoxyphenyl)-4,4,5,5-tetramethyl-1,3,2-dioxaborolane, PdCl₂(PPh₃)₂, Na₂CO₃, 1,4-dioxane, EtOH, H₂O, 130°C, MW, 1h, Ar; **c**: 138, BBr₃, DCM, -40°C to r.t., overnight, Ar; y = yield.*

4.2.2.   Structure-activity relationship (SAR) studies

All the developed pyrazines have been tested on CK1δ to explore the structure-activity relationship profile. Different substituents have been investigated, in particular at the 3- and 5- positions of the scaffold.

Studying the 6-position of the nucleus without substituents at 3- and 5-locations, 4-fluorophenyl moiety has led to inactive derivative **107**. Substituting the aromatic group with piperazine (**127**) and the Boc-protected

4. Synthesis and characterization of tri- and tetra-substituted pyrazines: new scaffold-based strategy

one (**126**), the situation does not change: IC$_{50}$s have not been registered since the activity percentage results higher than 50% at the concentration (**Table 12**).

Table 12: activity percentages of compounds **107, 126-127**.
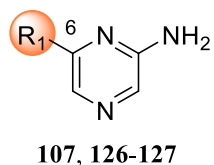
Cmpd	R$_1$	% Activity at 40 μM[a]
107	-(4-F)Ph	n.d. (87.5% ±10.5)
126	-BocPip	n.d. (97.2% ± 5.3)
127	-Pip	n.d. (75.2% ±1.2)

[a] Data represent the % of activity at 40 μM concentration expressed as a mean ± SD of two independent experiments.

Maintaining 4-fluorophenyl moiety at the 6-position of the main nucleus, some attempts have been conducted to functionalize the 3-position. Considering phenylpropyl chain as R$_1$, compound **114** has proved to be inactive on CK1δ revealing an activity percentage of 88.5%. The alkyl group has been substituted with amino moieties including morpholine (**128**) and functionalized piperazine with methyl group (**129**) and the benzyl one (**130**). The three substituents have conducted to non-active derivatives (**Table 13**).

Table 13: activity percentages of compounds **114, 128-130**.
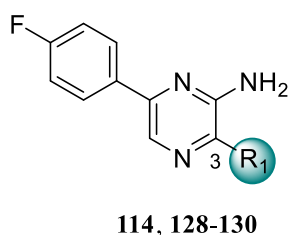
Cmpd	R$_1$	% Activity at 40 μM[a]
114	-(CH$_2$)$_3$Ph	n.d. (88.5% ±1.0)
128	-Morph	n.d. (135% ± 1)
129	-CH$_3$-Pip	n.d. (93.4% ± 2.2)
130	-BnPip	n.d. (85.0% ± 7.8)

[a] Data represent the % of activity at 40 μM concentration expressed as a mean ± SD of two independent experiments.

Trisubstituted pyrazines have been developed by substituting the 5-position of the scaffold inserting ethyl ester at the 3-location. 2-fluoro-6-methylpyridine group as R$_1$ has led to active compound in the high micromolar range with an IC$_{50}$ of 24.8 μM (**124**). Trying to change the functionalized pyridine with 4-fluorophenyl moiety, the activity improves achieving the IC$_{50}$ of 12.3 μM (**125**). From this preliminary SAR investigation, the substitution at 5-position results crucial to obtain an activity (**Table 14**).

Table 14: IC$_{50}$s of compounds **124-125** and activity percentages.
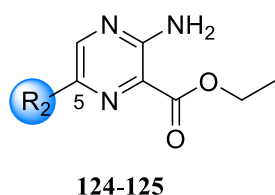
Cmpd	R$_1$	IC$_{50}$ μM [a] (% activity at 40 μM)[b]
124	-2F-6CH$_3$Pyr	24.8 ± 6.2
125	-4FPh	12.3 ± 5.3

[a] Data represent the mean ± SD of two independent experiments performed in technical duplicate. [b] Data represent the % of activity at 40 μM concentration expressed as a mean ± SD of two independent experiments.

4. Synthesis and characterization of tri- and tetra-substituted pyrazines: new scaffold-based strategy

A further SAR investigation has been carried out by studying the crucial 5-position of nucleus. Mente *et* coworkers have been conducted an optimization of the CK1δ/ε dual inhibitors PF-670462 (**9**) by improving its druglike properties developing a BBB-permeable candidate that is represented in **Fig. 81**. PF-670462 (**9**) has demonstrated IC$_{50}$s of 7.8 nM and 29.0 nM on CK1δ and ε, respectively, and it is used as tool for the investigation of circadian rhythm disorders on models. To improve the selectivity towards the isoform δ of CK1 and to develop a druglike compound, compounds **10-11** have been obtained as BBB-permeable optimized derivatives reporting 48.1 nM and 14.2 nM as IC$_{50}$ values, respectively.
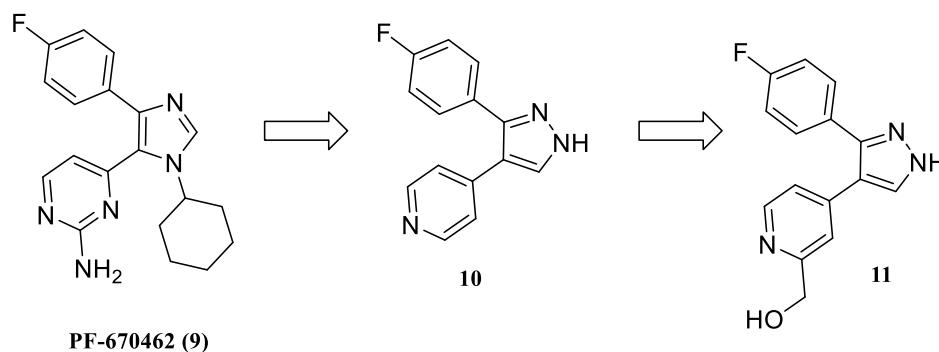
*Figure 81: representation of structures of PF-670462 (**9**) and its optimized derivatives **10-11**.*

The study of the 5-position of pyrazine nucleus includes some types of substituted aromatic rings. Starting from compound **137** with a 4-fluorophenyl moiety that has shown an IC$_{50}$ of 1.86 μM, a simple phenyl ring (**140**) as well as 4-methoxy (**139**) and the deprotected 4-hydroxyphenyl (**141**) moieties have been inserted but all the substitutions have proved to be ineffective. The hydroxy group, like a fluorine atom, is considered as a hydrogen bond acceptor even if in this case derivative **141** has resulted inactive on CK1δ differing from compound **137**. Therefore, observing the predicted binding pose of PF-670462 reporting in **1.6.1.1.2. paragraph**, 4-fluorophenyl moiety can position itself in the hydrophobic pocket stabilizing the structure in the ATP-binding site; probably the hydroxy moiety appears too hydrophilic in the case of compound **141**.

*Table 15: IC$_{50}$s of compounds **137-141** and activity percentages.*
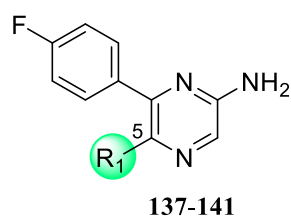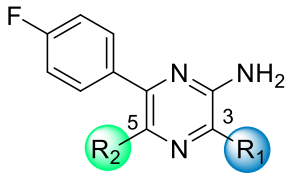
Cmpd	R$_1$	IC$_{50}$ μM [a] (% activity at 40 μM)[b]
137	-(4-F)Ph	1.86 ± 0.46
140	-Ph	n.d. (60.3% ± 0.4)
139	-(4OCH$_3$)Ph	n.d. (69.5% ± 0.4)
141	-(4OH)Ph	n.d. (90.2% ± 6.0)
138	-Pyr	0.069 ± 0.039

[a] Data represent the mean ± SD of two independent experiments performed in technical duplicate. [b] Data represent the % of activity at 40 μM concentration expressed as a mean ± SD of two independent experiments.

To corroborate this hypothesis the X-ray structure should be crucial. Instead, by substituting the 5-position of the scaffold with pyridine developing the 2-amino pyrazine analog of compound **9** developed by Mente and co-workers, a potent and promising lead derivative has been obtained (**138**) achieving an IC$_{50}$ of 0.069 μM (**Table 15**).

*Table 16: IC$_{50}$s of compounds **103-105**, **120** and **135-136** and activity percentages.*

Cmpd	R$_1$	R$_2$	IC$_{50}$ μM ^{a} (% activity at 40 μM)^b
103	-(CH$_2$)$_3$Ph	-(2-F)(6-CH$_3$)Pyr	21.9 ± 8.8
104	-(CH$_2$)$_4$Ph	-(2-F)(6-CH$_3$)Pyr	12.5 ± 4.8
105	-(CH$_2$)$_4$	-(2-F)(6-CH$_3$)Pyr	7.20 ± 3.37
120	-(CH$_2$)$_4$	-(4-F)Ph	0.20 ± 0.07
135	-BocPip	-(4-F)Ph	6.38 ± 0.85
136	-Pip	-(4-F)Ph	0.86 ± 0.09

^{a} *Data represent the mean ± SD of two independent experiments performed in technical duplicate.* ^{b} *Data represent the % of activity at 40 μM concentration expressed as a mean ± SD of two independent experiments.*

Tetrasubstituted pyrazines have been developed investigating alkyl chains as well as saturated cyclic amines. Compounds **103-105** are the precursors of the series screened on CK1δ that have reported IC$_{50}$s in the high micromolar range. Consequently, since in the ester derivatives (**124-125**) 4-fluorophenyl ring has proved to determine a better IC$_{50}$ value than 2-fluoro-6-methylpyridine derivative, compound **120** has been developed with double 4-fluorophenyl moiety at 5- and 6-positions determining IC$_{50}$ of 0.20 μM confirming itself as promising derivative. Analogs with cyclic amine have been obtained; the 3-Boc-piperazine compound (**135**) has reported an activity of 6.38 μM while the deprotected derivative (**136**) has registered an IC$_{50}$ of 0.86 on CK1δ (**Table 16**).

In this chapter a series of functionalized pyrazines has been discussed: the structure-activity relationship profile has been outlined investigating the four positions of the nucleus. Several promising derivatives have been found opening the possibility of exploring the druglike properties as well as the biochemical and biological characterization of the discovered hit candidates and compound **138** that has proved to be the best of the series.

4.2.3.   Evaluation of LiPE profile of this series

As discussed in the **chapter 3**, LiPE parameter allows to explore the druglike properties and attractiveness of candidates correlating the potency of compounds with their *C*logP. LiPE values of the pyrazine set of compounds have been calculated and plotted in the graph reported below. Agreeing with the color code, labeled dots have been colored in relation to IC$_{50}$s. In the upper left side of **Figure 82** the most promising derivative **138** places with the highest LiPE value given by an activity in the nanomolar range and a *C*logP of 2.0 (**Panel B** of **Fig. 83**) included in the ideal range of *C*logP values confirming it as most potent candidate with interesting druglike properties. Regards the other most active compounds **120** and **136**, LiPE values appear acceptable, nevertheless *C*logPs are higher than 3.0 determining a deviation from the range established. The same situation can be recorded for compound **137** reporting a *C*log P of 3.6 and a LiPE value of 2.2. In the lower left section of the graph compounds with ethyl ester moiety at the 3-position are reported (**124-125**) denoting good *C*log P values but IC$_{50}$s in the high micromolar range. The right part, instead, indicates 3-alkyl derivatives **103-105** and compound **120** with too high *C*logP values and too low IC$_{50}$s, consequently LiPE for these compounds appears unfavorable. Calculated LiPE values are reported in the histogram in **Fig. 83**, **Panel A**.

4. Synthesis and characterization of tri- and tetra-substituted pyrazines: new scaffold-based strategy
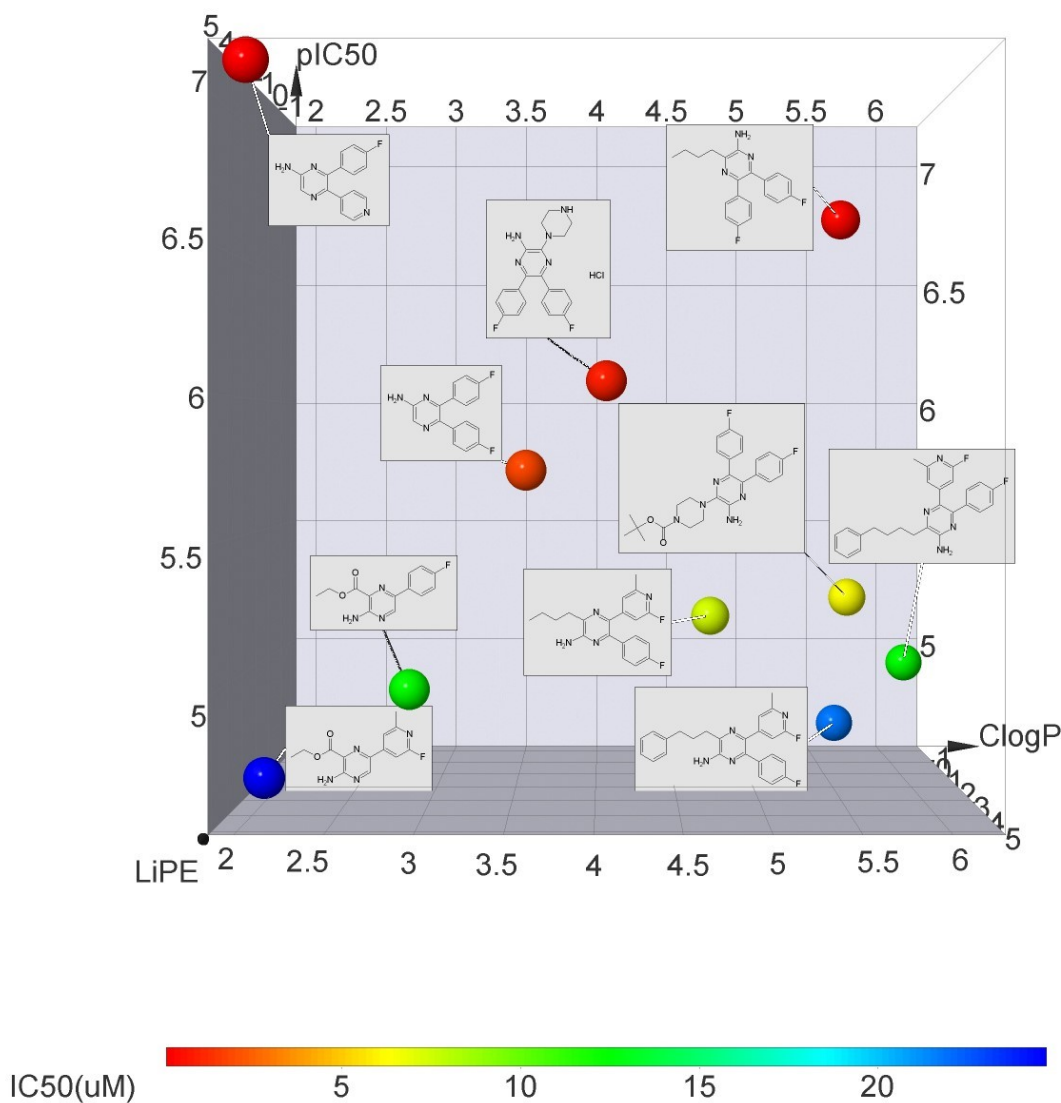
Figure 82: LiPE plot made using DataWarrior; in x and y axis ClogP and pIC₅₀ are reported while in z axis LiPE values of compounds are given. According to IC₅₀s of derivatives, colors of the labeled dots are chosen as represented in the color code below the figure.

Cmpd	ClogP
103	5.7
104	6.2
105	4.8
137	3.6
124	2.0
136	4.1
125	2.8
138	2.1
120	5.6
135	5.7
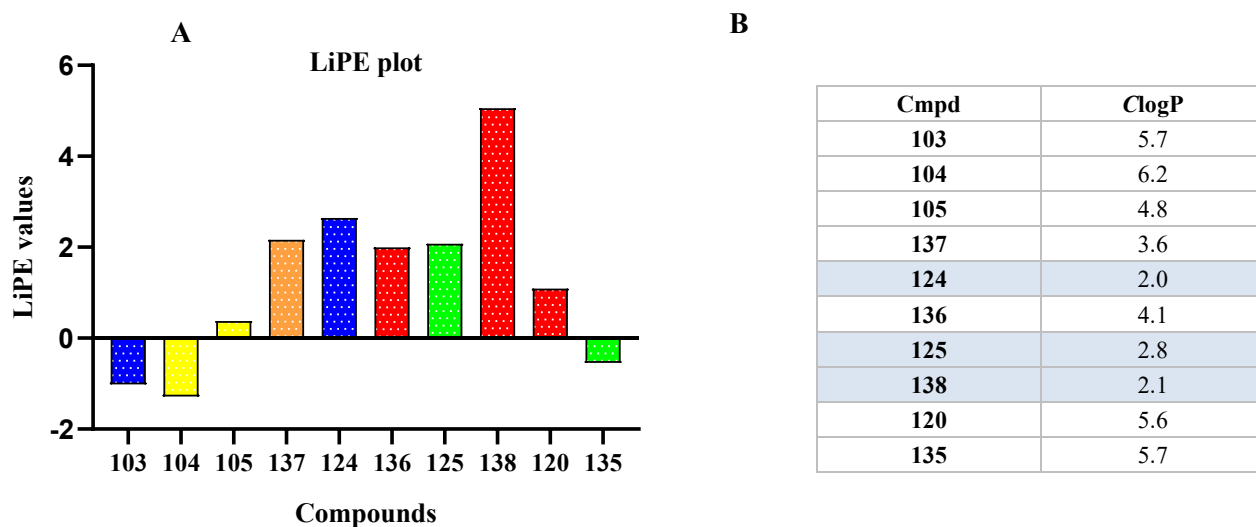
*Figure 83: LiPE values of active compounds are reported. Histogram made with GraphPad Prism 8.0. Panel B shows ClogP values, calculated with ChemDraw Professional of compounds **103-105**, **120**, **124-125**, **135-138**. Highlighted in light blue ClogP in the idea range.*

4.2.4. Biochemical and biological characterization

4.2.4.1. *In vitro* evaluation of BBB-permeability

The BBB-PAMPA assay, deeply discussed in **chapter 3**, has been conducted for most promising compounds that have displayed IC_{50}s below 2 μM (**136-138**). Moreover, the evaluation of CNS-permeability has been carried out also for derivative **105**, one of the precursors of the series to predict the passive transport for 3-alkyl derivatives. Unfortunately, the promising compound **120** has not been evaluated with BBB-PAMPA experiment since it has been developed in the final phase to conclude this subset of derivatives.

As mentioned in the **chapter 3**, obtained Pe were filtered according to the literature: the BBB permeability in humans is predicted as positive if it is higher than $4 \cdot 10^{-6}$ cm/s and negative if it is lower than $2 \cdot 10^{-6}$ cm/s. Therefore, applying these limits to the equation of calibrant line it is possible to establish cut-off values: in this case compounds with Pe higher than $2.1 \cdot 10^{-6}$ cm/s are classified as CNS+ while Pe permeations below $1.4 \cdot 10^{-6}$ cm/s represent CNS- derivatives. Giving the range of distant values, some compounds can obtain a borderline Pe and they are categorized as CNS+/-.

The collection of data, showed in **Figure 84** (**Panel A** and **B**), displays permeability values of four compounds of this series: 3-buthyl derivative **105** and double fluorophenyl molecule **137** have reported high Pe classified themselves as CNS+. The substitution of 3-position of the scaffold with piperazine moiety (**136**) has determined an increased hydrophilicity, therefore the CNS prediction has resulted borderline. The same prospect has been detected for compound **138**, the most potent of the series with pyridine at the 5-position. To improve druglike properties discussed in previous paragraph and CNS *in vitro* permeability maintaining an appealing IC_{50}, the challenge can be represented by 3-alkyl derivatives and by substituting pyridine moiety inserted at 5-location of candidate **138**.

A

BBB permeability evaluation

B

Cmpd	Bibl.	Pe (10^{-6} cm/s)	Prediction
Atenolol	0.8	0.1 ± 1.2	
Caffein	1.3	0.8 ± 0.9	
Desipramine	12	2.7 ± 3.2	
Enoxacin	1.6	1.3 ± 0.4	
Hydrocortisone	2.4	1.3 ± 0.3	
Ofloxacine	0.8	2.1 ± 0.7	
Piroxicam	2.5	1.7 ± 0.3	
Promazine	8.8	13.8 ± 10.2	
Testosterone	17	6.8 ± 2.1	
Verapamil	16	8.9 ± 2.8	
137		7.2 ± 0.1	**CNS+**
105		3.5 ± 0.5	**CNS+**
136		1.4 ± 0.4	**CNS+/-**
138		1.9 ± 0.6	**CNS+/-**
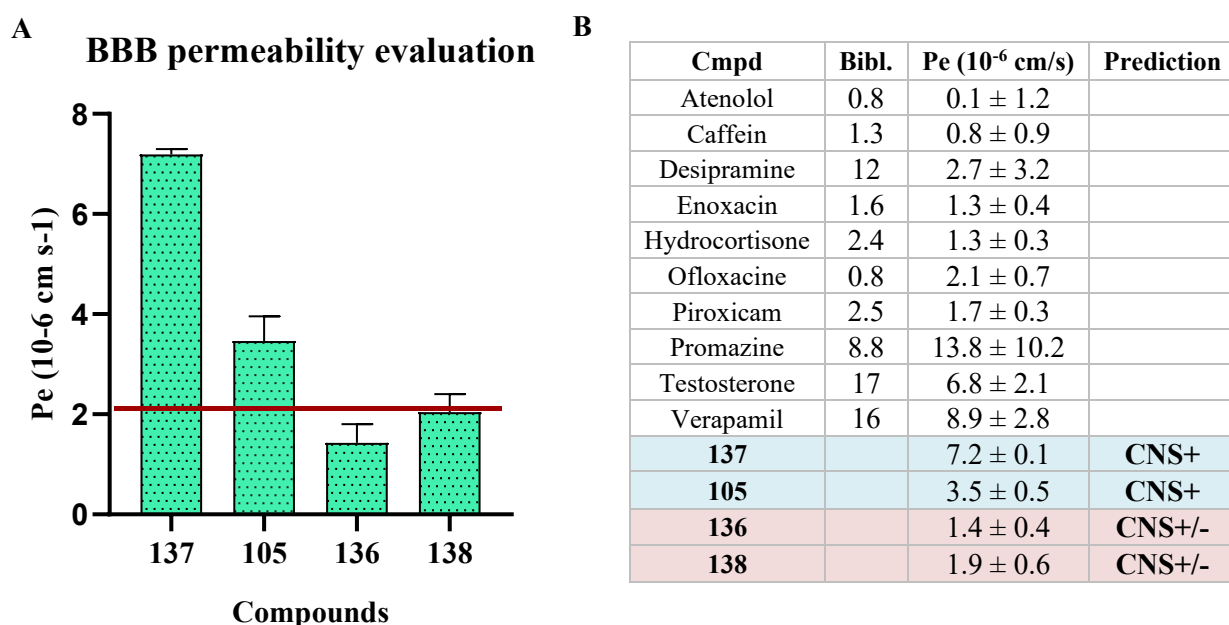
*Figure 84: **Panel A)** histogram of Pe values of compounds **105, 136-138** made with GraphPad 8.0. **Panel B)** Table of Pe and CNS predictions.*

4.2.4.2. ATP-competition

To assess the behavior of the most appealing compound (**138**) of this series, the Lineweaver-Burk plot, displayed in **Fig. 85**, has been carried out by performing the kinetic ATP-competition assay using Kinase-Glo Kit. Since derivative has shown an IC_{50} of 69 nM, it has been assayed at the concentrations of 0.1 μM and 0.2 μM using increasing ATP concentrations (1 μM, 2 μM, 10 μM, 50 μM). Observing **Fig. 85** and the zoom of the origin reported, it is possible to appreciate how the intercept of the three lines related to the inhibitor's concentrations and negative control, appears the same denoting and confirming this candidate as CK1δ ATP-competitive derivative (the **Table 17** reports the y-intercept values).
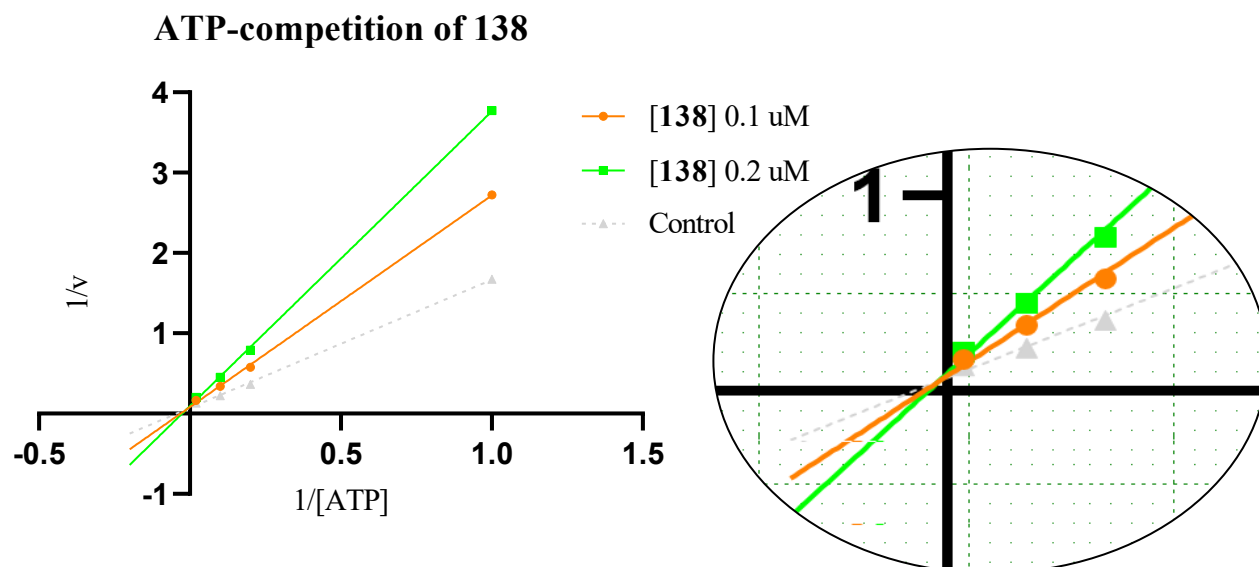
Figure 85: Double-reciprocal Lineweaver graph of compound 138 assaying at concentrations of 0.1 and 0.2 μM. The zoom of the intercept is reported on the right.

Table 17: y-intercept values of the Lineweaver-Burk plot reported in Fig.84 for compound 138.

Cmpd	y-intercept
[138] 0.1 μM	0.1
[138] 0.2 μM	0.1
Control	0.1

4.2.4.3. Thermal Shift Assay (TSA)

The TSA technique has been accurately described in the dedicated paragraph (**chapter 3.3.5.3.**). This experiment has been conducted for best derivative **138**, as displayed in **Fig. 86** it is possible to appreciate the shift of the melting curve of CK1δ when increasing amounts of ligand were added to the protein. This evidence collected by the assay allow to define that compound appears a very good binder of CK1δ: at a 15-fold concentration of **138** respect to kinase, a shift of about five degrees of T_m has been observed (**Table 18**).
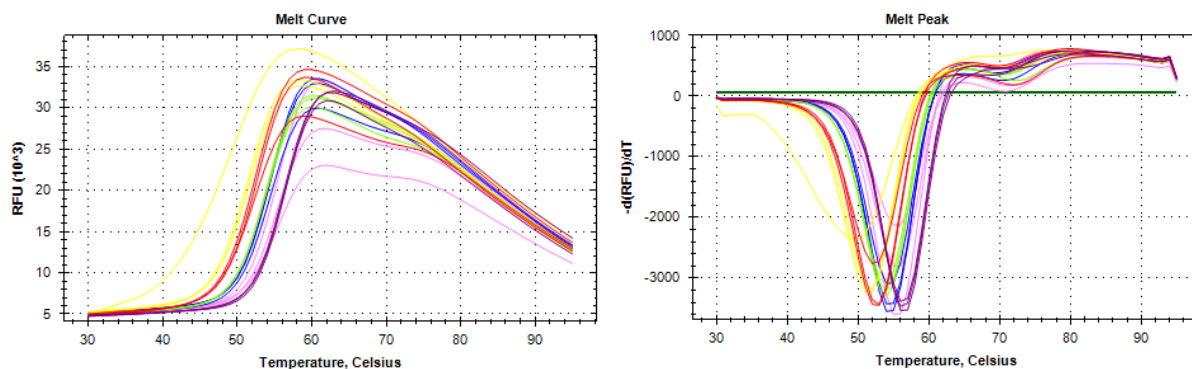
Colour code: yellow 0.5x; red 1x; green 3x; blue 5x; pink 10x; purple 15x

*Figure 86: melting curves of compound **138**. The first graph (melt curve) reports the temperature (C°) in x axis and RFU (relative fluorescence unit) in y axis. The second graph (dissociation curve) reports the temperature in x axis and the negative derivate of RLU in the y one.*

Table 18: table of shift values. The "condition" reports concentrations of compound (multiples of protein concentration), the "average" column indicates the mean of temperature of technical triplicate accompanied by the standard deviation ("SD") while the "DT°C" column reports the temperature shift.

Condition	Tm	DT°C	SD triplicates
CK1δ (3μM)	51	(0)	0
CK1δ + 2.5% DMSO	51	(0)	0
138 0.5X	51.3	+0.3	1.2
138 1X	52.6	+1.6	0.6
138 3X	54	+3	0
138 5X	54	+3	0
138 10X	55.6	+4.6	0.6
138 15X	56	+5	0

4.2.4.4.   Screening on GSK3β

For the most promising compounds the screening on GSK3β has been conducted during the Erasmus program in the Prof. Martinez' group (CSIC-Madrid-ES) not only to obtain useful information about the selectivity of developed derivatives but also to explore the behavior of this series towards another kinase involved in neurodegenerative diseases. As reported in the **chapter 3.3.5.4.**, compounds have been tested on full-length GSK3β (1 ng/μL) at the presence of GS-2 as substrate (0.2 μg/μL) and ATP at the final concentration of 1 μM. **Table 19** displays the percentage activity values assaying compounds **136-138** at the final concentration of 10 μM. It is possible to observe that IC_{50}s of derivatives have not been determined since activity percentages have resulted over than 50% at the tested concentration.

*Table 19: Activity percentages of compounds **134, 136-137** on GSK3β at the concentration of 10 μM. ᵃ Data represent the % of activity at 10 μM concentration expressed as a mean ± SD of two independent experiments performed in technical duplicate; n.d.: not determined.*

Cmpd	% Activity at 10 μMᵃ
137	n.d. (100% ± 0)
136	n.d. (100% ± 1)
138	n.d. (100% ± 0)

4.2.5. Biological *in vitro* characterization of the most promising derivatives on neuroblastoma cell lines

The best candidates **136-138** have been investigated from biological point of view during the Erasmus+ Traineeship program in the Prof. Martinez' group (CSIC-Madrid-ES) to evaluate neuroprotective behavior of compounds and if they are able to decrease the TDP-43 phosphorylation on neuroblastoma cell lines (SH-SY5Y). Detailed experiments and procedures are explained in **chapter 4.1.4.1.5.** and in experimental section, respectively. Firstly, to establish potential toxicity of derivatives, MTT assay plating 80000 cells/well has been conducted in triplicate testing compounds at the concentrations of 5 and 10 μM. Histograms of cell viability percentage are reported in **Fig. 87** and **88**. It is possible to observe that the three derivatives assayed have demonstrated to be harmless for cells.
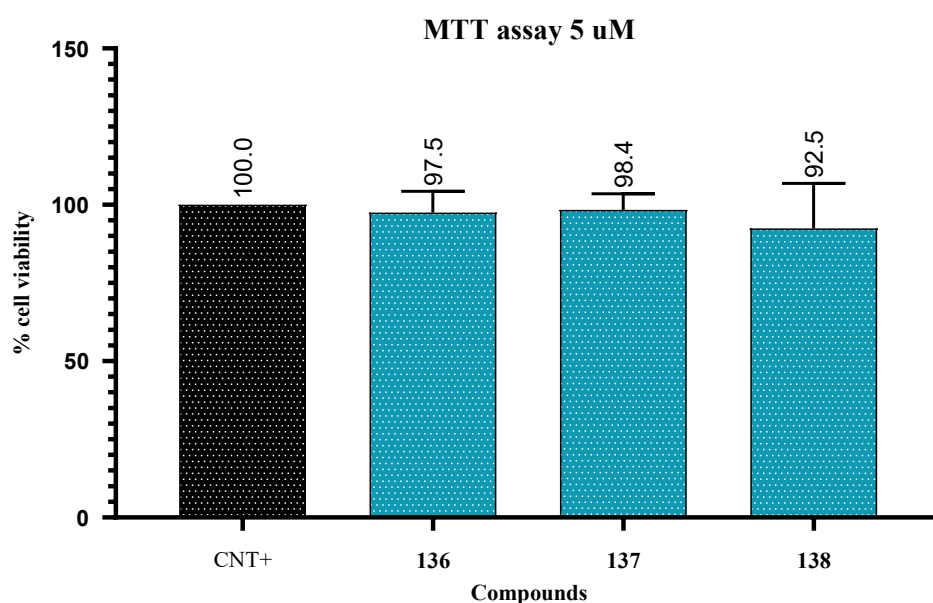
*Figure 87: MTT assay of compounds **136-138** at the concentration of 5 μM. In y axis the cell viability percentage is reported. The elaboration performed with GraphPad Prism 8.0 in "Anova" mode is the result of three independent experiments and each experiment is conducted using the mean of six wells per compound.*
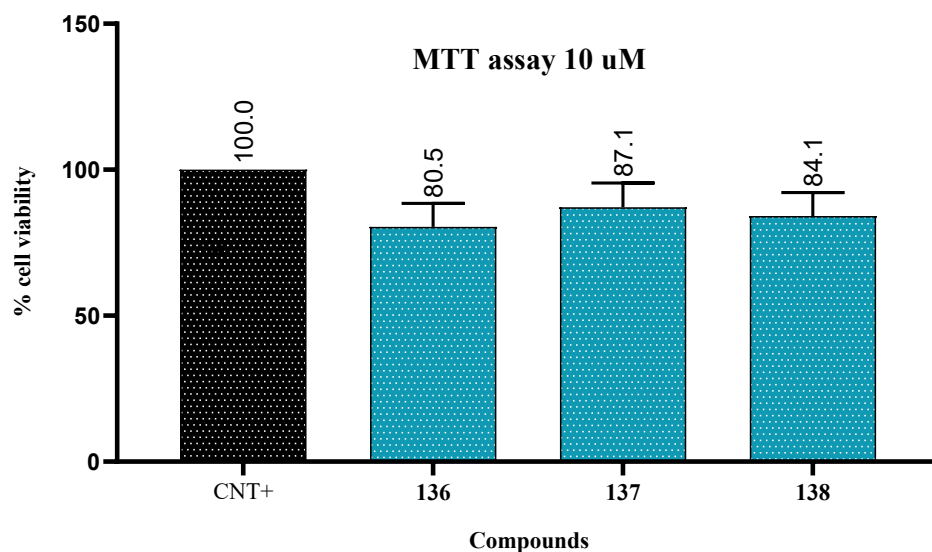
Figure 88: MTT assay of compounds 136-138 at the concentration of 10 μM. In y axis the cell viability percentage is reported. The elaboration performed with GraphPad Prism 8.0 in "Anova" mode is the result of three independent experiments and each experiment is conducted using the mean of six wells per compound.

Once completed the MTT assay, the three derivatives have been tested in the neuroprotection assay plating 60000 cells/well and observing the cell viability adding ethacrynic acid as toxic agent to simulate the neuronal death. Firstly, compound **138** has been tested at the concentrations of 1 and 5 μM. As **Figure 89** reports, the interested candidate has displayed a neuroprotective behavior at the concentration of 1 μM and, interestingly, this attitude has not been featured with the increased concentration of 5 μM. To rationalize the reported neuroprotection only at the lower concentration, a dose-effect curve should be provided. Also compound **136** has been assayed in the same experiment without showing any neuroprotective behavior.
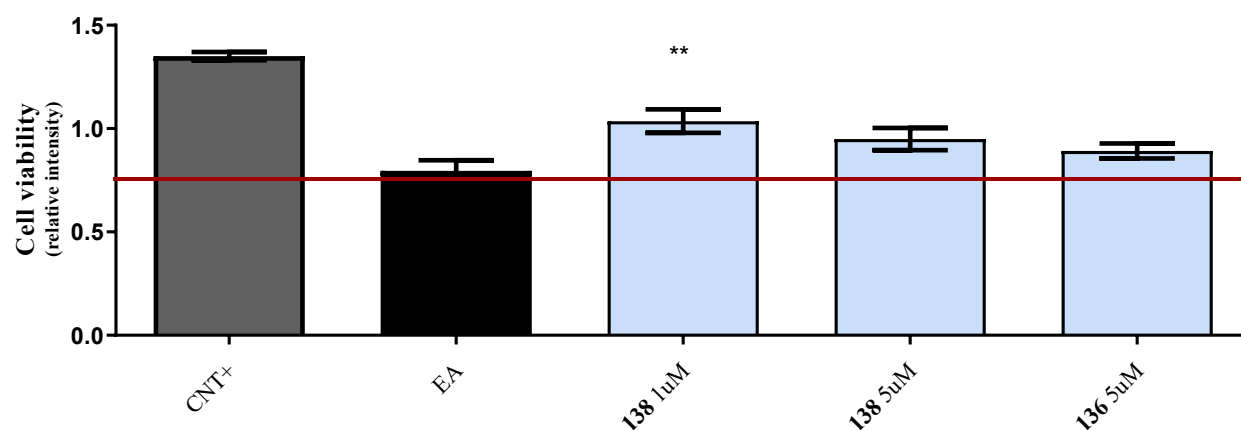
*Figure 89: neuroprotection assay's results. Three independent experiments have been conducted and the elaboration has been performed with GraphPad Prism 8.0 using the "Anova" mode with the mean of eight wells per compounds for each plate and then final data have been obtained with "T test" mode to compare the three experiments. EA has been used at 45 μM while chosen concentration for compound 136 is 5 μM while derivative 138 has been assayed at 1 and 5 μM. Results are expressed as the mean of three data ± standard error (error bars); ****p<0.0001 significantly different from control cells, ***p<0.001 significantly different from control cells, **p<0.01 significantly different from control cells, *p<0.1 significantly different from control cells.*

Derivative **137** has been evaluated in another experiment at the concentration of 5 μM but no significant data are reported, as **Fig. 90** showed, denoting a relative cell viability comparable to the negative control represented by the ethacrynic acid.
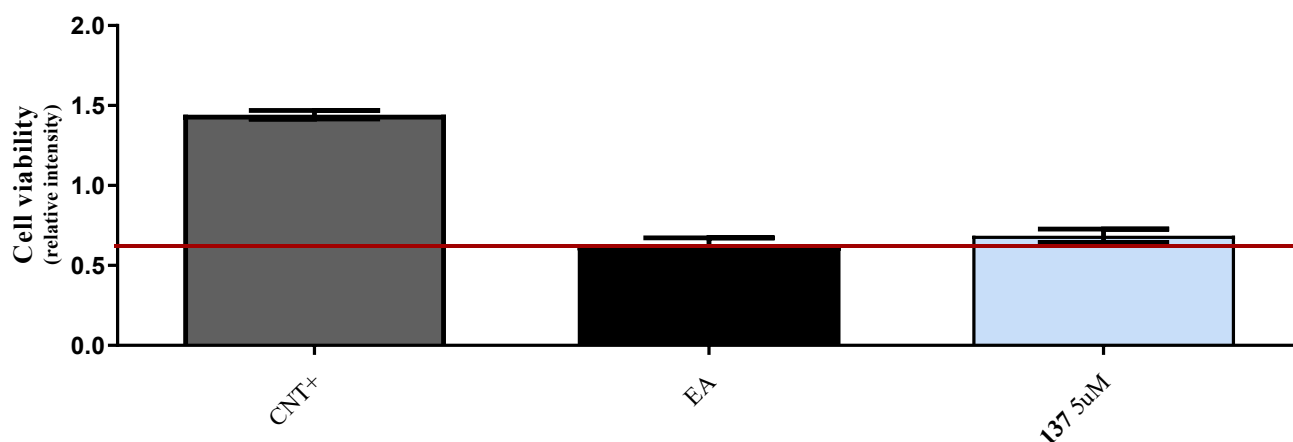
Figure 90: neuroprotection assay's results. Three independent experiments have been conducted and the elaboration has been performed with GraphPad Prism 8.0 using the "Anova" mode with the mean of eight wells per compounds for each plate and then final data have been obtained with "T test" mode to compare the three experiments. EA has been used at 45 μM while chosen concentration for compound 137 is 5 μM.

Since results for derivative **138** have indicated a neuroprotective behavior, Western Blot has been carried out to detect a decrease of pTDP-43. Details of the experiment have been explained in **chapter 3.3.5.5.**. Two experiments have been carried out obtaining some preliminary results, even though the triplicate could provide to have the statistic validation.

First Western Blot experiment is reported in **Fig. 91** (**Panel A** and **Panel B**); the fragment of 25 KDa has been detected. The intensity related to compound **138** appears minor than ethacrynic acid condition. To appreciate a quantitative decrease in pTDP-43, the normalization against total TDP-43 is given in **Panel B** denoting a significative improvement in comparison to the positive control. Nevertheless, an acceptable span between control and ethacrynic acid has not been recorded.
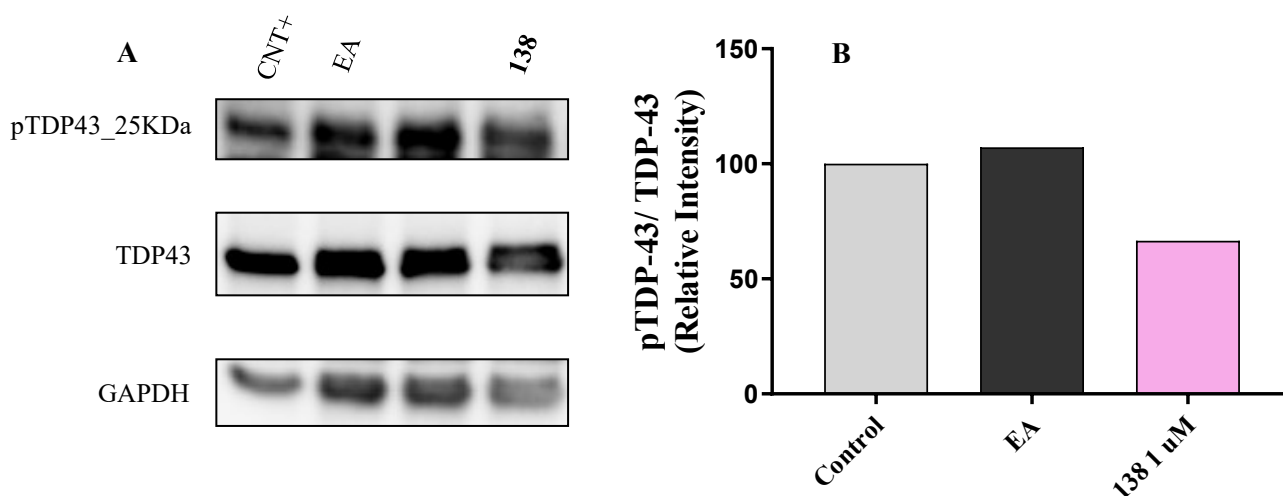
*Figure 91: **Panel A**) Western Blot results of the first experiments: the three windows report the pTDP-43 (25 KDa) overview, TDP-43 and GAPDH, respectively. **Panel B**) the histogram displays quantitative results of Immunoblotting. There is a significant decrease in pTDP-43 administrating **138** at the concentration of 1 μM. Quantitative results of Western Blot analysis are elaborated using ImageLab as program.*

Interestingly, the 25 kDa TDP-43 has been detected also in the insoluble fraction as it is possible to observe in **Fig. 92**. The intensity of ethacrynic acid appears marked related to the reported one for compound **138**, nevertheless normalizing it against total TDP-43 whose intensity seems distinct denoting different amounts in the loading process, thus it was not possible to obtain results from this fraction.
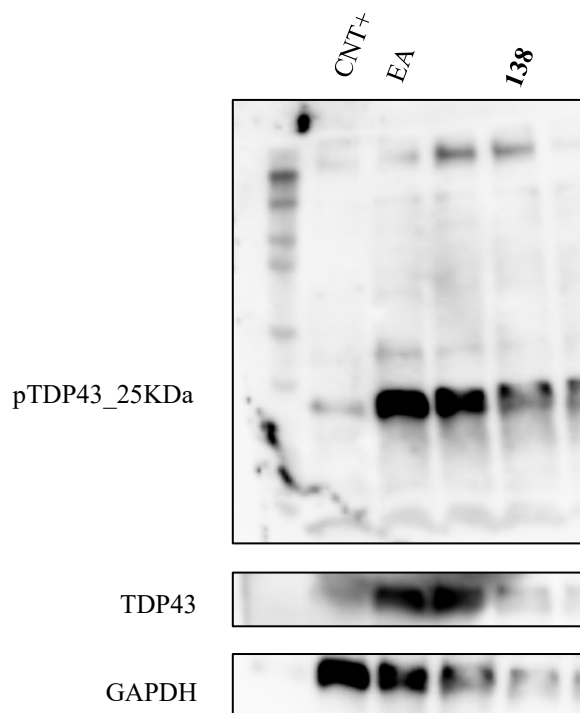
Figure 92: Western Blot results of the first experiments (insoluble fraction): the three windows report the pTDP-43 (25 KDa) overview, TDP-43 and GAPDH, respectively.

The second experiment conducted on the soluble fraction (**Fig. 93**) represents another situation in which the 37 kDa fragment has been recognized: there is enough span between control and ethacrynic acid; however, administration of compound **138** reveals a comparable percentage related to EA. Therefore, a decrease in pTDP-43 has not been recorded.
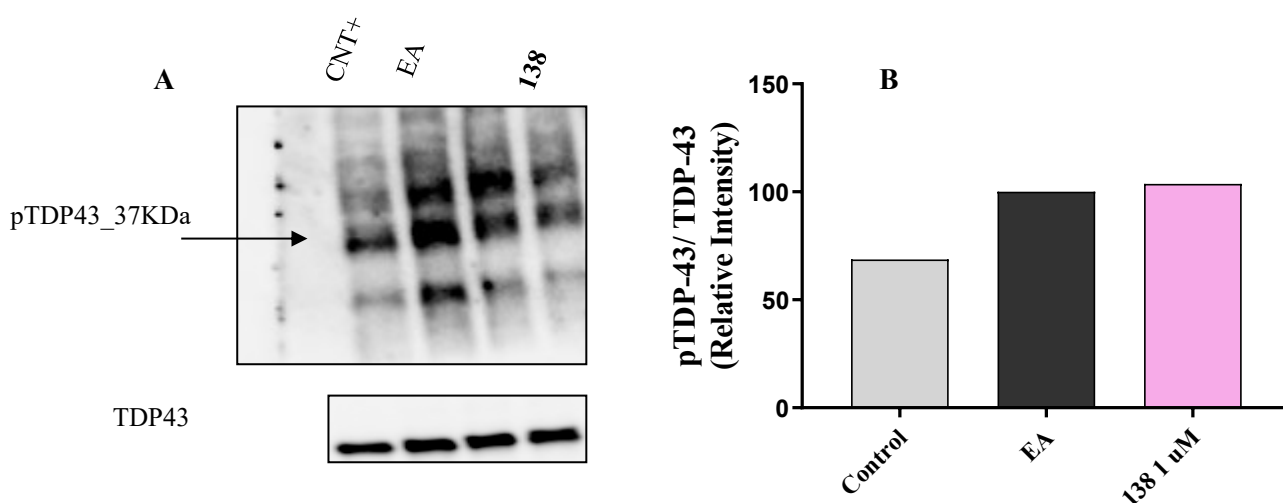
*Figure 93: **Panel A)** Western Blot results of the second experiments: the three windows report the pTDP-43 (37 KDa) overview and TDP-43, respectively. **Panel B)** the histogram displays quantitative results of Immunoblotting. There is not a decrease in pTDP-43 administrating **138** at the concentration of 1 μM. Quantitative results of Western Blot analysis are elaborated using ImageLab as program.*

Therefore, to conclude Western Blot analysis to establish if administrated candidates can reduce phosphorylation of TDP-43, at least a third experiment will be mandatory to obtain validated results, since combination of both experiments 1 and 2 does not provide significant data as **Fig. 94** displays.
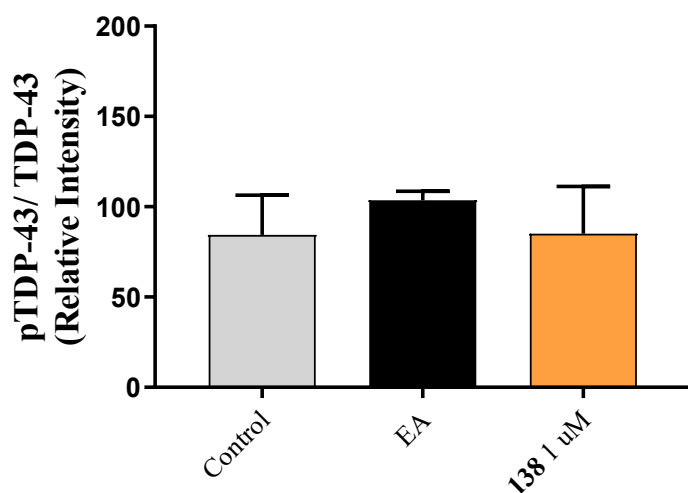
*Figure 94: histogram displays quantitative results of Immunoblotting (experiments 1 and 2). There is not a decrease in pTDP-43 administrating **138** at the concentration of 1 μM. Quantitative results of Western Blot analysis are elaborated using ImageLab as program.*

4.3.　Conclusions and future perspectives

In the **chapter 4** tri- and tetra-substituted pyrazines as CK1δ ATP-competitive inhibitors have been discussed exploring substitutions at three of the four positions of the nucleus. The structure-activity relationship profile has been outlined and druglike properties have been evaluated considering LiPE values and BBB permeability of the active subset of derivatives. From this first characterization, several compounds have been resulted potent and interesting denoting features agreeing with ideal druglike properties; in particular, derivative **138** bearing pyridine at the 5-position has reported an IC_{50} of 69.0 nM confirming itself as the most potent of the small library. Other appealing discovered compounds involve the tetra-substitution approach: 3-butyl derivative **120** synthesized rationalize alkyl-derivatives has shown an activity of 200 nM while the insertion of piperazine at the 3-location maintaining the double fluorophenyl ring at 5- and 6-positions has displayed an IC_{50} of 0.86 μM (**136**). Moreover, a biochemical investigation established an ATP-competitive behavior of the most promising candidate **138** and its ability to bind and stabilize CK1δ has been demonstrated by thermal shift assay. During the Erasmus+ program conducted in Prof. Martinez' group in Spain (CSIC-Madrid) the testing of most promising compounds on GSK3β has been carried out to obtain useful information about the activity over this other kinase involved in several neurodegenerative diseases. Tested compounds resulted to be inactive against GSK3β. Nevertheless, the selectivity of a wide panel of kinases should be conducted for compound **138**. In neuroprotection assays on neuroblastoma cell lines, derivative **138** has shown a neuroprotective behavior at the concentration of 1 μM, therefore, the Western Blot analysis, performed to detect the decrease in TDP-43 phosphorylation that represents the hallmark of ALS, gave promising results, but a third experiment will be required to have an appropriate statistical validation. As future perspectives, collecting all the evidences and starting from this derivative it is possible to deepen the SAR investigation developing a correspondent compound with pyridine at the 5-position and alkyl chain at the 3-location. The development of several candidates bearing a functionalized pyridine at the 5-location of the main scaffold could result interesting to develop more potent derivatives investigating druglike features as well as BBB-permeation. Nevertheless, a wider exploration of substituents could be performed investigating several types of moieties to insert at 6- and 3-positions since pyrazine nucleus lends itself to an extensive SAR analysis by substituting all the 4 positions.

4.4.   Experimental section

4.4.1.   General Chemistry

Reagents were obtained from commercial suppliers and used without further purification. Reactions were monitored by TLC, on precoated silica gel plates (Macherey-Nagel, 60FUV254). Final compounds and intermediates were purified by flash chromatography using as stationary phases silica gel (Macherey-Nagel, silica 60, 240-400 mesh) or preparative TLC (stationary phase silica gel, Mechery-Nagel, silica 60, 240-400 mesh, 0.25 mm). When used, light petroleum ether refers to the fractions boiling at 40-60°C. Melting points were determined with a Stuart SMP10 melting point apparatus, and they were not corrected. The ^{1}H NMR, ^{13}C NMR and gHSQCAD bidimensional spectra were determined in CDCl$_3$ or DMSO-d_6 and recorded on Varian 400 MHz or Varian 500 MHz spectrometers; chemical shifts (δ scale) are reported in parts per million (ppm) and referenced to residual solvent peak, with splitting patterns abbreviated to: s (singlet), d (doublet), dd (doublet of doublets), dt (doublet of triplets), t (triplet), m (multiplet) and bs (broad signal). Coupling constants (*J*) are given in Hz. MS-ESI analysis was performed using ESI Bruker 4000 Esquire spectrometer or microTOF-Q – Bruker, used also for the recording of accurate mass. Compound purities were determined by HPLC using the instrument SHIMADZU CBM-20A, column Gemini® 5 μm NX-C18 (Phenomenex®). Elution gradient was performed for 20 min at the flow of 1 ml/min from water-methanol 55:45 to 15:85. The detector was set at 254 nm.

4.4.2.   3-alkyl-5-substituted-6-(4-fluorophenyl)pyrazin-2-amino derivatives (**103-105**, **120**)

4.4.2.1.   Synthesis of 6-(4-fluorophenyl)pyrazin-2-amine (**107**)

To a stirred suspension of commercially available 6-chloropyrazin-2-amine (**106**) (0.0154 mol, 2.00 g) and (4-fluorophenyl)boronic acid (0.0185 mol, 2.60 g) in 90.4 mL of toluene, 8.50 mL of ethanol and 16.4 mL of a 2M solution of Na$_2$CO$_3$ 0.620 mmol (0.716 g) of Pd(PPh$_3$)$_4$ were added in an argon atmosphere. The mixture was refluxed for 4 h; once completed, the catalyst was removed by filtration through a celite pad, and the solvent was evaporated under *vacuum*. The crude product was dissolved in 120 mL of water and extracted with DCM (3 x 40 mL). Finally, organic phases were dried over anhydrous sodium sulfate and concentrated at reduced pressure. The crude residue was then purified with flash chromatography (light petroleum 70% - EtOAc 30% to light petroleum 60% - EtOAc 40%) affording compound **107** as a white solid with a 95% of yield; mp 153°C. ^{1}H-NMR (400 MHz, DMSOd_6) δ 8.27 (s, 1H), 8.04 (dd, $^3J_{H\text{-}F}$ = 8.9, $^4J_{H\text{-}F}$ =5.6 Hz, 2H), 7.85 (s, 1H), 7.29 (t, $^3J_{H\text{-}F}$, $^4J_{H\text{-}F}$= 8.9 Hz, 2H), 6.52 (s, 2H). ^{13}C-NMR (101 MHz, DMSOd_6) δ 163.81 (d, $^1J_{C\text{-}F}$ = 246.2 Hz), 155.19 (CH), 147.55 (CH), 133.71 (d, $^4J_{C\text{-}F}$ = 3.0 Hz), 131.05, 128.53 (d, $^3J_{C\text{-}F}$ = 8.4 Hz, CH), 128.14, 115.55 (d, $^2J_{C\text{-}F}$ = 21.5 Hz, CH). ES-MS (methanol) *m/z*: C$_{10}$H$_8$FN$_3$ 190.0 [M+H]$^+$.

4.4.2.2.   Synthesis of 3-bromo-6-(4-fluorophenyl)pyrazin-2-amine (**109**)

A stirred solution of 2.50 mmol of 6-(4-fluorophenyl)pyrazin-2-amine (**107**, 473 mg) in 25.0 mL of anhydrous DCM was cooled to 0°C and 2.73 mmol of NBS (486 mg) were added portionwise. The solution was allowed to warm to room temperature and stirred for 1h. Then, the reaction has been washed with 10 mL of NaHCO3, 10 mL of water and 10 mL of brine. The organic phase was dried over Na$_2$SO$_4$ and the solvent was removed under *vacuum* and, once completed, the crude residue was purified with flash chromatography (light petroleum 70% - EtOAc 30%) affording 202 mg of yellow solid (**103**, yield 43%); mp 196°C; ^{1}H-NMR (400 MHz, DMSOd_6) δ 8.15 (s, 1H), 8.10 (d, $^3J_{H\text{-}F}$ = 8.9, $^4J_{H\text{-}F}$ = 5.5 Hz, 2H), 7.32 (t, $^3J_{H\text{-}F}$, $^4J_{H\text{-}F}$ = 8.9 Hz, 2H), 6.82 (s, 2H). ^{13}C-NMR (101 MHz, DMSOd_6) δ 163.06 (d, $^1J_{C\text{-}F}$ = 246.9 Hz), 152.77 (CH), 147.65, 132.04 (d, $^4J_{C\text{-}F}$ = 3.0 Hz), 128.77 (d, $^3J_{C\text{-}F}$ = 8.5 Hz, CH), 128.22, 123.94, 115.73 (d, $^2J_{C\text{-}F}$ = 21.6 Hz, CH). ES-MS (methanol) *m/z*: C$_{10}$H$_7$BrFN$_3$ 268.0 [M+1]$^+$.

5-bromo-6-(4-fluorophenyl)pyrazin-2-amine (**108**): yellow solid; yield 11%; mp 170°C; ^{1}H-NMR (400 MHz,

DMSOd_6) δ 7.69 (s, 1H), 7.68 – 7.63 (m, 2H), 7.29 (t, $^3J_{H-F}$ = 8.9 Hz, 2H), 6.77 (s, 2H). ^{13}C-NMR (101 MHz, DMSOd_6) δ 162.26 (d, $^1J_{C-F}$ = 246.2 Hz), 154.68 (CH), 149.86, 134.31 (d, $^4J_{C-F}$ = 3.2 Hz), 131.43 (d, $^3J_{C-F}$ = 8.5 Hz, CH), 130.75, 122.14, 114.82 (d, $^2J_{C-F}$ = 21.6 Hz, CH). ES-MS (methanol) *m/z*: $C_{10}H_7BrFN_3$ 268.0 [M+1]$^+$.

4.4.2.3.   Synthesis of di-*tert*-butyl (3-bromo-6-(4-fluorophenyl)pyrazin-2-yl)carbamate (**110**)

27.0 mmol of di-*tert*-butyl-dicarbonate (5.90 g, 3.0 eq) and 40.0 mmol of 3-bromo-6-(4-fluorophenyl)pyrazin-2-amine (**109**, 2.40 g) were solved in 100 mL of THF. After cooled to 0°C the stirred reaction, 18.0 mmol of DMAP (0.22 g, 0.2 eq) were added and the mixture was refluxed for 2 h. After completed, the solvent was removed under *vacuum* and the crude residue was washed with 180 mL of brine and extracted with EtOAc (3 x 60 mL). Organic phases were dried over sodium sulfate and the solvent was evaporated under reduced pressure. Then the crude residue was purified with flash chromatography (light petroleum 70%-EtOAc 30%) to give 3.20 g of solid (**110**). White solid; yield 97%; mp 132°C; ^{1}H-NMR (400 MHz, DMSO-d_6) δ 9.15 (s, 1H), 8.19 (dd, $^3J_{H-F}$ = 8.9, $^4J_{H-F}$ = 5.4 Hz, 2H), 7.41 (t, $^3J_{H-F}$, $^4J_{H-F}$ =8.9 Hz, 2H), 1.37 (s, 18H). ^{13}C-NMR (101 MHz, DMSO-d_6) δ 164.06 (d, $^1J_{C-F}$= 249.1 Hz), 149.31, 149.24, 146.95, 141.34 (CH), 137.91, 130.44 (d, $^4J_{C-F}$= 3.1 Hz), 129.67 (d, $^3J_{C-F}$= 8.8 Hz, CH), 116.71 (d, $^2J_{C-F}$= 23.6 Hz, CH), 84,24, 27,65 (CH$_3$). ES-MS (methanol) *m/z*: $C_{20}H_{23}BrFN_3O_4$ 490.1 [M+Na]$^+$, 390.0 [M-Boc+Na]$^+$.

4.4.2.4.   General procedure for the synthesis of *tert*-butyl(6-(4-fluorophenyl)-3-alkyl substituted pyrazin-2-yl)carbamate (**111-113**)

11.0 mmol of magnesium (200 mg, 8.6 eq) were inserted under argon atmosphere to 16 mL of anhydrous THF (0.5 M). To the mixture a catalytic amount of iodine was added, and the stirred reaction was refluxed. Then, 7.60 mmol of desired alkyl halide (1.20 mL, 6.0 eq) were added dropwise and the mixture proceeded for 3 h until the reaction whitened. Once the preparation of Grignard reagent is completed, 1.28 mmol of di-*tert*-butyl (3-bromo-6-(4-fluorophenyl)pyrazin-2-yl)carbamate (**110**, 600 mg) were solved under argon atmosphere in 15 mL of THF and 1.5 mL of NMP. The mixture was cooled to 0°C and 0.031 mmol of Fe(acac)$_3$ (about 12.8 mg, 0.03 eq) and (3-phenylpropyl)magnesium bromide synthesized in the previous step was added. The reaction proceeded for 2h; then, the mixture was washed with 90 mL of water and extracted with diethyl ether (3 x 30 mL). Organic layers were washed with 40 mL of brine and dried over sodium sulfate. Once completed, the solvent was removed under *vacuum* and the crude residue was purified with flash chromatography (light petroleum 90% - EtOAc 10%) affording solid final compounds (**111-113**).

4.4.2.4.1.   *Tert*-butil(6-(4-fluorophenyl)-3-(3-phenylpropyl)pyrazin-2-yl)carbamate (**111**)
White solid; yield 60% (142 mg); mp 113°C. ^{1}H-NMR (400 MHz, DMSO-d_6) δ 9.50 (s,1H), 8.98 (s,1H), 8.13 (dd, $^3J_{H-F}$ = 8.9, $^4J_{H-F}$ = 5.5 Hz, 2H), 7.42-7.31 (m, 3H), 7.35-7.27 (m, 2H), 7.23-7.15 (m, 3H), 2.85-2.74 (m, 2H), 2.65-2.60 (m, 2H), 2.03-1.96 (m, 2H), 1.45 (s, 9H). ^{13}C-NMR (101 MHz, DMSO-d_6) δ 163.10 (d, $^2J_{C-F}$=21.3 Hz, CH), 79.57, 34.98, 32.02 (CH$_2$), 28.88 (CH$_2$), 28.04 (CH$_3$). ES-MS (methanol) *m/z*: $C_{24}H_{26}FN_3O_2$ 430.1 [M+Na]$^+$.

4.4.2.4.2.   *Tert*-butyl (6-(4-fluorophenyl)-3-(4-phenylbutyl)pyrazin-2-yl)carbamate (**112**)
White solid; yield 55% (285 mg); mp 106°C. ES-MS (methanol) *m/z*: $C_{25}H_{28}FN_3O_2$ 444.2 [M+Na]$^+$.

4.4.2.4.3.   *Tert*-butyl (3-butyl-6-(4-fluorophenyl)pyrazin-2-yl)carbamate (**113**)

Yellow solid; yield 54% (141 mg); mp 106°C. ^{1}H NMR (400 MHz, DMSO-d_6) δ 9.49 (s, 1H), 8.96 (s, 1H), 8.13 (dd, $^3J_{H-F}$ = 10.4, $^4J_{H-F}$ = 7.2 Hz, 2H), 7.35 (d, $^3J_{H-F}$, $^4J_{H-F}$ = 8.9 Hz, 2H), 2.82 – 2.74 (m, 2H), 1.66 (dd, J = 15.1, 7.4 Hz, 2H), 1.48 (s, 9H), 1.33 (dd, J = 14.8, 7.4 Hz, 2H), 0.89 (t, J = 7.3 Hz, 3H). ^{13}C NMR (101 MHz, DMSO-d_6) δ 163.53 (d, $^1J_{C-F}$ = 242.6 Hz), 153.65, 151.21, 146.71, 145.51, 137.68 (CH), 132.55 (d, $^4J_{C-F}$ = 3.0 Hz), 129.17 (d, $^3J_{C-F}$ = 8.6 Hz, CH), 116.32 (d, $^2J_{C-F}$ = 21.6 Hz, CH), 79.95, 32.56 (CH$_2$), 29.71, 28.47 (CH$_2$), 22.44 (CH$_2$), 14.22 (CH$_3$). ES-MS (methanol) *m/z*: C$_{19}$H$_{24}$FN$_3$O$_2$ 368.1 [M+Na]$^+$.

4.4.2.5. General procedure for the synthesis of 6-(4-fluorophenyl)-3-alkyl substituted-2-amine (**114-116**)

0.879 mmol of **111-113** were solved under stirring in 4.5 mL of HCl in 1,4-dioxane 4M (commercially available). The reaction was allowed at room temperature for 2 h; then, the solvent was removed under *vacuum* and the crude residue was purified with flash chromatography (light petroleum 80% - EtOAc 20%). Once completed, the solvent was evaporated under reduced pressure to obtain products **114-116**.

4.4.2.5.1.   6-(4-fluorophenyl)-3-(3-phenylpropyl)pyrazin-2-amine (**114**)

Yellow solid; yield 86% (233 mg), mp 134°C; ^{1}H NMR (400 MHz, DMSO-d_6) δ 8.22 (s, 1H), 8.06 – 7.96 (m, 2H), 7.31 – 7.11 (m, 7H), 6.29 (s, 2H), 2.66 (ddd, J = 8.7, 6.7, 1.7 Hz, 4H), 2.01 – 1.89 (m, 2H). ^{13}C NMR (101 MHz, DMSO-d_6) δ 164.25, 161.81, 153.38, 145.87, 142.60, 141.28, 133.93 (d, J = 3.0 Hz), 128.77 (CH), 128.66 (d, $^3J_{C-F}$ = 7.5 Hz, CH), 128.03, 126.12 (CH), 116.04, 115.83 (CH), 35.28 (CH$_2$), 32.20 (CH$_2$), 28.46 (CH$_2$). ES-MS (methanol) m/z 308.1 [M+H]$^+$; theoretical 307.15. HRMS (ESI-TOF) *m/z*: C$_{19}$H$_{18}$FN$_3$ experimental 308.1557 [M+H]$^+$, theoretical 308.1558 [M+H]$^+$, Δ = 0.0001. Purity HPLC: 96.1%.

4.4.2.5.2.   6-(4-fluorophenyl)-3-(4-phenylbutyl)pyrazin-2-amine (**115**)

Pale yellow solid; yield 65% (135 mg); mp 126°C. ^{1}H NMR (400 MHz, DMSO-d_6) δ 8.24 (s, 1H), 8.04 (dd, $^3J_{H-F}$ = 8.7, $^4J_{H-F}$ = 5.6 Hz, 2H), 7.35 – 6.99 (m, 9H), 2.72 (t, J = 6.8 Hz, 2H), 2.61 (dd, J = 34.7, 6.6 Hz, 2H), 1.66 (d, J = 6.7 Hz, 4H).^{13}C NMR (101 MHz, DMSO-d_6) δ 161.96, 153.50, 142.64, 133.38, 128.74 (dd, $^3J_{C-F}$ = 11.2, 6.6 Hz, CH), 126.06 (CH) , 116.13, 115.92 (CH), 35.48 (CH$_2$), 31.94 (CH$_2$), 31.15 (CH$_2$), 26.29 (CH$_2$). ES-MS (methanol) *m/z*: C$_{20}$H$_{20}$FN$_3$ 322.2 [M+H]$^+$.

4.4.2.5.3.   3-butyl-6-(4-fluorophenyl)pyrazin-2-amine (**116**)

Yellow solid; yield 22% (45.0 mg); mp 87°C. ^{1}H NMR (400 MHz, DMSO-d_6) δ 8.22 (s, 1H), 8.02 (dd, $^3J_{H-F}$ = 8.9, $^4J_{H-F}$ = 5.6 Hz, 2H), 7.28 (m, 2H), 6.25 (s, 2H), 2.63 (d, 2H), 1.63 (dd, J = 15.2, 7.5 Hz, 2H), 1.36 (dd, J = 14.6, 7.3 Hz, 2H), 0.91 (t, J = 7.3 Hz, 3H). ^{13}C NMR (101 MHz, DMSO-d_6) δ 164.22, 161.77, 153.31, 145.76, 141.71, 133.92 (d, $^4J_{C-F}$ = 3.0 Hz), 128.65 (d, $^3J_{C-F}$ = 4.6 Hz), 127.98 (CH), 116.02 (CH), 115.80 (CH), 32.26 (CH$_2$), 28.72 (CH$_2$), 22.39 (CH$_2$), 14.37 (CH$_3$). ES-MS (methanol) *m/z*: C$_{15}$H$_{18}$FN$_3$ 246.0 [M+H]$^+$.

4.4.2.6. General procedure for the synthesis of 5-bromo-6-(4-fluorophenyl)-3-alkyl substituted pyrazin-2-amine (**117-119**)

0.650 mmol of 6-(4-fluorophenyl)-3-akyl substitueted pyrazin-2-amine (**114-116**) were solved under argon atmosphere in 8.0 mL of anhydrous DCM. After cooling the mixture, 0.890 mmol of NBS (29.0 mg, 1.3 eq) were added portionwise. The reaction was warmed to room temperature for 5 h. Once completed, the mixture was washed with 9.0 mL of NaHCO$_3$, 9.0 mL of brine and 9.0 mL of water. The organic phase was dried over anhydrous sodium sulfate and the solvent was removed under *vacuum*. Then, the crude residue was purified with flash chromatography (light petroleum 80% - EtOAc 20%) affording compounds **117-119**.

4.4.2.6.1.   5-bromo-6-(4-fluorophenyl)-3-(3-phenylpropyl)pyrazin-2-amine (**117**)

Yellow solid; yield 87% (27.0 mg), mp 93°C. ^{1}H NMR (400 MHz, DMSO-d_6) δ 7.67 (m, 2H), 7.32-7.15 (m, 7H), 6.58 (s, 3H), 2.74 – 2.63 (m, 4H), 1.96 (dd, J = 15.2, 7.7 Hz, 2H). ^{13}C NMR (101 MHz, DMSO-d_6) δ 163.73, 152.93, 147.66, 142.44, 142.09, 134.82, 134.79 (d, $^4J_{C-F}$ = 3.2 Hz), 131.86 (d, $^3J_{C-F}$ = 8.5 Hz, CH),

128.75 (d, $^3J_{C-F}$=8.7 Hz, CH), 126.17 (CH), 121.82, 115.19 (d, $^2J_{C-F}$= 21.6 Hz, CH), 35.21(CH$_2$), 31.77 (CH$_2$), 28.42 (CH$_2$). ES-MS (methanol) *m/z*: C$_{20}$H$_{19}$BrFN$_3$ 386.1 [M+H]$^+$.

4.4.2.6.2. 5-bromo-6-(4-fluorophenyl)-3-(4-phenylbutyl)pyrazin-2-amine (**118**)
Yellow solid; yield 57% (87.0 mg); mp 128°C. ^{1}H NMR (400 MHz, DMSO-*d$_6$*) δ 7.64 (t, $^4J_{H-F}$ = 6.1 Hz, 2H), 7.20 (ddd, $^3J_{H-F}$ = 16.2, $^3J_{H-F}$ = 11.6, $^4J_{H-F}$ = 6.4 Hz, 7H), 6.54 (s, 2H), 2.62 (d, *J*= 6.9 Hz, 4H), 1.65 (d, *J*= 3.5 Hz, 4H). ^{13}C NMR (101 MHz, DMSO-*d$_6$*) δ 162.55 (d, $^1J_{C-F}$=245.9 Hz), 152.91, 147.67, 142.51 (d, $^3J_{C-F}$=20.5 Hz), 134.82, 134.79, 131.87 (d, $^4J_{C-F}$=,8.5 Hz, CH), 128.70 (d, $^4J_{C-F}$=3.1 Hz, CH), 126.08 (CH), 121.83, 115.18 (d, $^2J_{C-F}$=21.6 Hz, CH), 35.40 (CH$_2$), 31.92 (CH$_2$), 31.05 (CH$_2$), 26.27 (CH$_2$). ES-MS (methanol) *m/z*: C$_{21}$H$_{21}$BrFN$_3$ 400.0 [M+H]$^+$.

4.4.2.6.3. 5-bromo-3-butyl-6-(4-fluorophenyl)pyrazin-2-amine (**119**)
Yellow solid; yield 56% (81.5 mg); mp 125°C. ^{1}H NMR (400 MHz, DMSO-*d$_6$*) δ 7.66 (dd, $^3J_{H-F}$ = 8.9, $^4J_{H-F}$ =5.5 Hz, 2H), 7.27 (t, $^3J_{H-F}$ = 8.9 Hz, 2H), 6.54 (s, 2H), 2.67 – 2.58 (m, 2H), 1.62 (dt, *J*= 15.3, 7.5 Hz, 2H), 1.38 (dq, *J* = 14.6, 7.3 Hz, 2H), 0.92 (t, *J* = 7.3 Hz, 3H). ^{13}C NMR (101 MHz, DMSO-*d$_6$*) δ 162.54 (d, $^1J_{C-F}$ = 245.8 Hz), 152.89, 147.58, 142.55, 134.80 (d, $^4J_{C-F}$ = 3.2 Hz), 131.86 (d, $^3J_{C-F}$ = 8.5 Hz, 2CH), 121.82, 115.18 (d, $^2J_{C-F}$ = 21.6 Hz, 2CH), 31.85 (CH$_2$), 28.74 (CH$_2$), 22.36 (CH$_2$), 14.33 (CH$_3$). ES-MS (methanol) *m/z*: C$_{15}$H$_{17}$BrFN$_3$ 324.1 [M+H]$^+$.

4.4.2.7. General procedures for the synthesis of 5-(2-fluoro-6-methylpyridin-4-yl)-6-(4-fluorophenyl)-3-alkyl substituted pyrazin-2-amine (**103**-**105**, **120**)
0.155 mmol of 5-bromo-6-(4-fluorophenyl)-3-alkyl substituted pyrazin-2-amine (**117-119**) and an equimolar amount of 2-fluoro-6-methyl-4-(4,4,5,5-tetramethyl-1,3,2-dioxaborolan-2-yl)pyridine were suspended under argon atmosphere in a microwave tube in 1.0 mL of 1,4-dioxane, 1.0 mL of ethanol and 1.5 mL of water. Then, 0.220 mmol of Na$_2$CO$_3$ (2 eq) and 0.00750 mmol of PdCl$_2$(PPh$_3$)$_2$ (0.05 eq) were added and the mixture was allowed to react at 130°C for 1.20 h. Once completed, the reaction was washed with 6.0 mL of water and extracted with EtOAc (3 x 2 mL). The organic layer was dried over anhydrous sodium sulfate and the solvent was removed under *vacuum*. Then, the crude residue was purified with flash chromatography (light petroleum 85% - EtOAc 25%) and the solvent was evaporated under reduce pressure to give compounds **103-105**, **120**.

4.4.2.7.1. 5-(2-fluoro-6-methylpyridin-4-yl)-6-(4-fluorophenyl)-3-(3-phenylpropyl)pyrazin-2-amine (**103**)
White solid; yield 28% (17.4 mg), mp 136°C. ^{1}H NMR (400 MHz, DMSO-*d$_6$*) δ 7.41 – 7.32 (m, 2H), 7.32-7.09 (m, 7H), 7.11 – 7.04 (m, 1H), 6.77 (s, 2H), 6.62 (s, 1H), 2.79 – 2.66 (m, 4H), 2.30 (s, 3H), 2.04 (dd, *J*= 15.2, 7.6 Hz, 2H). ^{13}C NMR (101 MHz, DMSO-*d$_6$*) δ 163.88 (d, $^3J_{C-F}$ = 24.5 Hz), 161.32, 156.90, 153.29 (d, $^2J_{C-F}$ = 52.9 Hz), 147.48, 142.61, 140.79, 134.47, 131.93 (d, $^4J_{C-F}$ = 5.8 Hz, CH), 128.69 (CH), 126.17 (CH), 121.28 (CH), 115.67 (CH), 106.03 (CH), 35.38 (CH$_2$), 31.97 (CH$_2$), 28.26 (CH$_2$), 23.85 (CH$_3$). ES-MS (methanol) m/z 417.2 [M+H]$^+$. HRMS (ESI-TOF) m/z: C$_{25}$H$_{22}$F$_2$N$_4$ experimental 417.1854 [M+H]$^+$, theoretical 417.1855 [M+H]$^+$, Δ = 0.0001. Purity HPLC: 94.1%.

4.4.2.7.2. 5-(2-fluoro-6-methylpyridin-4-yl)-6-(4-fluorophenyl)-3-(4-phenylbutyl)pyrazin-2-amine (**104**)
White solid, yield 45% (32.5 mg), mp 121°C. ^{1}H NMR (400 MHz, DMSO-*d$_6$*) δ 7.35 (t, $^3J_{H-F}$ = 8.6 Hz, 2H), 7.32 – 7.13 (m, 7H), 7.04 (s, 1H), 6.76 (s, 2H), 6.60 (s, 1H), 2.74 (t, *J*= 6.9 Hz, 2H), 2.65 (t, *J*= 7.0 Hz, 2H), 2.31 (s, 3H), 1.87-1.57 (m, 4H). ^{13}C NMR (101 MHz, DMSO-*d$_6$*) δ 163,73, 156.74, 152.95, 147.56, 142.70, 141.16, 135.45, 132.00 (CH), 131.92 (CH), 128.72 d, $^3J_{C-F}$=6.1 Hz, CH), 126.0 (CH) 7, 121.21 (CH), 115.58 (d, $^2J_{C-F}$=17.1 Hz, CH), 106.03 (CH), 105.64, 35.48 (CH$_2$), 32.09 (CH$_2$), 31.14 (CH$_2$) , 26.21 (CH$_2$), 23.86 (CH$_2$). ES-MS (methanol) m/z 431.2 [M+H]$^+$. HRMS (ESI-TOF) m/z: C$_{26}$H$_{24}$F$_2$N$_4$ experimental 431.2041 [M+H]$^+$, theoretical 431.2042 [M+H]$^+$, Δ = 0.0001. Purity HPLC: 98.6%.

4.4.2.7.3.   3-butyl-5-(2-fluoro-6-methylpyridin-4-yl)-6-(4-fluorophenyl)pyrazin-2-amine (**105**)

White solid, yield 7% (88.6 mg), mp 134°C. ^{1}H NMR (400 MHz, DMSO-d_6) δ 7.40 – 7.34 (m, 2H), 7.19 (t, $^3J_{H-F}$ = 8.9 Hz, 2H), 7.05 (s, 1H), 6.75 (s, 2H), 6.62 (s, 1H), 2.77 – 2.66 (m, 2H), 2.31 (s, 3H), 1.70 (dt, J = 15.2, 7.5 Hz, 2H), 1.49 – 1.35 (m, 2H), 0.94 (t, J = 7.4 Hz, 3H). ^{13}C NMR (101 MHz, DMSO-d_6) δ 156.93, 153.48, 152.91, 147.49, 141.31, 131.90 (2CH), 120.15 (CH), 119.18, 115.75 (d, $^2J_{C-F}$ = 16.6 Hz, 2CH), 115.45, 106.04 (d, $^4J_{C-F}$ = 2.1 Hz, CH), 105.65, 32.11 (CH$_2$), 28.69 (CH$_2$), 23.83 (CH$_3$), 22.43 (CH$_2$), 14.36 (CH$_3$). ES-MS (methanol) m/z 355.0 [M+H]$^+$. HRMS (ESI-TOF) m/z: C$_{25}$H$_{22}$F$_2$N$_4$ experimental 355.1729 [M+H]$^+$, theoretical 355.1729 [M+H]$^+$, Δ = 0.0000. Purity HPLC: 95.5%.

4.4.2.7.4.   3-butyl-5,6-bis(4-fluorophenyl)pyrazin-2-amine (**120**)

White solid, yield 23% (19.0 mg), mp 157°C. ^{1}H NMR (400 MHz, DMSO-d_6) δ 7.36 – 7.23 (m, 4H), 7.17 – 7.04 (m, 4H), 6.41 (s, 2H), 2.73 – 2.66 (m, 2H), 1.69 (dt, J = 15.3, 7.5 Hz, 2H), 1.41 (dq, J = 14.6, 7.4 Hz, 2H), 0.93 (t, J = 7.3 Hz, 3H). ^{13}C NMR (101 MHz, DMSO-d_6) δ 154.00 (d, J = 4.0 Hz), 152.16 (s), 145.72 (s), 140.84 (s), 137.61 (s), 131.91 (d, J = 8.9 Hz, 2CH), 131.50 (d, $^4J_{C-F}$ = 8.3 Hz, 2CH), 115.24 (dd, $^2J_{C-F}$ = 21.4, $^2J_{C-F}$ =10.3 Hz, 4CH), 32.16 (CH$_2$), 28.83 (CH$_2$), 22.49 (CH$_2$), 14.40 (CH$_3$). ES-MS (methanol) m/z 340.3 [M+H]$^+$. HRMS (ESI-TOF) m/z: C$_{20}$H$_{20}$F$_2$N$_4$ experimental 340.1621 [M+H]$^+$, theoretical 340.1620 [M+H]$^+$, Δ = 0.0001. Purity HPLC: 93.0%.

4.4.3.   3-ester-5-substituted-6-(4-fluorophenyl)pyrazin-2-amino derivatives (**124-125**)

4.4.3.1. General procedure for the synthesis of ethyl 3-aminopyrazine-2-carboxylate (**122**)

5.00 g (1.0 eq, 36.0 mmol) of 3-aminopyrazine-2-carboxylic acid (**121**), commercially available, were allowed to react with 8.0 mL of thionyl chloride (3.0 eq, 107 mmol) and 200 mL of ethanol. The reaction was refluxed overnight. After removing the solvent, the crude product was extracted with DCM (3 x 100 mL) and water (3 x 50.0 mL) and washed with saturated solution of NaHCO$_3$ (3 x10 mL). The organic layers were dried over anhydrous sodium sulfate and the solvent was removed under reduced pressure. The crude was precipitated by using light petroleum – EtOAc. Yellow solid, yield 62% (3.70 g); mp 102°C. ^{1}H NMR (400 MHz, DMSO-d$_6$) δ 8.19 (d, $^3J_{H-F}$ = 2.2 Hz, 1H), 7.84 (d, $^3J_{H-F}$ = 2.2 Hz, 1H), 7.26 (s, 2H), 4.25 (q, J = 7.1 Hz, 2H), 1.25 (t, J = 7.1 Hz, 3H). ES-MS (methanol) m/z: C$_7$H$_9$N$_3$O$_2$ 190.0 [M+Na]$^+$.

4.4.3.2. Synthesis of ethyl 3-amino-6-bromopyrazine-2-carboxylate (**123**)

Under argon atmosphere, 0.96 g (1.0 eq) of compound **122** were solved in 70.0 mL of dry DCM. Once achieved the temperature of 0°C, 1.12 g (1.1. eq) of NBS have been added portionwise. The reaction has been stirred overnight at room temperature. The mixture has been washed with water (70.0 mL), saturated solution of NaHCO$_3$ and brine and dried over Na$_2$SO$_4$. The solvent has been removed under reduced pressure and the crude product has been purified with flash chromatography (light petroleum 70%– EtOAc 30%). A precipitation with light petroleum – EtOAc has been required to obtain 1.04 g of yellow product (yield 85%); mp 145°C. ^{1}H NMR (400 MHz, DMSO-d$_6$) δ 8.41 (s, 1H), 7.54 (s, 2H), 4.32 (q, $^3J_{C-H}$ = 7.1 Hz, 2H), 1.31 (t, $^3J_{C-H}$ = 7.1 Hz, 3H). ES-MS (methanol) m/z: C$_7$H$_8$BrN$_3$O$_2$ 267.9 [M+Na]$^+$.

4.4.3.3. General procedure for the synthesis of ethyl 3-amino-6-(substituted 4-yl)pyrazine-2-carboxylate (**124-125**)

Method A: 200 mg of compound **123** (0.8 mmol, 1.0 eq) was solved in 1,4-dioxane (2.0 mL), ethanol (2.0 mL) and water (1.0 mL) under argon atmosphere in a microwave tube. 169.6 mg of Na$_2$CO$_3$ (1.6 mmol, 2.0 eq), 28.0 mg of PdCl$_2$(PPh$_3$)$_2$ (0.04 mmol, 0.05 eq) and 189.7 mg of 2-fluoro-6-methyl-4-(4,4,5,5-tetramethyl-1,3,2-dioxaborolan-2-yl)pyridine (0.8 mmol, 1.0 eq) were added. The reaction was stirred 1 h at 130°C on microwave. Once completed, the mixture was extracted with water (120 mL) and EtOAc (3 x 40.0 mL) after removing catalyst through celite plug. The crude was purified with flash chromatography (light petroleum 80%– EtOAc 20%). The solvent was removed under reduced pressure affording 18.4 mg of product.

4. Synthesis and characterization of tri- and tetra-substituted pyrazines: new scaffold-based strategy

Method B: Under argon atmosphere, 1.00 g of compound **123** (1.0 eq) were solved in 25.0 mL of toluene, 2.8 mL of ethanol and 4.6 mL of 2M Na_2CO_3 solution. To the mixture, 718 mg (1.0 eq) of (4-fluorophenyl)boronic acid, commercially available and 215 mg (0.05 eq) of $Pd(PPh_3)_4$ were added. The reaction was refluxed at 110°C for 3 h. Once completed, the product was extracted with DCM (3 x 60.0 mL) and water (3 x 20.0 mL) and organic layers were dried over anhydrous Na_2SO_4. The solvent was removed under reduced pressure and the crude was purified with flash chromatography (light petroleum 80%– EtOAc 20%). The solvent was removed under *vacuum* to give 0.51 g of product.

4.4.3.3.1.   Ethyl 3-amino-6-(2-fluoro-6-methylpyridin-4-yl)pyrazine-2-carboxylate (**124**)
Method A; yellow solid; yield 8% (18.4 mg), mp 136°C. ^{1}H NMR (400 MHz, DMSO-d_6) δ 9.04 (s, 1H), 7.81 (s, 1H), 7.75 (s, 2H), 7.48 (s, 1H), 4.40 (q, J = 7.1 Hz, 2H), 2.52 (dd, J = 3.7, 1.8 Hz, 3H), 1.38 (t, J = 7.1 Hz, 3H).   ES-MS (methanol) m/z 277.1 [M+H]$^+$, 299.0 [M+Na]$^+$. HRMS (ESI-TOF) m/z: $C_{13}H_{13}FN_4O_2$ experimental 299.0916 [M+Na]$^+$, theoretical 299.0915 [M+Na]$^+$, Δ = 0.0001. Purity HPLC: 93.2%.

4.4.3.3.2.   Ethyl 3-amino-6-(4-fluorophenyl)pyrazine-2-carboxylate (**125**)
Method B; yellow solid; yield 58% (0.51 g); mp 121°C. ^{1}H NMR (400 MHz, DMSO-d_6) δ 8.89 (s, 1H), 8.14 – 7.91 (m, 2H), 7.44 (s, 2H), 7.31 (t, J = 8.5 Hz, 2H), 4.49 – 4.28 (m, 2H), 1.35 (t, J = 6.9 Hz, 3H). ^{13}C NMR (101 MHz, DMSO-d_6) δ 166.46, 155.09, 145.27 (CH), 139.13, 133.00 (d, $^4J_{C-H}$ = 3.0 Hz), 127.75 (d, $^3J_{C-H}$ = 8.4 Hz, 2CH), 122.43, 116.12 (d, $^2J_{C-H}$ = 21.6 Hz, 2CH), 61.47 (CH$_2$), 14.63 (CH$_3$). ES-MS (methanol) m/z 262.1 [M+H]$^+$, 284.1 [M+Na]$^+$, theoretical 261.09. HRMS (ESI-TOF) m/z: $C_{13}H_{12}FN_3O_2$ experimental 284.0808 [M+Na]$^+$, theoretical 284.0811 [M+Na]$^+$, Δ = 0.0001. Purity HPLC: 94.8%.

4.4.3.4. Synthesis of 6-aminopyrazin-2-piperazine derivative (**127**)

4.4.3.4.1.   *Tert*-butyl 4-(6-aminopyrazin-2-yl)piperazine-1-carboxylate (**126**)
3.30 mmol of 6-chloropyrazin-2-amine (1.0 eq) (**106**), commercially available, were diluted with butanol (25.0 mL). *Tert*-butyl piperazine-1-carboxylate (9.9 mmol, 3.0 eq) was added and the solution was refluxed overnight. Once completed, the solvent was removed under reduced pressure and the crude product was purified with flash chromatography (light petroleum 90% – EtOAc 10%) to afford 30.0 mg of **126**. Yellow solid; yield 3%; mp 123°C. ^{1}H NMR (400 MHz, DMSO-d_6) δ 7.34 (s, 1H), 7.19 (s, 1H), 5.99 (s, 2H), 3.40 (d, J = 2.1 Hz, 8H), 1.42 (s, 9H). MicrOTOF-Q (methanol) m/z 280.17 [M+H]$^+$, 302.15 [M+Na]$^+$. HRMS (ESI-TOF) m/z: $C_{13}H_{21}N_5O_2$ experimental 280.1767 [M+H]$^+$, theoretical 280.1768 [M+H]$^+$, Δ = 0.0001.

4.4.3.4.2.   6-(piperazin-1-yl)pyrazin-2-amine hydrochloride (**127**)
0.11 mmol of 122 (1.0 eq, 30.0 mg) were solved in 3.0 mL of HCl in 1,4-dioxane. The reaction was stirred at room temperature for 2 h, once completed, the solvent was removed under removed pressure affording 23.0 mg of compound **127**. Yield 100%; yellow solid; mp 156°C. ^{1}H NMR (400 MHz, DMSO-d_6) δ 9.50 (s, 2H), 7.54 (s, 1H), 7.19 (s, 1H), 3.85 – 3.75 (m, 4H), 3.16 (s, 4H). HRMS (ESI-TOF) m/z: $C_8H_{13}N_5$ experimental 180.1244 [M+H]$^+$, theoretical 180.1244 [M+H]$^+$, Δ = 0.0000.

4.4.4.   3-amino-6-substituted 2-aminopyrazine derivatives (**128-130**, **136**)

4.4.4.4.   6-(4-fluorophenyl)-3-substituted pyrazin-2-amine (**128-130**)
Precursors **107** and **109** were obtained according to the synthetic procedures described in the **paragraph 4.4. 2..**

General procedures to obtain 6-(4-fluorophenyl)-3-substituted pyrazin-2-amine: 1.0 eq of 3-bromo-6-(4-fluorophenyl)pyrazin-2-amine (**109**) was allowed to react in a microwave tube with desired amine (3.0 eq) in 6.0 mL of butanol. The reaction was stirred for 2 h at 130°C. Once completed, the solvent was removed under reduced pressure and the crude was purified with flash chromatography (light petroleum 70%– EtOAc 30%) affording compounds **128-130**.

4. Synthesis and characterization of tri- and tetra-substituted pyrazines: new scaffold-based strategy

4.4.4.4.1. 6-(4-fluorophenyl)-3-morpholinopyrazin-2-amine (**128**)

Yellow solid; yield 78% (198 mg); mp 160°C. ^{1}H NMR (400 MHz, DMSO-d$_6$) δ 8.05 (s, 1H), 8.01 – 7.94 (m, 2H), 7.31 – 7.21 (m, 2H), 6.16 (s, 2H), 3.81 – 3.74 (m, 4H), 3.10 – 3.04 (m, 4H). ES-MS (methanol) m/z 275.3 [M+H]$^+$, theoretical 274.12. HRMS (ESI-TOF) m/z: C$_{14}$H$_{15}$FN$_4$O experimental 275.1302 [M+H]$^+$, theoretical 275.1303 [M+H]$^+$, Δ = 0.0001. Purity HPLC: 92.0%.

4.4.4.4.2. 6-(4-fluorophenyl)-3-(4-methylpiperazin-1-yl)pyrazin-2-amine (**129**)

White solid; yield 49% (131 mg); mp 133°C. ^{1}H NMR (400 MHz, DMSO-d$_6$) δ 8.04 (s, 1H), 8.01 – 7.92 (m, 2H), 7.31 – 7.20 (m, 2H), 6.02 (s, 2H), 3.35 (s, 4H), 3.10 (s, 4H), 2.23 (s, 3H). ES-MS (methanol) m/z 288.1 [M+H]$^+$. HRMS (ESI-TOF) m/z: C$_{14}$H$_{16}$FN$_5$ experimental 288.1618 [M+H]$^+$, theoretical 288.1619 [M+H]$^+$, Δ = 0.0001.

4.4.4.4.3. 3-(4-benzylpiperazin-1-yl)-6-(4-fluorophenyl)pyrazin-2-amine (**130**)

Yellow solid; yield 8% (26.7 mg); mp 147°C. ^{1}H NMR (400 MHz, DMSO-d$_6$) δ 8.14 (s, 1H), 7.85 – 7.79 (m, 2H), 7.32 – 7.14 (m, 7H), 6.65 (s, 2H), 3.64 (s, 2H), 3.57 (m, 4H), 2.89 -2.81 (m, 4H). ES-MS (methanol) m/z 364.1 [M+H]$^+$. HRMS (ESI-TOF) m/z: C$_{21}$H$_{22}$FN$_5$ experimental 364.1930 [M+H]$^+$, theoretical 364.1932 [M+H]$^+$, Δ = 0.0002.

4.4.4.5. General procedures for the synthesis of 5,6-bis(4-fluorophenyl)-3-(piperazin-1-yl)pyrazin-2-amine hydrochloride (**136**)

3,5-dibromo-6-chloropyrazin-2-amine (**131**): 2.00 g (1.0 eq, 15.0 mmol) of 6-chloropyrazin-2-amine commercially available (**106**) was solved in 120 mL of dry DCM under argon atmosphere. Once achieved the temperature of 0°C, 5.52 g (2.0 eq, 30.0 mmol) of NBS were added portionwise and the mixture was allowed to react at room temperature for 1 h. The mixture was washed with water (40.0 mL), saturated solution of NaHCO$_3$ and brine and dried over Na$_2$SO$_4$. The solvent was removed under reduced pressure and the crude product was purified with flash chromatography (light petroleum 85%– EtOAc 15%) to obtain 3.29 g of yellow solid; yield 77%; mp 165°C. ^{1}H NMR (400 MHz, DMSO-d$_6$) δ 7.38 (s, 2H). 5-bromo-6-chloropyrazin-2-amine (**133**) and 3-bromo-6-chloropyrazin-2-amine (**132**) are obtained with 4 and 3% of yields, respectively.

4.4.4.5.1. *Tert*-butyl 4-(3-amino-6-bromo-5-chloropyrazin-2-yl)piperazine-1-carboxylate (**134**)

500 mg (0.87 mmol, 1.0 eq) of 3,5-dibromo-6-chloropyrazin-2-amine (**131**) were solved in 5.0 mL of butanol in a sealed tube. 648 mg (1.74 mmol, 2-0 eq) of *tert*-butyl piperazine-1-carboxylate were added and the system was stirred at 130°C overnight. Once completed, the solvent was removed under reduced pressure and the crude was purified with flash chromatography (light petroleum 85% – EtOAc 15%) affording 271 mg of compound **131**. White solid, yield 40%, mp: 172°C. ^{1}H NMR (400 MHz, DMSO-d$_6$) δ 6.75 (s, 2H), 3.53 – 3.44 (m, 4H), 3.03 - 2.92 (m, 4H), 1.41 (s, 9H). ES-MS (methanol) C$_{13}$H$_{19}$BrClN$_5$O$_2$ m/z 393.2 [M+H]$^+$.

4.4.4.5.2. *Tert*-butyl 4-(3-amino-5,6-bis(4-fluorophenyl)pyrazin-2-yl)piperazine-1-carboxylate (**135**)

250 mg (0.64 mmol, 1.0 eq) of *tert*-butyl 4-(3-amino-6-bromo-5-chloropyrazin-2-yl)piperazine-1-carboxylate (**134**) and 188 mg (1.34 mmol, 2.1 eq) of (4-fluorophenyl)boronic acid were solved in 1.3 mL of 1,4-dioxane, 1.3 mL of ethanol and 2.0 mL of water in a microwave tube. 136 mg (1.28 mmol, 2.0 eq) of Na$_2$CO$_3$ and 22.5 mg (0.03 mmol, 0.05 eq) of PdCl$_2$(PPh$_3$)$_2$ were added. The reaction was stirred at 130°C on microwave for 3h. Once completed, the catalyst was removed under celite plug and the mixture was extracted with DCM (3 x 10 mL) and water (30 mL) and dried over anhydrous Na$_2$SO$_4$. The crude was purified with flash chromatography (light petroleum 60% – EtOAc 40%) to afford 152 mg of compound **135**. White solid; yield 51%; mp 187°C. ^{1}H NMR (400 MHz, DMSO-d$_6$) δ 7.34 – 7.25 (m, 4H), 7.13 - 7.0 (m, 4H), 6.28 (s, 2H), 3.57 – 3.52 (m, 4H), 3.12 – 3.08 (m, 4H), 1.42 (s, 9H). MicrOTOF-Q (methanol) m/z 468.19 [M+H]$^+$, 390.18 [M+Na]$^+$. HRMS (ESI-TOF) m/z: C$_{22}$H$_{27}$F$_2$N$_5$O$_2$ experimental 490.2024 [M+Na]$^+$, theoretical 490.2025 [M+Na]$^+$, Δ = 0.0001.

4.4.4.5.3.   5,6-bis(4-fluorophenyl)-3-(piperazin-1-yl)pyrazin-2-amine hydrochloride (**136**)

147.5 mg (0.32 mmol, 1.0 eq) of *tert*-butyl 4-(3-amino-5,6-bis(4-fluorophenyl)pyrazin-2-yl)piperazine-1-carboxylate (**135**) have been stirred at room temperature overnight adding 7.0 mL of HCl in diethyl ether 1M. Once completed, the solvent has been removed under reduced pressure and the product has been precipitated with EtOAc to obtain 119 mg of compound **136**. White solid, yield 95%, mp 213°C. ^{1}H NMR (400 MHz, DMSO-d$_6$) δ 9.26 (s, 2H), 7.43 - 7.20 (m, 4H), 7.20 – 7.02 (m, 4H), 6.50 (s, 2H), 3.45-3.20 (m,, 8H). ^{13}C NMR (101MHz, DMSO-d$_6$) δ 158.55 (d, $^4J_{C-H}$ = 2.4 Hz), 146.21, 135.11, 131.51 (d, $^3J_{C-H}$ =7.9 Hz, CH), 131.12 (d, $^2J_{C-H}$ =8.2 Hz, CH), 115.13 (s, CH), 114.96 (d, $^3J_{C-H}$ = 6.8 Hz, CH), 109.58, 44.56 (s, CH$_2$), 42.39 (s, CH$_2$). ESI-MS (MeOH): [M+H]$^+$ m/z 368.2. HRMS (ESI-TOF) m/z: C$_{20}$H$_{19}$F$_2$N$_5$ experimental 368.1683 [M+H]$^+$, theoretical 368.1681 [M+H]$^+$, Δ = 0.0002. Purity HPLC: 97.7%.

4.4.5.   6-(4-fluorophenyl)-5-substituted pyrazin-2-amine (**137-141**)

Precursors **107** and **108** have been obtained according to the synthetic procedures described in the **paragraph 4.4.2.**.

4.4.5.4.   General procedures to obtain 6-(4-fluorophenyl)-5-substituted pyrazin-2-amine (**137-140**)

Method A: 100 mg (0.37 mmol, 1.0 eq) of 5-bromo-6-(4-fluorophenyl)pyrazin-2-amine (**108**) and 62.12 mg (0.44 mmol, 1.73 eq) of (4-fluorophenyl)boronic acid were solved in 3.0 mL of toluene, 0.5 mL of ethanol and 1.0 mL of 2M solution of Na$_2$CO$_3$. 16.62 mg (0.01 mmol, 0.054 eq) of Pd(PPh$_3$)$_4$ were added to the mixture that was then refluxed for 4h under argon atmosphere. Once completed, the catalyst was removed through a celite plug and the mixture was extracted using water (30.0 mL) and DCM (3 x 10.0 mL) and the organic layers were dried over Na$_2$SO$_4$. The crude was purified with flash chromatography (light petroleum 70% – EtOAc 30%) affording 62.5 mg of compound **137**.

Method B: 200 mg (0.75 mmol, 1.0 eq) of 5-bromo-6-(4-fluorophenyl)pyrazin-2-amine (**108**) and 103 mg (0.82 mmol, 1.1 eq) of pyridin-4-ylboronic acid were solved in a microwave tube in 1.5 mL of 1,4-dioxane, 2.3 mL of water and 1.5 mL of ethanol. To the reaction, 26.0 mg (0.038 mmol, 0.05 eq) of PdCl$_2$(PPh$_3$)$_2$ and 158 mg (1.5 mmol, 2.0 eq) of Na$_2$CO$_3$ were added. The reaction was stirred at 130°C on microwave for 3h. Once completed, the catalyst was removed through a celite plug and the solvent was eliminated under *vacuum*. The crude was purified with flash chromatography (light petroleum 60%– EtOAc 40%) affording compound **138**.

Method C: a) 669 μL (5.3 mmol, 1.0 eq) of 1-bromo-4-methoxybenzene was solved in 15.0 mL of 1,4-dioxane under argon atmosphere. To the mixture, 1.61 g (6.36 mmol, 1.2 eq) of 4,4,4',4',5,5,5',5'-octamethyl-2,2'-bi(1,3,2-dioxaborolane), 2.2 g (15.9 mmol, 3.0 eq) of K$_2$CO$_3$ and 306 mg (0.265 mmol, 0.2 eq) of Pd(PPh$_3$)$_4$ were added. The reaction was refluxed overnight. Once completed, the catalyst was eliminated through a celite plug and the solvent was removed under reduced pressure to obtain 1.04 g of 2-(4-methoxyphenyl)-4,4,5,5-tetramethyl-1,3,2-dioxaborolane, transparent liquid, yield 87%.

b) 120 mg (0.7 mmol, 1.0 eq) of 5-bromo-6-(4-fluorophenyl)pyrazin-2-amine (**108**) was solved in 1.5 mL of 1,4-dioxane, 1.5 mL of ethanol and 2.4 mL of water under argon atmosphere in a microwave tube. To the mixture 164 mg (0.7 mmol, 1.0 eq) of 2-(4-methoxyphenyl)-4,4,5,5-tetramethyl-1,3,2-dioxaborolane, 148.4 mg (1.4 mmol, 2.0 eq) of Na$_2$CO$_3$ and 25.0 mg (0.04 mmol, 0.05 eq) of PdCl$_2$(PPh$_3$)$_2$ were inserted. The reaction was stirred at 130°C on microwave for 30 min. Once completed, the solvent was removed through a celite plug and the mixture was extracted with water (30.0 mL) and EtOAc (3 x 10.0 mL). After removing the solvent under reduced pressure, the crude was purified with flash chromatography (light petroleum 60%– EtOAc 40%) to afford 82.9 mg of compound **139** and 14.7 mg of demethoxylated derivative **140**.

4.4.5.4.1. 5,6-bis(4-fluorophenyl)pyrazin-2-amine (**137**)

Method A. Pale yellow solid, yield 60% (62.5 mg); mp 269°C. ^{1}H NMR (400 MHz, DMSOd_6) δ 7.94 (s, 1H), 7.33 (dd, $^3J_{\text{H-F}}$ = 8.5, $^4J_{\text{H-F}}$ = 5.7 Hz, 2H), 7.26 (dd, $^3J_{\text{H-F}}$ = 8.5, $^4J_{\text{H-F}}$ = 5.7 Hz, 2H), 7.23 – 6.95 (m, 4H), 6.64 (bs, 2H). ^{13}C NMR (101 MHz, DMSOd_6) δ 162.75 (d, $^1J_{\text{C-F}}$ = 64.7 Hz), 160.31 (d, $^1J_{\text{C-F}}$ = 63.5 Hz), 153.95, 147.75, 138.04, 135.70 (d, $^4J_{\text{C-F}}$ = 3.2 Hz), 135.56 (d, $^4J_{\text{C-F}}$ = 3.2 Hz), 131.52 (d, $^3J_{\text{C-F}}$ = 8.4 Hz, CH), 131.07 (d, $^3J_{\text{C-F}}$ = 8.4 Hz, CH), 130.18 (s, CH), 114.96 (d, $^2J_{\text{C-F}}$ = 11.9 Hz, CH), 114.75 (d, $^2J_{\text{C-F}}$ = 11.8 Hz, CH). ESI-MS (MeOH): [M+H]$^+$ m/z 284.1. HRMS (ESI-TOF) m/z: $C_{16}H_{11}F_2N_3$ experimental 284.0996 [M+H]$^+$, theoretical 284.0994 [M+H]$^+$, Δ = 0.0002.

4.4.5.4.2. 6-(4-fluorophenyl)-5-(pyridin-4-yl)pyrazin-2-amine (**138**)

Method B. White solid; yield 64% (127 mg); mp 201°C. ^{1}H NMR (400 MHz, DMSO-d$_6$) δ 8.45 – 8.39 (m, 2H), 7.99 (s, 1H), 7.43 – 7.32 (m, 2H), 7.23 – 7.12 (m, 4H), 6.88 (s, 2H). ^{13}C NMR (101 MHz, DMSO-d$_6$) δ 162.85 (d, $^4J_{\text{C-F}}$ = 2.3 Hz), 155.59 (s), 148.15 (s), 133.55 (d, $^4J_{\text{C-F}}$ = 3.2 Hz), 131.99 (s), 131.38 (s), 129.01 (d, $^3J_{\text{C-F}}$ = 8.5 Hz), 128.50 (s), 116.05 (d, $^2J_{\text{C-F}}$ = 21.5 Hz), 109.99 (s). ESI-MS (MeOH): [M+H]$^+$ m/z 267.4. HRMS (ESI-TOF) m/z: $C_{15}H_{11}FN_4$ experimental 267.1041 [M+H]$^+$, theoretical 267.1041 [M+H]$^+$, Δ = 0.0000. Purity HPLC: 100%.

4.4.5.4.3. 6-(4-fluorophenyl)-5-(4-methoxyphenyl)pyrazin-2-amine (**139**)

Method C. Yellow solid; yield 40% (82.9 mg); mp 153°C. ESI-MS (MeOH): [M+H]$^+$ m/z 296.0. HRMS (ESI-TOF) m/z: $C_{17}H_{14}FN_3O$ experimental 296.1193 [M+H]$^+$, theoretical 296.1194 [M+H]$^+$, Δ = 0.0001. Purity HPLC: 91.7%.

4.4.5.4.4. 6-(4-fluorophenyl)-5-phenylpyrazin-2-amine (**140**)

Method C. Yellow solid, yield 8% (14.7 mg), mp 163°C. ^{1}H NMR (400 MHz, DMSO-d$_6$) δ 7.94 (s, 1H), 7.37 – 7.28 (m, 2H), 7.28 – 7.18 (m, 5H), 7.16 – 7.06 (m, 2H), 6.62 (s, 2H). ESI-MS (MeOH): [M+H]$^+$ m/z 266.3. HRMS (ESI-TOF) m/z: $C_{16}H_{12}FN_3$ experimental 266.1086 [M+H]$^+$, theoretical 266.1088 [M+H]$^+$, Δ = 0.0002. Purity HPLC: 94.6%.

4.4.5.2. General procedures to obtain 4-(5-amino-3-(4-fluorophenyl)pyrazin-2-yl)phenol (**141**)

73.0 mg (0.25 mmol, 1.0 eq) of compound **139** were solved under argon atmosphere in 1.5 mL of anhydrous DCM. The solution was cooled to -40°C. Once achieved, 250 μL (2.25 mmol, 9.0 eq) of BBr$_3$ were slowly added. The reaction was stirred overnight at room temperature. Once completed, it was quenched with 15 mL of cold MeOH and the solvent was removed under reduced pressure. The crude residue was purified with flash chromatography (light petroleum 70% - EtOAc 30%) to obtain 20 mg of white solid. Yield 28%; mp 172°C. ESI-MS (MeOH): [M+H]$^+$ m/z 282.3. HRMS (ESI-TOF) m/z: $C_{16}H_{13}FN_3O$ experimental 282.1049 [M+H]$^+$, theoretical 282.1037 [M+H]$^+$, Δ = 0.0012.

4.4.6. Computational procedures

4.4.6.1. LiPE plot procedures

Smiles of compounds' structures as well as Clog P (calculated by ChemDraw Professional), pIC$_{50}$ (M) and LiPE values obtained according to the formula reported in the **chapter 3.** were inserted in a Database converted into ".txt" format. The file was loaded in Osiris DataWarrior Software 3.5.0. to achieve a 3D representation. pIC50s were used in y axis, Clog P in x axis and LiPE value in z ones.

4.4.6. Biochemistry

4.4.6.4. CK1δ assays

Assays with truncated (1-294 aa) CK1δ. Compounds were tested on commercially available CK1δ (Merck Millipore, recombinant human, amino acids 1e294, GST-tagged N-terminal) with KinaseGlo® luminescence kit (Promega). Experiments were performed in 96-well plate (white, flat bottom) using buffer prepared as follow: 50 mM HEPES (pH 7.5), 1 mM EDTA, 1 mM EGTA and 15 mM magnesium acetate. Compound PF-

670462 (IC$_{50}$ CK1δ 0.014 μM) was used as a positive control at the concentration of 40 μM while a solution of DMSO/buffer as negative control. Firstly, 10 μL of inhibitor solution was inserted in the well (10 mM stock solution in DMSO was diluted with buffer) followed by 10 μL of enzyme (16 ng of CK1δ) and 20 μL of casein substrate 0.1% and 2 μM ATP (final concentration) (to perform ATP-competition increasing concentrations were chosen: 1, 2, 10, 50 μM). The final DMSO concentration in the mixture did not exceed 1-2%. After 60 minutes of incubation at 30°C, the enzymatic reaction was stopped with 40 μL of KinaseGlo reagent (Promega). Luminescence signal (RLU) was recorded after 10 minutes at 25°C using Tecan Infinite M100. The inhibitory activities were calculated in relation to the maximal activity (absence of inhibitor). As preliminary screening, each compound was assayed at the concentration of 40 μM, consequently, for derivative that reported an activity percentage less than 50% at the concentration, IC$_{50}$s were performed in triplicate and reported as mean ± standard error. Results were elaborated with Excel and GraphPad Prism 8.0.

ATP-competition assays were performed following the just described procedure by firstly performed the ATP calibration line to obtain the slope. The two chosen inhibitor's concentrations agree with the IC$_{50}$ of the compound (the concentration at its IC$_{50}$ and the double) and the experiment was conducted at the presence of increasing ATP concentrations: 1, 2, 10, 50 μM. The mean of the RLU value was divided for the slope of the calibration line and the mean of negative controls were subtracted by the ATP consumed; the reciprocal characterizes the x axis of the Lineweaver-Burk plot. The ATP consumed divided for volume of reaction (40 μL) provides the y value. Results were elaborated using Excel and GraphPad Prism 8.0.

4.4.6.5. GSK3β assays

GSK3β of most promising compounds was developed during the Erasmus program in the research group of Prof. Ana Martinez (CSIC-Madrid-ES). Compounds were tested on commercially available full-length GSK3β (Thermo-Scientific) with KinaseGlo® luminescence kit (Promega). Experiments were performed in 96-well plate (white, flat bottom) using buffer prepared as follow: 40 mM Tris pH 7.5, 20 mM magnesium chloride, 0.1% mg/mL BSA and 50 μM DTT. As a positive control, the reaction mixture without enzyme was used while the solution with enzyme, ATP and substrate as negative control. Firstly, 10 μL of inhibitor solution was inserted in the well (10 mM stock solution in DMSO has been diluted with buffer) followed by 10 μL of GS-2 as substrate (0.2 μg/μL), 10 μL of ATP (starting from a stock solution at 8 mM, it was diluted with buffer to achieve an initial concentration of 4 μM) and 10 μL of enzyme (1 ng/μL). The final DMSO concentration in the mixture did not exceed 1-2%. After 60 minutes of incubation at 25°C, the enzymatic reaction was stopped with 40 μL of KinaseGlo reagent (Promega). Luminescence signal (RLU) was recorded after 10 minutes at 25°C using Tecan Promega. The inhibitory activities were calculated in relation to the maximal activity (absence of inhibitor). As preliminary screening, each compound was assayed at the concentration of 10 μM, consequently, for derivative that reported an activity percentage less than 50% at the concentration, IC$_{50}$s were performed in triplicate and reported as mean ± standard error. Results were elaborated with Excel and GraphPad Prism 8.0.

4.4.6.6. CNS permeation prediction: BBB-PAMPA

CNS prediction of most promising derivatives was evaluated using Parallel Artificial Membrane Permeability Assay (PAMPA). Ten commercial drugs with known permeability were included in the experiment to obtain cut-off values (2-6 mg of Caffeine, Enoxacine, Hydrocortisone, Desipramine, Ofloxacine, Piroxicam, Testosterone and 12-15 mg of Promazine, Verapamil and 23 mg of Atenolol dissolved in 1000 μL of ethanol, then diluted with buffer when it is required). Compounds were dissolved in a 70/30 PBS pH 7.4 buffer/ethanol solution in the appropriate concentration determining absorbance values in the UV-VIS light spectrum. 5 mL of solutions were filtered with PVDF memnrane filters (diameter 30 mm, pore size 0.45 mm). The acceptor 96-well plate (MultiScreen 96-well Culture Tray clear, Merck Millipore) was filled with 180 μL of buffer (70/30). In the donor 96-well plate ((Multiscreen® IP Sterile Plate PDVF membrane, pore size is 0.45 mM, Merck Millipore) 4 μL/well of porcine lipid brain (Merck Millipore) in dodecane (20 mg/ml) were added and,

after 5 minutes, 180 μL of inhibitor solutions were inserted. Once completed, the donor plate was carefully located on the acceptor one to make a "sandwich" and, after 2.5h of incubation at 25°C, the dolor plate was removed. The absorbance values at dedicated wavelengths were red using Tecan Infinite M1000. Experiment was conducted in duplicate. The permeability coefficient (Pe) of each compound was established in centimeter per second.

$$Pe = \frac{Vd \cdot Vr}{(Vd + Vr) \cdot S \cdot t} \cdot \frac{100 \cdot Vd}{100 \cdot Vd - \%T(Vd + Vr)}$$

$$\%T = \frac{Vr \cdot Ar}{Ad \cdot Vd} \cdot 100$$

Where Vd and Vr are volumes of donor and acceptor solution (0.18 cm^3), S is the membrane area (0.266 cm^2), time of incubation (2.5 h = 9000 s), Ar is the absorbance of the receptor plate after the experiment and Ad0 is the absorbance in the donor compartment before incubation. Results are given as the mean and the average of the two runs ± standard deviation (SD) is reported. Obtained results for quality control drugs were then correlated to permeability data found in the literature. The linear correlation between experimental and literature permeability values was used for the classification of compounds in those able to cross the BBB by passive permeation (CNS+ which correlate with a bibliographic Pe > 4) and those not (CNS- which correlate with a bibliographic Pe < 2). Compounds correlating with reported Pe values from 2 to 4·10^{-6} cm s^{-1} are classified as CNS+/-.

4.4.6.7.   Thermal Shift Assay (TSA)

Thermal Shift Assays for the best compound was performed by Elelonora Cescon in the group of Prof. Paola Storici (BioLab-Elettra Sincrotrone-Trieste). All TSA experiments were conducted in triplicates. Recombinant CK1d 1-294, representing the catalytic core domain of the protein, was produced at Elettra Protein Facility in Elettra Synchrotron. Optimal concentration of protein and dye were tested from preliminary TSA in order to establish the most advantageous set up. Samples were prepared in white 96-multiwell plate (Biorad®) with a final volume of 20 mL into each well. A 5x stock of buffer and a 5x stock of protein solution were prepared hence 4 mL of both were added into the wells. Tested inhibitors were dissolved in 100% DMSO and a 40x stock of each concentration tested was prepared to keep a final concentration of DMSO at 2.5% in each condition tested. Thermal shift assay was performed in assay buffer containing 20 mM Tris pH 7.5, 180 mM NaCl and 0.5 mM TCEP as final concentrations, while protein was kept at 3 mM in all conditions of the analysis. Compounds were tested at final concentrations of 1.5, 3, 9, 15, 30 and 45 mM (0.5x, 1x, 3x, 5x, 10x, 15x). Once added buffer, protein and compounds stocks plus a proper volume of water to reach 20 mL, the multi-well plate was centrifugated at 100 xg, 4°C for 1 min to spin down and stir the components. Protein and inhibitors were then incubated at room temperature for 30 min. After incubation, SyproOrange dye (Protein Thermal shift dye, Thermo Fisher Scientific®) was added into each well to a final concentration of 0.5x from 1000x stock in 100% DMSO. The multiwell plate was centrifuged again and measurement was started. Measures were performed in a real-time PCR machine (CFX96, Biorad®), registering emission of the dye at 560-580 nm every 30 sec, with a temperature gradient of 2°C/min. Each analysis was executed in comparison to a negative control represented by the only buffer or the compounds with SyproOrange, and a positive control consisted of the protein or protein with 2.5% of DMSO plus the fluorophore.

4.4.7.   *In vivo* experiments on neuroblastoma cell lines (SH-SY5Y)

Biological investigation of most promising derivatives was conducted during the Erasmus program in the group of Prof. Ana Martinez (CSIC-Madrid-ES).

4.4.7.4.   MTT assays

The human neuroblastoma SH-SY5Y cell line was propagated in Dulbecco's Modified Eagle Medium (DMEM) containing L-glutamine (2mM), 1% non-essential amino acids, 1% penicillin/streptomycin and 10%

fetal bovine serum (FBS) under humidified 5% CO_2. Once semiconfluence was achieved, cells were countered using TC10™ Automated Cell Counter Bio-Rad Laboratories (CSIC-Madrid) and 80000 cells/well were plated in 96-well plate. After 24h of incubation, compounds were inserted at the concentrations of 5 and 10 μM (the stock solution in DMSO was diluted with DMEM to obtain the right final concentration) and, after another 24h of incubation, DMEM was removed and MTT reactive (3-[4,5- Dimethylthiazol-2-yl]-2,5- Diphenyltetrazolium Bromide) was added at the concentration of 20 mg/mL. After 2h, absorbance was recorded, and cell survival was estimated as percentage of value of untreated control (mean of six wells). Three independent experiments were carried out.

4.4.7.5. Neuroprotection assays

The human neuroblastoma SH-SY5Y cell line was propagated in Dulbecco's Modified Eagle Medium (DMEM) containing L-glutamine (2mM), 1% non-essential amino acids, 1% penicillin/streptomycin and 10% fetal bovine serum (FBS) under humidified 5% CO_2. Once semiconfluence was achieved, cells were countered using TC10™ Automated Cell Counter Bio-Rad Laboratories (CSIC-Madrid) and 60000 cells/well were plated in 96-well plate. After 24h of incubation, compounds were inserted at the concentrations of 5 and 10 μM (the stock solution in DMSO was diluted with DMEM to obtain the right final concentration) and, after 1h ethacrynic acid (45 μM starting from stock solution of 100 mM diluted in DMEM) was added. As negative control, a solution of DMSO 1% in DMEM was used while as positive control ethacrynic acid without compound. After 24h of incubation, DMEM was removed and MTT reactive (3-[4,5- Dimethylthiazol-2-yl]-2,5-Diphenyltetrazolium Bromide) was added at the concentration of 20 mg/mL. After 2h, absorbance was recorded, and cell survival was estimated as the mean of relative absorbance of six wells/compound. Three independent experiments were conducted, and statistical analysis of data was conducted using GraphPad Prism 8.0 one-way ANOVA for each plate and T-TEST to compare the three experiments.

4.4.7.6. Immunoblotting analysis

In a 6-well plate, 2000000 of cells were plated per well and, after 24h of incubation, compounds were inserted at the chosen concentration (starting from stock solution in DMSO diluted with DMEM). Ethacrynic acid was added at the concentration of 45 μM after 1h of incubation. To prepare the cell extraction, cells were harvested and washed with PBS and then they were lysed in ice-cold lysis buffer. The number of proteins in the extract was detected by the Pierce BCA Protein Assay kit (Thermo Scientific). 20-50 μg of protein of protein were fractionated on SDS poly-acrylamide gel and transferred to poly-vinylidene fluoride (PVDF) membranes (Millipore, Billerica, MA, USA). Membranes were blocked with 5% bovine serum albumin (BSA) (Sigma) for 1h and then they were incubated overnight at 4°C with primary antibodies (pTDP-43 mouse, BioRad) diluting 3μL in 3 mL of BCA. Signal from the primary antibody was amplified using species-specific secondary antibody (pTDP-43 anti-mouse, BioRad) to obtain the "sandwich" detected with a chemiluminescent substrate detection system ECL. Protein band densities were quantified using ChemiDoc station with Quantity One 1D analysis software (Bio-Rad Laboratories, Madrid, Spain).

5.   1,3,5-triazines as CK1δ inhibitors: a simplification strategy

5.4.   Introduction

As reported in the previous chapters, development of CK1δ inhibitors results interesting since this target is involved in several pathological processes. The research group in which I have carried out the PhD project has published a series of [1,2,4]triazolo[1,5-*c*]pyrimidine (TP) and [1,2,4]triazolo[1,5-*a*]triazine (TT) derivatives whose main backbone can be considered as "adenine-like" (**Fig. 95**) and outlining a structure-activity relationship profile . [209]

TP scaffold
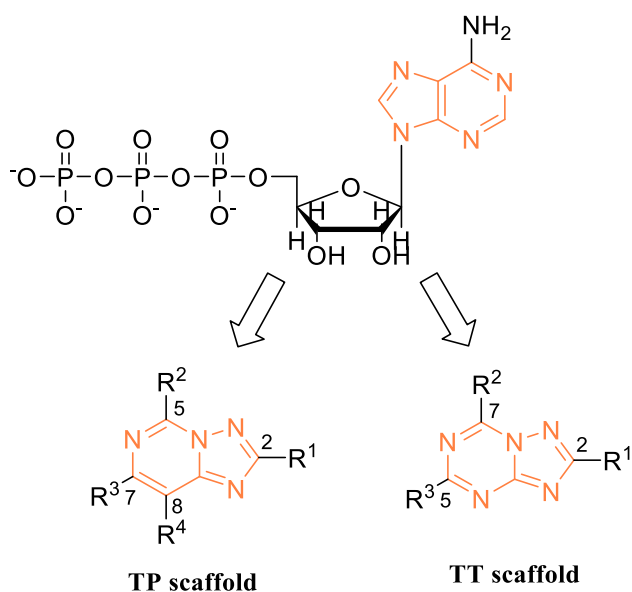
TT scaffold

Figure 95: representation of [1,2,4]triazolo[1,5-c]pyrimidine (TP) and [1,2,4]triazolo[1,5-a]triazine (TT) scaffolds.

Several compounds have displayed promising activities on CK1δ and several information about the SAR have been collected; the introduction of phenyl moieties functionalized with hydroxy groups at the 2-position of TT systems has led to the achievement of the best derivative showed in **Fig. 96 (35)**. Compound **35** has reported an IC_{50} of 0.18 μM [209] allowing a deeper characterization from biochemical and biological point of view that is discussed in the appendix.

35

IC_{50} CK1δ = 0.18 ± 0.04
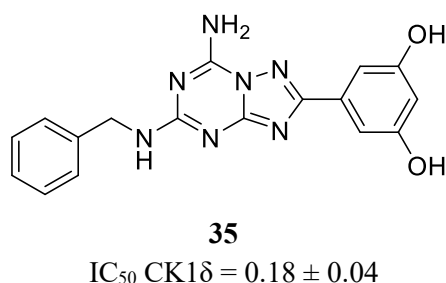
*Figure 96: compound **35** and its IC_{50} on CK1δ.*

5.5.   Aim of the work

The application of a molecular simplification approach encloses the possibility to decrease the synthetic steps for the achievement of a final product bypassing complicated intramolecular cyclization that leads to low yields. Therefore, to outline a deepen and quicker structure-activity relationship profile, a molecular simplification approach of bicyclic rings has been applied developing a series of 2,4,6-trisubstituted 1,3,5-triazines (**Fig. 97**). The 1,3,5-triazine system results challenging and versatile allowing selective step by step nucleophilic substitution by controlling the temperature performing the first reaction at 0°C, the second at room temperature and the last one at 110°C but it lends itself to other types of reactions including Suzuki-Miyaura. [210,211,212,213] Nevertheless, as a disadvantage, molecular simplification approach can determine a decrease in potency of the developed compounds.
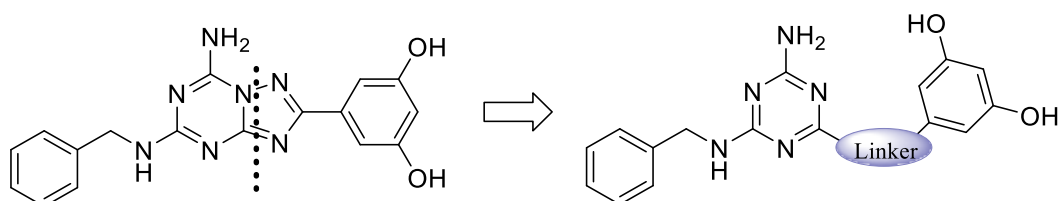
*Figure 97: molecular simplification approach starting from compound **35**.*

Phenyl moieties functionalized with methyl, methoxy and hydroxy groups have been inserted at the 2-position separated by a linker of different size and nature including hydrazide and amine spacers as well as ureido group and alkyl chains to explore the optimal distance between the main nucleus and the phenyl ring (**Fig. 98**).
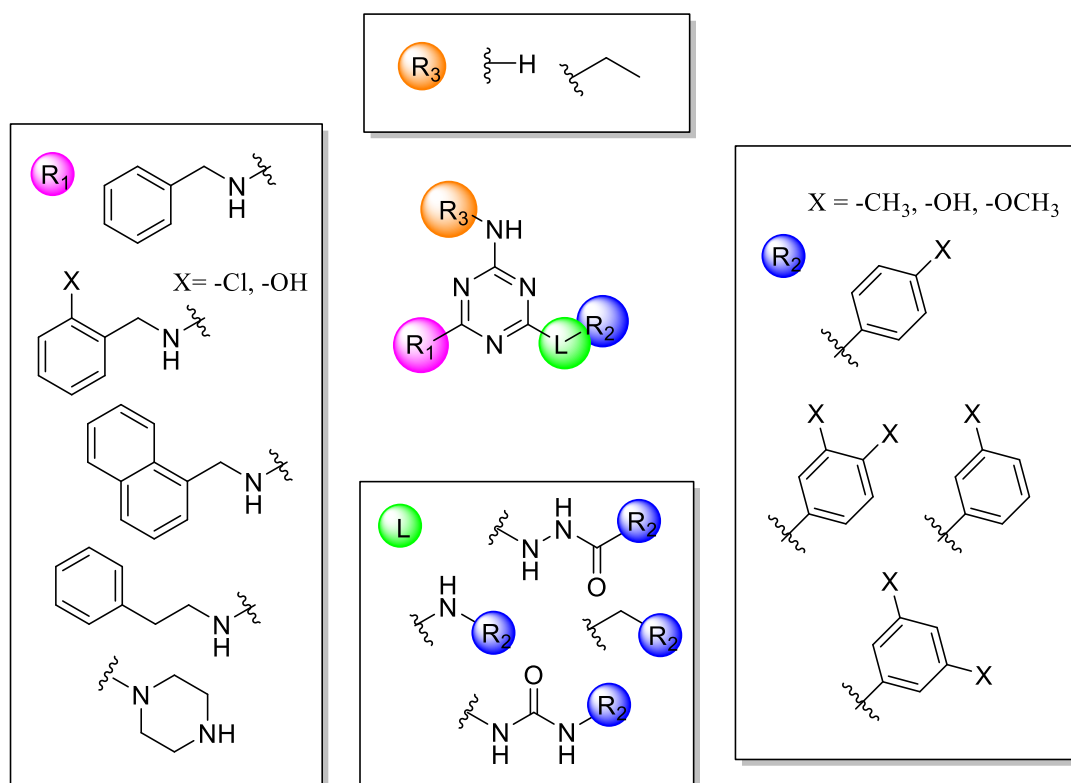
Figure 98: overview of the substituents inserted at the three positions of 1,3,5-triazine scaffold.

5. 1,3,5-triazines as CK1δ inhibitors: a simplification strategy

The amino group at the 4 position of system has resulted mandatory to achieve an activity in TT and TP bicycles [209], thus it has been maintained in 1,3,5-triazine series even if some attempts to functionalize the free amino moiety have been conducted with an ethyl chain. Different arylalkyl and bulky amines have been inserted at the 6-position and one attempt has been performed inserting piperazine to reduce the molecular flexibility of R_1 substituent (**Fig. 98**).

To develop a hit compound starting from this preliminary series, another approach has been applied: the development of a molecular hybrid by linking two fragments (**142**). Considering the N^2-benzyl-1,3,5-triazine-2,4,6-triamine moiety as a fragment, computational tools have been used to identify specific interactions with the target, hypothesizing the introduction of complementary fragments at the 4-position of 1,3,5-triazine scaffold, like the 1H-indazole molecule discovered in a previous fragment-based work conducted by our research group. [214] The fragment has reported an IC$_{50}$ on CK1δ in the high micromolar range of 24.86 μM (**Fig. 99**).

142
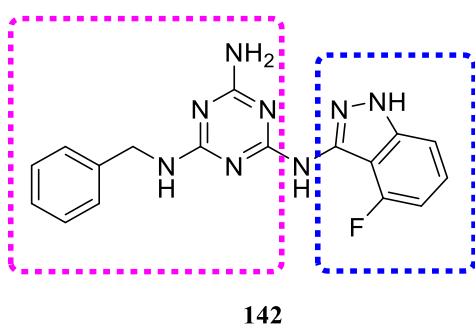
*Figure 99: structure of molecular hybrid developed by the combination of two fragments (**142**).*

5.6.   Discussion

5.6.3.   Chemistry

To develop 1,3,5-triazines with hydrazide moiety as linker connected to poli hydroxy and poli methoxyphenyl rings two synthetic pathways have been considered. [210] The pathway A involves the first nucleophilic substitution with hydrazide followed by the amination at the 4-position and the substitution of chlorine atom at the 6-position with the desired amine. Nevertheless, another synthetic strategy has been applied (pathway B) allowing to collect the 6-substituted-2-amino 1,3,5-triazine derivative performing afterward the amination at the 2-position of the ring and, as last reaction, the nucleophilic substitution to introduce the functionalized hydrazide or amino groups as well as arylalkyl systems *via* Suzuki-Miyaura. This synthetic pathway has been also used for the development of molecular hybrids: the insertion of fragment at the 2-position has been performed as the last reaction *via* nucleophilic substitution. A ureido-liker derivative has also been developed starting from 2,4-diamino-6-chloro-[1,3,5]triazines to allow the reaction with isocyanide and finally the last nucleophilic substitution to introduce the desired amine at the 6-position has been conducted.

5.6.3.4.   Synthesis of N'-(4-amino-6-substituted-1,3,5-triazin-2-yl)-polymethoxy and polyhydroxy benzohydrazide derivatives (Synthetic pathway A) (**146-149**)

Compounds **148**-**149** were obtained following the synthetic pathway reported in **Scheme 12.** The strategy, starting from commercially available cyanuric chloride **143**, has involved the formation of compound **144** *via* nucleophilic substitution with 3,5-dimethoxybenzohydrazide. The reaction has been conducted at 0°C in acetone with 3,5-dimethoxybenzohydrazide previously synthesized by esterification of 3,5-dimethoxy benzoic acid and subsequent reaction using monohydrate hydrazine.

R$_1$ = -NHBn (**146**, **147**)
       -NH(CH$_2$)$_2$Ph (**148**, **149**)
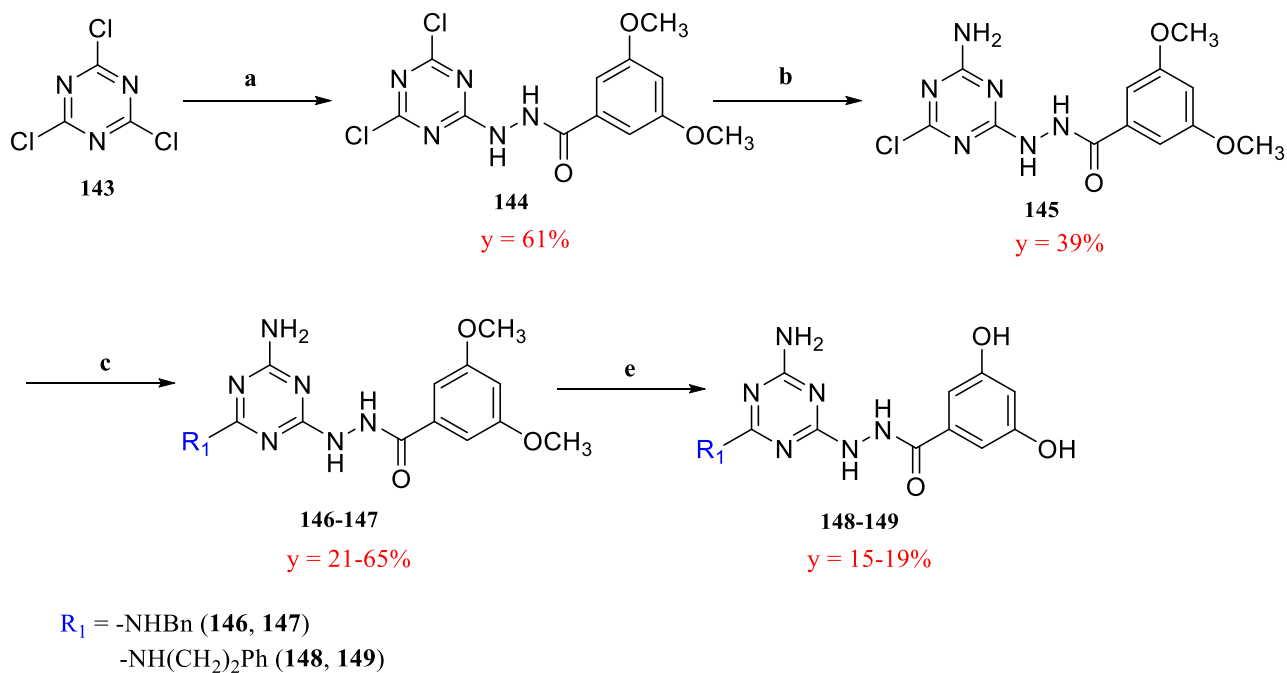
*Scheme 12: synthetic pathway (**A**) to obtain compounds **148-149**. Reagents and conditions. **a**: 3,5-dimethoxybenzo hydrazide, acetone, 0°C, 4-6h; **b**: NH$_4$OH, acetone, r.t., overnight; **c**: R$_1$, K$_2$CO$_3$, neat, 110°C, 2-6h; **d**: BBr$_3$, DCM, -40°C to r.t., overnight; y = yield.*

5. 1,3,5-triazines as CK1δ inhibitors: a simplification strategy

Compound **144** has been allowed to react in the presence of ammonium hydroxide to give derivative **145** at room temperature. The third substitution has been provided by increasing the temperature at 110°C adding the desired amine affording compounds **146-147** subjected to deprotection *via* BBr$_3$ (boron tribromide) to obtain 3,5-hydroxy derivatives **148-149**. The just discussed strategy allows to collect compound **145** to insert different amines at the position 6 of the scaffold. Nevertheless, the synthetic pathway showed in **Scheme 13 (B)** has been examined to collect 2-amino-6-substituted derivatives to perform afterward the insertion of functionalized hydrazide.

5.6.3.5. Synthesis of 2,4,6-trisubstituted 1,3,5-triazine derivatives (Synthetic pathway B) (**142**, **163**-**189**, **191**, **193**)

Starting from cyanuric chloride (**143**), the synthetic **pathway B** leads to the collection of 4-amino-6-substituted triazines to proceed with the achievement of different products. The first reaction has involved the nucleophilic substitution to insert desired amine at the 6-position affording derivatives **150-155**. Once completed, the amination using ammonium hydroxide has provided obtaining derivatives **156-162**. Following the **Scheme 13** for the development of hydrazide compounds, the third substitution has been conducted with previous synthesized hydrazides to afford polymethoxy benzohydrazide derivatives **163-174** except for compound **174** obtained by the directed nucleophilic substitution between precursor **156** and 4-hydroxybenzohydrazide. Nevertheless, given the too low yield and the difficulties during the purification, the protection of hydroxy moieties is required in this step. This reaction has been tried in three conditions considering the use of potassium carbonate as a base and the temperatu**r**e. Finally, the deprotection with BBr$_3$ onto demethoxylate derivatives **163-174** afforded compounds **175-185** (**Scheme 13, reactions a-g**). The strategy **B** has resulted more challenging than **A** to obtain final products, one example can be provided by comparing overall yields obtained for compounds **148** (strategy A) and **175** (strategy B); the reported percentages are 1.27% and 2.94%, respectively: results clear that the second strategy has proved to be the best. [210] Proceeding with the synthetic scheme, the arylalkyl derivative **186** has been developed starting from the collected precursor **159** *via* Suzuki-Miyaura to introduce a methylene spacer between the main scaffold and the substituted phenyl ring. Firstly, the boronic ester of 4-methyl benzyl moiety has been synthesized by reacting 1-(bromomethyl)-4-methylbenzene with 4,4,4',4',5,5,5',5'-octamethyl-2,2'-bi(1,3,2-dioxaborolane) at the presence of tetrakis(triphenylphosphine)palladium(0), Pd(PPh$_3$)$_4$. Then, using the same palladium catalyst, the boronic ester has been reacted in microwave with precursor **159** using Na$_2$CO$_3$ as base. (**Scheme 13, reactions a-c, h**) [211,212,213,215] Also amino derivatives have been synthesized according to the same **strategy B**: recursors **156** or **162** have been subjected to nucleophilic substitution to introduce the third substituent: the reaction has been tried in neat condition heating the mixture at 120°C leading to compounds **187-188** or in butanol achieving derivatives **142**, **189**, **191**, **193** (**Scheme 13, reactions a-d, e, i**).

R_3 = -OH (**175-177, 179, 181-183**)
-H (**178, 180, 184-185**)

R_4 = -OH (**176, 178, 180-181, 184-185**)
-H (**175, 177, 179, 182-183**)

R_5 = -OH (**182**)
-H (**175-181, 183-185**)

R_3 = -OCH$_3$ (**163-165, 167, 169-170, 172**)
-H (**166, 168, 171, 173-174**)

R_4 = -OCH$_3$ (**164, 166, 168-169, 171-173**)
-OH (**174**)
-H (**163, 165, 167, 170, 172**)

R_5 = -OCH$_3$ (**170**)
-H (**163-169, 171-174**)

175-185
y = 4-45%

163-174
y = 3-64%

R_2 = -H (**156, 158-187, 189, 191-192, 194**)
-CH$_2$CH$_3$ (**157, 188**)

142

150-155
y = 55%-q.y.

156-162   y = 26-82%

186   y = 37%

R_1 = -NHBn (**150, 156-157, 163-164, 174-176, 187-189,142, 193**)
-NH(CH$_2$)$_2$Ph (**151, 158, 165-166, 177-178**)
-NHCH$_2$Naph (**152, 159, 167-170, 179-182, 186**)
-NH(2-OCH$_3$)Ph (**153, 160, 171**)
-NH(2-Cl)Ph (**154, 161, 172-173, 183-184**)
-NH(2-OH)Ph (**185**)
-piperazine (**155, 162, 191**)

R_6 = -NHBn (**187-188**)
-piperazine (**189**)
-**190** (**142-191**)
-**192** (**193**)

190 =

192 =

142, 187-189, 191, 193
y = 3-45%

Scheme 13: synthetic pathway (B) for the development of compounds 142, 163-189, 191, 193. Reagents and conditions. a: amine, acetone, 0°C, 2-4h; b: NH$_4$OH, acetone, r.t., overnight; c: EtNH, acetone, r.t., overnight; d: hydrazide, K$_2$CO$_3$, neat, 110°C, 2h; e: hydrazide, neat, 150-170°C, 2-6h; f: hydrazide, neat, 110°C, MW, 3h; g: BBr$_3$, DCM, -40°C to r.t., overnight; h: 1-(bromomethyl)-4-methylbenzene, 4,4,4',4',5,5,5',5'-octamethyl-2,2'-bi(1,3,2-dioxaborolane), Pd(PPh$_3$)$_4$, K$_2$CO$_3$, 1,4-dioxane, rfx, 6 h/ 4,4,5,5-tetramethyl-2-(4-methylbenzyl)-1,3,2-dioxaborolane, Pd$_2$(PPh$_3$)$_2$, Na$_2$CO$_3$, 1,4-dioxane, EtOH, H$_2$O, 130°C, MW, 100W 2 h. i: amine, BuOH, 130°C, overnight. For details, see the experimental section; y = yield, q.y. = quantitative yield.

^{1}H-NMR spectra of hydrazide derivatives have provided split signals (temperature registered spectra have been reported for compound **175** in **Fig. 100** and square represent split peaks); the hypothesis of this phenomenon can be explained by the presence of different conformers. The rotation around single bonds leading to the formation of conformers appears slow; the slow exchange determines two discernible signals at 25°C in ^{1}H-NMR (**Fig. 100**, red spectrum). Increasing the temperature, at 45°C (green spectrum) it is possible to observe

that the rotation becomes faster determining broad signals that develop themselves as defined peak reaching the temperature of 65°C (blue spectrum) to achieve the coalescence temperature.
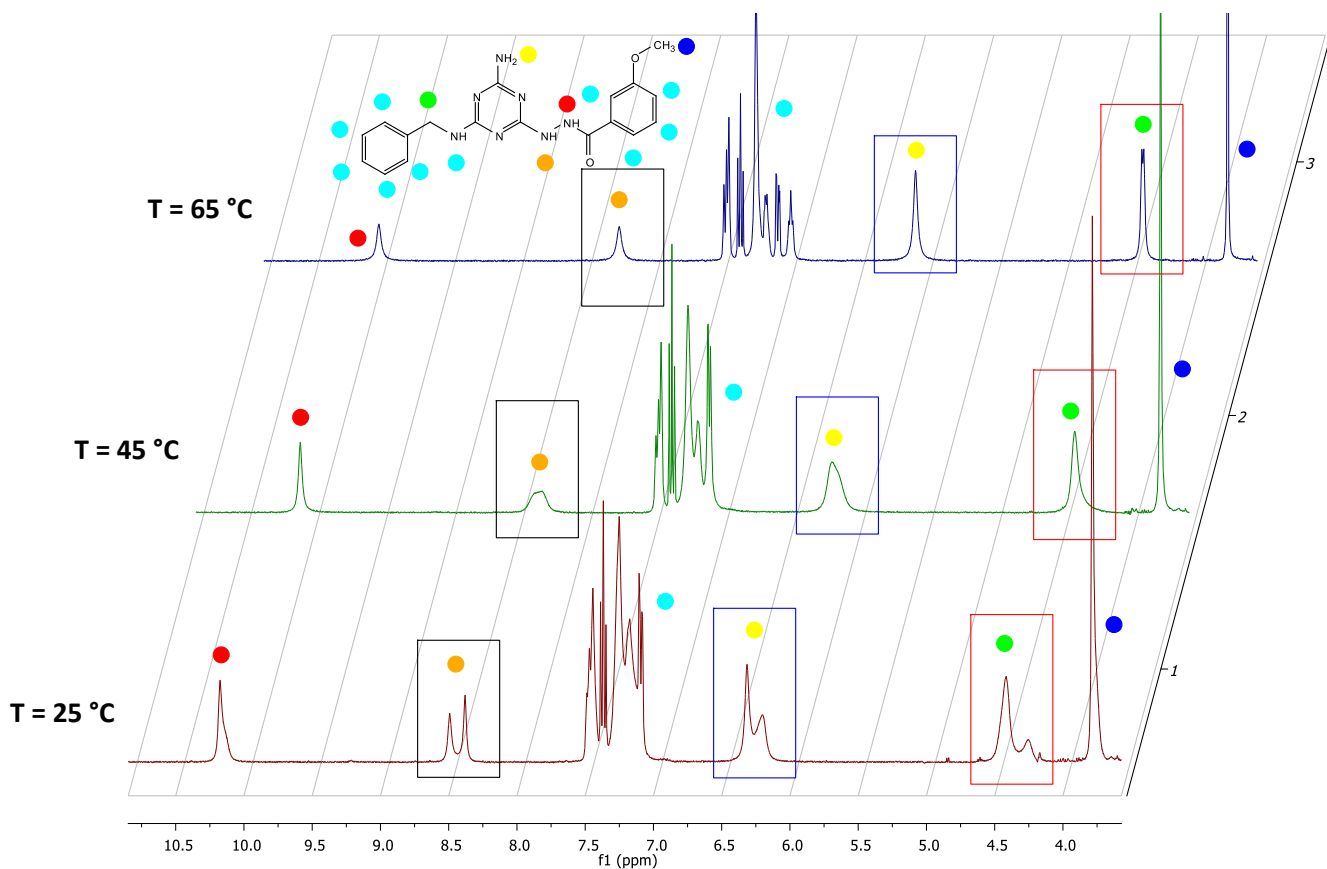
*Figure 100: registered ^{1}H-NMR (DMSO-d$_6$) spectra of compound **175** at the temperatures of 25°C, 45°C and 65°C.*

5.6.3.6.   Synthesis of 1-(4-amino-6-(benzylamino)-1,3,5-triazin-2-yl)-3-(p-tolyl)urea (**196**)

2,4-diamino-6-chloro-[1,3,5]triazine (**194**) has been synthesized using two equivalents of ammonia in acetone starting from cyanuric chloride (**143**). To develop the ureido precursor **195**, compound **194** has been allowed to react with the commercially available isocyanate in dry THF. Finally, the last reaction has involved a nucleophilic substitution with benzylamine to afford derivative **196** (**Scheme 14**). [216,217]
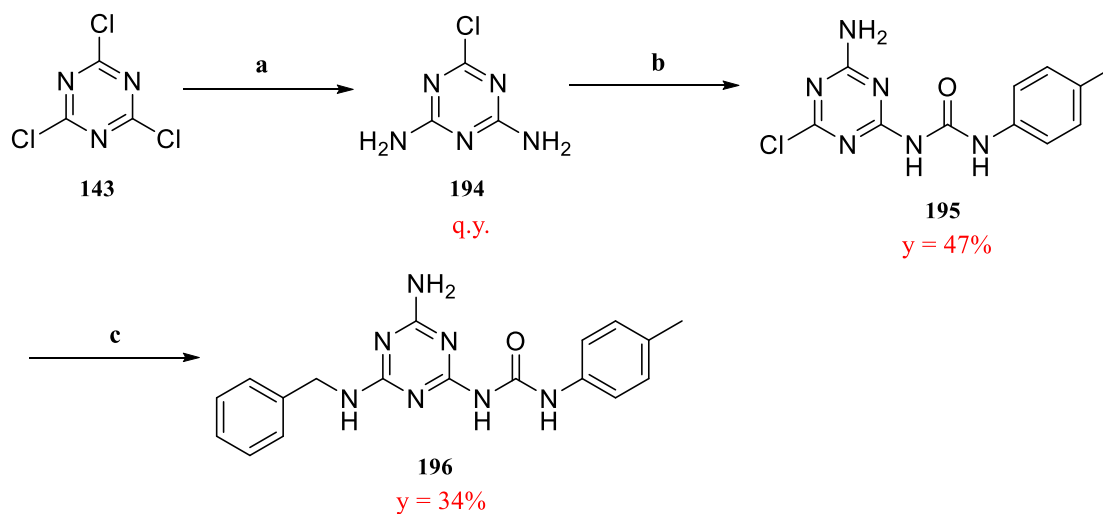
*Scheme 14: synthetic pathway to obtain compound **196**. Reagents and conditions. **a**: NH$_3$, acetone, 45°C, 5h; **b**: p-tolyl isocyanate, dry THF, rfx, overnight, Ar; **c**: benzylamine, neat, 80°C, overnight; y = yield, q.y. = quantitative yield.*

5.6.4. Structure-activity relationship studies

As discussed in the introduction of this chapter, in order to develop a series of 2,4,6-trisubstituted 1,3,5-triazines, a molecular simplification approach starting from compound **141** has been applied opening the possibility to explore the SAR profile inserting a wide variety of substituents. Several types of linkers have been chosen including hydrazide, amine, alkyl chains as well as ureido group and, connected to the spacer, polymethoxy and polyhydroxy moieties have been inserted. Different types of aromatic amines have been located at the 6-position of the main scaffold.

142, 146-149, 142, 163-189, 191, 193, 196
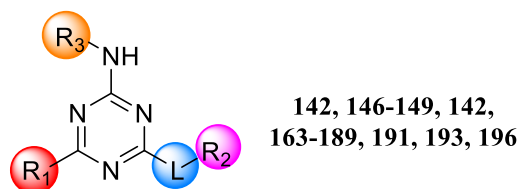
*Table 20: activity percentages and IC$_{50}$s of compounds **142**, **146-149**, **142**, **163-189**, **191**, **193**, **196** on CK1δ.*

Cmpd	R$_1$	L	R$_2$	R$_3$	IC$_{50}$ μM [a] (% activity at 40 μM)[b]
163	-NHBn	-NHNHCO-	-3-OCH$_3$Ph	-H	52.8% ± 14.3
164	-NHBn	-NHNHCO-	-3,4-OCH$_3$Ph	-H	57.3% ± 6.9
146	-NHBn	-NHNHCO-	-3,5-OCH$_3$Ph	-H	78.2% ± 3.2
175	-NHBn	-NHNHCO-	-3-OHPh	-H	72.4% ± 4.6
176	-NHBn	-NHNHCO-	-3,4-OHPh	-H	55.3% ± 2.5
148	-NHBn	-NHNHCO-	-3,5-OHPh	-H	35.5% ± 12.9 23.8 ± 4.8
174	-NHBn	-NHNHCO-	-4OHPh	-H	33.4% ± 6.5 **19.6 ± 2.5**
165	-NH(CH$_2$)$_2$Ph	-NHNHCO-	-3-OCH$_3$Ph	-H	98.0% ± 2.8
166	-NH(CH$_2$)$_2$Ph	-NHNHCO-	-4-OCH$_3$Ph	-H	75.5% ± 1.0
147	-NH(CH$_2$)$_2$Ph	-NHNHCO-	-3,5-OCH$_3$Ph	-H	78.2% ± 3.2
177	-NH(CH$_2$)$_2$Ph	-NHNHCO-	-3-OHPh	-H	83.4% ± 3.7
178	-NH(CH$_2$)$_2$Ph	-NHNHCO-	-4OHPh	-H	63.2% ± 6.2
149	-NH(CH$_2$)$_2$Ph	-NHNHCO-	-3,5-OHPh	-H	42.6% ± 0.6 36.8 ± 5.0
167	-NHCH$_2$Naph	-NHNHCO-	-3-OCH$_3$Ph	-H	90.1% ± 1.8
168	-NHCH$_2$Naph	-NHNHCO-	-4-OCH$_3$Ph	-H	85.7% ± 2.9
169	-NHCH$_2$Naph	-NHNHCO-	-3,4-OCH$_3$Ph	-H	66.3% ± 5.7
170	-NHCH$_2$Naph	-NHNHCO-	-3,5-OCH$_3$Ph	-H	86.0% ± 1.8
179	-NHCH$_2$Naph	-NHNHCO-	-3-OHPh	-H	73.3% ± 2.9
180	-NHCH$_2$Naph	-NHNHCO-	-4OHPh	-H	67.1% ± 0.9
181	-NHCH$_2$Naph	-NHNHCO-	-3,4-OHPh	-H	87.4% ± 6.1
182	-NHCH$_2$Naph	-NHNHCO-	-3,5-OHPh	-H	75.1% ± 4.7
185	-NH(2-OH)Bn	-NHNHCO-	-4-OHPh	-H	89.3% ± 12.4
172	-NH(2-Cl)Bn	-NHNHCO-	-3-OCH$_3$Ph	-H	75.0% ± 7.0
173	-NH(2-Cl)Bn	-NHNHCO-	-4-OCH$_3$Ph	-H	57.3% ± 2.1
183	-NH(2-Cl)Bn	-NHNHCO-	-3-OHPh	-H	59.8% ± 5.8
184	-NH(2-Cl)Bn	-NHNHCO-	-4OHPh	-H	65.5% ± 3.5
186	-NHCH$_2$Naph	-CH$_2$-	-4-CH$_4$Ph	-H	90.0% ± 5.9
187	-NHBn	-NHCH$_2$-	Ph	-H	52.2% ± 1.8
188	-NHBn	-NHCH$_2$-	Ph	-CH$_2$CH$_3$	64.3% ± 2.1
189	-NHPiperazine	-NHCH$_2$-	Ph	-H	69.3% ± 0.4
196	-NHBn	-NHCONH-	-4-CH$_4$Ph	-H	30.7% ± 3.4 52.9 ± 7.6

5. 1,3,5-triazines as CK1δ inhibitors: a simplification strategy

Examining the derivatives developed with the hydrazide linker (**Table 20**), different types of amines have been explored as R_1 including substituted and not benzylamine, phenylethylamine and naphthylmethyl amine. Considering benzylamine as substituent at the 6-position of the heteroaromatic ring, mono and polymethoxy phenyl moieties separated by the hydrazide spacer have conducted to inactive compounds (**146**, **163-164**). Proceeding with the deprotection, hydroxyphenyl derivatives have not registered an improvement in the activity (**148**, **175-176**) except for 4-hydroxyphenyl ring that has led to an IC_{50} of 19.6 µM (**174**) proving to be the best compound of this series. This activity in the high micromolar range appears so far from the reported ones for TP and TT derivatives from which this series is inspired. Increasing the amine substituent of one carbon atom, the situation does not change: methoxy precursors **147**, **165-166** have proved to be inactive on CK1δ while final deprotected compounds **178-179** bearing 3- and 4-hydroxy substitutions have not reported any activity. Maintaining the phenylethyl amine at the 6-position, the 3,5-dihydroxyphenyl moiety derivative (**149**), instead, has provided an IC_{50} of 36.8 µM. By substituting R_1 with bulky aromatic amine like naphthylmethyl amine, 3-, 4-, 3,4-, 3,5-polymethoxy derivatives have been developed and they have reported activity percentages at 40 µM more than 50% (**167-170**). The activities have not been improved with the deprotection (**179-182**). Since the substitution of benzylamine with phenylethylamine and naphthylmethyl amine increasing the size and steric hindrance of R_1 substituent has not led to active compounds, some attempts have been carried out by functionalizing benzylamine. Therefore, (2-hydroxyphenyl)methenamine has been inserted maintaining the 4-hydroxybenzo hydrazide but the derivative **185** has proved to be inactive. 2-chloro substitution on benzylamine has been considered developing protected precursors **172-173** denoting the same prospect even demethoxylating R_2 substituents (**183-184**).

Because most of the synthesized derivatives have reported activity percentages more than 50% at 40 µM concentration, linker has been changed. Derivative **186** that bears naphthylmethyl amine and 4-methylphenyl moiety separated by a CH_2 bridge has denoted a percentage value of 90.0%. Trying to insert three amino substituents the situation has not improved (**187-189**): the symmetric 1,3,5-triazine **187** has reported an activity of 52.2%, proceeding with the correspondent derivative with ethyl group on amine at the 2-position (**188**) the percentage has worsened. By changing benzylamine with a saturated cycle such as piperazine, compound **189** has proved to be inactive on the enzyme. Another attempt has been conducted by inserting ureido moiety as spacer (**196**) denoting the achievement of IC_{50} in the high micromolar range (e.g. 52.9 µM).

This investigation has led to the development of several derivatives in which only three compounds have reported IC_{50}s in the high micromolar range. The molecular simplification approach has allowed to obtain lots of candidates in a faster way in comparison to TP and TT series, nevertheless an almost complete loss of inhibitory power has been recorded linked to an increase in molecular flexibility of 1,3,5-triazine series.

Even if the just discussed results have highlighted poor inhibitors, it is possible to collect these data treating them as starting points to obtain a hit compound with the support of computational studies. In **Fig. 101** the predicted binding pose on the active site of CK1δ is reported for located compound **174** characterized by benzylamine as R_1 and 4-hydroxyphenyl moiety as R_2 separated by hydrazide linker that has recorded the best activity with an IC_{50} of 19.6 µM.
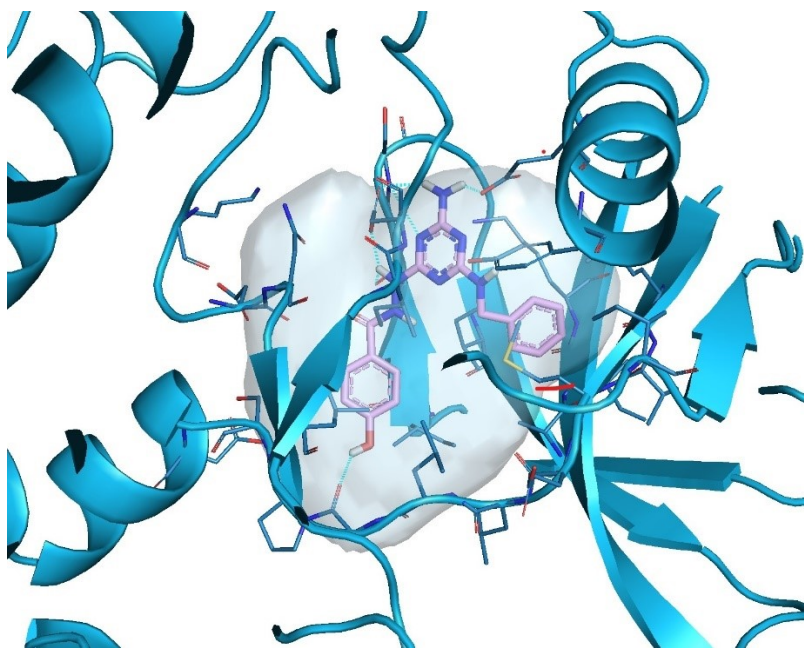
*Figure 101: predicted binding pose of compound **174** on CK1δ. Image made with Flap. PDB Code: 4HNF.*

Observing the residues map (**Fig. 102**) of the conformation with higher score the amino group at the 2-position of the main scaffold seems to interact with Asp149 confirming a completely different accommodation in comparison to the TT derivative **35 (Panel B, Fig. 102)** [209] Some interactions seem to be carried out by the phenyl ring of the R_2 substituents without a substantial contribute of hydroxy moiety as well as hydrazide spacer. Benzylamine group, instead, seems to engage the gatekeeper residue Met82 located in the hinge region of the kinase. Collecting these considerations, the key element bond to the main scaffold is represented by benzylamine chosen as R_1 substituent.
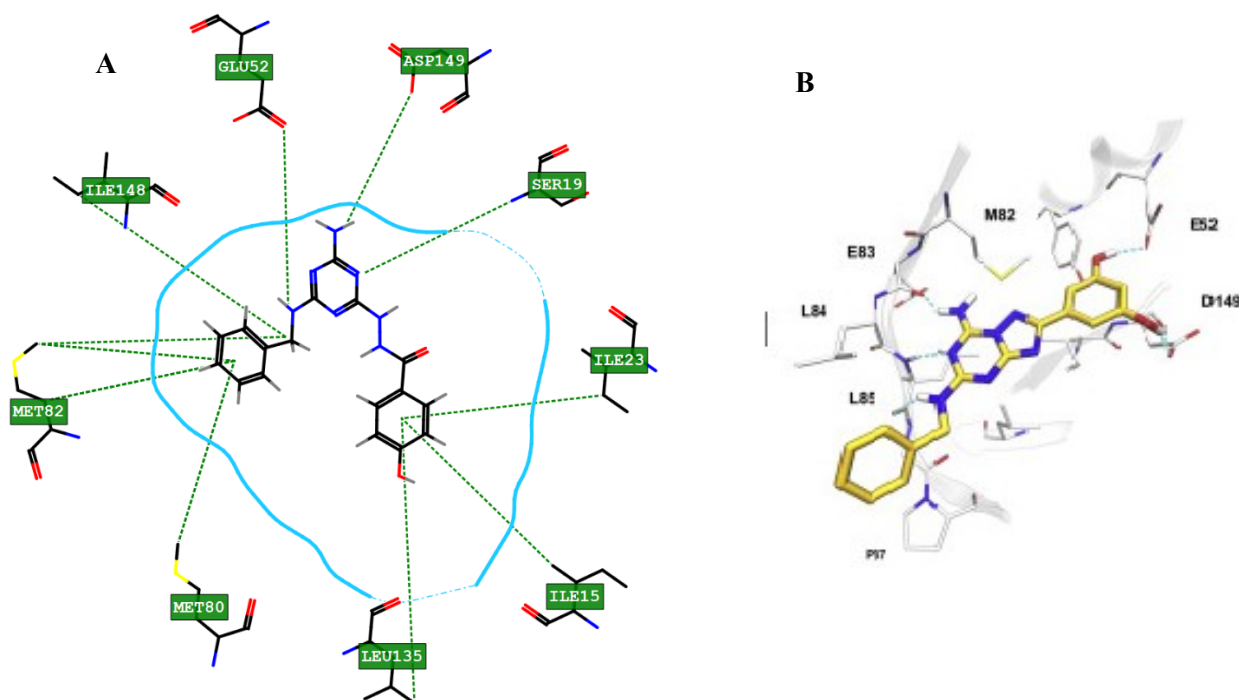
*Figure 102: Panel A) map of interactions of derivative **174** with residues. Image made with Flap. PDB Code: 4HNF, Panel B) predicted binding pose of compound **35** (for details see the Appendix); PDB Code: 4HNF.*

5. 1,3,5-triazines as CK1δ inhibitors: a simplification strategy

The **174**'s IC$_{50}$ value of 19.6 μM suggests that it behaves more as fragment than full inhibitor. Moreover, the predicted binding pose of compound has suggested that some moieties inserted have not covered important roles in establishing interaction with the enzyme. Consequently, the turning point can be the connection of **174** with another fragment by developing a molecular hybrid.

The research group in the publication of Bolcato *et al.* have assayed several fragments on CK1δ with a fragment-based approach. The Fragment-Based Drug Discovery (FBDD) appears as a useful technique for the development of lead compounds starting from the screening of fragments. Considering the appropriate features that characterize commercial drugs, 90% of these agrees with the druglike properties detailed discussed in the **chapter 3**. Examining the chemical space, more than 10^{60} molecules can be identified, and it is evident that achieving of new promising candidates *via* FBDD, the chemical space becomes wider that the estimated one for the druglike derivatives. Therefore, this approach opens the possibility to explore greater range of molecules and main nuclei. Several kinase inhibitors have been discovered using this approach, many of these are in clinic phases. In the preliminary process, the screening of identified fragments with a low molecular weight leads to activities in the high micromolar range, which can be used as starting points for the achievement of potent lead compounds *via* optimization processes. [214,218]

In the just mentioned work the *in silico* screening of 272000 commercially available fragments has been carried out by applying filters including docking protocols to generate the pharmacophoric model. The selected molecules applying this filter have then been screened with the dynamic obtaining 66 promising fragments assayed on CK1δ. Results of enzymatic test have highlighted 7 active molecules. [214]

Among the active fragments, 4-fluoro-1*H*-indazol-3-amine (**190**, **Fig. 103**) has been detected with an IC$_{50}$ of 24.9 μM. [214]
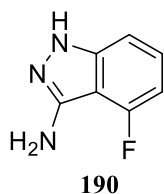
Figure 103: structure of 4-fluoro-1H-indazol-3-amine (**190**). [214]

190

Collecting these informations, derivative **174** has been fused with fragment **190** discovered from the fragment-based approach as represented in **Fig. 104** creating a molecular hybrid. Derivative **142**, as showed in **Table 20**, has displayed an IC$_{50}$ on CK1δ of 3.86 μM denoting an important increase in potency in comparison to the starting compound **174**. To rationalize the improvement of the activity, the predicted binding pose of candidate **142** has been reported in **Fig. 105**.

142
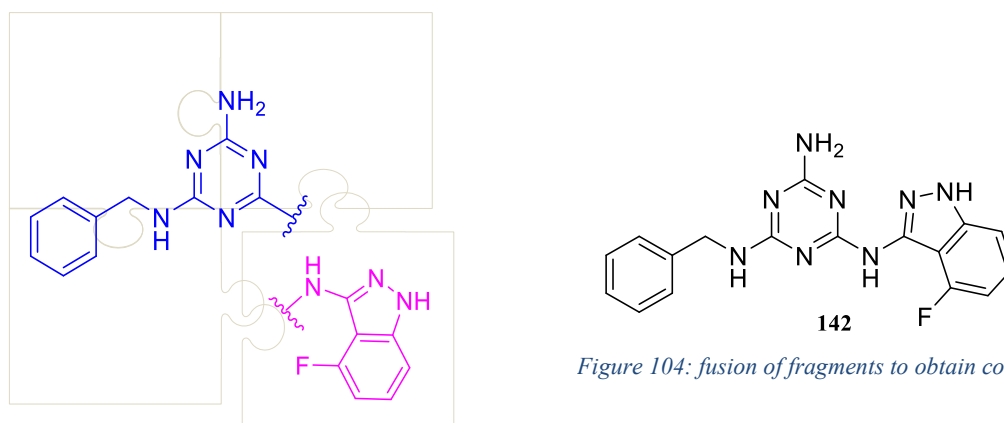
Figure 104: fusion of fragments to obtain compound **142**.
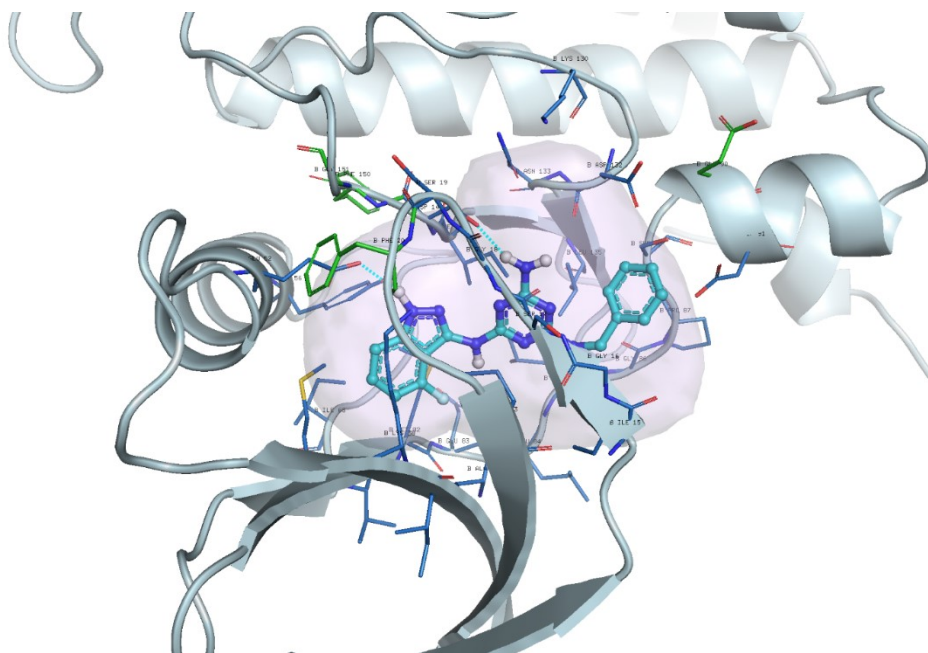
*Figure 105: predicted binding pose of compound **142**. Image made with Flap. PDB Code: 4HNF.*

It is possible to appreciate mainly hydrogen bonds establishing by free ammino group at the 2-position of 1,3,5-triazine scaffold and another one of the indazole moiety. To better exploit interactions, the stylized map of the compound in the active site of the kinase is represented in **Fig. 106**.

Curiously, interactions with Met82 of the hinge region have been established by the indazole nucleus that becomes the main fragment of the molecule while triazine scaffold seems to act as accessory member giving hydrogen bond of -NH$_2$ with Asp149 and other hydrophobic interactions of benzylamine towards several residues. Nevertheless, both the main actor **190**, free amino group and benzylamine have resulted crucial for the activity.
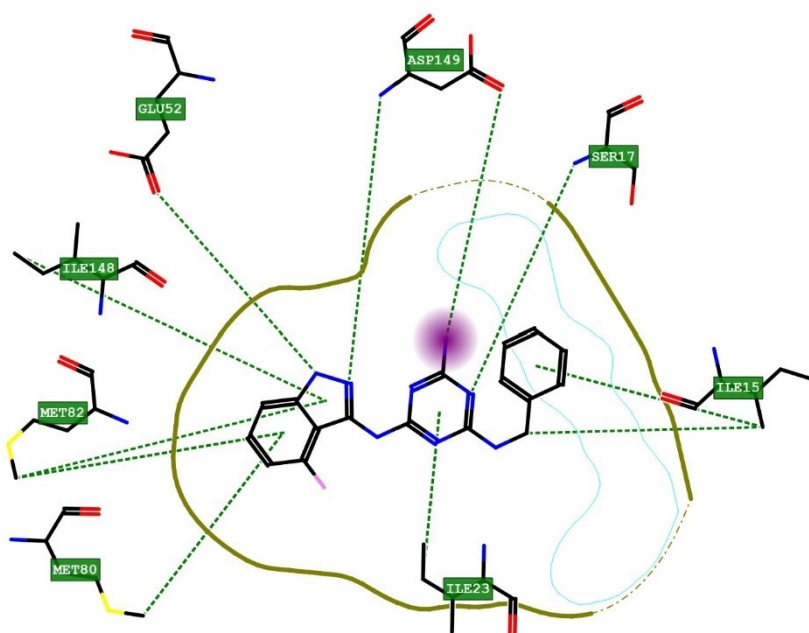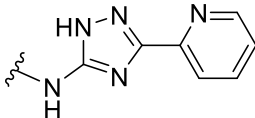
*Figure 106: representation of map of interactions giving by residues in the active site of CK1δ of compound **142**. Image made with Flap. PDB Code: 4HNF.*

5. 1,3,5-triazines as CK1δ inhibitors: a simplification strategy

The reliability of this idea has been validated by trying to change benzylamine with amine of different nature such as piperazine. The obtained derivative **191** has proved to be inactive reporting an activity percentage of 66.2%. Moreover, to corroborate the hybrid approach and the important role of benzylamine as R_1 substituent inserted at the 6-location of the main scaffold, derivative **193** has been developed by changing the fragment **190** with another type of molecule (**192**) that allows the possibility of establishing hydrogen bond. Synthesized compound **193** has been assayed on CK1δ demonstrating an activity of 6.65 μM (**Table 21**).

Table 21: activity percentages and IC₅₀s of compounds 142, 191, 193 on CK1δ.

Cmpd	R₁	R₂	IC$_{50}$ μM [a] (% activity at 40 μM)[b]
142	-NHBn		32.4% ± 8.4 **3.86 ± 0.90**
191	-piperazine		66.2% ± 6.0
193	-NHBn		31.3% ± 11.4 **6.65 ± 1.86**
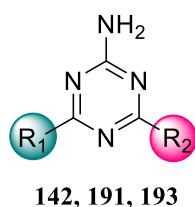
142, 191, 193

[a] *Data represent the mean ± SD of two independent experiments performed in technical duplicate.* [b] *Data represent the % of activity at 40 μM concentration expressed as a mean ± SD of two independent experiments.*

Concluding this SAR section, a series of poor and mediocre derivatives have been used as a starting point for the achievement of promising hit derivative opening the possibility to explore the hybrid approach to optimize again the discovered candidate **142**. The new developed derivatives will be investigated to develop a new series of 1,3,5-triazines.

5.6.5. Biochemical and biological characterization

5.6.5.4. In vitro evaluation of BBB-permeability

The BBB-PAMPA assay, deeply discussed in **chapter 3**, have been performed for compounds **174** and **142** in order to estimate a possible passive transport at the central level.

As mentioned in the **chapter 3**, obtained Pe are filtered according to the literature: the BBB permeability in humans is predicted as positive if it is higher than $4 \cdot 10^{-6}$ cm/s and negative if it is lower than $2 \cdot 10^{-6}$ cm/s. Therefore, applying these limits to the equation of calibration line it is possible to establish cut-off values: in this case compounds with Pe higher than $2.1 \cdot 10^{-6}$ cm/s are classified as CNS+ while Pe permeations below $1.4 \cdot 10^{-6}$ cm/s represent CNS- derivatives.

As reported in **Fig. 107**, derivative **174** that bears benzylamine as R_1 and 4-hydroxybenzo hydrazide at the 4-position of the scaffold has shown a poor predicted permeation reporting a Pe value of $1.0 \cdot 10^{-6}$ cm/s. On the contrary, hit compound **142**, derived from the fusion of the two fragments, has displayed to be able to cross the BBB revealing itself as a promising candidate.

A

BBB permeability evaluation

B

Cmpd	Bibl.	Pe (10^{-6} cm/s)	Prediction
Atenolol	0.8	0.1 ± 1.2	
Caffein	1.3	0.8 ± 0.9	
Desipramine	12	2.7 ± 3.2	
Enoxacin	1.6	1.3 ± 0.4	
Hydrocortisone	2.4	1.3 ± 0.3	
Ofloxacine	0.8	2.1 ± 0.7	
Piroxicam	2.5	1.7 ± 0.3	
Promazine	8.8	13.8 ± 10.2	
Testosterone	17	6.8 ± 2.1	
Verapamil	16	8.9 ± 2.8	
174		1.0 ± 0.1	**CNS-**
142		2.8 ± 0.7	**CNS+**

*Figure 107: **Panel A)** histogram of Pe values of compounds **174** and **142** made with GraphPad 8.0. **Panel B)** Table of Pe and CNS predictions.*

5.6.5.5.   ATP-competition

To establish the ATP-competitive behavior of compound **142**, the Lineweaver-Burk graph has been reported in **Fig. 108**. Derivative has been tested at the concentrations of 4.0 and 8.0 μM considering its IC_{50} value of 3.86 μM using increasing ATP concentrations (1 μM, 2 μM, 10 μM, 50 μM). In x axis the reciprocal ATP consumed has been given while in the y axis the correspondent per minute has been reported. It is possible to appreciate, observing the zoom indicated in the right side of the **Fig. 108**, that the intercept results the same for the three conditions assayed (the two concentrations of compound **142** and the control). Therefore, the derivative has been confirmed as ATP-competitive. The **Table 22** reports the y-intercept values.
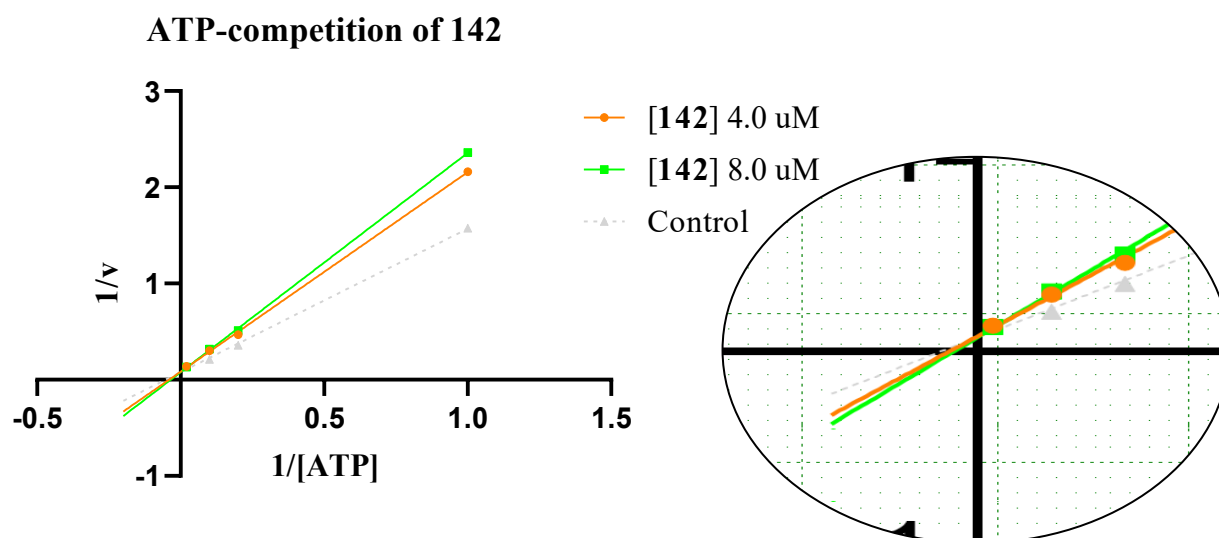
*Figure 108: Lineweaver-Burk plot testing compound **142** at the concentrations of 4.0 μM and 8.0 μM. Experiment has been conducted in technical duplicate and two independent experiments have been carried out. In the left-side of the figure, the zoom of the intercept of the three lines has been reported.*

Table 22: y-intercept values of the Lineweaver-Burk plot reported in Fig.107 for compound 142.

Cmpd	y-intercept
[142] 4 μM	0.08
[142] 8 μM	0.08
Control	0.08

5.6.5.6. Screening on GSK3β

Derivative **142** has been screened on the kinase GSK3β in the group of Prof. Ana Martinez during the Erasmus traineeship program (CSIC-Madrid-ES) in order to obtain useful information about the activity of the compound towards another target involved in neurodegenerative diseases. As described in the **chapter 3.**, derivative **142** has been tested on full-length GSK3β (1 ng/μL) at the presence of GS-2 as substrate (0.2 μg/μL) and ATP at the final concentration of 1 μM. As reported in **Table 23**, the candidate has displayed an activity percentage of 100% denoting a complete inactivity towards GSK3β.

Table 23: Activity percentage of compound 142 on GSK3β at the concentration of 10 μM

Cmpd	% Activity at 10 μM[a]
142	n.d. (100 % ± 0)

[a] *Data represent the % of activity at 10 μM concentration expressed as a mean ± SD of three independent experiments performed in technical duplicate; n.d.: not determined*

Derivative **142**, therefore, results interesting from several point of views and it could be an appealing starting point for the development of new more potent lead compounds with good druglike properties able to cross the BBB and selective on CK1δ.

5.6.5.7. Biological characterization on neuroblastoma cell lines

Developed candidate **142** has been assayed on neuroblastoma cell lines (SH-SY5Y) as described in the **chapter 3**. As a preliminary step, the toxicity of compound has been evaluated by performing the MTT assay plating 80000 cells/well testing **142** at the concentrations of 5 and 10 μM. The histogram reported in **Figure 109** shows the results of derivative at the two concentrations screened denoting an increasing toxicity on neuroblastoma cells. Therefore, the investigation in neuroprotection and the Western Blot experiment to view a decrease in pTDP-43 cannot be available for this compound and biological exploration has been interrupted at this point for the displayed toxicity of the candidate.
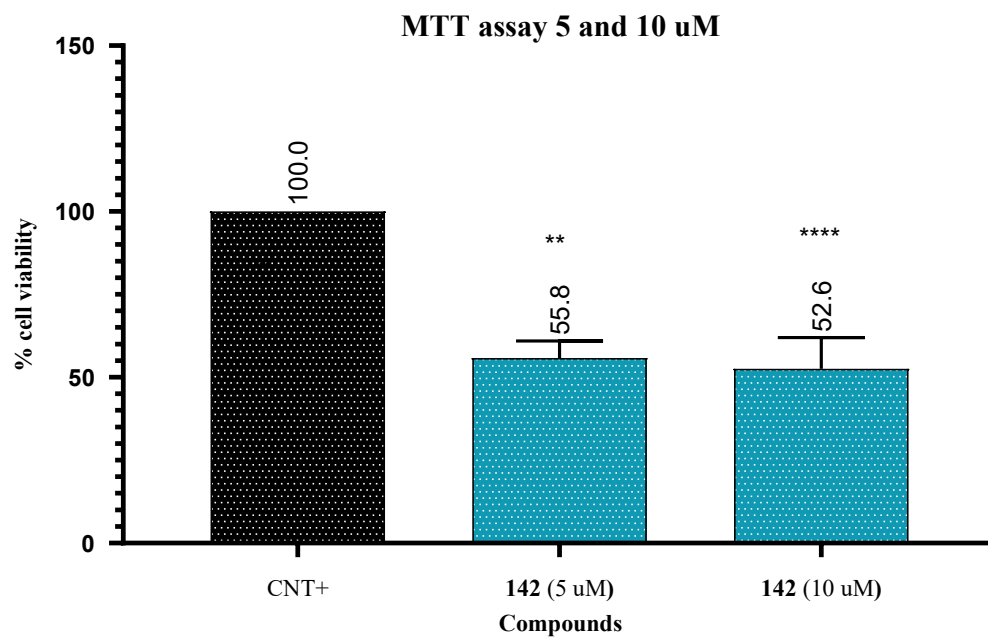
*Figure 109: MTT assay of compound **142** at the concentrations of 5 and 10 μM. In y axis the cell viability percentage is reported. The elaboration performed with GraphPad Prism 8.0 in "Anova" mode is the result of three independent experiments and each experiment is conducted using the mean of six wells per compound.*

5.7.   Conclusions and future perspectives

A series of 2,4,6-trisubstitued 1,3,5-triazines has been developed by applying a molecular simplification approach of the TT scaffold compound **35** that showed an IC_{50} of 0.18 μM on CK1δ. Several derivatives have been obtained investigating all the three positions of the main nucleus to outline a SAR profile. Different types of amines have been considered for the 6-location while polymethyl, methoxy and hydroxy phenyl moieties have been inserted as R_2 separated by a linker of different size and nature including hydrazide groups, amine and ureido moieties as well as alkyl bridge. Only three compounds of the series have proved to be active on the kinase in a high micromolar range and in particular derivative **174** has reported an IC_{50} of 19.6 μM demonstrating itself as the best compound of the series. Its activity suggests that it behaves more as fragment than full inhibitor, therefore it has been fused with a published indazole fragment (**190**) by applying a fragment-based approach. The molecular hybrid (**142**) has reported an activity of 3.86 μM achieving a promising result also in according with the computational support. The candidate **142** has displayed a good BBB passage and no activity towards GSK3β. Nevertheless, the derivative has denoted a toxicity in the MTT assay conducted at CSIC in Madrid on neuroblastoma cell lines, thus the neuroprotective behavior has not been investigated. Compound **142** has been featured as a promising starting point opening the possibility of exploring similar fragments and functionalized indazole molecules to insert at the 4-position of the 1,3,5-triazine scaffold to obtain a more potent lead derivative. The strategy used to achieve a more active compound has proved to be challenging transforming poor potent derivatives into a turning point. Nevertheless, a more focused optimization of the final derivative can be carried out by functionalizing the 1H-indazole ring or by substituting this fragment with other types of aromatic moieties allowing to outline a new SAR investigation analysis.

5.8.   Experimental section

5.8.3.   General chemistry

Reagents were obtained from commercial suppliers and used without further purification. Reactions were monitored by TLC, on precoated silica gel plates (Macherey-Nagel, 60FUV254). Final compounds and intermediates were purified by flash chromatography using as stationary phases silica gel (Macherey-Nagel, silica 60, 240-400 mesh) or preparative TLC (stationary phase silica gel, Mechery-Nagel, silica 60, 240-400 mesh, 0.25 mm). When used, light petroleum ether refers to the fractions boiling at 40-60°C. Melting points were determined with a Stuart SMP10 melting point apparatus, and they were not corrected. The ^{1}H NMR, ^{13}C NMR and gHSQCAD bidimensional spectra were determined in CDCl$_3$ or DMSO-d_6 and recorded on Varian 400 MHz or Varian 500 MHz spectrometers; chemical shifts (δ scale) are reported in parts per million (ppm) and referenced to residual solvent peak, with splitting patterns abbreviated to: s (singlet), d (doublet), dd (doublet of doublets), dt (doublet of triplets), t (triplet), m (multiplet) and bs (broad signal). Coupling constants (*J*) are given in Hz. MS-ESI analysis was performed using ESI Bruker 4000 Esquire spectrometer or microTOF-Q – Bruker, used also for the recording of accurate mass. Compound purities were determined by HPLC using the instrument SHIMADZU CBM-20A, column Gemini® 5 μm NX-C18 (Phenomenex®). Elution gradient was performed for 20 min at the flow of 1 ml/min from water-methanol 55:45 to 15:85. The detector was set at 254 nm.

5.8.4.   Synthesis of N'-(4-amino-6-substituted-1,3,5-triazin-2-yl)-polymethoxy and polyhydroxy benzohydrazide derivatives (**Synthetic pathway A**)

5.8.4.4.   Synthesis of N'-(4,6-dichloro-1,3,5-triazin-2-yl)-3,5-dimethoxybenzohydrazide (**144**)

1.0 equivalent (7.39 g, 40 mmol) of 2,4,6-trichloro-1,3,5-triazine (cyanuric chloride, 143), commercially available, was solved in acetone (20.0 mL/mmol of **143**). To the solution at 0°C, 1.0 equivalent of 3,5-dimethoxybenzohydrazide (7.84 g, 40 mmol) previously solved in acetone (17.0 mL/mmol) was added dropwise in 30-45 minutes. The reaction was stirred for 16 h. Once completed, the solvent was removed under reduced pressure and 50.0 mL of water were added and the mixture was filtered to collect 8.31 g of white solid on the filter. Yield 61%; mp 217°C. ^{1}H-NMR (400 MHz, DMSO-d_6) δ 11.02 (s, 1H), 10.88 (s, 1H), 7.06 (d, *J* = 2.3 Hz, 2H), 6.74 (t, *J* = 2.3 Hz, 1H), 3.81 (s, 6H). ES-MS (methanol) *m/z* C$_{12}$H$_{11}$Cl$_2$N$_5$O$_3$: 342.1 [M-H]$^+$.

5.8.4.5.   Synthesis of N'-(4-amino-6-chloro-1,3,5-triazin-2-yl)-3,5-dimethoxybenzohydrazide (**145**)

To 90 mg (1.0 eq, 0.26 mmol) of N'-(4,6-dichloro-1,3,5-triazin-2-yl)-3,5-dimethoxybenzohydrazide (**144**) solved in 10.0 mL of acetone, a solution of 0.076 mL of ammonium hydroxide (7.5 eq, 1.96 mmol of a solution 23%) in 5.0 mL of acetone was added dropwise in 15 minutes. The reaction was stirred for 6 hours. 7.5 eq of ammonium hydroxide solution was then added and, after 16 h, the solvent was removed under reduced pressure. The crude was purified with flash chromatography (light petroleum 60% - EtOAc 40% to EtOAc 90% - MeOH 10%) to obtain 33.0 mg of white solid. Yield 39%; mp 243°C. ^{1}H-NMR (400 MHz, DMSO-d_6) δ 10.44 + 9.57 (bs, 1H),7.48 + 7.07 (bs, 2H), 6.69 (s, 1H), 3.79 (s, 6H). ES-MS (methanol) *m/z* C$_{12}$H$_{13}$ClN$_6$O$_3$: 325.1 [M+H]$^+$, 347.0 [M+Na]$^+$, 363.0 [M+K]$^+$.

5.8.4.6.   General procedure for the synthesis of N'-(4-amino-6-(amino-substituted)-1,3,5-triazin-2-yl)-3,5-dimethoxybenzohydrazide (**146-147**)

1.0 equivalent of N'-(4-amino-6-chloro-1,3,5-triazin-2-yl)-3,5-dimethoxybenzohydrazide (**145**) was reacted in a sealed tube with excess of desired amine (17.0 equivalents) and 3.0 eq. of K$_2$CO$_3$ at 110°C for 2 h. Once completed, excess of amine was removed under reduced pressure and the crude was purified with flash chromatography.

5.8.4.6.1.   N'-(4-amino-6-(benzylamino)-1,3,5-triazin-2-yl)-3,5-dimethoxybenzohydrazide (**146**)
Flash chromatography eluent (EtOAc 95% - MeOH 5% to EtOAc 90% - MeOH 10%). White solid; yield 65% (207 mg); mp 246°C. ^{1}H-NMR (400 MHz, DMSO-d_6) δ 10.17 (bs, 1H), 8.51 + 8.39 (bs, 1H), 7.51 – 6.94 (m, 8H), 6.66 (s, 1H), 6.34 + 6.22 (bs,2H), 4.44 + 4.29 (bs, 2H), 3.78 (s, 6H). ^{13}C NMR (101 MHz, DMSO-d_6) δ 167.92, 167.92, 166.28, 165.15, 160.29, 140.70, 134.99, 128.05 (CH), 126.95 (CH), 126.40 (CH), 105.30 (CH), 103.51 (CH), 55.40 (CH$_3$), 43.00 (CH$_2$). ES-MS (methanol) *m/z* C$_{19}$H$_{21}$N$_7$O$_3$: 396.2 [M+H]$^+$, 418.2 [M+Na]$^+$.

5.8.4.6.2.   N'-(4-amino-6-(phenethylamino)-1,3,5-triazin-2-yl)-3,5-dimethoxybenzohydrazide (**147**)
Flash chromatography eluent (EtOAc 95% - MeOH 5%). White solid; yield 21% (149.5 mg); mp 244°C. ^{1}H NMR (400 MHz, DMSO-d_6) δ 10.17 (s, 1H), 8.43 (d, *J* = 71.5 Hz, 1H), 7.40 – 6.55 (m, 9H), 6.26 (d, *J* = 64.6 Hz, 2H), 3.77 (d, *J* = 15.0 Hz, 6H), 3.42 (s, 5H), 3.22 (s, 2H), 2.72 (d, *J* = 59.7 Hz, 2H). ^{13}C NMR (101 MHz, DMSO-d_6) δ 188.79, 165.51, 160.65, 135.57, 132.74, 128.98 (CH), 126.48 (CH), 105.62 (CH), 103.91 (CH), 87.23, 73.27, 56.27 (CH$_3$), 42.31 (CH$_2$), 35.74 (CH$_2$). ES-MS (methanol) m/z: 410.2 [M+H]$^+$, 432.2 [M+Na]$^+$. HRMS *m/z* C$_{20}$H$_{23}$N$_7$O$_3$: experimental 410.1933 [M+H]$^+$, theoretical 410.1935 [M+H]$^+$, Δ = 0.0002. Purity HPLC: 98.8%.

5.8.4.7.   General procedure for the synthesis of N'-(4-amino-6-substituted-1,3,5-triazin-2-yl)-3,5-dihydroxybenzohydrazide (**148-149**)
Under   argon   atmosphere   1.0   eq.   of   N'-(4-amino-6-(amino-substituted)-1,3,5-triazin-2-yl)-3,5-dimethoxybenzohydrazide derivative (**146-147**) was solved in anhydrous DCM (1.0 mL/mmol of **146-147**). The reaction was cooled to -40°C and 9-12 equivalents of BBr$_3$ in anhydrous DCM (1.0 mL/mmol of BBr$_3$) were added slowly. The reaction was stirred at room temperature overnight and once completed, the solution was cooled at 0°C and cold MeOH (15 mL/mmol BBr$_3$) was slowly inserted. The solvent was removed under reduced pressure and the crude residue was purified with flash chromatography.

5.8.4.7.1.   N'-(4-amino-6-(benzylamino)-1,3,5-triazin-2-yl)-3,5-dihydroxybenzohydrazide (**148**)
Flash chromatography eluent (EtOAc 90% - MeOH 10%). White solid; yield 19% (34.3 mg); mp 161°C. ^{1}H-NMR a 25, 45 and 65 °C: ^{1}H-NMR T = 65 °C (400 MHz, DMSO-d_6) δ 9.77 (s, 1H), 9.27 (s, 2H), 8.21 (bs, 1H), 7.39 – 7.13 (m, 5H), 6.98 (t, *J* = 6.0 Hz, 1H), 6.76 (d, *J* = 2.1 Hz, 2H), 6.39 (t, *J* = 2.1 Hz, 1H), 6.07 (s, 2H), 4.43 (d, *J* = 5.9 Hz, 2H). ^{13}C-NMR (101 MHz, DMSO-d_6) δ 167.94, 166.28, 165.83, 158.22, 140.68, 135.05, 128.07 (CH), 126.94 (CH), 126.39 (CH), 105.74 (CH), 105.37 (CH), 42.99 (CH$_2$). ES-MS (methanol) *m/z*: 368.2 [M+H]$^+$, 390.1 [M+Na]$^+$. HRMS *m/z* C$_{17}$H$_{17}$N$_7$O$_3$: experimental 368.1467 [M+H]$^+$, theoretical 368.1466 [M+H]$^+$, Δ = 0.0001. Purity HPLC: 100%.

5.8.4.7.2.   N'-(4-amino-6-(phenethylamino)-1,3,5-triazin-2-yl)-3,5-dihydroxybenzohydrazide (**149**)
Flash chromatography eluent (EtOAc 95% - MeOH 5% to EtOAc 90% - MeOH 10%). White solid; yield 15% (31.7 mg); mp 156°C. ^{1}H NMR (400 MHz, DMSO-d_6) δ 9.95 (s, 1H), 9.46 (s, 2H), 8.51 – 8.16 (m, 1H), 7.37 – 6.58 (m, 8H), 6.51 – 6.04 (m, 3H), 3.22 (s, 2H), 2.70 (d, *J* = 70.0 Hz, 2H). ^{13}C NMR (101 MHz, DMSO-d_6) δ 178.68, 158.54, 142.54, 140.12, 135.57, 129.62 (CH), 128.61 (CH), 126.17, 117.35, 106.48 (CH), 106.16 (CH), 43.76 (CH$_2$), 35.11 (CH$_2$). ES-MS (methanol) *m/z*: 382.2 [M+H]$^+$, 404.1 [M+Na]$^+$. HRMS *m/z* C$_{18}$H$_{19}$N$_7$O$_3$: experimental 404.1441 [M+Na]$^+$, theoretical 404.1442 [M+H]$^+$, Δ = 0.0001. Purity HPLC: 93.7%.

5.8.5. Synthesis of 2,4,6-trisubstituted 1,3,5-triazine derivatives (**Synthetic pathway B**) (**142**, **163-189**, **191**, **193**)

5.5.3.1. General procedure for the synthesis of 4,6-dichloro-N-substituetd-1,3,5-triazin-2-amine (**150-155**)

1.0 equivalent of 2,4,6-trichloro-1,3,5-triazine (cyanuric chloride, **143**), commercially available, was solved in acetone (20.0 mL/mmol of **143**). To the solution at 0°C, 1.0 equivalent of desired amine previously solved in acetone (17.0 mL/mmol) was added dropwise in 30-45 minutes. The reaction was stirred for 16 h. Once completed, the solvent was removed under reduced pressure and 50.0 mL of water were added and the mixture was filtered to collect the solid on the filter.

5.5.3.1.2. N-benzyl-4,6-dichloro-1,3,5-triazin-2-amine (**150**)

The solid was suspended in water and extracted with EtOAc (1:1 volume ratio). The solvent was removed under reduced pressure to collect 5.55 g of white solid. Yield 55%; mp 127°C. ^{1}H-NMR (400 MHz, DMSO-d_6) δ 9.61 (t, J = 6.2 Hz, 1H), 7.37 – 7.25 (m, 5H), 4.53 (d, J = 6.3 Hz, 2H). ES-MS (methanol) m/z $C_{10}H_{18}Cl_2N_4$: 255.0 [M+H]$^+$.

5.5.3.1.3. 4,6-dichloro-N-phenethyl-1,3,5-triazin-2-amine (**151**)

White solid; yield 94% (9.55 g); mp 135°C. ^{1}H NMR (400 MHz, DMSO-d_6) δ 9.20 (s, 1H), 7.28 – 7.17 (m, 5H), 3.52 – 3.46 (m, 2H), 2.80 (d, J = 7.2 Hz, 2H). ES-MS (methanol) m/z $C_{11}H_{10}Cl_2N_4$: 267.0 [M+H]$^+$.

5.5.3.1.4. 4,6-dichloro-N-(naphthalen-1-ylmethyl)-1,3,5-triazin-2-amine (**152**)

White solid; yield 58% (6.22 g); mp 142°C. ^{1}H NMR (400 MHz, DMSO-d_6) δ 9.71 (t, J = 5.8 Hz, 1H), 8.11 (dd, J = 7.9, 1.2 Hz, 1H), 8.03 – 7.94 (m, 1H), 7.89 (dd, J = 6.9, 2.5 Hz, 1H), 7.59 (dqd, J = 8.2, 6.8, 1.6 Hz, 2H), 7.53 – 7.42 (m, 2H), 4.99 (d, J = 5.9 Hz, 2H). ES-MS (methanol) m/z $C_{14}H_{10}Cl_2N_4$: 303.1 [M+H]$^+$.

5.5.3.1.5. 4,6-dichloro-N-(2-methoxybenzyl)-1,3,5-triazin-2-amine (**153**)

White solid; yield q.y. (10.76 g); mp 132°C.

5.5.3.1.6. 4,6-dichloro-N-(2-chlorobenzyl)-1,3,5-triazin-2-amine (**154**)

White solid; yield q.y. (10.97 g); mp 153°C. ^{1}H NMR (400 MHz, DMSO-d_6) δ 8.67 (s, 1H), 7.69 – 7.62 (m, 1H), 7.56 – 7.50 (m, 1H), 7.45 – 7.39 (m, 2H), 4.11 (dd, J = 5.5 Hz, 2H). ES-MS (methanol) *m/z* $C_{10}H_7Cl_3N_4$: 326.3 [M+H]$^+$.

5.5.3.1.7. *Tert*-butyl 4-(4,6-dichloro-1,3,5-triazin-2-yl)piperazine-1-carboxylate (**155**)

White solid; yield 58% (2.80 g); mp 164°C. ES-MS (methanol) m/z $C_{12}H_{17}Cl_2N_5O_2$: 334.1 [M+H]$^+$.

5.5.3.2. General procedure for the synthesis of 6-chloro-N^2-(2-substituted)-1,3,5-triazine-2,4-diamine (**156-162**)

1.0 eq. of 4,6-dichloro-N-substituetd-1,3,5-triazin-2-amine (**150-155**) was solved in acetone (25.0 mL/mmol of **150-155**) and 10 eq. of solution of ammonium hydroxide in acetone (1.3 mL/mmol of NH$_4$OH) were added dropwise in 30 minutes. The reaction was stirred for 20 h, then 5.0 eq. of ammonium hydroxide solution in acetone were added. After 5 h, the solvent was removed under vacuum and the crude residue was purified with flash chromatography (light petroleum 50% - EtOAc 50%). After removing solvent, the product was precipitated using EtOAc to achieve white solid.

Compound **157** was obtained previously, and the experiment procedure is not reported.

5. 1,3,5-triazines as CK1δ inhibitors: a simplification strategy

5.5.3.2.1.   N^2-benzyl-6-chloro-1,3,5-triazine-2,4-diamine (**156**)
Yield 49% (908 mg); mp 210°C. ^{1}H-NMR (400 MHz, DMSO-d_6) δ 8.24 (t, J = 6.3 Hz, 1H), 7.44 – 7.06 (m, 7H), 4.46 (d, J = 6.4 Hz, 2H). ES-MS (methanol) m/z C$_{10}$H$_{10}$ClN$_5$: 236.0 [M+H]$^+$.

5.5.3.2.2.   6-chloro-N^2-phenethyl-1,3,5-triazine-2,4-diamine (**158**)
Yield 31% (1.74 g); mp 232°C. ^{1}H NMR (400 MHz, DMSO-d_6) δ 7.80 (t, J = 63.5 Hz, 2H), 7.21 (dd, J = 45.1, 38.0 Hz, 6H) 3.42 (s, 2H), 2.79 (s, 2H). ES-MS (methanol) m/z C$_{11}$H$_{12}$ClN$_5$: 250.0 [M+H]$^+$.

5.5.3.2.3.   6-chloro-N^2-(naphthalen-1-ylmethyl)-1,3,5-triazine-2,4-diamine (**159**)
yield 82% (4.70 g); mp 243°C. ^{1}H NMR (400 MHz, DMSO-d_6) δ 8.33 (t, J = 6.1 Hz, 1H), 8.20 – 8.07 (m, 1H), 7.98 – 7.93 (m, 1H), 7.83 (d, J = 7.9 Hz, 1H), 7.59 – 7.51 (m, 2H), 7.44 (dt, J = 23.2, 7.1 Hz, 3H), 7.33 (s, 1H), 4.91 (dd, J = 12.0, 6.1 Hz, 2H). ES-MS (methanol) m/z C$_{14}$H$_{12}$ClN$_5$: 286.1 [M+H]$^+$.

5.5.3.2.4.   6-chloro-N^2-(2-methoxybenzyl)-1,3,5-triazine-2,4-diamine (**160**)
Yield 45% (831 mg); mp 203°C. ES-MS (methanol) m/z C$_{11}$H$_{12}$ClN$_5$O: 266.1 [M+H]$^+$.

5.5.3.2.5.   6-chloro-N^2-(2-chlorobenzyl)-1,3,5-triazine-2,4-diamine (**161**)
Yield 26% (2.70 g); mp 253°C. ^{1}H NMR (400 MHz, DMSO-d_6) δ 8.56 – 7.98 (m, 2H), 7.56 – 7.04 (m, 5H), 4.57 – 4.42 (m, 2H). ES-MS (methanol) m/z C$_{10}$H$_9$Cl$_2$N$_5$: 270.0 [M+H]$^+$.

5.5.3.2.6.   *Tert*-butyl 4-(4-amino-6-chloro-1,3,5-triazin-2-yl)piperazine-1-carboxylate (**162**)
Yield 63% (1.82 g); mp 272°C. ES-MS (methanol) m/z C$_{12}$H$_{19}$ClN$_6$O$_2$: 315.2 [M+H]$^+$.

5.5.3.3.   General procedure for the synthesis of N'-(4-amino-6-substituted-1,3,5-triazin-2-yl)methoxybenzohydrazide derivatives (**163-174**)
Method A: 1.0 eq. of 6-chloro-N^2-(2-substituted)-1,3,5-triazine-2,4-diamine (**156-162**) was reacted with desired substituted methoxybenzohydrazide or amine (15.0 eq.) in a sealed tube. 3.0 eq. of K$_2$CO$_3$ were added and the reaction was stirred at neat condition for 2-6 h at 110-140°C. The excess of amine was removed under reduced pressure and the crude residue was purified with flash chromatography.

Method B: 1.0 eq. of 6-chloro-N^2-(2-substituted)-1,3,5-triazine-2,4-diamine (**156-162**) was reacted, under neat condition, with 1.0 eq. of desired substituted methoxybenzohydrazide or amine in a sealed tube heating the mixture at 170°C. The reaction was allowed for 2-6 h and, once completed, the crude residue was purified with flash chromatography.

Method C: 1.0 eq. of 6-chloro-N^2-(2-substituted)-1,3,5-triazine-2,4-diamine (**156-162**) was reacted, under neat condition, with 1.0 eq. of desired substituted methoxybenzohydrazide or amine in a microwave tube heating the mixture at 130°C. The reaction was allowed for 3 h on microwave and, once completed, the crude residue was purified with flash chromatography.

5.5.3.2.1.   N'-(4-amino-6-(benzylamino)-1,3,5-triazin-2-yl)-3-methoxybenzohydrazide (**163**)
Method A; flash chromatography eluents (DCM 90% - MeOH 10%, EtOAc 92% - MeOH 8%). White solid; yield 37% (284 mg); mp 190°C. ^{1}H-NMR (400 MHz, DMSO-d_6) δ 10.20 (bs, 1H), 8.49 + 8.38 (bs, 1H), 7.54 – 7.05 (m, 10H), 6.34 + 6.22 (bs,2H), 4.42 + 4.26 (bs, 2H), 3.80 (s, 3H). ^{13}C-NMR (101 MHz, DMSO-d_6) δ 168.38, 166.72, 159.55, 141.11, 134.78, 129.92, 128.50, 127.38, 126.83, 120.14, 117.90, 112.91, 55.71, 43.42. ES-MS (methanol) m/z: 366.2 [M+H]$^+$, 388.1 [M+Na]$^+$, 404.1 [M+K]$^+$. HRMS (ESI-TOF) m/z C$_{18}$H$_{19}$N$_7$O$_2$: experimental 366.1671 [M+H]$^+$, theoretical 366.1673 [M+H]$^+$, Δ = 0.0002. Purity HPLC: 97.7%.

5.5.3.2.2. N'-(4-amino-6-(benzylamino)-1,3,5-triazin-2-yl)-3,4-dimethoxybenzohydrazide (**164**)

Method A; flash chromatography eluents (acetone 80% - DCM 20% + 1% NH$_4$OH, DCM 90% - MeOH 10% whit alumine as stationary phase). White solid; yield 38% (323 mg); mp 146°C. ^{1}H-NMR (400 MHz, DMSO-d_6) δ 10.09 (bs, 1H), 8.45 + 8.32 (bs, 1H), 7.53 (d, J = 8.5 Hz, 1H), 7.49 (s, 1H), 7.38-7.06 (m, 6H), 7.02 (d, J = 8.5 Hz, 1H), 6.30 + 6.18 (bs, 2H), 4.43 + 4.25 (bs, 2H), 3.80 (s, 6H). ^{1}H-NMR (400 MHz, DMSO-d_6, 65 °C) δ 9.92 (s, 1H), 8.18 (s, 1H), 7.65 – 7.41 (m, 2H), 7.41 – 7.10 (m, 5H), 7.10 – 6.85 (m, 2H), 6.05 (s, 2H), 4.41 (d, J = 4.7 Hz, 2H), 3.93 – 3.67 (m, 6H). ^{13}C-NMR (101 MHz, DMSO-d_6) δ 168.46, 166.63, 165.68, 151.87, 148.60, 141.08, 128.51 (CH), 127.38 (CH), 126.84 (CH), 125.52, 121.27 (CH), 111.35 (CH), 111.09 (CH), 56.03 (CH$_3$), 43.43 (CH$_2$). ES-MS (methanol) m/z: 396.2 [M+H]$^+$, 413.2 [M+NH$_4$]$^+$, 418.2 [M+Na]$^+$, 434.1 [M+K]$^+$. HRMS (ESI-TOF) m/z C$_{19}$H$_{21}$N$_7$O$_3$: experimental 396.1779 [M+H]$^+$, theoretical 396.1779 [M+H]$^+$, Δ = 0.0000. Purity HPLC: 100%.

5.5.3.2.3. N'-(4-amino-6-(benzylamino)-1,3,5-triazin-2-yl)-4-hydroxybenzohydrazide (**174**)

Method A; obtained directly the 4-hydroxy derivative. flash chromatography eluents (DCM 90% - MeOH 10%, DCM 90% - MeOH 10% + 1% NH$_4$OH). White solid; yield 3% (8.8 mg); mp 169°C. ^{1}H-NMR (400 MHz, CD$_3$OD) δ 7.78 (s, 2H), 7.51 – 7.03 (m, 5H), 6.84 (d, J = 8.6 Hz, 2H), 4.53 (s, 2H). ^{13}C-NMR (101 MHz, CD$_3$OD) δ 130.76 (CH), 129.37 (CH), 128.26 (CH), 127.91 (CH), 116.14 (CH), 45.04 (CH$_2$). No signals of quaternary carbons were detected. ES-MS (methanol) m/z: 352.2 [M+H]$^+$, 374.1 [M+Na]$^+$. HRMS (ESI-TOF) m/z C$_{17}$H$_{17}$N$_7$O$_2$: experimental 352.1519 [M+H]$^+$, theoretical 352.1516 [M+H]$^+$, Δ = 0.0003. Purity HPLC: 95.2%.

5.5.3.2.4. N'-(4-amino-6-(phenethylamino)-1,3,5-triazin-2-yl)-3-methoxybenzohydrazide (**165**)

Method B; flash chromatography eluent (EtOAc 70% - light petroleum 30%). White solid; yield 50% (222 mg); mp 153°C. ^{1}H NMR (400 MHz, DMSO-d_6) δ 10.20 (s, 1H), 8.47 (d, J = 78.0 Hz, 1H), 7.60 – 7.45 (m, 2H), 7.38 (t, J = 7.9 Hz, 1H), 7.32 – 6.98 (m, 6H), 6.83 (d, J = 21.6 Hz, 2H), 6.29 (d, J = 55.4 Hz, 2H), 3.78 (d, J = 14.5 Hz, 3H), 3.40 (s, 2H), 2.71 (d, J = 56.1 Hz, 2H). ^{13}C NMR (101 MHz, DMSO-d_6) δ 195.16, 185.77, 168.27, 165.78, 159.58, 140.20, 134.74, 129.95 (CH), 128.86 (d, J = 38.1 Hz, CH), 126.38 (CH), 120.15 (CH), 117.91 (CH), 112.94 (CH), 55.77 (CH$_3$), 42.08 (CH$_2$), 35.72 (CH$_2$). ES-MS (methanol) m/z: 380.2 [M+H]$^+$. HRMS (ESI-TOF) m/z C$_{19}$H$_{21}$N$_7$O$_2$: experimental 380.1827 [M+H]$^+$, theoretical 380.1829 [M+H]$^+$, Δ = 0.0002. Purity HPLC: 99.0%.

5.5.3.2.5. N'-(4-amino-6-(phenethylamino)-1,3,5-triazin-2-yl)-4-methoxybenzohydrazide (**166**)

Method C; flash chromatography eluent (EtOAc 70% - light petroleum 30%). White solid; yield 47% (511.8 mg); mp 152°C. ^{1}H NMR (400 MHz, DMSO-d_6) δ 11.18 (s, 1H), 8.77 (s, 1H), 7.93 (d, J = 8.5 Hz, 2H), 7.27 (dd, J = 18.7, 12.8 Hz, 7H), 7.01 (d, J = 8.6 Hz, 3H), 3.82 (s, 3H), 3.52 (s, 2H), 2.83 (s, 2H). ES-MS (methanol) m/z: 380.2 [M+H]$^+$. HRMS (ESI-TOF) m/z C$_{19}$H$_{21}$N$_7$O$_2$: experimental 380.1827 [M+H]$^+$, theoretical 380.1829 [M+H]$^+$, Δ = 0.0002. Purity HPLC: 99.0%.

5.5.3.2.6. N'-(4-amino-6-((naphthalen-1-ylmethyl)amino)-1,3,5-triazin-2-yl)-3-methoxybenzohydrazide (**167**)

Method B; flash chromatography eluent (EtOAc 80% - light petroleum 20% to EtOAc 100%). White solid; yield 64% (742 mg); mp 173°C. ^{1}H NMR (400 MHz, DMSO-d_6) δ 10.37 (d, J = 19.0 Hz, 2H), 8.16 – 7.78 (m, 4H), 7.60 – 7.34 (m, 7H), 7.13 (d, J = 6.5 Hz, 1H), 4.96 (s, 2H), 3.80 (d, J = 6.1 Hz, 3H). ^{13}C NMR (101 MHz, DMSO-d_6) δ 194.90, 191.99, 184.09, 159.60, 133.66 (s, CH), 131.10 (s, CH), 130.12 (s, CH), 128.97 (s, CH), 126.67 (s, CH), 126.24 (s, CH), 125.90 (s, CH), 125.61 (s, CH), 123.73 (s, CH), 120.28 (s, CH$_2$), 54.80 (d, J = 192.3 Hz, CH$_3$). ES-MS (methanol) m/z: 416.2 [M+H]$^+$, 438.2 [M+Na]$^+$. HRMS (ESI-TOF) m/z C$_{21}$H$_{19}$N$_7$O$_2$: experimental 416.1827 [M+H]$^+$, theoretical 416.1829 [M+H]$^+$, Δ = 0.0002. Purity HPLC: 94.0%.

5.5.3.2.7. N'-(4-amino-6-((naphthalen-1-ylmethyl)amino)-1,3,5-triazin-2-yl)-4-methoxybenzohydrazide (**168**)

Method B; flash chromatography eluent (EtOAc 80% - light petroleum 20%). White solid; yield 39% (392.6 mg); mp 165°C. ^{1}H NMR (400 MHz, DMSO-d_6) δ 10.10 (s, 1H), 8.42 (d, J = 52.9 Hz, 1H), 7.85 (dd, J = 41.0, 4.7 Hz, 5H), 7.56 – 7.20 (m, 5H), 6.96 (t, J = 24.6 Hz, 1H), 6.31 (d, J = 43.0 Hz, 2H), 4.86 (d, J = 51.5 Hz, 2H), 3.81 (s, 3H). ^{13}C NMR (101 MHz, DMSO-d_6) δ 168.35, 162.38, 158.50, 135.68, 133.65, 131.51 (CH), 131.23 (CH), 128.93 (CH), 128.14 (CH), 126.67 (CH), 126.26 (CH), 125.93 (d, J = 9.4 Hz, CH), 123.94 (CH), 113.78 (CH), 55.73 (CH$_3$), 41.60 (CH$_2$). ES-MS (methanol) *m/z*: 416.2 [M+H]$^+$. HRMS (ESI-TOF) m/z C$_{21}$H$_{19}$N$_7$O$_2$: experimental 416.1828 [M+H]$^+$, theoretical 416.1829 [M+H]$^+$, Δ = 0.0001. Purity HPLC: 98.1%.

5.5.3.2.8. N'-(4-amino-6-((naphthalen-1-ylmethyl)amino)-1,3,5-triazin-2-yl)-3,4-dimethoxy benzohydrazide (**169**)

Method B; flash chromatography eluent (EtOAc 60% - light petroleum 40% to EtOAc 80% - light petroleum 20%). White solid; yield 27% (427 mg); mp 239°C. 1H NMR (499 MHz, DMSO-d6) δ 10.26 (s, 1H), 10.09 (s, 1H), 8.10 (d, J = 45.0 Hz, 1H), 7.84 (dd, J = 74.5, 18.2 Hz, 3H), 7.64 – 7.37 (m, 8H), 7.07 (d, J = 8.5 Hz, 1H), 4.88 (d, J = 6.0 Hz, 2H), 3.82 (d, J = 4.3 Hz, 6H). HRMS (ESI-TOF) m/z C$_{23}$H$_{23}$N$_7$O$_3$: experimental 446.1938 [M+H]$^+$, theoretical 446.1935 [M+H]$^+$, Δ = 0.0003. Purity HPLC: 97.8%.

5.5.3.2.9. N'-(4-amino-6-((naphthalen-1-ylmethyl)amino)-1,3,5-triazin-2-yl)-3,5-dimethoxy benzohydrazide (**170**)

Method B; flash chromatography eluent (EtOAc 60% - light petroleum 40% to EtOAc 80% - light petroleum 20%). White solid; yield 25% (385 mg); mp 241°C. ^{1}H NMR (499 MHz, DMSO-d_6) δ 10.17 (s, 1H), 8.49 (d, J = 94.9 Hz, 1H), 8.17 – 7.70 (m, 5H), 7.47 (d, J = 40.2 Hz, 6H), 7.08 – 6.60 (m, 3H), 4.94 – 4.70 (m, 2H), 3.70 (d, J = 54.2 Hz, 6H). ES-MS (methanol) *m/z*: 446.2 [M+H]$^+$. HRMS (ESI-TOF) m/z C$_{23}$H$_{23}$N$_7$O$_3$: experimental 446.1938 [M+H]$^+$, theoretical 446.1935 [M+H]$^+$, Δ = 0.0003. Purity HPLC: 99.9%.

5.5.3.2.10. N'-(4-amino-6-((2-methoxybenzyl)amino)-1,3,5-triazin-2-yl)-4-methoxybenzohydrazide (**171**)

Method B; flash chromatography eluent (EtOAc 60% - light petroleum 40% to EtOAc 80% - light petroleum 20%). White solid; yield 47% (562 mg); mp 231°C. ^{1}H NMR (400 MHz, DMSO-d_6) δ 10.25 (s, 1H), 10.09 (s, 1H), 7.93 – 7.76 (m, 2H), 7.00 (dt, J = 45.4, 43.3 Hz, 8H), 6.32 (d, J = 15.6 Hz, 1H), 4.40 (s, 2H), 3.80 (d, J = 7.1 Hz, 6H). HRMS (ESI-TOF) m/z C$_{19}$H$_{21}$N$_7$O$_3$: experimental 396.1779 [M+H]$^+$, theoretical 396.1779 [M+H]$^+$, Δ = 0.0000.

5.5.3.2.11. N'-(4-amino-6-((2-chlorobenzyl)amino)-1,3,5-triazin-2-yl)-3-methoxybenzohydrazide (**172**)

Method B; flash chromatography eluent (EtOAc 70% - light petroleum 30% to EtOAc 100%). Grey solid; yield 11% (146 mg); mp 253°C. ^{1}H NMR (400 MHz, DMSO-d_6) δ 10.68 (s, 1H), 8.50 (s, 1H), 7.62 – 7.06 (m, 11H), 4.67 – 4.51 (m, 2H), 3.83 (s, 3H). ^{13}C NMR (101 MHz, DMSO-d_6) δ 179.37, 178.03, 170.77, 164.92, 159.59, 133.07, 132.91, 132.29, 130.02 (t, J = 6.2 Hz, CH), 129.53 (CH), 128.95 (CH), 127.62 (d, J = 2.9 Hz, CH), 120.10 (CH), 117.77 (d, J = 1.6 Hz, CH), 113.18 (d, J = 4.2 Hz, CH), 55.81 (CH3), 41.48 (CH2). ES-MS (methanol) *m/z*: 400.2 [M+H]$^+$. HRMS (ESI-TOF) m/z C$_{18}$H$_{18}$ClN$_7$O$_2$: experimental 400.1282 [M+H]$^+$, theoretical 400.1283 [M+H]$^+$, Δ = 0.0001. Purity HPLC: 99.5%.

5.5.3.2.12. N'-(4-amino-6-((2-chlorobenzyl)amino)-1,3,5-triazin-2-yl)-4-methoxybenzohydrazide (**173**)

Method B; flash chromatography eluent (EtOAc 70% - light petroleum 30% to EtOAc 100%). White solid; yield 46% (680 mg); mp 250°C. ^{1}H NMR (400 MHz, DMSO-d_6) δ 10.16 (s, 1H), 8.42 (s, 1H), 7.83 (d, J = 7.4 Hz, 2H), 7.28 (q, J = 40.3 Hz, 7H), 6.36 (s, 2H), 4.49 (s, 2H), 2.36 (s, 3H). ^{13}C NMR (101 MHz, DMSO-d_6) δ 190.23, 187.71, 173.09, 169.07, 157.05, 141.52, 130.17, 129.75 (CH), 129.32 (t, J = 11.2 Hz, CH), 129.18 (CH), 127.88 (d, J = 1.6 Hz, CH), 127.27 (CH), 122.31, 41.55 (CH$_2$), 21.40 (s, CH$_3$). ES-MS (methanol) *m/z*:

400.2 [M+H]$^+$. HRMS (ESI-TOF) m/z C$_{18}$H$_{18}$ClN$_7$O$_2$: experimental 400.1282 [M+H]$^+$, theoretical 400.1283 [M+H]$^+$, Δ = 0.0001. Purity HPLC: 99.5%.

5.5.3.4. General procedure for the synthesis of N'-(4-amino-6-(amino substituted)-1,3,5-triazin-2-yl)-4-hydroxybenzohydrazide derivatives (**175-185**)

Under argon atmosphere 1.0 eq. of N'-(4-amino-6-substituted-1,3,5-triazin-2-yl)methoxybenzohydrazide derivatives (**163-174**) was solved in anhydrous DCM (1 mL/mmol of **163-164**). The solution was cooled to -40°C and 9-12 eq. of BBr$_3$ in anhydrous DCM (1mL/mmol BBr$_3$) was added slowly. The reaction was stirred overnight at room temperature and once completed, the mixture was cooled to 0°C and cold MeOH (15.0 mL/mmol of BBr$_3$) was inserted slowly. The solvent was removed under reduced pressure and the crude residue was purified with flash chromatography.

5.5.3.4.1.   N'-(4-amino-6-((2-hydroxybenzyl)amino)-1,3,5-triazin-2-yl)-4-hydroxybenzohydrazide (**185**)
Flash chromatography eluent (EtOAc 80% - light petroleum 20% to EtOAc 90% - MeOH 10%). White solid; yield 36% (187 mg); mp 240°C. ^{1}H-NMR (400 MHz, DMSO-d_6) δ 11.92 (s, 1H), 9.96 (d, J = 17.2 Hz, 2H), 8.40 (s, 1H), 7.74 (d, J = 8.6 Hz, 2H), 7.01 (s, 3H), 6.74 (dd, J = 22.0, 6.9 Hz,3H), 6.35 (d, J = 52.8 Hz, 2H), 4.29 (d, J = 30.4 Hz, 2H). ES-MS (methanol) m/z: 368.1 [M+H]$^+$. HRMS (ESI-TOF) m/z C$_{17}$H$_{17}$N$_7$O$_3$: experimental 368.1460 [M+H]$^+$, theoretical 368.1466 [M+H]$^+$, Δ = 0.0006. Purity HPLC: 99.9%.

5.5.3.4.2.   N'-(4-amino-6-(benzylamino)-1,3,5-triazin-2-yl)-3-hydroxybenzohydrazide (**175**)
Flash chromatography eluent (DCM 88% - MeOH 12%). White solid; yield 30% (83 mg); mp 272°C. ^{1}H-NMR (400 MHz, DMSO-d_6) δ 10.70 + 10.52 (bs, 1H), 10.00 + 9.79 (bs, 1H), 9.12 – 7.57 (m, 1H), 7.57 – 7.12 (m, 9H), 7.01 (bs, 1H), 4.55 + 4.38 (bs, 2H). ^{1}H-NMR (400 MHz, DMSO-d_6, 80 °C) δ 10.39 (s, 1H), 9.95 (bs, 1H), 9.51 (bs, 1H), 8.49 (bs, 1H), 7.70 (bs, 2H), 7.51 – 7.12 (m, 8H), 7.00 (d, J = 6.3 Hz, 1H), 4.53 (s, 2H). ^{13}C-NMR (400 MHz, DMSO-d_6) δ 43.30 (CH$_2$), 114.43 (CH), 118.03 (CH), 119.04 (CH), 127.04 (CH), 127.93 (CH), 128.19 (CH), 129.40 (CH). No signals were detected for quaternary carbons. HRMS (ESI-TOF) m/z C$_{17}$H$_{17}$N$_7$O$_2$: experimental 352.1518 [M+H]$^+$, theoretical 352.1516 [M+H]$^+$, Δ = 0.0002. Purity HPLC: 97.8%.

5.5.3.4.3.   N'-(4-amino-6-(benzylamino)-1,3,5-triazin-2-yl)-3,4-dihydroxybenzohydrazide (**176**)
Flash chromatography eluent (DCM 90% - MeOH 10%). White solid; yield 12% (29 mg); mp 236°C. ^{1}H-NMR (400 MHz, CD$_3$OD) δ 7.51 – 7.06 (m, 7H), 6.82 (d, J = 8.2 Hz, 1H), 4.53 (bs, 2H). ES-MS (methanol) m/z: 368.2 [M+H]$^+$, 390.1 [M+Na]$^+$. HRMS (ESI-TOF) m/z C$_{17}$H$_{17}$N$_7$O$_2$: experimental 368.1464 [M+H]$^+$, theoretical 368.1466 [M+H]$^+$, Δ = 0.0002. Purity HPLC: 100%.

5.5.3.4.4.   N'-(4-amino-6-(phenethylamino)-1,3,5-triazin-2-yl)-3-hydroxybenzohydrazide (**177**)
Flash chromatography eluent (DCM 90% - MeOH 10%). White solid; yield 5% (9.1 mg); mp 231°C. ^{1}H NMR (400 MHz, DMSO-d_6) δ 11.21 (s, 1H), 10.09 (s, 1H), 9.79 – 9.57 (m, 1H), 7.86 (t, J = 52.8 Hz, 2H), 7.52 – 7.05 (m, 8H), 6.91 (dd, J = 20.8, 5.8 Hz, 2H), 3.47 (d, J = 33.7 Hz, 2H), 2.85 (dd, J = 17.9, 10.6 Hz, 2H). ES-MS (methanol) m/z: 366.2 [M+H]$^+$. HRMS (ESI-TOF) m/z C$_{18}$H$_{19}$N$_7$O$_2$: experimental 366.1675 [M+H]$^+$, theoretical 366.1673 [M+H]$^+$, Δ = 0.0002. Purity HPLC: 99.2%.

5.5.3.4.5.   N'-(4-amino-6-(phenethylamino)-1,3,5-triazin-2-yl)-4-hydroxybenzohydrazide (**178**)
Flash chromatography eluent (EtOAc 90% - MeOH 10%). White solid; yield 8% (37 mg); mp 243°C. ^{1}H NMR (400 MHz, DMSO-d_6) δ 9.99 (d, J = 37.9 Hz, 2H), 8.31 (d, J = 85.3 Hz, 1H), 7.78 (d, J = 8.2 Hz, 2H), 7.40 – 6.94 (m, 5H), 6.80 (d, J = 8.7 Hz, 3H), 6.23 (d, J = 65.7 Hz, 2H), 3.40 (s, 2H), 2.69 (d, J = 63.5 Hz, 2H). ^{13}C NMR (101 MHz, DMSO-d_6) δ 197.39, 196.27, 173.61, 170.78, 160.83, 143.87, 141.39, 129.84 (CH), 129.07 (d, J = 2.3 Hz, CH), 128.66 (d, J = 3.4 Hz, CH), 124.02 (d, J = 0.9 Hz, CH), 115.27 (CH), 42.07 (CH$_2$), 35.73

(CH$_2$). ES-MS (methanol) m/z: 366.2 [M+H]$^+$. HRMS (ESI-TOF) m/z C$_{18}$H$_{19}$N$_7$O$_2$: experimental 366.1675 [M+H]$^+$, theoretical 366.1673 [M+H]$^+$, Δ = 0.0002. Purity HPLC: 99.8%.

5.5.3.4.6. N'-(4-amino-6-((naphthalen-1-ylmethyl)amino)-1,3,5-triazin-2-yl)-3-hydroxybenzohydrazide (**179**)

Flash chromatography eluent (EtOAc 90% - MeOH 10%). White solid; yield 4% (6.6 mg); mp 250°C. ^{1}H NMR (400 MHz, DMSO-d_6) δ 10.09 (s, 1H), 9.64 (s, 1H), 8.44 (d, J = 44.1 Hz, 1H), 8.27 – 7.66 (m, 3H), 7.65 – 7.16 (m, 8H), 6.93 (d, J = 9.2 Hz, 1H), 6.27 (d, J = 58.0 Hz, 1H), 4.86 (d, J = 44.5 Hz, 2H). ^{13}C NMR (101 MHz, DMSO-d_6) δ 198.63, 184.81, 162.82, 157.93 (d, J = 57.6 Hz), 157.64, 136.90, 135.56 (CH), 135.12 (d, J = 88.0 Hz, CH), 133.60 (CH), 129.82 (CH), 128.87 (CH), 127.39 (CH), 123.79 (CH), 118.82 (CH), 114.62 (CH), 41.58 (CH$_2$). ES-MS (methanol) m/z: 401.2 [M+H]$^+$, 424.2 [M+Na]$^+$. HRMS (ESI-TOF) m/z C$_{21}$H$_{19}$N$_7$O$_2$: experimental 402.1671 [M+H]$^+$, theoretical 402.1673 [M+H]$^+$, Δ = 0.0002. Purity HPLC: 82.2%.

5.5.3.4.7. N'-(4-amino-6-((naphthalen-1-ylmethyl)amino)-1,3,5-triazin-2-yl)-4-hydroxybenzohydrazide (**180**)

Flash chromatography eluent (EtOAc 100%). White solid; yield 8% (17.9 mg); mp 264°C. ^{1}H NMR (400 MHz, DMSO-d_6) δ 8.29 (d, J = 3.4 Hz, 4H), 8.13 (d, J = 7.9 Hz, 2H), 7.98 (t, J = 8.0 Hz, 3H), 7.68 – 7.51 (m, 5H), 4.53 (dd, J = 10.6, 4.7 Hz, 2H). ES-MS (methanol) m/z: 401.2 [M+H]$^+$. HRMS (ESI-TOF) m/z C$_{21}$H$_{19}$N$_7$O$_2$: experimental 402.1674 [M+H]$^+$, theoretical 402.1673 [M+H]$^+$, Δ = 0.0001. Purity HPLC: 91.4%.

5.5.3.4.8. N'-(4-amino-6-((naphthalen-1-ylmethyl)amino)-1,3,5-triazin-2-yl)-3,4-dihydroxybenzohydrazide (**181**)

Flash chromatography eluent (EtOAc 70% - light petroleum 30% to EtOAc 90% - MeOH 10%). White solid; yield 8% (31 mg); mp 262°C. ES-MS (methanol) m/z C$_{21}$H$_{19}$N$_7$O$_3$: 418.2 [M+H]$^+$. Purity HPLC: 98.4%.

5.5.3.4.9. N'-(4-amino-6-((naphthalen-1-ylmethyl)amino)-1,3,5-triazin-2-yl)-3,5-dihydroxybenzohydrazide (**182**)

Flash chromatography eluent (EtOAc 70% - light petroleum 30% to EtOAc 90% - MeOH 10%). White solid; yield 26% (92 mg); mp 265°C. ^{1}H NMR (499 MHz, DMSO-d_6) δ 11.09 (s, 1H), 10.42 (s, 1H), 9.61 (s, 1H), 9.59 (s, 1H), 8.11 (s, 2H), 7.96 (d, J = 10.0 Hz, 2H), 7.86 (d, J = 22.5 Hz, 1H), 7.59 – 7.42 (m, 3H), 6.76 (s, 2H), 6.68 – 6.64 (m, 1H), 6.46 – 6.38 (m, 2H), 5.01 (s, 2H). ES-MS (methanol) m/z: 418.1 [M+H]$^+$, 440.0 [M+Na]$^+$. HRMS (ESI-TOF) m/z C$_{21}$H$_{19}$N$_7$O$_3$: experimental 402.1639 [M+H]$^+$, theoretical 402.1622 [M+H]$^+$, Δ = 0.0017. Purity HPLC: 95.3%.

5.5.3.4.10. N'-(4-amino-6-((2-chlorobenzyl)amino)-1,3,5-triazin-2-yl)-3-hydroxybenzohydrazide (**183**)

Flash chromatography eluent (EtOAc 70% - light petroleum 30% to EtOAc 90% - MeOH 10%). White solid; yield 45% (111 mg); mp 260°C. ^{1}H NMR (400 MHz, DMSO-d_6) δ 11.91 (s, 1H), 10.26 (d, J = 49.0 Hz, 1H), 9.70 (d, J = 21.0 Hz, 1H), 7.23 (ddd, J = 131.5, 74.7, 17.9 Hz, 11H), 4.65 – 4.40 (m, 2H). ^{13}C NMR (101 MHz, DMSO-d_6) δ 185.95, 183.52, 162.59, 158.11, 157.37, 140.05, 129.46 (CH), 129.24 (CH), 128.84 (d, J = 11.4 Hz, CH), 119.25 (CH), 118.43 (CH), 114.61 (CH), 41.76 (CH$_2$). ES-MS (methanol) m/z: 386.1 [M+H]$^+$, 408.1 [M+Na]$^+$. HRMS (ESI-TOF) m/z C$_{16}$H$_{17}$ClN$_7$O$_2$: experimental 386.1122 [M+H]$^+$, theoretical 386.1127 [M+H]$^+$, Δ = 0.0005. Purity HPLC: 94.2%.

5.5.3.4.11. N'-(4-amino-6-((2-chlorobenzyl)amino)-1,3,5-triazin-2-yl)-4-hydroxybenzohydrazide (**184**)

Flash chromatography eluent (EtOAc 70% - light petroleum 30% to EtOAc 90% - MeOH 10%). White solid; yield 22% (42.4 mg); mp 261°C. ^{1}H NMR (400 MHz, DMSO-d_6) δ 11.88 (s, 1H), 10.08 (d, J = 62.4 Hz, 1H), 8.37 (d, J = 31.8 Hz, 1H), 7.80 (dd, J = 15.3, 9.4 Hz, 2H), 7.55 – 6.97 (m, 6H), 6.78 (dd, J = 14.6, 8.6 Hz, 1H), 6.34 (s, 2H), 4.47 (s, 2H). ES-MS (methanol) m/z: 408.1 [M+Na]$^+$. HRMS (ESI-TOF) m/z C$_{16}$H$_{17}$ClN$_7$O$_2$: experimental 386.1127 [M+H]$^+$, theoretical 386.1127 [M+H]$^+$, Δ = 0.0000. Purity HPLC: 95.1%.

5.5.3.5. Synthesis of 6-(4-methylbenzyl)-N^2-(naphthalen-1-ylmethyl)-1,3,5-triazine-2,4-diamine (**186**)

A) 1.20 g (6.40 mmol, 1.0 eq) of 1-(bromomethyl)-4-methylbenzene and 1.95 g (7.68 mmol, 1.0 eq) of 4,4,4',4',5,5,5',5'-octamethyl-2,2'-bi(1,3,2-dioxaborolane) were solved in 25.0 mL of 1,4-dioxane under argon atmosphere. To the solution, 2.65 g (19.2 mmol, 3.0 eq) of K_2CO_3 and 370 mg (0.32 mmol, 0.05 eq) of Pd(PPh$_3$)$_4$ were added. The reaction was refluxed for 6 h and once completed, the solvent was removed under reduced pressure and the crude was solved in 90 mL of water and extracted with EtOAc (3 x 30 mL). The solvent was eliminated under vacuum to obtain a yellow oil directly used in the following step. ES-MS (methanol) m/z $C_{14}H_{21}BO_2$: 255.0 [M+Na]$^+$.

B) 102 mg (0.36 mmol, 1.0 eq) of 6-chloro-N^2-(naphthalen-1-ylmethyl)-1,3,5-triazine-2,4-diamine (**x**) and 100 mg (0.43 mmol, 1.2 eq) of 4,4,5,5-tetramethyl-2-(4-methylbenzyl)-1,3,2-dioxaborolane synthesized in step A were solved in 2.0 mL of 1,4-dioxane, 2.0 mL of ethanol and 1.0 mL of water in a microwave tube under argon atmosphere. To the mixture 76.0 mg (0.72 mmol, 3.0 eq) of Na_2CO_3 and 13 mg (0.018 mmol, 0.05 eq) of PdCl$_2$(PPh$_3$)$_2$ were added and the reaction was stirred at 130°C for 2 h on microwave. Once completed, the catalyst was removed over celite plug and the mixture was extracted with EtOAc (10 mL) and washed with water. The crude residue was purified with flash chromatography (light petroleum 80% - EtOAc 20%) to afford 55 mg of white solid; yield 37%; mp 276°C. ES-MS (methanol) m/z: 356.2 [M+H]$^+$. HRMS (ESI-TOF) m/z $C_{22}H_{21}N_5$: experimental 356.1866 [M+H]$^+$, theoretical 356.1870 [M+H]$^+$, $\Delta = 0.0004$.

5.5.3.6. General procedure for the synthesis of N^2-benzyl-N^4-substituted-1,3,5-triazine-2,4,6-triamine derivatives (**187-189**)

Method A) 1.0 eq. of N^2-benzyl-6-chloro-N^4-substituted-1,3,5-triazine-2,4-diamine (**156-157**) was allowed to react with 1.0 eq. of desired amine in a sealed tube. The reaction was heated to 120°C and stirred for 3-12h. Once completed, the crude residue was purified with flash chromatography.

Method B) 1.0 eq. of N^2-benzyl-6-chloro-N^4-substituted-1,3,5-triazine-2,4-diamine (**172**) was solved in BuOH (1.0 mL/mmol of **x**) in a sealed tube. To the solution 1.0 eq. of desired amine was added and the reaction was stirred at 130°C overnight. Once completed, the crude residue was purified with flash chromatography.

5.5.3.6.1. N^2,N^4-dibenzyl-1,3,5-triazine-2,4,6-triamine (**187**)
Method A. Flash chromatography eluent (light petroleum 70% - EtOAc 30%). White solid; yield 45% (413 mg); mp 256°C. ^{1}H NMR (400 MHz, DMSO-d_6) δ 7.15 (dd, $J = 76.9, 39.0$ Hz, 12H), 6.09 (d, $J = 60.1$ Hz, 2H), 4.44 (s, 4H). MicrOTOF-Q (methanol) m/z $C_{17}H_{18}N_6$: 307.1591 [M+H]$^+$. Purity HPLC: 99.5%.

5.5.3.6.2. N^2-benzyl-6-(piperazin-1-yl)-1,3,5-triazine-2,4-diamine (**189**)
Method B. Flash chromatography eluent (EtOAc 90% - light petroleum 10%). White solid; yield 3% (10 mg); mp 232°C. ^{1}H NMR (400 MHz, DMSO-d_6) δ 7.30 – 7.06 (m, 6H), 6.15 (d, $J = 49.2$ Hz, 2H), 4.38 (d, $J = 7.2$ Hz, 2H), 3.69 – 3.55 (m, 4H), 2.71 (d, $J = 4.7$ Hz, 4H). ES-MS (methanol) m/z: 286.4 [M+H]$^+$. HRMS (ESI-TOF) m/z $C_{14}H_{19}N_7$: experimental 286.1776 [M+H]$^+$, theoretical 286.1775 [M+H]$^+$, $\Delta = 0.0001$. Purity HPLC: 98.4%.

5.5.3.6.3. N^2,N^4-dibenzyl-N^6-ethyl-1,3,5-triazine-2,4,6-triamine (**188**)
Method A. Flash (light petroleum 70% - EtOAc 30%). White solid; yield 24% (85 mg); mp 265°C. ^{1}H NMR (400 MHz, DMSO-d_6) δ 7.11 (dd, $J = 98.4, 60.8$ Hz, 10H), 6.46 (d, $J = 61.4$ Hz, 2H), 4.40 (s, 4H), 3.26 – 3.11 (m, 2H), 1.02 (d, $J = 5.3$ Hz, 3H). MicrOTOF-Q (methanol) m/z $C_{10}H_{22}N_6$: 335.1918 [M+H]$^+$. Purity HPLC: 99.5%.

5.5.3.6.4.   N^2-benzyl-N^4-(4-fluoro-1H-indazol-3-yl)-1,3,5-triazine-2,4,6-triamine (142)
Method B. Flash chromatography eluent (EtOAc 90% - light petroleum 10%). Dark yellow solid; yield 18% (27.2 mg); mp 276°C. ^{1}H NMR (400 MHz, DMSO-d_6) δ 12.22 (s, 1H), 9.17 (s, 1H), 8.79 – 8.30 (m, 1H), 8.13 (d, J = 8.0 Hz, 1H), 7.29 (dd, J = 115.6, 65.3 Hz, 9H), 6.19 (s, 1H), 4.57 (s, 2H). ^{13}C NMR (101 MHz, DMSO-d_6) δ 187.53, 168.28, 162.85, 157.03, 152.99, 150.31, 137.80, 136.08 (CH), 135.72 (CH), 128.80 (d, J = 11.6 Hz, CH), 128.01 (CH), 127.87 – 127.62 (CH), 127.29 (CH), 109.99 (CH), 102.13 (CH$_2$). ES-MS (methanol) m/z: 351.2 [M+H]$^+$.

5.5.3.6.5.   N^2-(4-fluoro-1H-indazol-3-yl)-6-(piperazin-1-yl)-1,3,5-triazine-2,4-diamine (191)
Obtained directly deprotected; method B. Flash chromatography eluent (EtOAc 100%). White solid; yield 14% (22.3 mg); mp 286°C. ^{1}H NMR (400 MHz, DMSO-d_6) δ 12.80 (s, 1H), 7.75 (s, 1H), 7.50 – 7.38 (m, 1H), 7.07 – 6.89 (m, 2H), 6.26 (dt, J = 15.5, 8.2 Hz, 1H), 3.63 (d, J = 47.0 Hz, 4H), 2.82 – 2.56 (m, 4H). ES-MS (methanol) m/z: 330.1 [M+H]$^+$. HRMS (ESI-TOF) m/z C$_{14}$H$_{16}$FN$_9$: experimental 330.1586 [M+H]$^+$, theoretical 330.1585 [M+H]$^+$, Δ = 0.0001. Purity HPLC: 98.4%.

5.5.3.6.6.   N^2-benzyl-N^4-(3-(pyridin-2-yl)-1H-1,2,4-triazol-5-yl)-1,3,5-triazine-2,4,6-triamine (193)
Method B. Flash chromatography eluent (EtOAc 90% - light petroleum 10%). White solid; yield 9% (20 mg); mp 291°C. ^{1}H NMR (400 MHz, DMSO-d_6) δ 8.61 (dd, J = 10.1, 4.1 Hz, 1H), 7.91 (d, J = 20.9 Hz,12H), 7.46 – 7.06 (m, 10H), 4.51 (dd, J = 21.0, 5.0 Hz, 2H). ES-MS (methanol) m/z: 361.6 [M+H]$^+$. HRMS (ESI-TOF) m/z C$_7$H$_{16}$N$_{10}$: experimental 361.1632 [M+H]$^+$, theoretical 361.1632 [M+H]$^+$, Δ = 0.0000.

5.5.4.   Synthesis of 1-(4-amino-6-(benzylamino)-1,3,5-triazin-2-yl)-3-(p-tolyl)urea (196)

5.5.4.1. Synthesis of 6-chloro-1,3,5-triazine-2,4-diamine (194)
5.0 g (27.1 mmol, 1.0 eq) of 2,4,6-trichloro-1,3,5-triazine (193) was dissolved in 80 mL of hot acetone. 7.36 mL (108 mmol, 4.0 eq) of ammonia and 28 mL of water were added and the reaction was refluxed at 45°C for 5 h. Once completed, the mixture was filtered and washed with water. The product was dried in oven at 100°C to afford 4.9 g of x. White solid, yield q.y. ES-MS (methanol) m/z C$_3$H$_4$ClN$_5$: 145.8 [M+H]$^+$.

5.5.4.2. Synthesis of 1-(4-amino-6-chloro-1,3,5-triazin-2-yl)-3-(p-tolyl)urea (195)
300 mg (2.06 mmol, 1.0 eq) of 6-chloro-1,3,5-triazine-2,4-diamine (194) were solved under argon atmosphere in 4.0 mL of THF. 350 μL of (2.68 mmol, 1.3 eq) 1-isocyanato-4-methylbenzene were added and the reaction was refluxed overnight. Once completed, the mixture was filtered to collect 267 mg of white solid. Yield 47%. ES-MS (methanol) m/z C$_{11}$H$_{11}$ClN$_6$O: 279.1 [M+H]$^+$.

5.5.4.3. Synthesis of 1-(4-amino-6-(benzylamino)-1,3,5-triazin-2-yl)-3-(p-tolyl)urea (196)
In a sealed tube 260 mg (0.93 mmol, 1.0 eq) of 1-(4-amino-6-chloro-1,3,5-triazin-2-yl)-3-(p-tolyl)urea (195) were reacted with 102 μL (0.93 mmol, 1.0 eq) of benzylamine. The reaction was heated to 90°C overnight. Once completed, the crude residue was purified with flash chromatography (light petroleum 60% - EtOAc 40%) affording 112 mg of a white solid. Yield 34%; mp 253°C. HRMS (ESI-TOF) m/z C$_{18}$H$_{19}$N$_7$O: experimental 372.1542 [M+Na]$^+$, theoretical 372.1543 [M+Na]$^+$, Δ = 0.0001. Purity HPLC: 97.0%.

5.5.5.   Computational procedures
5.5.5.6.   Docking studies

Docking studies were performed using Flap 2.2.1 as software. GRID MIF protocol was used to obtain docking 3D binding pose and residue interaction 2D map. Target (PDB ID:4HNF) and dataset of smiles of molecules ("*.smi*") were loaded. The structure-based analysis was settled using dry, H, N, O probes and the binding mode with higher S-score was chosen. The 3D docking representation was provided with highlighted hydrogen bonds while the residue interactions 2D map was given with hydrophobic interactions and hydrogen bonds.

5.5.6.   Biochemistry

5.5.6.6.   CK1δ activity assays

Assays with truncated (1-294 aa) CK1δ. Compounds were tested on commercially available CK1δ (Merck Millipore, recombinant human, amino acids 1e294, GST-tagged N-terminal) with KinaseGlo® luminescence kit (Promega). Experiments were performed in 96-well plate (white, flat bottom) using buffer prepared as follow: 50 mM HEPES (pH 7.5), 1 mM EDTA, 1 mM EGTA and 15 mM magnesium acetate. Compound PF-670462 (IC$_{50}$ CK1δ 0.014 μM) was used as a positive control at the concentration of 40 μM while a solution of DMSO/buffer as negative control. Firstly, 10 μL of inhibitor solution was inserted in the well (10 mM stock solution in DMSO was diluted with buffer) followed by 10 μL of enzyme (16 ng of CK1δ) and 20 μL of casein substrate 0.1% and 2 μM ATP (final concentration) (to perform ATP-competition increasing concentrations were chosen: 1, 2, 10, 50 μM). The final DMSO concentration in the mixture did not exceed 1-2%. After 60 minutes of incubation at 30°C, the enzymatic reaction was stopped with 40 μL of KinaseGlo reagent (Promega). Luminescence signal (RLU) was recorded after 10 minutes at 25°C using Tecan Infinite M100. The inhibitory activities were calculated in relation to the maximal activity (absence of inhibitor). As preliminary screening, each compound was assayed at the concentration of 40 μM, consequently, for derivative that reported an activity percentage less than 50% at the concentration, IC$_{50}$s were performed in triplicate and reported as mean ± standard error. Results were elaborated with Excel and GraphPad Prism 8.0.

ATP-competition assays were performed following the just described procedure by firstly performed the ATP calibration line to obtain the slope. The two chosen inhibitor's concentrations agree with the IC$_{50}$ of the compound (the concentration at its IC$_{50}$ and the double) and the experiment was conducted at the presence of increasing ATP concentrations: 1, 2, 10, 50 μM. The mean of the RLU value was divided for the slope of the calibration line and the mean of negative controls were subtracted by the ATP consumed; the reciprocal characterizes the x axis of the Lineweaver-Burk plot. The ATP consumed divided for volume of reaction (40 μL) provides the y value. Results were elaborated using Excel and GraphPad Prism 8.0.

5.5.6.7.   GSK3β activity assays

<u>GSK3β of most promising compounds was developed during the Erasmus program in the research group of Prof. Ana Martinez (CSIC-Madrid-ES).</u> Compounds were tested on commercially available full-length GSK3β (Thermo-Scientific) with KinaseGlo® luminescence kit (Promega). Experiments were performed in 96-well plate (white, flat bottom) using buffer prepared as follow: 40 mM Tris pH 7.5, 20 mM magnesium chloride, 0.1% mg/mL BSA and 50 μM DTT. As a positive control, the reaction mixture without enzyme was used while the solution with enzyme, ATP and substrate as negative control. Firstly, 10 μL of inhibitor solution was inserted in the well (10 mM stock solution in DMSO has been diluted with buffer) followed by 10 μL of GS-2 as substrate (0.2 μg/μL), 10 μL of ATP (starting from a stock solution at 8 mM, it was diluted with buffer to achieve an initial concentration of 4 μM) and 10 μL of enzyme (1 ng/μL). The final DMSO concentration in the mixture did not exceed 1-2%. After 60 minutes of incubation at 25°C, the enzymatic reaction was stopped with 40 μL of KinaseGlo reagent (Promega). Luminescence signal (RLU) was recorded after 10 minutes at 25°C using Tecan Promega. The inhibitory activities were calculated in relation to the maximal activity (absence of inhibitor). As preliminary screening, each compound was assayed at the concentration of 10 μM, consequently, for derivative that reported an activity percentage less than 50% at the concentration, IC$_{50}$s were performed in triplicate and reported as mean ± standard error. Results were elaborated with Excel and GraphPad Prism 8.0.

5.5.6.8.   CNS permeation prediction: BBB-PAMPA

CNS prediction of most promising derivatives was evaluated using Parallel Artificial Membrane Permeability Assay (PAMPA). Ten commercial drugs with known permeability were included in the experiment to obtain cut-off values (2-6 mg of Caffeine, Enoxacine, Hydrocortisone, Desipramine, Ofloxacine, Piroxicam, Testosterone and 12-15 mg of Promazine, Verapamil and 23 mg of Atenolol dissolved in 1000 μL of ethanol,

then diluted with buffer when it is required). Compounds were dissolved in a 70/30 PBS pH 7.4 buffer/ethanol solution in the appropriate concentration determining absorbance values in the UV-VIS light spectrum. 5 mL of solutions were filtered with PVDF memnrane filters (diameter 30 mm, pore size 0.45 mm). The acceptor 96-well plate (MultiScreen 96-well Culture Tray clear, Merck Millipore) was filled with 180 μL of buffer (70/30). In the donor 96-well plate ((Multiscreen® IP Sterile Plate PDVF membrane, pore size is 0.45 mM, Merck Millipore) 4 μL/well of porcine lipid brain (Merck Millipore) in dodecane (20 mg/ml) were added and, after 5 minutes, 180 μL of inhibitor solutions were inserted. Once completed, the donor plate was carefully located on the acceptor one to make a "sandwich" and, after 2.5h of incubation at 25°C, the dolor plate was removed. The absorbance values at dedicated wavelengths were red using Tecan Infinite M1000. Experiment was conducted in duplicate. The permeability coefficient (Pe) of each compound was established in centimeter per second.

$$Pe = \frac{Vd \cdot Vr}{(Vd + Vr) \cdot S \cdot t} \cdot \frac{100 \cdot Vd}{100 \cdot Vd - \%T(Vd + Vr)}$$

$$\%T = \frac{Vr \cdot Ar}{Ad \cdot Vd} \cdot 100$$

Where Vd and Vr are volumes of donor and acceptor solution (0.18 cm^3), S is the membrane area (0.266 cm^2), time of incubation (2.5 h ¼ 9000 s), Ar is the absorbance of the receptor plate after the experiment and Ad0 is the absorbance in the donor compartment before incubation. Results are given as the mean and the average of the two runs ± standard deviation (SD) is reported. Obtained results for quality control drugs were then correlated to permeability data found in the literature. The linear correlation between experimental and literature permeability values was used for the classification of compounds in those able to cross the BBB by passive permeation (CNS+ which correlate with a bibliographic Pe > 4) and those not (CNS- which correlate with a bibliographic Pe < 2). Compounds correlating with reported Pe values from 2 to 4·10^{-6} cm s^{-1} are classified as CNS+/-.

5.5.7. *In vitro* experiments on neuroblastoma cell lines (SH-SY5Y)
Biological investigation of most promising derivatives was conducted during the Erasmus program in the group of Prof. Ana Martinez (CSIC-Madrid-ES).

5.5.7.6. MTT assays
The human neuroblastoma SH-SY5Y cell line was propagated in Dulbecco's Modified Eagle Medium (DMEM) containing L-glutamine (2mM), 1% non-essential amino acids, 1% penicillin/streptomycin and 10% fetal bovine serum (FBS) under humidified 5% CO$_2$. Once semiconfluence was achieved, cells were countered using TC10™ Automated Cell Counter Bio-Rad Laboratories (CSIC-Madrid) and 80000 cells/well were plated in 96-well plate. After 24h of incubation, compounds were inserted at the concentrations of 5 and 10 μM (the stock solution in DMSO was diluted with DMEM to obtain the right final concentration) and, after another 24h of incubation, DMEM was removed and MTT reactive (3-[4,5- Dimethylthiazol-2-yl]-2,5-Diphenyltetrazolium Bromide) was added at the concentration of 20 mg/mL. After 2h, absorbance was recorded, and cell survival was estimated as percentage of value of untreated control (mean of six wells). Three independent experiments were carried out.

6.   Conclusions and future perspectives

Series of ATP-competitive CK1δ inhibitors by exploring heteroaromatic systems were developed outlining the SAR profile. Three main strategies have been applied to rationalize the scaffolds selection. Several substituents of different size and nature were inserted to functionalize the free positions of the main nuclei.

1) **Metabolism-based design**. Starting from riluzole (**34**) that proved to be active on CK1δ, its N-hydroxylamine metabolite (**39**) was developed confirming the hypothesis of the activity towards the target. This is an important achievement contributing to explain the mechanism of action of candidate **34** that is still unclear. The hydrazine derivative (**42**) was developed improving the IC_{50} and a series of functionalized benzo[*d*]thiazole compounds was synthesized obtaining promising results and more potent derivatives. Riluzole and best candidates were characterized from biological point of view with encouraging data. As future perspectives further experiments of western blot analysis as well as the conclusion of *in vivo* investigation on *Drosophila* will be conducted for riluzole (**34**).

2) **New scaffold-based strategy**. A screening of in-house compounds led to the development of a series of tri- and tetra-substituted pyrazines. Several appealing compounds were highlighted achieving an IC_{50} of 69.0 nM, this lead derivative displayed neuroprotective features. The SAR investigation will be deepened studying lots of substituents to be inserted in the four positions of the scaffold.

3) **Simplification approach**. Considering the [1,2,4]triazolo[1,5-*a*]triazine **35** that reported an IC_{50} of 0.18 μM, the simplification of the bicyclic ring allows to reduce the number and the complexity of the synthetic steps. A series of 1,3,5-triazines was investigated obtaining activities in the high micromolar range. Derivative **174** (IC_{50} = 19.6 μM) was combined with an indazole fragment achieving a molecular hybrid that proved to be more active on CK1δ with an IC_{50} of 3.86 μM (**142**). Therefore, this strategy will be followed to optimize the obtained hit compound.

Promising results were achieved with series of heteroaromatic candidates. To conclude, the SAR investigation as well as the biological characterization will be deepened.

7.   Appendix

7.1. Developing of lead compound 5-(7-amino-5-(benzylamino)-[1,2,4]triazolo[1,5-*a*][1,3,5]triazin-2-yl)benzene-1,3-diol (**35**): biochemical and biological investigation

7.1.1. Aim of the work

A series of TP and TT bicyclic scaffold compounds have been developed and published exploring the four positions of the rings to outline a deep SAR investigation (**Fig. 110**). [209]

TP scaffold   **TT scaffold**
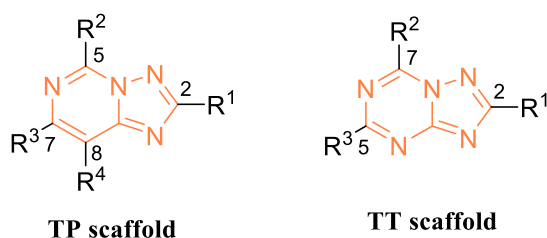
Figure 110: representation of TP and TT scaffolds.

 As previously discussed, compound **35** has proved to be the best compound showing an IC_{50} on truncated CK1δ of 0.18 μM. Given the promising activity, the derivative, previously synthesized by the research group, has been collected in a large amount in order to achieve a complete characterization from the biochemical and biological point of view. In addition to enzymatic assays conducted and BBB-permeability prediction, the appealing candidate has been screened in a panel of 452 kinases exploring its selectivity profile. [209] Moreover, **35** has been tested *in vitro* in non-tumoral lymphocytes in collaboration with Prof. Viola of University of Padua [209] and in neuroblastoma cell lines during the Erasmus program in Prof. Ana Martinez's group investigating neuroprotection features (CSIC-Madrid-ES). *In vivo* preliminary results have then collected on *Drosophila* by Prof. Marco Bisaglia (University of Padua). Finally, an example of application has been provided by trying to include the compound in Superparamagnetic Iron Oxide Nanoparticles in collaboration with Dr. Stefano Valente (Prof. Pasquato's research group, University of Trieste) to improve BBB properties providing the explication of its function at the central level.

7.1.2. Discussion

7.1.2.1.   Chemistry

Compound **35** has been *de novo* synthesized by optimizing synthetic pathway as showed in **Scheme 15** to improve overall yield achieving the percentage of 2.4% starting from 0.36% and to collect a large amount of final product. 3,5-dimethoxybenzo hydrazide **200** has been obtained through an initial esterification catalyzed by H_2SO_4 (**198**) and subsequential methoxylation (**199**). Precursor **200** has been allowed to react with triphenoxy triazine, previously synthesized starting from cyanuric chloride (**201**), in DBU. Proceeding in **scheme 15**, intramolecular cyclization has occurred using hexamethyldisiloxane (HMDSO) and phosphorus pentoxide (P_2O_5) to afford compound **202**, that was successively aminated (**203**). Benzylamine has been inserted at the 5-position of the bicyclic ring (**204**) and finally, derivative **35** has been achieved *via* deprotection using boron tribromide (BBr_3).
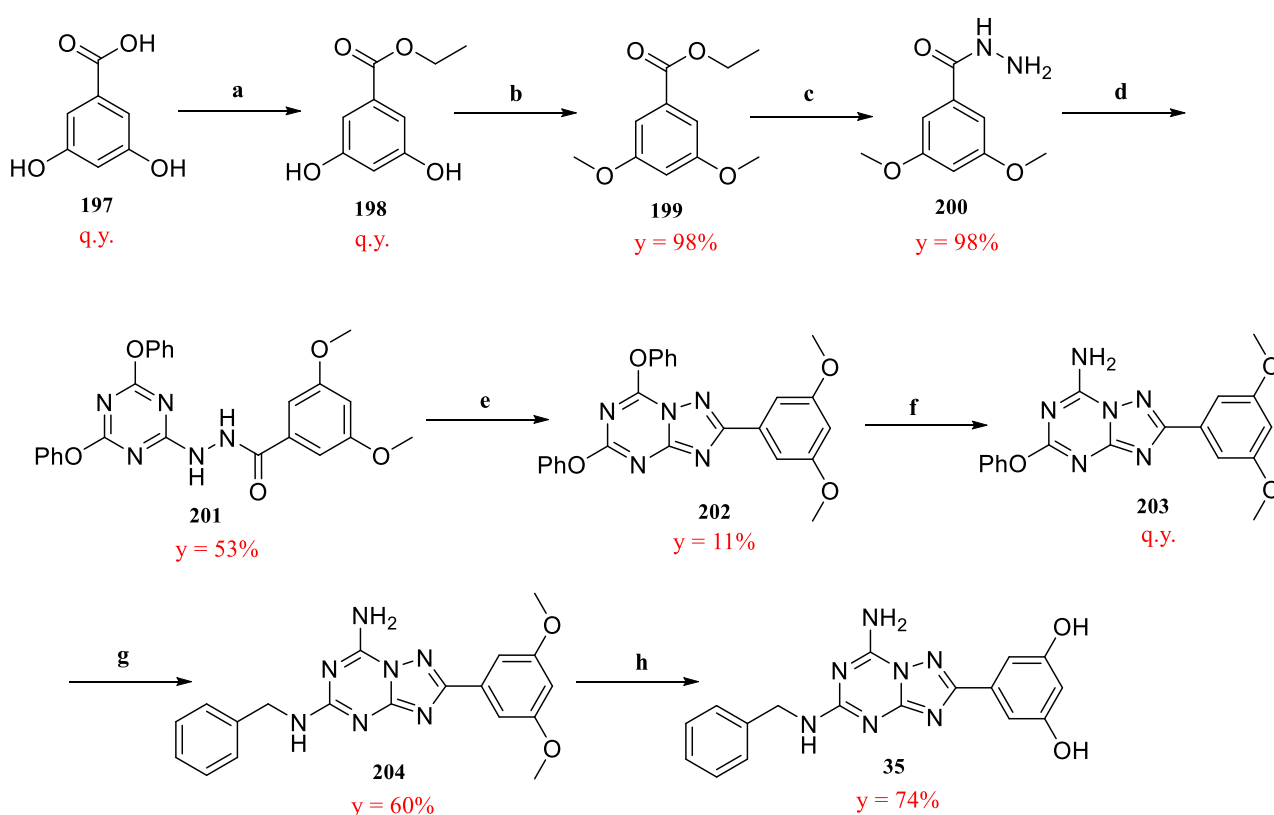
Scheme 15: synthesis of compound 35. Reagents and conditions. a: EtOH, H₂SO₄, rfx, overnight; b: CH₃I, K₂CO₃, acetone, rfx, overnight; c: NH₂NH₂·H₂O, EtOH, rfx, overnight; d: 2,4,6-triphenoxytriazine, DBU, dry THF, r.t., overnight, Ar; e: P₂O₅, HMDSO, xylene, 140°C, 3h, Ar; f: NH₃ 7N, MeOH, r.t., overnight; g: benzylamine, BuOH, 170°C, MW, 100W, 2h; h: BBr₃, dry DCM, -40°C to r.t., overnight, Ar; y = yield, q.y. = quantitative yield.

Yields of the reactions for the achievement of compound **35** have been improved as displayed in **Table 23**. A marked difference can be displayed in reactions **g** and **h**; in *de novo* synthesis of compound **35**, the nucleophilic substitution with benzylamine to obtain derivative **204** has been performed in microwave achieving a yield of 60% (**g**). Regarding the deprotection of **204**, work-up of the reaction has been improved to arrive at a 74% of yield (**h**).

*Table 23: comparison of yields registered in the initial synthesis of **35** and the optimized ones to achieve an overall yield of 2.4%. q.y. = quantitative yield.*

Reaction	Initial yield	Final yield
a	q.y.	q.y.
b	84%	q.y.
c	78%	98%
d	38%	53%
e	25%	11%
f	q.y.	q.y.
g	10%	60%
h	40%	74%

7.1.2.2. Computation studies and biological investigation

Compound **35** has been assayed on truncated (1-294 aa) CK1δ reporting an IC_{50} of 0.18 μM. The predicted binding pose of the derivative displayed in **Figure 111** suggests that TT nucleus can engage a tridentate hydrogen bond with Glu83 and Leu85 belonging to the hinge region. The resorcinol-like moiety at the 2-position, instead, establishes interactions with Glu52 and Asp149 (**Fig. 111, Panel B**). **Panel A** shows the electrostatic and hydrophobic contributions of residues (x axis) in comparison to all the active derivatives of series (y axis), respectively, by using an heatmap with a colorimetric scale of colors: proceeding with a darker shade it is possible to appreciate an increased magnitude of interaction. [209]
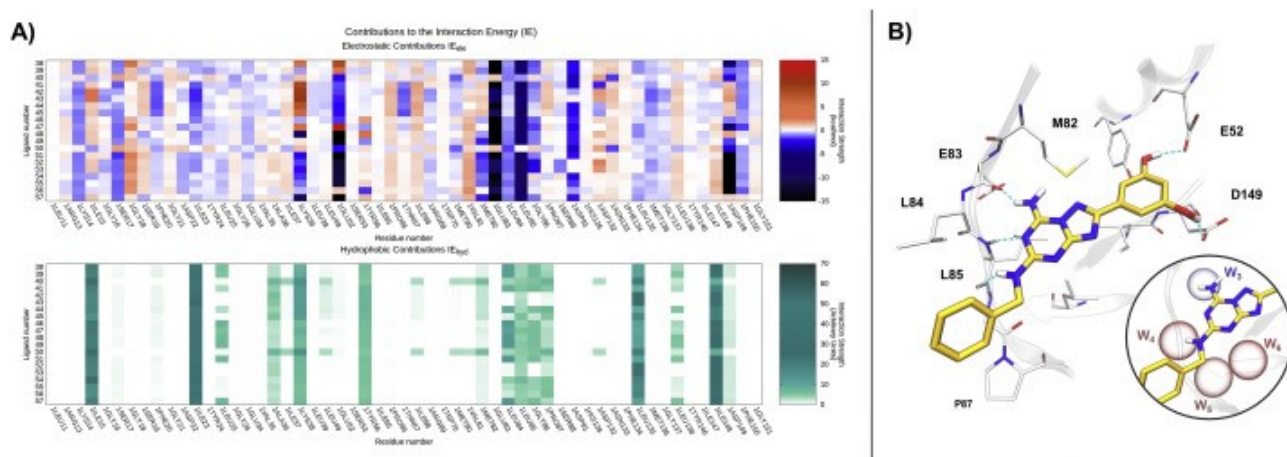
*Figure 111: **Panel A**) Interaction Energy (IE) fingerprints that represent electrostatic (IEele) and hydrophobic (IEhyd) interaction between each 5-substituted TT derivate (y-axis) and each CK1δ binding site residue (x-axis). The intensity of the electrostatic interactions is rendered by a colorimetric scale going from blue to red (for negative to positive values) while for the hydrophobic interactions a scale going from white to dark green (for low to high values) is exploited. **Panel B**) Representation of the docking-predicted structure of the complex between protein kinase CK1d (grey) and compound **141**. Hydrogen bond interactions are depicted as cyan dotted lines. [209]*

Derivative **35** has been assayed from the biochemical point of view; firstly, the IC_{50} on full-length CK1δ has been performed. The full-length kinase contains all its autophosphorylation sites, thus the activity can be different but more reliable than the truncated one. This compound has reported an activity of 0.30 μM as reported in **Figure 112** in which the concentration-inhibition curve has been displayed. [209]
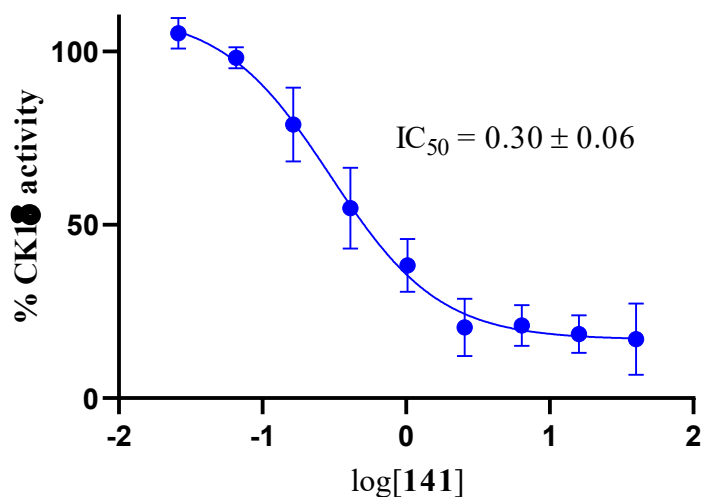
Figure 112: concentration-inhibition curve of compound 35 on full-length CK1δ.

Moreover, the ATP-competitive behavior has been confirmed by testing candidate **35** at the presence of increasing ATP concentrations (2 μM, 20 μM, 200 μM) denoting an enhancement of activity percentage. (**Fig. 113**). [209]
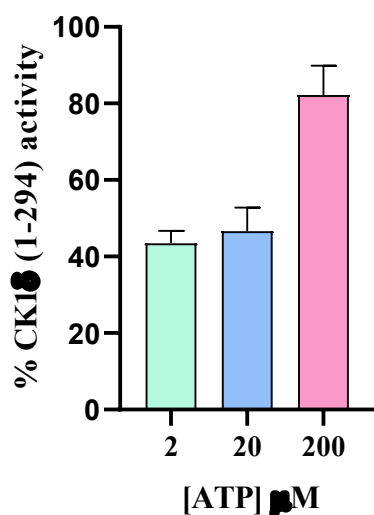
Figure 113: ATP-competition of compound 35 on CK1δ using increasing ATP concentrations (2 μM, 20 μM, 200 μM).

To establish the possible passive permeability of compound **35**, BBB-PAMPA investigation has been carried out. As detailed described in **chapter 3**, the experiment has been conducted by detecting the amount of compound at the level of the acceptor compartment using the absorbance mode considering cut-off values of $1.1 \cdot 10^{-6}$ cm/s and $0.6 \cdot 10^{-6}$ cm/s to determine CNS+ and CNS-, respectively. The recorded Pe for candidate **35** has achieved the permeability value of 0.62 classifying itself as borderline permeable derivative. [209]

Since derivative **35** has proved to be the best of TP and TT series, it has been screened in a panel of 452 kinases by Discoverex® to explore the selectivity of this compound. As it is possible to appreciate in **Fig. 114**, candidate **35** has displayed an excellent selectivity profile even if it is able to bind all the isoforms of CK1δ. **Table 24** shows the binding percentage assaying **35** at the concentration of 10 μM; an important activity has been recorded on CK1ε that demonstrates an high homology with the isoform δ reporting a value of 1.4%. [209]

*Table 24: Competition binding assay KINOMEscan™. Data are reported as % of binding to kinases related to compound **35** at the concentration of 10 μM. [209]*

Isoform	CK1α₁	CK1α₁L	CK1δ	CK1ε	CK1γ₁	CK1γ₂	CK1γ₃
Binding percentage	3.2	14	14	1.4	32	20	14

Observing **Fig. 114**, best binding percentages are reported in dark blue while the opposite situation is registered with light blue according to the color code below, nevertheless intermediate values have been evaluated. Compound **35** has displayed a strong activity towards Mitogen Activated Protein Kinase 5 (MEK5) which is involved in several pathways with other MAP kinases in regulating gene expression, apoptosis, and cell division. Deregulation can lead to the occurrence of some pathological conditions including cancer and neurodegenerative diseases. [219,220] In a recent publication the role of MEK5 in a mTOR-independent lysosome-autophagy pathway has been reported reducing the hyperphosphorylation of TDP-43 in ALS. [221] Nevertheless, MEK5 has been also detected as biomarker in Alzheimer's disease since its expression increases with the formation of protein aggregates that characterize the disease progression as detailed discussed in the introductive chapter of this thesis. [220] Therefore, the activity recorded for compound **35** towards this kinase can be an added value allowing the study of another target acting the neurodegenerative disease but also to obtain more results in *in vitro* and *in vivo* investigation for the treatment of AD, PD and ALS.

Legend:
- 0≤x<0.1
- 0.1≤x<1
- 1≤x<10
- 10≤x<35
- x≥35

7.1.2.2.1. *In vitro* investigation of compound 35

Derivative **35** has been assayed on peripheral blood lymphocytes (PBL) by Prof. Giampietro Viola of University of Padua stimulated and not with phytohematoagglutinin (PHA) and human fibroblasts of healthy volunteers. As displayed in **Table 25**, the candidate has proved to be not toxic on non-tumoral cells. [209]

Table 25: compound 35 concentration required to inhibit 50% of the cell growth in peripheral blood lymphocytes (PBL) stimulated and not (resting) and human fibroblasts.

IC_{50} (μM) $PBL_{resting}$	>10
IC_{50} (μM) PBL_{PHA}	>10
IC_{50} (μM) Human fibroblast	>10

Lead compound **35**, moreover, has been tested on neuroblastoma cell lines (SH-SY5Y) during the Erasmus program in the research group of Prof Ana Martinez (CSIC-Madrid-ES). Firstly, as deeply described in the **chapter 3**, derivative has been screened at the concentrations of 5 and 10 μM plating 80000 cells/well. As showed in **Fig. 115**, compound has displayed to be harmless for cells at the two assayed concentrations.
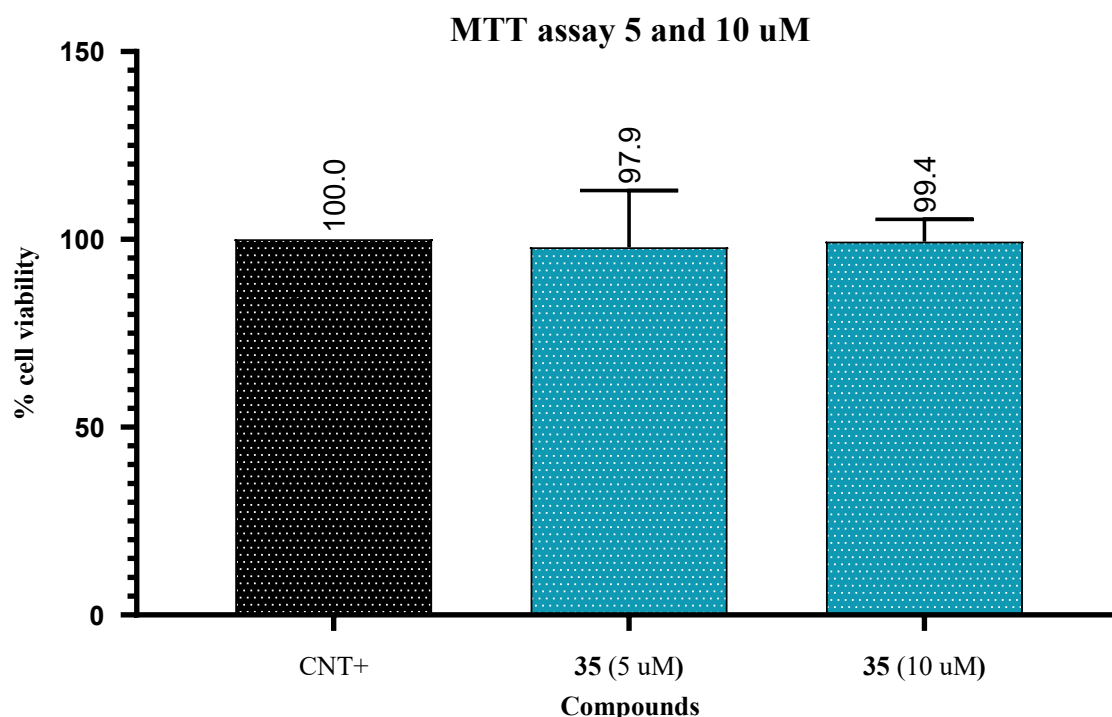
Figure 115: MTT assay of compound 35 at the concentrations of 5 and 10 μM. In y axis the cell viability percentage is reported. The elaboration performed with GraphPad Prism 8.0 in "Anova" mode is the result of three independent experiments and each experiment is conducted using the mean of six wells per compound.

Consequently, neuroprotection investigation has been conducted at the concentration of 5 μM of **35** plating 60000 cells/well. Results have highlighted an improvement in relative cell viability value in comparison to the

ethacrynic acid at 45 μM that simulates neuronal death; nevertheless, neuroprotective behavior of the candidate has not been registered with the statistical validation of reported data (**Fig. 116**).
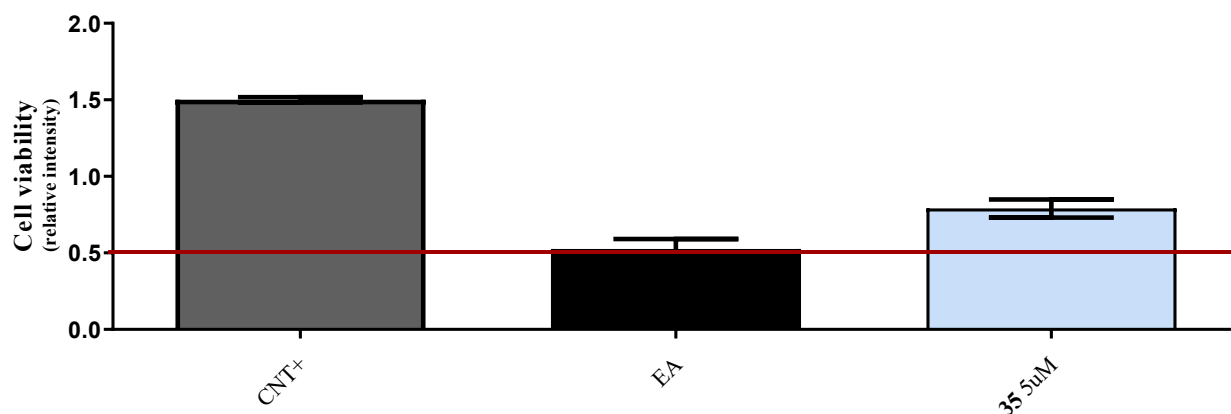
Figure 116: neuroprotection assay's results. Three independent experiments have been conducted and the elaboration has been performed with GraphPad Prism 8.0 using the "Anova" mode with the mean of eight wells per compounds for each plate and then final data have been obtained with "T test" mode to compare the three experiments. EA has been used at 45 μM while chosen concentration for compound 35 is 5 μM.

7.1.2.2.2. *In vivo* investigation of compound **35**

Despite results in neuroprotective assays for derivative **35** have not demonstrated a solid neuroprotective behavior, candidate has been tested *in vivo* on *Drosophila* specie that overexpress TDP-43 in glial cells considered "astrocyte-like" in collaboration with Prof. Marco Bisaglia of University of Padua. From preliminary results the compound administered at the concentration of 0.25 mM has shown, as reported in **Fig. 117**, the increase of lifespan of *Drosophila* achieving 36 days in comparison to control (31 days).
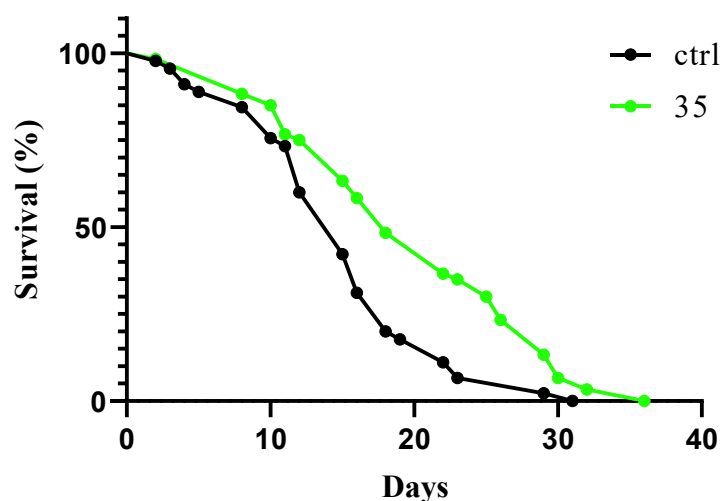
Figure 117: survival percentage on Drosophila testing compound 35 at the concentration of 0.25 mM.

Figure 118 reports the survival proportions of candidate **35** in comparison to the control. Nevertheless, a deeper investigation should be required to confirm obtained results.

Survival proportions: Survival cntr vs 35
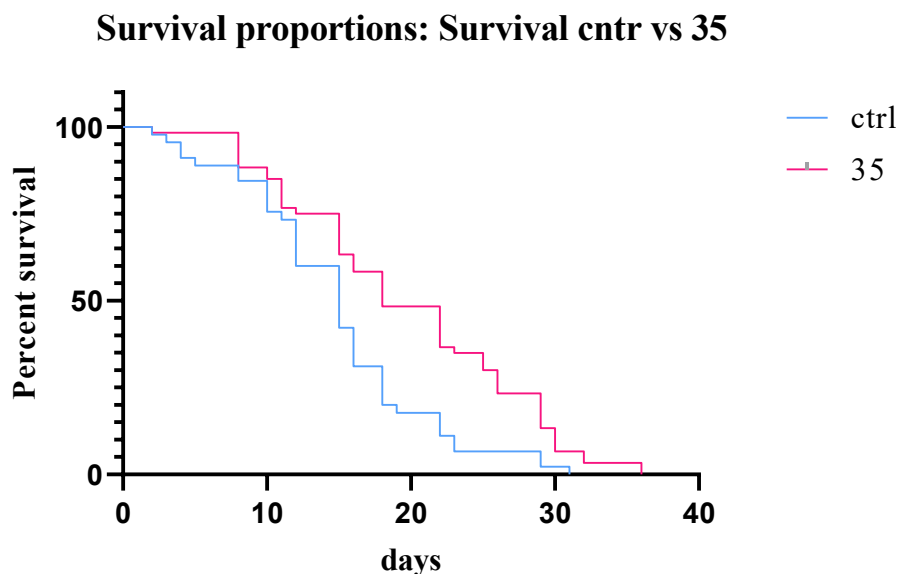
Figure 118: survival proportions graph. Survival percentage of compound 141 in comparison to the control.

7.1.2.3. Example of application: inclusion of compound 35 in Superparamagnetic Iron Oxide Nanoparticles

Over the years, nanotechnology has gained more attraction in medical field for diagnosis, therapy and drug delivery becoming important tool. Among nanosystems, magnetic nanoparticles have acquired challenging features in magnetic resonance imagining (MRI), cell separation as well as drug delivery. Superparamagnetic Iron Oxide Nanoparticles including Fe_3O_4 (magnetite) and γ-Fe_2O_3 (maghemite) are characterized by small size achieving 10-20 nm, thus suitable for clinical applications for their stability, safety and compatibility with the physiological environment. [222] Coating of nanoparticles results important to avoid the oxidation process and to confer specific properties; several polymeric materials can be used including dextran, polyethylene glycol (PEG), polyvinyl alcohol (PVA), chitosan and starch. Many developed drug candidates are characterized by poor druglike properties: too hydrophobic to gain appropriate oral properties and too hydrophilic to allow the permeation through membranes. Consequently, drug delivery systems can be useful to bypass drug's pharmacokinetic limits. Moreover, considering SPIONs, the possibility to apply a magnetic guide can be implemented, especially to vehicle drugs in precise districts of organism to exploit their function: one example is provided by helping the transport at the central level but SPIONs are also involved in thermal therapy [223]

The increasing role of Superparamagnetic Iron Oxide Nanoparticles in medical field has been explained in the introductive section of the chapter. As previously discussed, compound **35** has demonstrated a borderline value in the in vitro BBB-permeation experiment and the arrival at the central level results essential to exploit its function. With the collaboration of Prof. Lucia Pasquato (University of Trieste), SPIONs have been synthesized and derivative **35** has been included in the system for drug delivery purposes. To obtain reliable results, a commercial drug, riluzole (**34**), discussed in **chapter 3**, has been also incorporated since it is well-known established that it is a substrate of P-glycoprotein, therefore all the commercial formulations involve a drug delivery system.

Polymeric SPIONs nanosystems have been developed by using PVA (13 KDa and 57 KDa) and Pluronic F127 checking stability and dimensions using TEM (Transmission electron microscopy) and NTA (Nanoparticle Tracking Analysis). Since riluzole has been shown a poor solubility in water like **35**, the organic layer containing SPIONs and compound **34** has been inserted in the aqueous one composed by polymers by creating

a micellar system that include the drug. The encapsulation has been successful achieved with a percentage of 97.70% conserving an overall dimension below than 200 nm (system with PVA 13 KDa). The same procedure has been applied for the inclusion of compound **35** (78.96%) validating the used method. Regarding the SPIONs with PVA coating of 57 KDa, riluzole (**34**) has been included with a percentage of 97.81%, and derivative **35** with a value of 79.92%.

To corroborate the functioning of the drug delivery system, one attempt has been conducted by adapting BBB-PAMPA technique to observe an improvement of the passage of candidates in comparison to their permeability without SPIONs. Nevertheless, the used experiment has not revealed an increase in the transport of riluzole (**34**) as well as compound **35** denoting the necessity to use a more complex system to corroborate the inclusion and release. Therefore, release studies will be carried out as a preliminary step to assay the developed systems in cell models.

7.1.3. Conclusions and future perspectives

In this section the development of a lead compound (**35**) has been discussed; in order to characterize the candidate from the biochemical and biological point of view, the collection of a larger amount of derivative has been required. Therefore, the synthetic pathway has been optimized achieving an overall yield of 2.4% in eight synthetic steps. Molecule **35** has been assayed in luminescence assay to establish IC_{50}s on truncated and full-length CK1δ and to demonstrate its ATP-competitive behavior. To screen the activity of **35** on kinoma, it has been tested on a panel of 452 kinases denoting an excellent selectivity profile even if it has shown to be able to bind all the isoforms of CK1 and MEK5, another kinase involved in neurodegenerative diseases unlocking the possibility to explore for the future another new target. Compound **35** has been assayed also in cell models: firstly, in collaboration with Prof. Viola (University of Padua) it has displayed to be not cytotoxic against non-tumoral cells (activated and not peripheral blood lymphocytes and human fibroblast) and it has proved to be harmless on neuroblastoma cells (SH-SY5Y) by performing the experiment during the Erasmus program in the group of Prof. Ana Martinez (CSIC-Madrid-ES). Despite the innocuousness of derivative **35** on SH-SY5Y, neuroprotective behavior has not been detected. Preliminary *in vivo* investigations have been carried out by Prof. Marco Bisaglia (university of Padua) on *Drosophila* specie overexpressing TDP-43 for which the candidate has shown encouraging results. Finally, an example of implication has been given with the inclusion of compound **35** in Superparamagnetic Iron Oxide Nanoparticles denoting a successful encapsulation (Prof. Pasquato's groups, University of Trieste). Nevertheless, the improvement of the permeability using SPIONs has not been highlighted for the compound that has shown a borderline permeability in BBB-PAMPA experiment. As future perspective, releases studies for compound **35** incorporated in nanosystems will be conducted using to observe an improvement in drug delivery. Preliminary *in vivo* results will be corroborated to achieve an appealing candidate that can be used as tool for disease's investigation and treatment. Moreover, candidate **35** can provide a new starting point for the exploration of another target involved in neurodegeneration.

7.1.4. Experimental section

7.1.4.1. Chemistry

7.1.4.1.1. General chemistry

Reagents were obtained from commercial suppliers and used without further purification. Reactions were monitored by TLC, on precoated silica gel plates (Macherey-Nagel, 60FUV254). Final compounds and intermediates were purified by flash chromatography using stationary phases silica gel (Macherey-Nagel, silica 60, 240e400 mesh). When used, light petroleum ether refers to the fractions boiling at 40e60 _C. Melting points were determined with a Stuart SMP10 melting point apparatus and were not corrected. The ^{1}H NMR and ^{13}C NMR spectra were determined in CDCl$_3$ or DMSO-d$_6$ solutions and recorded Jeol GX 270 MHz and Varian 400 MHz spectrometers; chemical shifts (d scale) are reported in parts per million (ppm) and referenced to residual solvent peak, with splitting patterns abbreviated to: s (singlet), d (doublet), dd (doublet of doublets), dt (doublet of triplets), t (triplet), m (multiplet) and bs (broad signal). Coupling constants (J) are given in Hz. MS-ESI analysis were performed using ESI Bruker 4000 Esquire spectrometer while for the accurate mass the instrument microTOF-Q e Bruker have been used. Compound purities were determined by HPLC-DAD (Waters 515 HPLC pump; Waters PDA 2998 Detector) using Luna C18(2) HPLC column (150 x 4.6 mm, particle size 3 mm). Isocratic elution was performed for 40 min at a flow rate of 300 mL/min in water-methanol 30:70. UV absorption was detected from 220 to 400 nm using a diode array detector; purity was determined at the maximum absorption wavelength of the compound and at 254 nm.

7.1.4.2.2. N'-(4,6-diphenoxy-1,3,5-triazin-2-yl)-3,5dimethoxybenzohydrazide (**201**)

2,4,6-triphenoxy-[1,3,5]triazine (121, 10.0 g, 0.028 mol) and 3,5dimethoxybenzohydrazide(0.0476 mmol) was dissolved in anhydrous THF (200 mL) while DBU (7.1 mL, 0.0476 mmol) was added dropwise at 0°C. The mixture was stirred at room temperature for 12 h. The solvent was then removed, the residue was dissolved in DCM (300 mL), and the resulting solution was washed with water (3 x 100 mL). The organic layer was concentrated, dried over anhydrous sodium sulfate, and purified by flash chromatography (DCM-EtOAc 90:10) Yield 38% (4.89 g); white solid; mp 212-213°C (EtOEt-light petroleum). ^{1}H NMR (270 MHz, DMSO-d^6): d 10.45 (s, 1H), 10.05 (s, 1H), 7.53-7.35 (m, 2H), 7.35-7.04 (m, 8H), 7.04-6.89 (m, 2H), 6.73-6.68 (m, 1H), 3.79 (s, 6H). ES-MS (methanol) m/z: 460.2 [M+H]$^+$, 482.1 [M+Na]$^+$.

7.1.4.2.3. 2-(3,5-dimethoxyphenyl)-5,7-diphenoxy-[1,2,4]triazolo[1,5-*a*][1,3,5]triazine (**202**)

The mixture of phosphorous pentoxyde (0.075 mol) and hexamethyldisiloxane (0.075 mol) in anhydrous xylene (150 mL) was heated to 90°C over 1.5 h and then stirred for 1 h at 90°C, under argon atmosphere. The well dried hydrazides compound **x** (0.015 mol, 1 equivalent) was then added to the clear solution and the temperature is increased to reflux and stirred for 2e4 h. The solvent was then removed, the residue dissolved in DCM (300 mL) and the resulting solution was washed with water (3 x 100 mL). The organic layer was concentrated, dried over anhydrous sodium sulfate, and purified with flash chromatography eluent (DCM 100%). Yield 25% (1.65 g); white solid; mp 211°C (EtOEt-light petroleum). ^{1}H NMR (270 MHz, CDCl$_3$): d 7.59-7.47 (m, 4H), 7.47e7.34 (m, 5H), 7.34-7.12 (m, 3H), 6.68-6.55 (m, 1H), 3.86 (s, 6H). ^{13}C NMR (101 MHz, CDCl$_3$): d 167.18, 164.67, 161.00, 160.32, 154.72, 151.77, 150.51, 131.19, 130.09, 129.64, 127.53, 126.22, 121.49, 121.18, 105.27, 104.65, 55.64. ES-MS (acetonitrile) m/z: 442.2 [M+H]$^+$, 464.1 [M+Na]$^+$.

7.1.4.2.4. 2-(3,5-dimethoxyphenyl)-5-phenoxy-[1,2,4]triazolo[1,5-*a*][1,3,5] triazin-7-amine (**203**)

A solution of the 2-(3,5-dimethoxyphenyl)-5,7-diphenoxy-[1,2,4]triazolo[1,5-*a*][1,3,5]triazine (**202**) (2 mmol) in methanol (20 mL) with methanolic ammonia 7 N (12 mmol) was stirred for 2 h at room temperature. The solvent was removed under reduced pressure and the residue purified by the directly crystallized from EtOEt-

light petroleum to afford the desired compounds as white solid. Yield 95% (0.692 mg); mp 274°C (EtOEt-light petroleum). ^{1}H NMR (400 MHz, DMSO-d$_6$): d 9.12 (s, 1H), 8.78 (s, 1H), 7.46 (t, J = 7.8 Hz, 2H), 7.36-7.20 (m, 5H), 6.65 (s, 1H), 3.81 (s, 6H). ^{13}C NMR (101 MHz, DMSO-d$_6$): d 165.3,164.0,161.1, 159.4,152.8, 152.4, 132.5, 130.0, 125.9,122.3, 110.0, 105.0, 103.1, 55.8. ES-MS (methanol) m/z C$_{18}$H$_{16}$N$_6$O$_3$: 365.1 [M+H]$^+$, 387.1 [M+Na]$^+$.

7.1.4.2.5. N^5-benzyl-2-(3,5-dimethoxyphenyl)-[1,2,4]triazolo[1,5-*a*][1,3,5] triazine-5,7-diamine (**204**)

A solution of 2-(3,5-dimethoxyphenyl)-5-phenoxy-[1,2,4]triazolo[1,5-*a*][1,3,5] triazin-7-amine (**203**) (2 mmol) with 6 mmol of benzylamine in ethanol (20 mL) was stirred at 95-100°C in a sealed tube for 24-72 h. The solvent was removed under reduced pressure and the residue was purified, when necessary, by flash chromatography (EtOAc 70%-light petroleum 30%). Yield 10% (19 mg); white solid; mp 279e281°C (EtOEt-light petroleum). ^{1}H NMR (400 MHz, DMSO-d$_6$): d 8.46-7.84 (m, 3H), 7.43-7.13 (m, 7H), 6.59 (bs, 1H), 4.51 (bs, 2H), 3.79 (s, 6H). ES-MS (methanol) m/z: 378.1 [M+H]$^+$, 400.1 [M+Na]$^+$, 416.1 [M+K]$^+$. HRMS (ESI-TOF) m/z: C$_{19}$H$_{19}$N$_7$O$_2$ experimental 378.1672 [M+H]$^+$, theoretical 378.1672 [M+H]$^+$, Δ=0.0000. Purity HPLC: 97.7%.

7.1.4.2.6. 5-(7-amino-5-(benzylamino)-[1,2,4]triazolo[1,5-a][1,3,5]triazin-2-yl)benzen-1,3-diol (**35**)

3 equivalents of a 1M solution of boron tribromide in DCM were slowly added to a cooled (-78°C) solution of N^5-benzyl-2-(3,5-dimethoxyphenyl)-[1,2,4]triazolo[1,5-*a*][1,3,5] triazine-5,7-diamine (**204**, 0.25 mmol, 1 equivalent) in dichloromethane (10 mL/mmol **x**) under argon atmosphere. The cooling bath was removed, and the suspension was slowly warmed up to room temperature and stirred for 12 h. Once completed, at least an equal volume of cool methanol was added dropwise, and the solution stirred for 15 minutes-1 hour. Then the volatile species were removed under reduced pressure, thus giving the corresponding deprotected derivative **x** that were purified by flash chromatography (DCM 96%-MeOH 4%). Yield 40% (35 mg); white solid; mp > 300°C (EtOEt-light petroleum). ^{1}H NMR (400 MHz, DMSO-d$_6$): d 9.39 (s, 2H), 7.93-7.82 (m, 2H), 7.39-7.14 (m, 6H), 7.00-6.92 (m, 2H), 6.28 (bs, 1H), 4.57-4.43 (m, 2H). ^{13}C NMR (101 MHz, DMSO-d$_6$): d 163.5, 161.5, 159.6, 158.9, 150.5, 140.5, 132.9, 128.6, 127.5, 127.0, 105.5, 104.7, 44.2. ES-MS (methanol) m/z: 350.1 [M+H]$^+$. HRMS (ESI-TOF) m/z: C$_{17}$H$_{15}$N$_7$O$_2$ experimental 350.1360 [M+H]$^+$, theoretical 350.1359 [M+H]$^+$, Δ = 0.0001. Purity HPLC: 99.4%.

7.1.4.3. Biochemistry

7.1.4.3.1. CK1d activity assays

Assay with truncated CK1δ. Compounds were evaluated towards CK1δ (Merck Millipore, recombinant human, amino acids 1-294, with N-terminal GST-tagged) with the KinaseGlo® luminescence assay (Promega) following procedures reported in literature. In detail, luminescent assays were performed in black 96-well plates, using the following buffer: 50 mM HEPES (pH 7.5), 1 mM EDTA, 1 mM EGTA, and 15 mM magnesium acetate. Compound CR8 (IC$_{50}$ = 0.4 mM) was used as a positive control for CK1δ while DMSO/buffer solution was used as a negative control. In a typical assay, 10 mL of inhibitor solution (dissolved in DMSO at 10 mM concentration and diluted in assay buffer to the desired concentration) and 10 mL (16 ng of CK1d) of enzyme solution were added to the well, followed by 20 mL of assay buffer containing 0.1% casein substrate and 4 mM ATP (or 40 mM and 400 mM for ATP competition experiment). The final DMSO concentration in the reaction mixture did not exceed 1-2%. After 60 min of incubation at 30°C for CK1δ the enzymatic reactions were stopped with 40 mL of Kinase-Glo reagent (Promega). Luminescence signal (relative light unit, RLU) was recorded after 10 min at 25°C using Tecan Infinite M100 or FLUOstar Optima multimode readers. The activity is proportional to the difference of the total and consumed ATP. The inhibitory activities were calculated on the basis of maximal activities measured in the absence of inhibitor. First, enzyme activity percentage was determined at 40 mM for each inhibitor with respect to DMSO; subsequently, for the most

active compounds the IC$_{50}$ values were determined. Data were analyzed using Excel and GraphPad Prism software (version 8.0).

Assay with full length CK1δ. Compounds were evaluated towards CK1δ (full length, ThermoFisher) with the KinaseGlo® luminescence assay (Promega). In detail, luminescent assays were performed in black 96-well plates, using the following buffer: 50 mM HEPES (pH 7.5),1 mM EDTA, 1 mM EGTA, and 15 mM magnesium acetate. Compound PF-670462 was used as positive control for CK1δ while DMSO/buffer solution was used as negative control. In a typical assay, 10 mL of inhibitor solution (dissolved in DMSO at 10 mM concentration and diluted in assay buffer to the desired concentration) and 10 mL (26 nM) of enzyme solution were added to the well, followed by 20 mL of assay buffer containing 0.1% casein substrate and 4 mM ATP. The final DMSO concentration in the reaction mixture did not exceed 1-2%. After 10 min of incubation at 30°C the enzymatic reactions were stopped with 40 mL of KinaseGlo® reagent (Promega). Luminescence signal (relative light unit, RLU) was recorded after 10 min at 30°C using Tecan Infinite M100. For IC$_{50}$ determination, ten different inhibitor concentrations ranging from 100 to 0.026 mM were used. IC$_{50}$ values are reported as means ± standard errors of three independent experiments. Data were analyzed using GraphPad Prism software (version 8.0).

7.1.4.3.2. Competition binding assays on other kinases

KINOMEscan™ platform by DiscoverX has been applied to 6 human protein kinase CK1 isoforms: CK1α1, CK1α1L, CK1γ1-3, CK1δ and CK1ε, by testing compound 51 at a concentration of 10 mM.

7.1.4.4. Cytotoxicity in non-tumoral cells

Cytotoxicity assays were performed by Prof. Giampietro Viola (University of Padua). Peripheral blood lymphocytes (PBL) from healthy donors were obtained from human peripheral blood (leucocyte rich plasma buffy coats) from healthy volunteers using the Lymphoprep (Fresenius KABI Norge AS) gradient density centrifugation. Buffy coats were obtained from the Blood Transfusion Service, Azienda Ospedaliera of Padova and provided at this institution for research purposes. Therefore, no informed consent was further needed. In addition, buffy coats were provided without identifiers. The experimental procedures were carried out in strict accordance with approved guidelines. After extensive washing, cells were resuspended (1.0 x 106 cells/ mL) in RPMI-1640 with 10% FBS and incubated overnight. For cytotoxicity evaluations in proliferating PBL cultures, non-adherent cells were resuspended at 5 x 105 cells/mL in growth medium, containing 2.5 mg/mL Phytohematoagglutinin (PHA, Irvine Scientific). For cytotoxicity evaluations in resting PBL cultures, nonadherent cells were resuspended (5 x 105 cells/mL) and treated for 72 h with the test compounds, as described above. Normal human adult fibroblasts were purchased by ATCC (PCS- 201-012) and were cultivated in DMEM auditioned of 10% fetal Bovine serum. 2 x 104 cells were plated in 96 well plate and after 24 h, different concentrations of the test compounds were added, and viability was determined 72 h later. For both cell lines viability was evaluated by resazurin-based cell, measuring the relative fluorescence intensity at 590 nm with a Spark (Tecan) multiwell plate reader during a 4 h timespan.

7.1.4.5. CNS permeation prediction: PAMPA-BBB assay

Prediction of the brain penetration of active compounds was evaluated using a parallel artificial membrane permeability assay (PAMPA). Ten drugs of known BBB permeability (2-6 mg of Caffeine, Enoxacine, Hydrocortisone, Desipramine, Ofloxacine, Piroxicam, Testosterone, 12-15 mg of Promazine and Verapamil and 23 mg of Atenolol dissolved in 1000 mL of ethanol) were included in each experiment to validate the analysis set. Compounds were dissolved in a 70/30 PBS pH = 7.4 buffer/ethanol solution in a concentration that ensures adequate absorbance values in the UV-VIS light spectrum. 5 mL of these solutions were filtered with PDVF membrane filters (diameter 30 mm, pore size 0.45 mm). The acceptor indented 96-well microplate (MultiScreen 96-well Culture Tray clear, Merck Millipore) was filled with 180 mL of PBS/ethanol (70/30).

The donor 96-well filtrate plate (Multiscreen® IP Sterile Plate PDVF membrane, pore size is 0.45 mM, Merck Millipore) was coated with 4 mL of porcine brain lipid (Spectra 2000) in dodecane (20 mg/mL) and after 5 min, 180 mL of each compound solution were added. Then the donor plate was carefully put on the acceptor plate to form a "sandwich", which was left undisturbed for 2.5 h at 25°C. During this time the compounds diffused from the donor plate through the brain lipid membrane into the acceptor plate. After incubation, the donor plate was removed. The concentrations of compounds and commercial drugs were determined by measuring the absorbance in the donor (before the incubation) and the acceptor wells (after the incubation) with UV plate reader Tecan Infinite M1000. Every sample was analyzed at two to five wavelengths in 3 replicates and in two independent experiments. The permeability coefficient (Pe) of each drug, in centimeter per second, was calculated applying the following formula:

$$Pe = \frac{Vd \cdot Vr}{(Vd \cdot Vr) \cdot S \cdot t} \cdot \frac{100 \cdot Vd}{100 \cdot Vd - \%T(Vd \cdot Vr)}$$

$$\%T = \frac{Vr \cdot Ar}{Ad \cdot Vd} \cdot 100$$

where Vd and Vr are the volumes of the donor and the receptor solutions (0.18 cm^3), S is the membrane area (0.266 cm^2), t is the time of incubation (2.5 h = 9000 s), Ar is the absorbance of the receptor plate after the experiment and Ad0 is the absorbance in the donor compartment before incubation. Results are given as the mean and the average of the two runs ± standard deviation (SD) is reported. Obtained results for quality control drugs were then correlated to permeability data found in the literature. The linear correlation between experimental and literature permeability values was used for the classification of compounds in those able to cross the BBB by passive permeation (CNS + which correlate with a bibliographic Pe > 4) and those not (CNS- which correlate with a bibliographic Pe < 2). Compounds correlating with reported Pe values from 2 to 4 10x6 cm s^{-1} are classified as CNS +/-.

7.1.4.6. Thermal Shift Assay (TSA)

<u>Thermal Shift Assays for the best compound was performed by Elelonora Cescon in the group of Prof. Paola Storici (BioLab-Elettra Sincrotrone-Trieste).</u> All TSA experiments were conducted in triplicates. Recombinant CK1d 1-294, representing the catalytic core domain of the protein, was produced at Elettra Protein Facility in Elettra Synchrotron. Optimal concentration of protein and dye were tested from preliminary TSA in order to establish the most advantageous set up. Samples were prepared in white 96-multiwell plate (Biorad®) with a final volume of 20 mL into each well. A 5x stock of buffer and a 5x stock of protein solution were prepared hence 4 mL of both were added into the wells. Tested inhibitors were dissolved in 100% DMSO and a 40x stock of each concentration tested was prepared to keep a final concentration of DMSO at 2.5% in each condition tested. Thermal shift assay was performed in assay buffer containing 20 mM Tris pH 7.5, 180 mM NaCl and 0.5 mM TCEP as final concentrations, while protein was kept at 3 mM in all conditions of the analysis. Compounds were tested at final concentrations of 1.5, 3, 9, 15, 30 and 45 mM (0.5x, 1x, 3x, 5x, 10x, 15x). Once added buffer, protein and compounds stocks plus a proper volume of water to reach 20 mL, the multi-well plate was centrifugated at 100 xg, 4°C for 1 min to spin down and stir the components. Protein and inhibitors were then incubated at room temperature for 30 min. After incubation, SyproOrange dye (Protein Thermal shift dye, Thermo Fisher Scientific®) was added into each well to a final concentration of 0.5x from 1000x stock in 100% DMSO. The multiwell plate was centrifuged again and measurement was started. Measures were performed in a real-time PCR machine (CFX96, Biorad®), registering emission of the dye at 560-580 nm every 30 sec, with a temperature gradient of 2°C/min. Each analysis was executed in comparison to a negative control represented by the only buffer or the compounds with SyproOrange, and a positive control consisted of the protein or protein with 2.5% of DMSO plus the fluorophore

7.1.4.7. Molecular docking

Molecular docking analysis of compound x was performed by the group of Prof. Stefano Moro (Molecular Modeling Section University of Padua). Three-dimensional structures of the ligands were built by the MOE-builder tool. Ionization states were predicted using the MOEprotonate 3D tool and structures were minimized by the MMFF94x until the root mean square (RMS) gradient fell below 0.1 kcal mol^{-1} Å^{-1}. PLANTS docking protocol was selected as a conformational search program and ChemPLP as a scoring function. For each compound investigated, 20 docking simulation runs were performed, searching on a sphere of 10 Å radius, build around the coordinates of ligand 16W center of mass (PDB ID: 4HNF). For each derivate herein investigated, a single conformation was chosen as representative of the bound state, based on the docking score and a visual inspection of each complex, in such a way to optimize the ligand-protein interaction network. Electrostatic and hydrophobic interactions, respectively IEele and IEhyd, were computed between each selected ligand pose and each protein residue involved in binding (residues within 10 Å with respect to the binding site center of mass). Both these contributions were computed using MOE software and, in particular, IEele were calculated as non-bonded electrostatic interactions energy term of the force field (expressed in kcal/mol). Instead, IEhyd were computed as contact hydrophobic surfaces and are associated with an adimensional score (the higher the better). The data obtained by this analysis were reported in a graphic, representing residues (x-axis) in the form of equally high rectangles rendered according to a colorimetric scale. As regards IEele, colors from blue to red represent energy values ranging from negative to positive values; for IEhyd, colors from white to dark green depict scores going from 0 to positive values.

7.1.4.8. *In vivo* experiments on neuroblastoma cell lines (SH-SY5Y)

Biological investigation of most promising derivatives was conducted during the Erasmus program in the group of Prof. Ana Martinez (CSIC-Madrid-ES).

7.1.4.8.1. MTT assays

The human neuroblastoma SH-SY5Y cell line was propagated in Dulbecco's Modified Eagle Medium (DMEM) containing L-glutamine (2mM), 1% non-essential amino acids, 1% penicillin/streptomycin and 10% fetal bovine serum (FBS) under humidified 5% CO_2. Once semiconfluence was achieved, cells were countered using TC10™ Automated Cell Counter Bio-Rad Laboratories (CSIC-Madrid) and 80000 cells/well were plated in 96-well plate. After 24h of incubation, compounds were inserted at the concentrations of 5 and 10 μM (the stock solution in DMSO was diluted with DMEM to obtain the right final concentration) and, after another 24h of incubation, DMEM was removed and MTT reactive (3-[4,5- Dimethylthiazol-2-yl]-2,5-Diphenyltetrazolium Bromide) was added at the concentration of 20 mg/mL. After 2h, absorbance was recorded, and cell survival was estimated as percentage of value of untreated control (mean of six wells). Three independent experiments were carried out.

7.1.4.8.2. Neuroprotection assays

The human neuroblastoma SH-SY5Y cell line was propagated in Dulbecco's Modified Eagle Medium (DMEM) containing L-glutamine (2mM), 1% non-essential amino acids, 1% penicillin/streptomycin and 10% fetal bovine serum (FBS) under humidified 5% CO_2. Once semiconfluence was achieved, cells were countered using TC10™ Automated Cell Counter Bio-Rad Laboratories (CSIC-Madrid) and 60000 cells/well were plated in 96-well plate. After 24h of incubation, compounds were inserted at the concentrations of 5 and 10 μM (the stock solution in DMSO was diluted with DMEM to obtain the right final concentration) and, after 1h ethacrynic acid (45 μM starting from stock solution of 100 mM diluted in DMEM) was added. As negative control, a solution of DMSO 1% in DMEM was used while as positive control ethacrynic acid without compound. After 24h of incubation, DMEM was removed and MTT reactive (3-[4,5- Dimethylthiazol-2-yl]-2,5-Diphenyltetrazolium Bromide) was added at the concentration of 20 mg/mL. After 2h, absorbance was recorded, and cell survival was estimated as the mean of relative absorbance of six wells/compound. Three

independent experiments were conducted, and statistical analysis of data was conducted using GraphPad Prism 8.0 one-way ANOVA for each plate and T-TEST to compare the three experiments.

7.1.4.9. *In vivo* experiments on Drosophila

Compound **35** was tested on *Drosophila* that overexpresses TDP-43 at the concentration of 0.25 mM. *In vivo* assays were performed by Prof. Marco Bisaglia (University of Padua).

7.1.4.10. Inclusion of compound **35** in SPIONs

Compound **35** was included in SPIONs by Dr. Stefano Valente (Prof. Pasquato's group, University of Trieste).

8. Bibliography

1. Manning G, Whyte DB, Martinez R, Hunter T, Sudarsanam S. The protein kinase complement of the human genome. *Science (80)*. 2002;298(5600):1912-1934. doi:10.1126/science.1075762.

2. Duong-Ly KC, Peterson JR. The human kinome and kinase inhibition. *Curr Protoc Pharmacol*. 2013;(SUPPL.60):1-14. doi:10.1002/0471141755.ph0209s60.

3. Fabbro D, Cowan-Jacob WS, Mobitz H, Martiny-Baron G. *Targeting Cancer with Small-Molecular-Weight Kinase Inhibitors*. Vol 795.; 2012. doi:10.1002/9783527674381.ch2.

4. Seok SH. Structural insights into protein regulation by phosphorylation and substrate recognition of protein kinases/phosphatases. *Life*. 2021;11(9). doi:10.3390/life11090957.

5. Wang Z, Cole PA. Catalytic mechanisms and regulation of protein kinases. *Methods Enzymol*. 2014;548:1-21. doi:10.1016/B978-0-12-397918-6.00001-X.

6. Cormie KW, Woodgett JR. Protein Kinases: Physiological Roles in Cell Signalling. *Biochemistry*. 2016:1-9. doi: 10.1002/9780470015902.a0002710.pub3.

7. Hanks SK, Hunter T. The eukaryotic protein kinase superfamily: (catalytic) domain structure and classification. *FASEB J*. 1995;6:576-596. doi:10.1096/fasebj.9.8.7768349.

8. Teylor SS, Kornev AP. Protein Kinases: Evolution of Dynamic Regulatory Proteins Susan. *Trends Biochem Sci*. 2011;36(2):65-77. doi:10.1016/j.tibs.2010.09.006.

9. Modi V, Dunbrack RL. Defining a new nomenclature for the structures of active and inactive kinases. *PNAS*. Published online 2019:1-10. doi:10.1073/pnas.1814279116.

10. Guimaraes CRW, Rai BK, Munchhof MJ, et al. Understanding the Impact of the P-loop Conformation on Kinase Selectivity. *J Chem Inf Model*. 2011;51:1199-1204. doi: 10.1021/ci200153c.

11. Xu P, Ianes C, Gärtner F, Liu C, Burster T, Bakulev V. Structure , regulation , and (patho-) physiological functions of the stress- induced protein kinase CK1 delta (CSNK1D). *Gene*. 2019;715(144005):1-16. doi:10.1016/j.gene.2019.144005.

12. Leipe DD, Koonin E V, Aravind L. Evolution and Classification of P-loop Kinases and Related Proteins. *J Med Chem*. 2003;333:781-815. doi:10.1016/j.jmb.2003.08.040.

13. Kusuda J, Hidari N, Hirai M, Hashimoto K. Sequence Analysis of the cDNA for the Human Casein Kinase I d (CSNK1D) Gene and Its Chromosomal Localization. *Genomics*. 1996;32(91):140-143. doi: 10.1006/geno.1996.0091.

14. Peng Y, Shiao H, Tu C, et al. Protein Kinase Inhibitor Design by Targeting the Asp-Phe-Gly (DFG) Motif: The Role of the DFG Motif in the Design of Epidermal Growth Factor Receptor Inhibitors. *J Med Chem*. 2013;56:3889-3903. doi: 10.1021/jm400072p.

15. Treiber DK, Shah NP. Preview Ins and Outs of Kinase DFG Motifs. *Chem Biol*. 2013;20(6):745-746. doi:10.1016/j.chembiol.2013.06.001.

16. Huse M, Kuriyan J. The Conformational Plasticity of Protein Kinases. *Cell*. 2002;109:275-282. doi: 10.1016/s0092-8674(02)00741-9.

17. Knippschild U, Krüger M, Richter J, et al. The CK1 family: Contribution to cellular stress response and its role in carcinogenesis. *Front Oncol*. 2014;4(96):1-32. doi:10.3389/fonc.2014.00096.

18. Traxler P, Furet P. Strategies toward the design of novel and selective protein tyrosine kinase inhibitors. *Pharmacol Ther*. 1999;82(2-3):195-206. doi:10.1016/S0163-7258(98)00044-8.

19. Cozza G, Pinna LA. Casein kinases as potential therapeutic targets. *Expert Opin Ther Targets*. 2015;20(3):319-340. doi:10.1517/14728222.2016.1091883.

20. Davidson G, Wu W, Shen J, et al. Casein kinase 1γ couples Wnt receptor activation to cytoplasmic signal transduction. *Nature*. 2005;438(7069):867-872. doi:10.1038/nature04170.

21. Long AM, Zhao H, Huang X. Structural basis for the potent and selective inhibition of casein kinase 1 epsilon. *J Med Chem*. 2012;55(22):10307-10311. doi:10.1021/jm301336n.

22. Huang H, Acquaviva L, Berry V, et al. Structure-based design of potent and selective CK1γ inhibitors. *ACS Med Chem Lett*. 2012;3(12):1059-1064. doi:10.1021/ml300278f.

23. Bischof J, Leban J, Zaja M, et al. 2-Benzamido-N-(1H-benzo[d]imidazol-2-yl)thiazole-4-carboxamide derivatives as potent inhibitors of CK1δ/ε. *Amino Acids*. 2012;43(4):1577-1591. doi:10.1007/s00726-012-1234-x.

24. Mente S, Arnold E, Butler T, et al. Ligand-protein interactions of selective casein kinase 1δ inhibitors. *J Med Chem*. 2013;56(17):6819-6828. doi:10.1021/jm4006324.

25. Halekotte J, Witt L, Ianes C, et al. Optimized 4,5-Diarylimidazoles as Potent/Selective Inhibitors of Protein Kinase CK1δ and Their Structural Relation to P38α MAPK. *Molecules*. 2017; 22. doi:10.3390/molecules22040522.

26. García-Reyes B, Witt L, Jansen B, et al. Discovery of Inhibitor of Wnt Production 2 (IWP-2) and Related Compounds As Selective ATP-Competitive Inhibitors of Casein Kinase 1 (CK1) δ/ε. *J Med Chem*. 2018;61(9):4087-4102. doi:10.1021/acs.jmedchem.8b00095.

27. Minzel W, Venkatachalam, Avanthika Fink A, Hung E, et al. Small Molecules Co-targeting CKIα and the Transcriptional Kinases CDK7/9 Control AML in Preclinical Models Waleed. *Cell*. 2019;175(1):171-185. doi:10.1016/j.cell.2018.07.045.

28. Gebel J, Tuppi M, Chaikuad A, et al. p63 uses a switch-like mechanism to set the threshold for induction of apoptosis. *Nat Chem Biol*. 2020;16:1078-1086. doi: 10.1038/s41589-020-0600-3.

29. Cullati SN, Chaikuad A, Chen J-S, et al. Kinase domain autophosphorylation rewires the activity and substrate specificity of CK1 enzymes. *Mol Cell*. 2022;28(11):2006-2020. doi: 10.1016/j.molcel.2022.03.005.

30. Giamas G, Hirner H, Shoshiashvili L, et al. Phosphorylation of CK1δ: Identification of Ser370 as the major phosphorylation site targeted by PKA in vitro and in vivo. *Biochem J*. 2007;406(3):389-398. doi:10.1042/BJ20070091.

31. Clokie S, Falconer H, MacKie S, Dubois T, Aitken A. The interaction between casein kinase Iα and 14-3-3 is phosphorylation dependent. *FEBS J*. 2009;276(23):6971-6984. doi:10.1111/j.1742-4658.2009.07405.

32. Rivers A, Gietzen KF, Vielhaber E, Virshup DM. Regulation of casein kinase I ε and casein kinase I δ by an in vivo futile phosphorylation cycle. *J Biol Chem*. 1998;273(26):15980-15984. doi:10.1074/jbc.273.26.15980.

33. Kawakami F, Suzuki K, Ohtsuki K. A novel consensus phosphorylation motif in sulfatide- and cholesterol-3-sulfate-binding protein substrates for CK1 in vitro. *Biol Pharm Bull*. 2008;31(2):193-200. doi:10.1248/bpb.31.193.

34. Francisco JC, Virshup DM. Casein Kinase 1 and Human Disease: Insights From the Circadian Phosphoswitch. *Front Mol Biosci*. 2022;9(911764):1-8. doi:10.3389/fmolb.2022.911764.

35.   Wodarz A, Nusse R. Mechanisms of Wnt signaling in development. *Annu Rev Cell Dev Biol*. 1998;14:59-88. doi:10.1146/annurev.cellbio.14.1.59.

36.   Yamaguchi TP. Heads or tails: Wnts and anterior-posterior patterning. *Curr Biol*. 2001;11(17):713-724. doi:10.1016/S0960-9822(01)00417-1.

37.   Clevers H, Nusse R. Wnt/β-catenin signaling and disease. *Cell*. 2012;149(6):1192-1205. doi:10.1016/j.cell.2012.05.012.

38.   Kinzler KW, Nilbert MC, Su LK, et al. Identification of FAP locus genes from chromosome 5q21. *Science*. 1991;253(5020):661-665. doi: 10.1126/science.1651562.

39.   Rubinfeld B, Robbins P, El-Gamil M, Albert I, Porfiri E, Polakis P. Stabilization of β-Catenin by Genetic Defects in Melanoma Cell Lines. *Science*. 1997;275:1790-1792. doi: 10.1126/science.275.5307.1790.

40.   Reya T, Clevers H. Wnt signalling in stem cells and cancer. 434, 843–850 (2005). *Nature*. 2005;434:843-850. doi: 10.1038/nature03319.

41.   Takeda H, Lyle S, Lazar AJF, Zouboulis CC, Smyth I, Watt FM. Human sebaceous tumors harbor inactivating mutations in LEF1. *Nat Med*. 2006;12(4):395-397. doi:10.1038/nm1386.

42.   Merlos-Suárez A, Barriga FM, Jung P, et al. The intestinal stem cell signature identifies colorectal cancer stem cells and predicts disease relapse. *Cell Stem Cell*. 2011;8(5):511-524. doi:10.1016/j.stem.2011.02.020.

43.   Zhan T, Rindtorff N, Boutros M. Wnt signaling in cancer. *Oncogene*. 2017;36(11):1461-1473. doi:10.1038/onc.2016.304.

44.   MacDonald BT, Tamai K, He X. Wnt/β-Catenin Signaling: Components, Mechanisms, and Diseases. *Dev Cell*. 2009;17(1):9-26. doi:10.1016/j.devcel.2009.06.016.

45.   Zeng X, Huang H, Tamai K, et al. Initiation of Wnt signaling: Control of Wnt coreceptor Lrp6 phosphorylation/activation via frizzled, dishevelled and axin functions. *Development*. 2008;135(2):367-375. doi:10.1242/dev.013540.

46.   Cruciat CM. Casein kinase 1 and Wnt/β-catenin signaling. *Curr Opin Cell Biol*. 2014;31(Dvl):46-55. doi:10.1016/j.ceb.2014.08.003.

47.   Myant K, Sansom OJ. Wnt/Myc interactions in intestinal cancer: Partners in crime. *Exp Cell Res*. 2011;317(19):2725-2731. doi:10.1016/j.yexcr.2011.08.001.

48.   Gianferrara T, Cescon E, Grieco I, Spalluto G, Federico S. Glycogen Synthase Kinase 3β Involvement in Neuroinflammation and Neurodegenerative Diseases. *Curr Med Chem*. 2022;29(27):4631-4697. doi:10.2174/0929867329666220216113517.

49.   Wu D, Pan W. GSK3: a multifaceted kinase in Wnt signaling Dianqing. *Trends Biochem Sci*. 2010;35(3):161-168. doi:10.14670/HH-19.495.

50.   Aberle H, Bauer A, Stappert J, Kispert A, Kemler R. B-Catenin Is a Target for the Ubiquitin-Proteasome Pathway. *EMBO J*. 1997;16(13):3797-3804. doi:10.1093/emboj/16.13.3797.

51.   Cheong JK, Virshup DM. The International Journal of Biochemistry Casein kinase 1 : Complexity in the family. *Int J Biochem Cell Biol*. 2011;43(4):465-469. doi:10.1016/j.biocel.2010.12.004.

52.   Umar S, Wang Y, Morris AP, Sellin JH. Dual alterations in casein kinase I-epsilon and GSK-3beta modulate beta-catenin stability in hyperproliferating colonic epithelia. *Am J Physiol Liver Physiol*. 2022;292:599-607. doi:10.1152/ajpgi.00343.2006.

53.   Peters JM, McKay RM, McKay JP, Graff JM. Casein kinase I transduces Wnt signals. *Nature*.

1999;401:345-350.

54. Cruciat C-M, Dolde C, de Groot REA, Ohkawara B, Reinhard C, Korswagen, Hendrik C. Niehrs C. RNA Helicase DDX3 Is a Regulatory Subunit of Casein Kinase 1 in Wnt . *Science (80)*. 2013;339:1436-1442. doi: 10.1126/science.1231499.

55. Tree DRP, Shulman JM, Rousset R, Scott MP, Gubb D, Axelrod JD. Prickle mediates feedback amplification to generate asymmetric planar cell polarity signaling. *Cell*. 2002;109(3):371-381. doi:10.1016/S0092-8674(02)00715-8.

56. Kikuchi A, Yamamoto H, Sato A, Matsumoto S. New Insights into the Mechanism of Wnt Signaling Pathway Activation. *Int Rev Cell Mol Biol*. 2011;291:21-71. doi: 10.1016/B978-0-12-386035-4.00002-1.

57. Habas R, Kato Y, He X. Wnt/Frizzled activation of Rho regulates vertebrate gastrulation and requires a novel formin homology protein Daam1. *Cell*. 2001;107(7):843-854. doi:10.1016/S0092-8674(01)00614-6.

58. Gao B, Song H, Bishop K, et al. Wnt signaling gradients establish planar cell polarity by inducing Vangl2 phosphorylation through Ror2. *Dev Cell*. 2011;20(2):163-176. doi:10.1016/j.devcel.2011.01.001.

59. Gao C, Chen YG. Dishevelled: The hub of Wnt signaling. *Cell Signal*. 2010;22(5):717-727. doi:10.1016/j.cellsig.2009.11.021.

60. Sheldahl LC, Slusarski DC, Pandur P, Miller JR, Kühl M, Moon RT. Dishevelled activates Ca2+ flux, PKC, and CamKII in vertebrate embryos. *J Cell Biol*. 2003;161(4):769-777. doi:10.1083/jcb.200211094.

61. Harvey KF, Zhang X, Thomas DM. The Hippo pathway and human cancer. *Nat Rev Cancer*. 2013;13:246-257. doi: 10.1038/nrc3458.

62. Zhao B, Li L, Tumaneng K, Wang C, Guan K. A coordinated phosphorylation by Lats and CK1 regulates YAP stability through SCFb-TRCP. *Genes Dev*. 2010;24:72-85. doi:10.1101/gad.1843810.

63. Dong J, Feldmann G, Huang J, et al. Elucidation of a Universal Size-Control Mechanism in Drosophila and Mammals. *Cell*. 2007;130:1120-1133. doi:10.1016/j.cell.2007.07.019.

64. Harvey K, Tapon N. The Salvador–Warts–Hippo pathway — an emerging tumour-suppressor network. *Nat Rev Cancer*. 2007;7:182-191. doi: 10.1038/nrc2070.

65. Liu C, Witt L, Ianes C, Bischof J, Peifer C, Knippschild U. Newly Developed CK1-Specific Inhibitors Show Specifically Stronger E ff ects on CK1 Mutants and Colon Cancer Cell Lines. *Int J Mol Sci*. 2019;20(6184):1-26. doi: 10.3390/ijms20246184.

66. Ingham PW, Mcmahon AP. Hedgehog signaling in animal development : paradigms and principles. *Genes Dev*. 2001;15:3059-3087. doi:10.1101/gad.938601.look.

67. Beachy PA, Karhadkar SS, Berman DM. Tissue repair and stem cell renewal in carcinogenesis. *Nature*. 2004;432:324-331. doi: 10.1038/nature03100.

68. Carol W, Smyth I, Allen B. The hedgehog signalling pathway in tumorigenesis and development. *Oncogene*. 1999;18:7844-7851. doi: 10.17305/bjbms.2018.2756.

69. Lindemann RK. Stroma-Initiated Hedgehog Signaling Takes Center Stage in B-Cell Lymphoma. *Cancer Res*. 2008;68(4):961-964. doi:10.1158/0008-5472.CAN-07-5500.

70. Alteba RAI, Mas C, Stecca B. The Gli code : an information nexus regulating cell fate , stemness and cancer. *Trends Cell Biol*. 2007;17(9):438-447. doi:10.1016/j.tcb.2007.06.007.

71. Varjosalo M, Taipale J. Hedgehog : functions and mechanisms. *Genes Dev*. 2008;22:2454-2472. doi:10.1101/gad.1693608.

72. Aza-blanc P, Lin H, Ruiz A, Kornberg TB. Expression of the vertebrate Gli proteins in Drosophila reveals a distribution of activator and repressor activities. *Development*. 2000;127:4293-4301. doi: 10.1242/dev.127.19.4293.

73. Hammerschmidt M, Bitgood MJ, McMahon AP. Protein kinase A is a common negative regulator of Hedgehog signaling in the vertebrate embryo. *Genes Dev*. 1996;10:647-658. doi: 10.1101/GAD.10.6.647.

74. Mering C von, Basler K. Distinct and regulated activities of human Gli proteins in Drosophila. *Curr Biol*. 1999;9:1319-1322. doi: 10.1016/s0960-9822(00)80054-8.

75. Wang B, Li Y. Evidence for the direct involvement of βTrCP in Gli3 protein processing. *PNAS*. 2005;103(1):33-38. doi:10.1073/pnas.0509927103.

76. Chen Y, Sasai N, Ma G, et al. Sonic Hedgehog Dependent Phosphorylation by CK1 a and GRK2 Is Required for Ciliary Accumulation and Activation of Smoothened. *PLOS Biol*. 2011;9(6):1-16. doi:10.1371/journal.pbio.1001083.

77. Harms K, Nozell S, Chen X. The common and distinct target genes of the p53 family transcription factors. *Cell Mol Life Sci*. 2004;61:822-842. doi:10.1007/s00018-003-3304-4.

78. Iwakuma T, Lozano G. MDM2, an introduction. *Mol Cancer Reaserch*. 2003;1(14):993-1000. PMID: 14707282.

79. Huart A, Maclaine NJ, Meek DW, Hupp TR. CK1α Plays a Central Role in Mediating MDM2 Control of p53 and E2F-1 Protein Stability. *J Biol Chem*. 2009;284(47):32384-32394. doi:10.1074/jbc.M109.052647.

80. Philpott JM, Narasimamurthy R, Ricci CG, et al. Casein kinase 1 dynamics underlie substrate selectivity and the PER2 circadian phosphoswitch. *elifesciences*. 2020;9:1-28. doi: 10.7554/eLife.52343.

81. Blennow K, de Leon MJ, Zetterberg H. Alzheimer's disease. *Lancet*. 2006;368(9533):387-403. doi:10.1016/S0140-6736(06)69113-7.

82. Weller J, Budson A. Current understanding of Alzheimer's disease diagnosis and treatment. *F1000Research*. 2018;7:1-9. doi:10.12688/f1000research.14506.1.

83. Rios-Romenets S, Lopera F, Sink KM, et al. Baseline demographic, clinical, and cognitive characteristics of the Alzheimer's Prevention Initiative (API) Autosomal-Dominant Alzheimer's Disease Colombia Trial. *Alzheimer's Dement*. 2020;16:1023-1030. doi:10.1002/alz.12109.

84. Lewis J, Dickson DW, Lin WL, et al. Enhanced neurofibrillary degeneration in transgenic mice expressing mutant tau and APP. *Science (80-)*. 2001;293(5534):1487-1491. doi:10.1126/science.1058189.

85. Hurtado DE, Molina-Porcel L, Iba M, et al. Aβ accelerates the spatiotemporal progression of tau pathology and augments tau amyloidosis in an Alzheimer mouse model. *Am J Pathol*. 2010;177(4):1977-1988. doi:10.2353/ajpath.2010.100346.

86. Reitz C. Alzheimer ' s Disease and the Amyloid Cascade Hypothesis : A Critical Review. *Int J Alzheimers Dis*. 2012;2012:1-11. doi:10.1155/2012/369808.

87. Rissman RA, Poon WW, Blurton-Jones M, et al. Caspase-cleavage of tau is an early event in Alzheimer disease tangle pathology. *J Clin Invest*. 2004;114(1):121-130. doi:10.1172/jci20640.

88. Bloom GS. Amyloid-β and tau: The trigger and bullet in Alzheimer disease pathogenesis. *JAMA*

Neurol. 2014;71(4):505-508. doi:10.1001/jamaneurol.2013.5847.

89.   Takami M, Funamoto S. γ -Secretase-Dependent Proteolysis of Transmembrane Domain of Amyloid Precursor Protein : Successive Tri- and Tetrapeptide Release in Amyloid β -Protein Production. *Int J Alzheimers Dis*. 2012;2012:1-7. doi:10.1155/2012/591392.

90.   Chen C, Gu J, Basurto-islas G, Jin N, Wu F. Up-regulation of casein kinase 1 ε is involved in tau pathogenesis in Alzheimer ' s disease. *Sci Rep*. 2017;7(13478):1-15. doi:10.1038/s41598-017-13791-5.

91.   Chen GF, Xu TH, Yan Y, et al. Amyloid beta: Structure, biology and structure-based therapeutic development. *Acta Pharmacol Sin*. 2017;38(9):1205-1235. doi:10.1038/aps.2017.28.

92.   Li Z, Wang M, Moniruzzaman M, et al. Astrocytes deliver CK1 to neurons via extracellular vesicles in response to inflammation promoting the translation and amyloidogenic processing of APP. *J Extracell Vesicles*. 2020;10:1-21. doi:10.1002/jev2.12035.

93.   Wong PC, Cai H, Borchelt DR, Price DL. Genetically engineered mouse models of neurodegenerative. *Nat Neurosci*. 2002;5(2):633-639. doi:10.1038/nn0702-633.

94.   Flajolet M, He G, Heiman M, Lin A, Nairn AC, Greengard P. Regulation of Alzheimer ' s disease amyloid- ₙₗ formation by casein kinase I. *PNAS*. 2007;104(10):4159-4164. doi:10.1073/pnas.0611236104.

95.   Kelleher RJ, Shen J. Presenilin-1 mutations and Alzheimer ' s disease. *Proc Natl Acad Sci U S A*. 2017;114(4):629-631. doi:10.1073/pnas.1619574114.

96.   Fedeli C, Filadi R, Rossi A, Mammucari C, Pizzo P. PSEN2 (presenilin 2) mutants linked to familial Alzheimer disease impair autophagy by altering Ca2+ homeostasis. *Autophagy*. 2019;15(12):2044-2062. doi:10.1080/15548627.2019.1596489.

97.   Walters J, Schindzielorz A, Grünberg J, Haass C. Phosphorylation of presenilin-2 regulates its cleavage by caspases and retards progression of apoptosis. *PN*. 1999;96:1391-1396. doi: 10.1073/pnas.96.4.1391.

98.   Avila J, Lucas JJ, Pérez M, Hernández F. Role of Tau Protein in Both Physiological and Pathological Conditions. *Physiol Rev*. 2004;84(2):361-384. doi:10.1152/physrev.00024.2003.

99.   Avila J, Jiménez JS, Sayas CL, et al. Tau Structures. *Front Aging Neurosci*. 2016;8(262):1-10. doi:10.3389/fnagi.2016.00262.

100.   Tang Y, Lutz MW, Xing Y. A systems-based model of Alzheimer's disease. *Alzheimer's Dement*. Published online 2018:1-4. doi:10.1016/j.jalz.2018.06.3058.

101.   Kadavath, Harindranath Jaremko M, Jaremko Ł, Biernat J, Mandelkow E, Zweckstetter M. Folding of the Tau Protein on Microtubules. *Angew Chemie*. 2015;54(35):10347-10351. doi: 10.1002/anie.201501714.

102.   Congdon, Erin E. and Sigurdsson EM. Tau-targeting therapies for Alzheimer disease. *Nat Rev Neurol*. 2018;14(7):399-415. doi:10.1038/s41582-018-0013-z.

103.   Luna-Viramontes NI, Campa-Córdoba BB, Ontiveros-Torres MA, et al. PHF-Core Tau as the Potential Initiating Event for Tau Pathology in Alzheimer's Disease. *Front Cell Neurosci*. 2020;14(247):1-11. doi:10.3389/fncel.2020.00247.

104.   Hanger DP, Anderton BH, Noble W. Tau phosphorylation: the therapeutic challenge for neurodegenerative disease. *Trends Mol Med*. 2009;15(3):112-119. doi:10.1016/j.molmed.2009.01.003.

105.   Roth A, Sander A, Oswald MS, Gärtner F, Knippschild U, Bischof J. Comprehensive Characterization

of CK1 δ -Mediated Tau Phosphorylation in Alzheimer ' s Disease. *Front Mol Biosci*. 2022;9(872171):1-16. doi:10.3389/fmolb.2022.872171.

106. Augustinack JC, Schneider A, Mandelkow EM, Hyman BT. Specific tau phosphorylation sites correlate with severity of neuronal cytopathology in Alzheimer 's disease. *Acta Neuropathol*. 2002;103:26-35. doi:10.1007/s004010100423.

107. Kimura T, Fukuda T, Sahara N, et al. Aggregation of detergent-insoluble tau is involved in neuronal loss but not in synaptic loss. *J Biol Chem*. 2010;285(49):38692-38699. doi:10.1074/jbc.M110.136630.

108. Li G, Yin H, Kuret J. Casein Kinase 1 Delta Phosphorylates Tau and Disrupts Its Binding to Microtubules *. *J Biol Chem*. 2004;279(16):15938-15945. doi:10.1074/jbc.M314116200.

109. Lei P, Ayton S, Finkelstein DI, Adlard PA, Masters CL, Bush AI. Tau protein : Relevance to Parkinson's disease. *Int J Biochem Cell Biol*. 2010;42:1775-1778. doi:10.1016/j.biocel.2010.07.016.

110. Leon-Espinosa G, Garcia E, Garcia-Escudero V, Hernandez F, DeFelipe J, Avila J. Changes in Tau Phosphorylation in Hibernating Rodents. *J Neurosci Res*. Published online 2013:1-9. doi:10.1002/jnr.23220.

111. Roth A, Gärtner F, Mayer K, et al. CK1 δ -Derived Peptides as Novel Tools Inhibiting the Interactions between CK1 δ and APP695 to Modulate the Pathogenic Metabolism of APP. *Int J Mol Sci*. 2021;22(6423):1-18. doi: 10.3390/ijms22126423.

112. Kannanayakal TJ, Tao H, Vandre DD, Kuret J. Casein kinase-1 isoforms differentially associate with neurofibrillary and granulovacuolar degeneration lesions. *Acta Neuropathol*. 2006;111:413-421. doi:10.1007/s00401-006-0049-9.

113. Kalia L V, Lang AE, Shulman G. Parkinson ' s disease. *Lancet*. 2015;386:896-912. doi:10.1016/S0140-6736(14)61393-3.

114. Lotankar S, Prabhavalkar KS, Bhatt LK. Biomarkers for Parkinson's Disease: Recent Advancement. *Neurosci Bull*. 2017;33(5):585-597. doi:10.1007/s12264-017-0183-5.

115. Chen P-C, Lao C-L, Chen J-C. The D3 dopamine receptor inhibits dopamine release in PC-12/hD3 cells autoreceptor signaling via PP-2B, CK1, and Cdk-5. *J Neurochem*. 2009;110:1180-1190. doi:10.1111/j.1471-4159.2009.06209.

116. Li D-W, Liu Z-Q, Chen W, Yao M, Li G-R. Association of glycogen synthase kinase - 3 β with Parkinson ' s disease (Review). *Mol Med Rep*. 2014;9:2043-2050. doi:10.3892/mmr.2014.2080.

117. Martín-Bastida A, Lao-Kaim NP, Roussakis AA, et al. Relationship between neuromelanin and dopamine terminals within the Parkinson's nigrostriatal system. *Brain*. 2019;142(7):2023-2036. doi:10.1093/brain/awz120.

118. Bisaglia M, Greggio E, Beltramini M, Bubacco L. Dysfunction of dopamine homeostasis: Clues in the hunt for novel Parkinson's disease therapies. *FASEB J*. 2013;27(6):2101-2110. doi:10.1096/fj.12-226852.

119. Hisahara S, Shimohama S. Dopamine Receptors and Parkinson ' s Disease Shin Hisahara and Shun Shimohama. *Inernational J Med Chem*. 2011;2011:1-16. doi:10.1155/2011/403039.

120. Kosten J, Binol A, Stuiver M, et al. Efficient Modification of Alpha-Synuclein Serine 129 by Protein Kinase CK1 Requires Phosphorylation of Tyrosine 125 as a Priming Event. *ACS Cgemical Neurosci*. 2014;5:1203-1208. doi.org/10.1021/cn5002254.

121. Dzamko N, Zhou J, Huang Y, Halliday GM, Berg WD Van De. Parkinson 's disease-implicated kinases in the brain; insights into disease pathogenesis. *Front Mol Neurosci*. 2014;7(57):1-15. doi:10.3389/fnmol.2014.00057.

122.	Anderson JP, Walker DE, Goldstein JM, et al. Phosphorylation of Ser-129 Is the Dominant Pathological Modification of α-Synuclein in Familial and Sporadic Lewy Body Disease. *J Biol Chem*. 2006;281(40):29739-29752. doi:10.1074/jbc.M600933200.

123.	Elsholz L, Wasser Y, Ziegler P, Habib P. Independent of Serine 129 Phosphorylation. *Cells*. 2021;10(2830):1-22.

124.	Bancher C, Braak H, Fischer P, Jellinger KA. Neuropathological staging of Alzheimer lesions and intellectual status in Alzheimer's and Parkinson's disease patients. *Neurosci Lett*. 1993;162(1-2):179-182. doi:10.1016/0304-3940(93)90590-H.

125.	Muntané G, Dalfó E, Martinez A, Ferrer I. Phosphorylation of Tau and α-synuclein in synaptic-enriched fractions of the frontal cortex in Alzheimer's disease, and in Parkinson's disease and related α-synucleopathies. *Neuroscience*. 2008;152:913-923. doi:10.1016/j.neuroscience.2008.01.030.

126.	Cookson MR. The biochemistry of Parkinson's disease. *Annu Rev Biochem*. 2005;74:29-52. doi:10.1146/annurev.biochem.74.082803.133400.

127.	Eck RJ, Kraemer BC, Liachko NF. Regulation of TDP-43 phosphorylation in aging and disease. *GeroScience*. 2021;43:1605-1614. doi:10.1007/s11357-021-00383-5.

128.	Ayala YM, Pantano S, Ambrogio AD, et al. Human , Drosophila , and C . elegans TDP43 : Nucleic Acid Binding Properties and Splicing Regulatory Function. *J Mol Biol*. 2005;348:575-588. doi:10.1016/j.jmb.2005.02.038.

129.	Arseni D, Hasegawa M, Murzin AG, Kametani F, Arai M. Structure of pathological TDP-43 filaments from ALS with FTLD. *Nature*. 2022;601:139-143. doi:10.1038/s41586-021-04199-3.

130.	Mcaleese KE, Walker L, Erskine D, Thomas AJ, Mckeith IG, Attems J. TDP-43 pathology in Alzheimer ' s disease , dementia with Lewy bodies and ageing. *Brain Pathol*. 2017;27:472-479. doi:10.1111/bpa.12424.

131.	Neumann M, Sampathu DM, Kwong LK, et al. Ubiquitinated TDP-43 in Frontotemporal Lobar Degeneration and Amyotrophic Lateral Sclerosis. *Science (80-)*. 2006;314(5796):130-133. doi:10.1002/ana.21425.

132.	Dong Y, Chen Y. The role of ubiquitinated TDP-43 in amyotrophic lateral sclerosis. *Neuroimmunol Neuroinflammation*. 2018;5(5):1-10. doi:10.20517/2347-8659.2017.47.

133.	Herhaus L, Dikic I. Expanding the ubiquitin code through post-translational modification. *EMBO Rep*. 2015;16(9):1071-1083. doi: 10.15252/embr.201540891.

134.	Hu WT, Grossman M. TDP-43 and frontotemporal dementia. *Curr Neurol Neurosci Rep*. 2009;9(5):353-358. doi: 10.1007/s11910-009-0052-3.

135.	Nonaka T, Suzuki G, Tanaka Y, et al. Phosphorylation of TAR DNA-binding Protein of 43 kDa (TDP-43) by Truncated Casein Kinase 1 δ Triggers Mislocalization and Accumulation of TDP-43. *J Biol Chem*. 2016;291(11):5473-5483. doi:10.1074/jbc.M115.695379.

136.	Kametani F, Nonaka T, Suzuki T, Arai T, Dohmae N. Biochemical and Biophysical Research Communications Identification of casein kinase-1 phosphorylation sites on TDP-43. *Biochem Biophys Res Commun*. 2009;382(2):405-409. doi:10.1016/j.bbrc.2009.03.038.

137.	Alquezar C, Salado IG, Encarnación A De, Pérez DI, Moreno F, Gil C. Targeting TDP-43 phosphorylation by Casein Kinase-1 δ inhibitors : a novel strategy for the treatment of frontotemporal dementia. *Mol Neurodegener*. 2016;11(36):1-14. doi:10.1186/s13024-016-0102-7.

138.	Choksi DK, Roy B, Chatterjee S, et al. TDP-43 Phosphorylation by casein kinase I 1 promotes oligomerization and enhances toxicity in vivo. *Hum Mol Genet*. 2014;23(4):1025-1035.

doi:10.1093/hmg/ddt498.

139.   Deng X, Sun X, Yue W, et al. CHMP2B regulates TDP-43 phosphorylation and cytotoxicity independent of autophagy via CK1. *J Cell Biol*. 2021;221(1):1-16.

140.   Roskoski Jr R. Classification of small molecule protein kinase inhibitors based upon the structures of their drug-enzyme complexes. *Pharmacol Res*. 2016;103:26-48. doi:10.1016/j.phrs.2015.10.021.

141.   Zuccotto F, Ardini E, Casale E, Angiolini M. Through the " Gatekeeper Door ": Exploiting the Active Kinase Conformation. *J Med Chem Perspect*. 2010;53:2681-2694. doi:10.1021/jm901443h.

142.   Traxler P, Furet P. Strategies toward the design of novel and selective protein tyrosine kinase inhibitors. *Pharmacol Ther*. 1999;82:195-206. doi: 10.1016/s0163-7258(98)00044-8.

143.   Garuti L, Roberti M, Bottegoni G. Non-ATP competitive protein kinase inhibitors. *Curr Med Chem*. 2010;17(25):2804-2821. doi: 10.2174/092986710791859333.

144.   Müller S, Chaikuad A, Nathanael GS, Knapp S. The ins and outs of selective kinase inhibitor development. *Nat Chem Biol*. 2015;11:818-821. doi: 10.1038/nchembio.1938.

145.   Lamba V, Indraneel G. New directions in targeting protein kinases: focusing upon true allosteric and bivalent inhibitors. *Curr Pharm Des*. 2012;18(20):2936-2945. doi: 10.2174/138161212800672813.

146.   Barf T, Kaptein A. Irreversible Protein Kinase Inhibitors: Balancing the Bene fi ts and Risks. *J Med Chem*. 2012;55:6243-6262. doi: 10.1021/jm3003203.

147.   Singh J, Petter RC, Baillie TA, Whitty A. The resurgence of covalent drugs. *Nat Rev Drug Discov*. 2011;10:307-317. doi:10.1038/nrd3410.

148.   Liu Q, Sabnis Y, Zhao Z, et al. Developing irreversible inhibitors of the protein kinase cysteinome. *Chem Biol*. 2014;20(2):146-159. doi:10.1016/j.chembiol.2012.12.006.

149.   Mashhoon N, Demaggio AJ, Tereshko V, et al. Crystal Structure of a Conformation-selective Casein Kinase-1 Inhibitor. *J Biol Chem*. 2000;275(26):20052-20060. doi:10.1074/jbc.M001713200.

150.   Brockschmidt C, Hirner H, Huber N, et al. Anti-apoptotic and growth-stimulatory functions of CK1 delta and epsilon in ductal adenocarcinoma of the pancreas are inhibited by IC261 in vitro and in vivo. *Gut*. 2008;57(6):799-806. doi: 10.1136/gut.2007.123695.

151.   Rena G, Bain J, Elliott M, Cohen P. D4476, a cell-permeant inhibitor ofCK1, suppresses the site-specific phosphorylationandnuclear exclusion of FOXO1a. *EMBO Rep*. 2004;5(1):60-65. doi:10.1038/sj.embor.7400048.

152.   Peifer C, Abadleh M, Bischof J, et al. 3 , 4-Diaryl-isoxazoles and -imidazoles as Potent Dual Inhibitors of p38 r Mitogen Activated Protein Kinase and Casein Kinase 1 δ †. *J Med Chem*. 2009;52:7618-7630. doi:10.1021/jm9005127.

153.   Badura L, Swanson T, Adamowicz W, et al. An Inhibitor of Casein Kinase I ε Induces Phase Delays in Circadian Rhythms under Free-Running and Entrained Conditions. *J Pharmacol*. 2007;322(2):730-738. doi:10.1124/jpet.107.122846.

154.   Ihara T, Nakamura Y, Mitsui T, Tsuchiya S, Kanda M. Intermittent restraint stress induces circadian misalignment in the mouse bladder , leading to nocturia. *Sci Rep*. 2019;9(10069):1-11. doi: 10.1038/s41598-019-46517-w.

155.   Storz SS, Tovin A, Mracek P, Alon S, Foulkes NS, Gothilf Y. Casein Kinase 1 d Activity : A Key Element in the Zebrafish Circadian Timing System. *PLoS One*. 2013;8(1):1-10. doi:10.1371/journal.pone.0054189.

156.   Janovska P, Verner J, Kohoutek J, et al. Casein kinase 1 is a therapeutic target in chronic lymphocytic

leukemia. *Blood*. 2018;131(11):1206-1218. doi:10.1182/blood-2017-05-786947.

157. Luxenburger A, Schmidt D, Ianes C, et al. Design, Synthesis and Biological Evaluation of Isoxazole-Based CK1 Inhibitors Modified with Chiral Pyrrolidine Scaffolds. *Molecules*. 2019;24(873):1-34. doi:10.3390/molecules24050873.

158. Oumata N, Bettayeb K, Ferandin Y, et al. Roscovitine-Derived , Dual-Specificity Inhibitors of Cyclin-Dependent Kinases and Casein Kinases 1. *J Med Chem*. 2008;51:5229-5242. doi: 10.1021/jm800109e.

159. Delehouzé C, Godl K, Loae C, et al. CDK / CK1 inhibitors roscovitine and CR8 downregulate amplified MYCN in neuroblastoma cells. *Oncogene*. Published online 2013:1-13. doi:10.1038/onc.2013.513.

160. Bibian M, J. Rahaim R, Yong CJ, et al. Development of highly selective casein kinase 1δ/1ε (CK1δ/ε) inhibitors with potent antiproliferative properties. *Bioorg Med Chem Lett*. 2013;23(15):1-7. doi:10.1016/j.bmcl.2013.05.075.

161. Monastyrskyi A, Nilchan N, Quereda V, et al. Development of dual casein kinase 1δ/1ε (CK1δ/ε) inhibitors for treatment of breast cancer. *Bioorg Med Chem Lett*. 2019;26(3):590-602. doi:10.1016/j.bmc.2017.12.020.

162. Richter J, Bischof J, Zaja M, et al. Di fluoro-dioxolo-benzoimidazol-benzamides As Potent Inhibitors of CK1δ and ε with Nanomolar Inhibitory Activity on Cancer Cell Proliferation. *J Med Chem*. 2014;57:7933-7946. doi:10.1021/jm500600b.

163. Salado IG, Redondo M, Bello MB, et al. Protein Kinase CK-1 Inhibitors As New Potential Drugs for Amyotrophic Lateral Sclerosis. *J Med Chem*. 2014;57:2755-2772. doi:10.1021/jm500065f.

164. Martínez-gonzález L, Rodríguez-cueto C, Cabezudo D, Martín-requero Á, Fernández-ruiz J, Martínez A. Motor neuron preservation and decrease of in vivo TDP-43 phosphorylation by protein CK-1 δ kinase inhibitor treatment. *Nat Res*. 2020;10(4449):1-12. doi:10.1038/s41598-020-61265-y.

165. Benn CL, Dawson LA. Clinically Precedented Protein Kinases: Rationale for Their Use in Neurodegenerative Disease. *Front Aging Neurosci*. 2020;12(242):1-29. doi:10.3389/fnagi.2020.00242.

166. Mikitsh JL, Chacko AM. Pathways for small molecule delivery to the central nervous system across the blood-brain barrier. *Perspect Medicin Chem*. 2014;(6):11-24. doi:10.4137/PMc.s13384.

167. Cardoso FL, Brites D, Brito MA. Looking at the blood-brain barrier: Molecular anatomy and possible investigation approaches. *Brain Res Rev*. 2010;64(2):328-363. doi:10.1016/j.brainresrev.2010.05.003.

168. Wohnsland F, Faller B. High-throughput permeability pH profile and high-throughput alkane/water log P with artificial membranes. *J Med Chem*. 2001;44(6):923-930. doi:10.1021/jm001020e.

169. Ottaviani G, Martel S, Carrupt PA. Parallel artificial membrane permeability assay: A new membrane for the fast prediction of passive human skin permeability. *J Med Chem*. 2006;49(13):3948-3954. doi:10.1021/jm060230+.

170. Di L, Kerns EH, Fan K, McConnell OJ, Carter GT. High throughput artificial membrane permeability assay for blood-brain barrier. *Eur J Med Chem*. 2003;38(3):223-232. doi:10.1016/S0223-5234(03)00012-6. doi: 10.1016/s0223-5234(03)00012-6.

171. AG M, K N, F L, et al. Fundamental Methods in Drug Permeability, pKa, LogP and LogDx Determination. *J Drug Res Dev*. 2019;4(2):1-6. doi:10.16966/2470-1009.146.

172. Mhambi S, Fisher D, Tchokonte MBT, Dube A. Permeation Challenges of Drugs for Treatment of Neurological Tuberculosis and HIV and the Application of Magneto-Electric Nanoparticle Drug Delivery Systems. *Pharmaceutics*. 2021;13(1479):1-15. doi: 10.3390/pharmaceutics13091479.

173. Freeman-cook KD, Hoffman RL, Johnson TW. Lipophilic efficiency : the most important efficiency metric in medicinal chemistry. *Future Med Chem*. 2013;5(2):113-115. doi: 10.4155/fmc.12.208.

174. Walters WP, Green J, Weiss JR, Murcko MA. What Do Medicinal Chemists Actually Make ? A 50-Year Retrospective. *J Med Chem*. 2011;54:6405-6416. doi: 10.1021/jm200504p.

175. Arnott JA, Kumar R, Planey SL. Lipophilicity Indices for Drug Development Lipophilicity Indices for Drug Development. *Biopharm Pharmacokinet*. 2013;1(1):31-36. doi:10.14205/2309-4435.2013.01.01.6.

176. Jaiswal MK. Riluzole and edaravone : A tale of two amyotrophic lateral sclerosis drugs. *Med Res Rev*. Published online 2018:1-16. doi:10.1002/med.21528.

177. Prasad Ranjeet D, R Jayachandra B, Nuggehally RS. Two Decades-Long Journey from Riluzole to Edaravone : Revisiting the Clinical Pharmacokinetics of the Only Two Amyotrophic Lateral Sclerosis Therapeutics. *Clin Pharmacokinet*. 2018;57(11):1385-1398. doi:10.1007/s40262-018-0655-4.

178. EMEA. *Scientific Discussion for the Approval of RILUTEK*.; 2004.

179. Doble A. The pharmacology and mechanism of action of riluzole. *Neurology*. 1996;47(S4):S233-S241. doi:10.1212/WNL.47.6.

180. Bissaro M, Federico S, Salmaso V, Sturlese M, Spalluto G, Moro S. Targeting protein kinase CK1δ with Riluzole: could it be one of the possible missing bricks to interpret its effect in the treatment of ALS from a molecular point of view? *ChemMedChem*. 2018;13(24):2601-2605. doi:10.1002/cmdc.201800632.

181. Bissaro M, Moro S. Rethinking to riluzole mechanism of action : the molecular link among protein kinase CK1δ activity , TDP-43 phosphorylation , and amyotrophic lateral sclerosis pharmacological treatment. *Neural Regen Res*. 2019;14(12):2083-2085. doi:10.4103/1673-5374.262578.

182. Martinet M, Montay G, Rhodes G. Pharmacokinetics and metabolism of riluzole. *Drugs of todey*. 1996;33(8):587-594.

183. Sanderink G, Bournique B, Stevens J, Petry M, Martinet M. Involvement of Human CYP1A Isoenzymes in the Metabolism and Drug Interactions of Riluzole In Vitro 1. *J Pharmacol Exp Ther*. 1997;282(3):1465-1472.

184. Kan HJM Van, Groeneveld GJ, Straaten RJHM Van Der, Vught PWJ Van. Pharmacokinetics of Riluzole : Evidence for Glucuronidation as a Major Metabolic Pathway not Associated with UGT1A1 Genotype. *Biopharm drug Dispos*. 2008;29:139-144. doi:10.1002/bdd.

185. Jimonet P, Audiau F, Barreau M, et al. Riluzole series. synthesis and in vivo "antiglutamate" activity of 6- substituted-2-benzothiazolamines and 3-substituted-2-imino-benzothiazolines. *J Med Chem*. 1999;42(15):2828-2843. doi:10.1021/jm980202u.

186. Gazette. Fascicule de brevet européen. Derivés de 6 polyfluoroalcoxy et 6 polyfluoroalkyle 2 aminobenzothiazole. WO 96/13492. Exemple 1. Published online 1996.

187. Pierce AC, Arnost M, Davies RJ, et al. Preparation of 3,5 diamino- triazoles as protein kinase inhibitors. PCT International Application. WO2004046120. Published online 2004.

188. Too K, Brown DM, Bongard E, Yardley V, Vivas L, Loakes D. Anti-malarial activity of N6-modified purine analogues. *Bioorganic Med Chem*. 2007;15(16):5551-5562. doi:10.1016/j.bmc.2007.05.038.

189. Ewan HS, Muli CS, Touba S, et al. Synthesis of sugar oxime ether surfactants. *Tetrahedron Lett*. 2014;55(35):4962-4965. doi:10.1016/j.tetlet.2014.07.036.

190. Lernen GS, Giampietro NC, Hay MB, Wolfe JP. Influence of hydroxylamine conformation on stereocontrol in Pd-catalyzed isoxazolidine-forming reactions. *J Org Chem*. 2009;74(6):2533-2540. doi:10.1021/jo8027399.

191. Fors BP, Buchwald SL. A multiligand based Pd catalyst for C-N cross-coupling reactions. *J Am Chem*

Soc. 2010;132(45):15914-15917. doi:10.1021/ja108074t.

192.   Toulot S, Heinrich T, Leroux FR. Convenient and reliable routes towards 2-aminothiazoles: Palladium-catalyzed versus copper-catalyzed aminations of halothiazoles. *Adv Synth Catal*. 2013;355(16):3263-3272. doi:10.1002/adsc.201300591.

193.   Rasmussen LK. Facile synthesis of mono-, di-, and trisubstituted alpha-unbranched hydrazines. *J Org Chem*. 2006;71(9):3627-3629. doi:10.1021/jo0525783.

194.   Guha R, Drie JH Van. Structure-Activity Landscape Index : Identifying and Quantifying Activity Cliffs. *J Chem Inf Model*. 2008;48:646-658. doi: 10.1021/ci7004093.

195.   Yang T, Ferrill L, Gallant L, et al. Verapamil and riluzole cocktail liposomes overcome pharmacoresistance by inhibiting P-glycoprotein in brain endothelial and astrocyte cells: A potent approach to treat amyotrophic lateral sclerosis. *Eur J Pharm Sci*. 2018;120(December 2017):30-39. doi:10.1016/j.ejps.2018.04.026.

196.   Bhayani JA, Ballicora MA. Determination of dissociation constants of protein ligands by thermal shift assay. *Biochem Biophys Res Commun*. 2022;590:1-6. doi:10.1016/j.bbrc.2021.12.041.

197.   Huynh K, Partch CL. Analysis of Protein Stability and Ligand Interactions by Thermal Shift Assay. *Curr Protoc Protein Sci*. 2015;79:1-14. doi: 10.1002/0471140864.ps2809s79.

198.   Boivin S, Kozak S, Meijers R. Optimization of protein purification and characterization using Thermofluor screens. *Protein Expr Purif*. 2013;91:192-206. doi:10.1016/j.pep.2013.08.002.

199.   Meerloo J van, Kaspers GJL, Cloos J. Cell sensitivity assays: the MTT assay. *Methods Mol Biol*. 2011;731:237-245. doi: 10.1007/978-1-61779-080-5_20.

200.   Iguchi Y, Katsuno M, Takagi S, Ishigaki S, Niwa J. Neurobiology of Disease Oxidative stress induced by glutathione depletion reproduces pathological modi fi cations of TDP-43 linked to TDP-43 proteinopathies. *Neurobiol Dis*. 2012;45:862-870. doi:10.1016/j.nbd.2011.12.002.

201.   ONG KT, LIU Z-Q, TAY MG. Review on the Synthesis of Pyrazine and Its Derivatives. *Borneo J Resour Sci Technol*. 2017;7(2):60-75. doi:10.33736/bjrst.591.2017.

202.   Vidal Juan B, Esteve Trias C, Soca Pueyo L, Eastwood P, Eastwood R. WO2007017096A1. Published online 2007:1-193.

203.   Mori K, Yang CY. Pheromone synthesis. Part 261: Synthesis of four pyrazines produced by females of the Korean apricot wasp, Eurytoma maslovskii. *Tetrahedron*. 2017;73(32):4766-4769. doi:10.1016/j.tet.2017.06.055.

204.   Philippi F, Rauber D, Zapp J, Präsang C, Scheschkewitz D, Hempelmann R. Multiple Ether-Functionalized Phosphonium Ionic Liquids as Highly Fluid Electrolytes. *ChemPhysChem*. Published online 2019:S1-S30. doi: 10.1002/cphc.201800939.

205.   Lennox AJJ, Lloyd-Jones GC. Selection of boron reagents for Suzuki-Miyaura coupling. *Chem Soc Rev*. 2014;43(1):412-443. doi:10.1039/c3cs60197h.

206.   Furstner A, Leitner A, Mendez M, Krause H. Iron-Catalyzed Cross-Coupling Reactions. *Jacs*. 2002;124:13856-13863. doi: 10.1021/ja027190t.

207.   Nikishkin NI, Huskens J, Verboom W. Transition metal-catalyzed functionalization of pyrazines. *Org Biomol Chem*. 2013;11(22):3583-3602. doi:10.1039/c3ob40460a.

208.   Phan DP, Le VN, Kim J, Lee EY. Controlled hydrodeoxygenation of lignin-derived anisole over supported Pt on UiO-66 based-catalysts through defect engineering approach. *Fuel Process Technol*. 2021;224. doi:10.1016/j.fuproc.2021.107001.

209. Grieco I, Bissaro M, Benedetto D, et al. Developing novel classes of protein kinase CK1 d inhibitors by fusing [1 , 2 , 4] triazole with different bicyclic heteroaromatic systems. *Eur J Med Chem*. 2021;216:113331. doi:10.1016/j.ejmech.2021.113331.

210. Blotny G. Recent applications of 2,4,6-trichloro-1,3,5-triazine and its derivatives in organic synthesis. *Tetrahedron*. 2006;62(41):9507-9522. doi:10.1016/j.tet.2006.07.039.

211. Cascioferro S, Parrino B, Spanò V, et al. 1,3,5-Triazines: A promising scaffold for anticancer drugs development. *Eur J Med Chem*. 2017;142:523-549. doi:10.1016/j.ejmech.2017.09.035.

212. Bork JT, Lee JW, Chang YT. Palladium-catalyzed cross-coupling reaction of resin-bound chlorotriazines. *Tetrahedron Lett*. 2003;44(32):6141-6144. doi:10.1016/S0040-4039(03)01451-5.

213. Langmead CJ, Andrews SP, Congreve M, et al. Identification of novel adenosine A 2A receptor antagonists by virtual screening. *J Med Chem*. 2012;55:1904-1909. doi:10.1021/jm201455y.

214. Bolcato G, Cescon E, Pavan M, et al. Article a computational workflow for the identification of novel fragments acting as inhibitors of the activity of protein kinase ck1δ. *Int J Mol Sci*. 2021;22(9741):1-13. doi:10.3390/ijms22189741.

215. Giroux A. Synthesis of benzylic boronates via palladium-catalyzed cross-coupling reaction of bis(pinacolato)diboron with benzylic halides. *Tetrahedron Lett*. 2003;44(2):233-235. doi:10.1016/S0040-4039(02)02566-2.

216. Shaikh MS, Rana J, Gaikwad D, et al. Antifolate Agents Against Wild and Mutant Strains of Plasmodium falciparum. *Indian J Pharm Sci*. Published online 2014:116-124.

217. Baraldi PG, Cacciari B, Romagnoli R, et al. Pyrazolo[4,3-e]1,2,4-Triazolo[1,5-c]Pyrimidine Derivatives as Adenosine Receptor Ligands: A Starting Point for Searching A2B Adenosine Receptor Antagonists. *Drug Dev Res*. 2001;53:225-235. doi: 10.1021/jm991114s.

218. Hall RJ, Mortenson PN, Murray CW. Efficient exploration of chemical space by fragment-based screening. *Prog Biophys Mol Biol*. 2014;116(2-3):82-91. doi:10.1016/j.pbiomolbio.2014.09.007.

219. Drew BA, Borow ME, Beckman BS. MEK5 / ERK5 Pathway : The first fifteen years. *Biochim Biophys Acta*. 2014;1825(1):37-48. doi:10.1016/j.bbcan.2011.10.002.MEK5/ERK5.

220. Polyakov A, Phillips W, Clark K. (10) International Publication Number WO2008/132464 A2. Published online 2008:1-94.

221. Jo M, Lee S, Kim K, Lee S, Kim SR, Kim HJ. Inhibition of MEK5 suppresses TDP-43 toxicity via the mTOR-independent activation of the autophagy-lysosome pathway. *Biochem Biophys Res Commun*. 2019;513(4):925-932. doi:10.1016/j.bbrc.2019.04.088.

222. Arias Salomão L, Pessan Pelim J, Miranda Vieira AP, Toito de Lima TM, Botazzo Delbem AC, Monteiro DR. Iron Oxide Nanoparticles for Biomedical Applications : A Perspective on Synthesis , Drugs , Antimicrobial Activity , and Toxicity. *Antibiotics*. 2018;7(46):1-32. doi:10.3390/antibiotics7020046.

223. Demirer GS, Okur AC, Kizilel S. Synthesis and Design of Biologically Inspired Biocompatible Iron Oxide Nanoparticles for Biomedical Applications. *J Mater Chem B*. 2015;00(1-3):1-23. doi:10.1039/x0xx00000x.

9. Acknowledgements